THE UNIVERSITY OF
WARWICK

AUTHOR: **Rachel Lauren Tunnicliffe** DEGREE: **Ph.D.**

TITLE: **Constraining the Progenitors of Short Gamma-Ray Bursts**

DATE OF DEPOSIT: .....

I agree that this thesis shall be available in accordance with the regulations governing the University of Warwick theses.

I agree that the summary of this thesis may be submitted for publication.

I **agree** that the thesis may be photocopied (single copies for study purposes only).

Theses with no restriction on photocopying will also be made available to the British Library for microfilming. The British Library may supply copies to individuals or libraries. subject to a statement from them that the copy is supplied for non-publishing purposes. All copies supplied by the British Library will carry the following statement:

> "Attention is drawn to the fact that the copyright of this thesis rests with its author. This copy of the thesis has been supplied on the condition that anyone who consults it is understood to recognise that its copyright rests with its author and that no quotation from the thesis and no information derived from it may be published without the author's written consent."

AUTHOR'S SIGNATURE: .....

USER'S DECLARATION

1. I undertake not to quote or make use of any information from this thesis without making acknowledgement to the author.
2. I further undertake to allow no-one else to use this thesis while it is in my care.

DATE SIGNATURE ADDRESS

.....

.....

.....

.....

.....

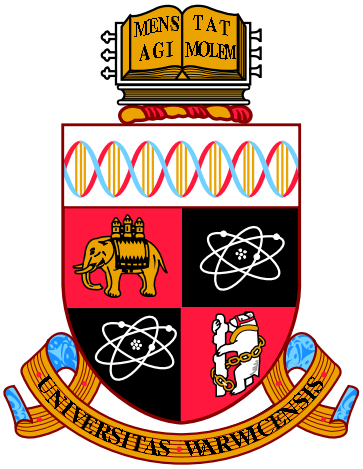

Constraining the Progenitors of Short Gamma-Ray Bursts

by

Rachel Lauren Tunnicliffe

Thesis

Submitted to the University of Warwick

for the degree of

Doctor of Philosophy

Department of Physics

January 2014

THE UNIVERSITY OF WARWICK

Contents

List of Tables

List of Figures

Acknowledgments

First and foremost I would like to thank my supervisor Dr. Andrew Levan for always being present with a wealth of knowledge and an open door, giving useful insight and direction to all my work. In addition I would like to thank, for the start of my PhD, Karl Svensson and, thoughout, Prof. Nial Tanvir for additional help, insight and many ideas. Without these people and many others, this work could not have been completed.

I have been very privileged to be a member of the Astronomy and Astrophysics group at Warwick and the Physics department as a whole. I would like to thank all those people, past and present, who have been a part of my experience here. It really is a very special group and I hope that, though it will change, it never loses the essence which made it such a wonderful place for me to study and just to grow as a person.

In particular I would like to thank the following people: Joao, Steve Parsons and George for being the people who, after gentle persuasion, really made me feel a part of the group when I first started; Steve Gallagher, Pete, Simon and Zoe for being such an integral part of my experience at Warwick and for the many times they helped me even if they didn't know they were; John, Phil and Penelope for some much needed and helpful tea breaks, your company and insight was and always will be appreciated and finally, Greg and Tom who, along with everyone else, made my time thesis writing a lot less impossible and a lot more bearable.

As ever, my family, in particular my mum, dad and grandad have been unendingly supportive in every choice I've ever made. I cannot thank them enough for everything they have ever done for me and without them this work would not

have been possible.

Finally, my partner Matt who just makes me a better, and in times of stress perhaps more bearable, person. His love, support and most of all understanding kept me afloat whenever I felt at sea and I thank him for his patience, kindness and joviality throughout.

Declarations

This is a declaration of the extent of the original work within this thesis and of the work published/submitted for publication. This thesis has not been submitted in part or full to any other institution for any other qualification.

Chapter 3 is based on a paper published in the *Monthly Notice of the Royal Astronomical Society (MNRAS)* entitled "On the nature of the 'hostless' short GRBs" (Tunnicliffe et al., 2014). Any presented spectroscopy, including that for a galaxy in the field of GRB 111020A, was produced by Andrew Levan. Figure 3.8, displaying the neutron star binary offset as well as $P_{\rm chance}$ was also created by Andrew Levan. All other work presented was completed by the author. The main collaborators for this work are Andrew Levan and Nial Tanvir.

Chapter 4 was completed entirely by the author utilising some data available from the literature with references therein. The work regarding kilonova was also included, in part, in the Tanvir et al, 2013 paper entitled "A 'kilonova' associated with short-duration gamma-ray burst 130603B" published in *Nature* (Tanvir et al., 2013).

In Chapter 5 all photometric data reduction and subtraction for GRB 100816A was performed by the author and all spectroscopic analysis perfomed by Andrew Levan and Nial Tanvir. All additional analysis was performed by the author.

Abstract

So far the progenitors of short γ-ray bursts (SGRBs) have proved elusive. Their presence within both old and young environments and their bias against star-forming regions provide tantalising evidence of a neutron star binary or neutron star - black hole merger origin. Within this thesis we study an array of characteristics of the population of SGRBs focussing in particular on their host environments and afterglow properties in the optical and X-ray bands.

In particular we consider a set of SGRBs with no detectable host galaxy to deep limits and no clear host in the field from probabilistic arguments. These GRBs either represent a population at high redshift or with high offsets from low redshift hosts. Comparing the offsets of these GRBs from their potential hosts with random positions on the sky we find they are somewhat closer than expected, suggesting these GRBs are more likely to have been kicked from relatively local hosts.

We also consider the issue of classification, given suggestions that the often used two second duration divide for SGRBs may produce a sample with a high contamination from collapsar objects or potentially a suggested third class of intermediate objects. We look at a sample of optically-detected SGRBs below the nominal two second divide and go on to consider properties of a larger sample of GRBs comparing varying duration bins. From constructed optical lightcurves and SEDs, we constrain the presence of extinction, jet breaks, supernovae and kilonovae. Though there is a suggestion that such a sample would be 40% contaminated from collapsar objects we find, from supernova constraints combined with duration and spectral hardness fits from Bromberg et al. (2013) that only 22% of objects in our sample could have been collapsars.

The optical constraints placed on a kilonova (an r-process transient associated with neutron star mergers), suggest this transient is fainter than has sometimes been predicted but is consistent when considering additional opacities from the r-process material which could cause strong reddening to the infra-red.

Finally, we do not find evidence for a distinct class of intermediate GRBs, though there are likely additional progenitors which create GRB-like objects. At the intermediate duration we do find two unusual individual events not typical of LGRBs: GRBs 100816A and 060505. We find that GRB 100816A is most likely a mis-classified SGRB, from its position within its host and the constraint on any associated supernova.

Chapter 1

Introduction

1.1 History of GRB discovery

1.1.1 Discovery

The most exciting discoveries are often fortuitous. This is true across the whole range of science from the discovery of penicillin to the cosmic microwave background. This is also the case with gamma-ray bursts (GRBs) which were first detected in 1969 by the *Vela* satellites. The initial function of these satellites was military, launched to ensure compliance to the Nuclear Test Ban Treaty of 1963 by detecting any γ-rays produced from nuclear tests made in space. The presence of multiple satellites allowed a basic constraint of the direction of any detected γ-rays due to measurable time lag between multiple detections and Earth occultations. No nuclear test was ever reported, but in 1973 details of sixteen flashes of gamma-rays were published by Klebesadel et al. (1973). They were unlike previous phenomena and, from the weak directional constraint, not emerging from the Earth or the Sun. This opened up a new era of discovery with GRBs proving enigmatic but ultimately providing us with a wealth of information regarding their origins, their place in the Universe as well as details about the Universe itself.

1.1.2 Afterglow revolution

GRBs are characterised by a brief, bright flash of γ-rays with durations typically between tens of milliseconds and thousands of seconds. Initially, the brevity of these events, as well as the difficulty of focussing γ-rays, meant an accurate position could not be provided from the γ-rays alone. For methods using photon arrival times, for example, errors on locations were several degrees across (though more recent method involving using a coded mask provide positions on the order of several arcminutes).

This meant that for many years after their discovery the distance scales of GRBs could not be determined, precluding measurement of the energetics behind their production. As large samples of GRBs were collected, in particular by the *BATSE* instrument onboard the Compton Gamma-Ray Observatory (CGRO) launched in 1991, it became clear that their distribution on the sky was isotropic (Meegan et al., 1992; Briggs et al., 1996). The apparent lack of preference for the Galactic plane or centre ruled out some progenitors with a local origin but still allowed for GRBs to be extremely local ($\sim$ 100AU) (White, 1993) or present in a Galactic neutron star corona ($\sim 100 - 400$kpc, $z \lesssim 0.01$) (Lamb, 1995). However, this distribution most naturally pointed towards GRBs being extra-galactic and residing at cosmological distances ($\gtrsim$ 40Mpc, $z \gtrsim 0.01$) (Paczyński, 1995).

In most cosmological scenarios, as well as a few Galactic ones, the large energy density at the source implies that the plasma produced (e^+, e^-, γ fireball) undergoes relativistic expansion (Rees and Meszaros, 1992; Begelman et al., 1993). For extragalactic sources, without this relativistic expansion the high density of photons would create an effective high energy cutoff due to e^+-e^- pair creation at $\sim 1\,\mathrm{MeV}$, which is not seen. Because the observed photons are blue-shifted and the observed timescales are shortened pair creation is reduced since, in the comoving frame, the photons are softer and the density is decreased (Vedrenne and Atteia, 2009, pgs. 219-222). Another important consequence of this scenario, as well as creation of γ-ray emission from internal shocks, is the prediction that this fireball will produce X-ray, optical and radio afterglow emission after ploughing into the external medium (Meszaros and Rees, 1993; Meszaros et al., 1994; Meszaros and Rees, 1997). Counterpart searches in the *BATSE* era were, however, unsuccesful with searches generally occurring a few days after the initial GRB detection (e.g. Hurley et al. 1994; Frail et al. 1994), though a few searches were completed within a few hours (e.g. Schaefer et al. 1994). Nonetheless, the limits placed on this emission were still generally consistent with cosmological models where searches for counterparts needed to be initiated even more quickly in order to detect these transients.

The first afterglows were detected over 25 years after the first detection of a GRB, from rapid follow-up with the BeppoSAX satellite. BeppoSAX was equipped with both γ-ray wide field (GRB Monitor for detection and multiple Wide Field Cameras for localisation) and X-ray narrow field instruments (NFI) allowing follow-up to occur hours after the GRB detection. Detections of an accompanying X-ray transient provided enough precision for ground and space-based optical follow-up, as well as searches for radio transients, providing sub-arcsecond precision (Costa et al.,

1997; van Paradijs et al., 1997). The first GRB redshift was measured in 1997 from the host galaxy spectrum of optically-localised GRB 970508 (Metzger et al., 1997) at $z = 0.835$ (Bloom et al., 1998) (GRB 970228 was actually detected earlier but the redshift of the host galaxy was measured after that for GRB 970508; Djorgovski et al. 1999; Bloom et al. 2001). Measurements such as this for many GRBs confirmed that they were of extra-galactic origin and, in fact, can be detected out to very high redshifts.

This distance scale implies isotropic equivalent γ-ray energies of $E_{iso} \sim 10^{50} - 10^{54}$ erg. However, there is also likely significant collimation of the GRB outflow into narrow jets, with evidence seen for some GRBs (Frail et al., 2001; Bloom et al., 2003; Racusin et al., 2009). The true energy is not always possible to determine due to unknown jet opening angles but where the true energy can be measured Racusin et al. (2009) found the energy budget is clustered around $E_\gamma \sim 10^{50}$ erg, though some GRBs are sub-luminous outliers to this distribution.

This period of time, known as the "Afterglow Revolution", settled the debate about the distance scales and energetics of GRBs, provided clues about the progenitor, and paved the way for the next generation of telescopes, in particular *HETE-II*, *Swift* and, more recently, *Fermi* by providing the best strategy for consistently detecting and localising GRBs to high levels of precision. We will now go on to talk in more detail about the population of detected GRBs themselves, their properties, environment and origins as well as the physics behind their production.

1.2 Classification of GRBs

For a GRB the initial emission, primarily in γ-rays, is termed the prompt emission and, as has been discussed in section 1.1.2, this is often followed by detectable afterglow emission in the X-ray, and sometimes optical and radio bands (e.g. Gehrels et al. 2009). The spectra of both the prompt and afterglow emission is non-thermal, often best fit by a series of connected power-laws (when absorption is accounted for) though, depending on the spectral energy range, the prompt emission also has an exponential high energy cutoff.

From burst to burst the lightcurve structure of the prompt γ-ray emission is highly variable. As can be seen in Figure 1.1, some GRBs are comprised of single, simple peaks sometimes showing a fast-rise, exponential decay (FRED) profile whereas others contain multiple distinct peaks sometimes separated by quiescent periods. The emission can also contain fine structure showing anywhere from millisecond variability to thousands of seconds. Thus, classification requires some careful

consideration.

From the prompt emission, one useful quantity is the duration, often expressed as T_{90} which is the time for 90% (between 5% and 95% above the background) of the total fluence from the γ-ray emission to arrive. Fluence here is the γ-ray flux received in the detector integrated over the duration of the GRB. Along with T_{90}, the property of spectral hardness, as defined as the ratio between two γ-ray sub-channels covering different parts of the spectrum, can be used to show that there are at least two populations of objects which produce GRBs, known ostensibly as long-soft GRBs (LGRBs) and short-hard GRBs (SGRBs) (Kouveliotou et al., 1993).

However, as can be seen in Figure 1.2, though there are at least two populations in the parameter space there is clearly overlap. In addition, there are suggestions that the population could be fit by three log-normal distributions (Horváth, 1998; Řípa et al., 2009; Huja et al., 2009; Horváth et al., 2010) introducing a third intermediate class between the original two. Based on the original BATSE data a basic split between SGRBs and LGRBs was formed at $T_{90} = 2\,\mathrm{s}$ (Kouveliotou et al., 1993), within an energy range of $50 - 300\,\mathrm{keV}$. The measured duration of GRBs is dependant on the spectral band being sampled. Figure 1.2 also shows the population of GRBs detected by the *Swift*/BAT instrument which has a softer spectral energy band of $15 - 150\,\mathrm{keV}$ than BATSE. This means that, even though this split is still often used, it is not necessarily appropriate with Bromberg et al. (2013) suggesting a value of $T_{90} = 0.80\,\mathrm{s}$ should be used instead. In addition, some "short" GRBs are composed of a short initial spike of hard γ-rays followed by a period of softer extended emission (Norris and Bonnell, 2006). In these cases, it may be best to separate the spectrally distinct parts of the emission and to look only at the duration of the initial, hard pulse (Norris et al., 2010b).

It is clear that classification simply based on the duration and spectral properties, though useful, has its problems. It is also useful to consider other properties associated with the GRB such as its environment, energy and any associated supernova signature (e.g. Zhang et al. 2009).

1.3 Host galaxies and associated supernova

Studying the host galaxies and environments of both the long and short populations of GRBs provides information about the types of progenitor systems which formed them. For LGRBs, their host environment clearly shows a strong link with massive stars. Their host galaxies are blue, low metallicity, actively star-forming dwarf

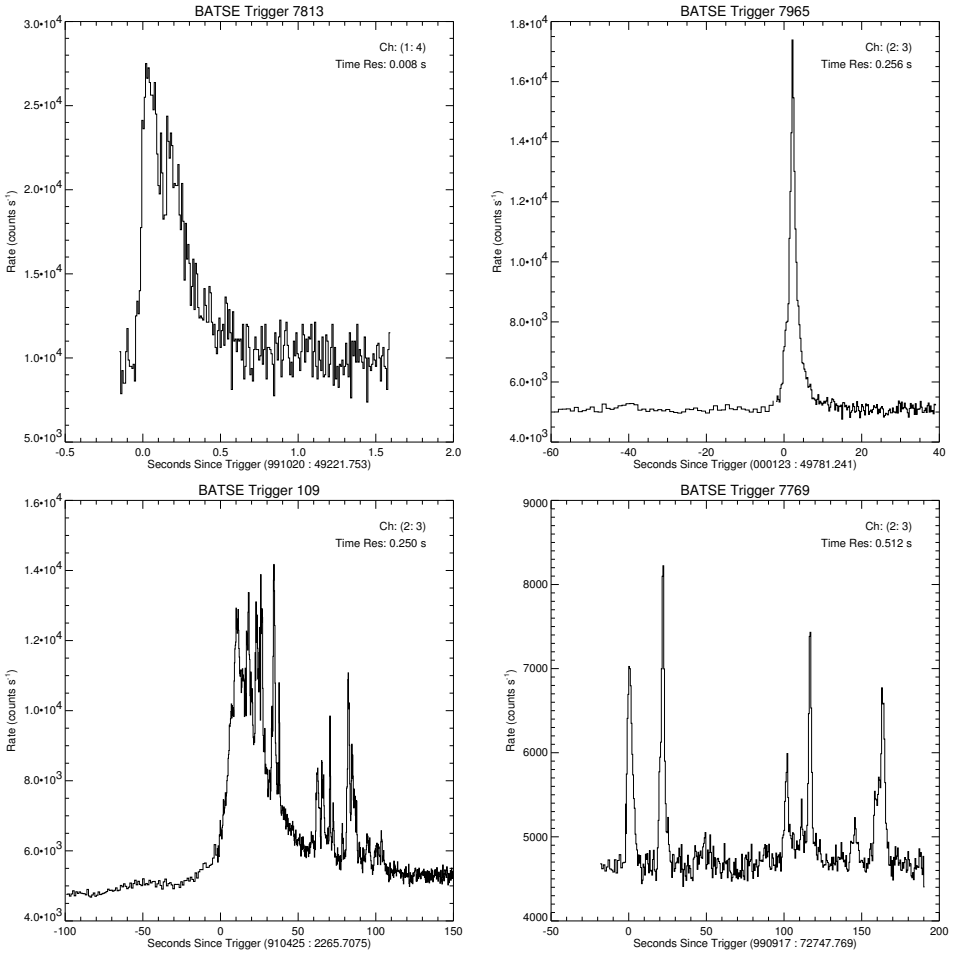

Figure 1.1: *BATSE* GRB lightcurves in energy range $50 - 300\,\mathrm{keV}$. The top two panels show GRBs which display a single peak: on the left is a (short) GRB with a fast-rise, exponential decay (FRED) profile and on the right a simple peak. The bottom left hand panel shows a GRB with multiple peaks and fast variability and the bottom right a GRB with multiple peaks separated by quiescent, or at least low level emission, periods. GRBs occur over a range of different timescales covering a range in these examples from 0.6 to just under 200 s. All BATSE lightcurves shown here have been taken from http://www.batse.msfc.nasa.gov/batse/grb/lightcurve/

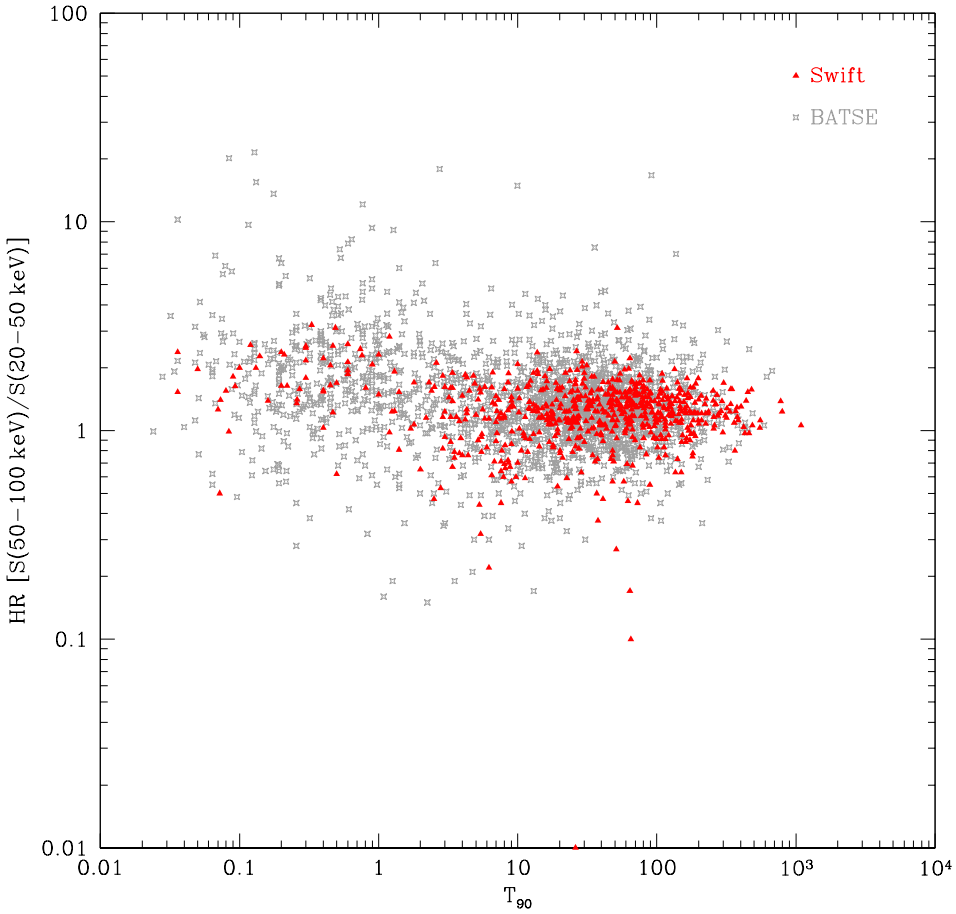

Figure 1.2: T_{90} vs Hardness Ratio for *BATSE* (grey starred points) and *Swift* (red triangles). The Hardness Ratio (HR) is taken as the ratio between the fluence in the $50-100$ keV channel and the $20-50$ keV channel. Within the population of GRBs there are at least two overlapping classes: one with a shorter duration and harder spectrum and the other, larger population with a long duration and softer spectrum.

galaxies with masses consistent with the LMC (covering a range $10^{8.5} - 10^{10.3} M_{\odot}$) but with much higher star formation rates (median$\sim 2.5 M_{\odot}\,\mathrm{yr}^{-1}$) (Savaglio et al., 2009; Fan et al., 2010; Levesque et al., 2010b). In addition, LGRBs lie within the brightest regions of their host galaxies (Fruchter et al., 2006; Svensson et al., 2010) placing them within these star-forming regions.

The most convincing link between LGRBs and massive stars is their association with supernova. SN 1998bw, the first supernova associated with a GRB, was a luminous Type Ic event pointing to a hydrogen-deficient core-collapse supernova (Galama et al., 1998; Patat et al., 2001), measurable because of its low redshift. Following this discovery, associated supernova have been detected for a number of local LGRBs (e.g. Hjorth et al. 2003; Stanek et al. 2003; Malesani et al. 2004; Bersier et al. 2006; Pian et al. 2006; Campana et al. 2006; Starling et al. 2011; Melandri et al. 2012) though there are also two notable examples of robust non-detections (GRBs 060614 & 060505) where the lack of a supernova is constrained down to deep limits (Fynbo et al., 2006; Gal-Yam et al., 2006; Della Valle et al., 2006).

SGRBs are found in much more varied environments, within host galaxies both with and without active star formation. Fong et al. (2013) found for a sample of 36 SGRBs with strongly associated host galaxies, of these hosts 47% were late-type whereas only 17% were found in early-type hosts with some notable examples being: GRBs 050509B, 050724, 100117A & 100625A (Gehrels et al., 2005; Bloom et al., 2006; Berger et al., 2005; Fong et al., 2011b, 2013). The remaining GRBs in the sample had host galaxies of inconclusive type or were not firmly associated with any one host. Even accounting for the unidentified hosts, this observed early-to-late type ratio shows there is a tendency for SGRBs to be found in star-forming galaxies perhaps suggesting the SGRB rate traces not only stellar mass but also star formation (Fong et al., 2013). Comparing the late-type host galaxies of SGRBs to LGRBs, they are typically more massive ($\sim 10^{9.5} - 10^{12.1}\,M_{\odot}$ when considering maximum possible masses), higher metallicity ($Z \sim 0.6 - 1.6 Z_{\odot}$) and have lower specific star formation rates (star formation rate per unit mass, $SFR = 0.2 - 6 M_{\odot}\,\mathrm{yr}^{-1}$) (Berger, 2009; Leibler and Berger, 2010). Hence, even when only considering the host galaxies with active star formation, the SGRB and LGRB host galaxies are not drawn from the same underlying distribution (Leibler and Berger, 2010).

Within their host galaxies, unlike LGRBs, SGRBs are often found in faint regions and do not appear to directly trace star-formation (Fong et al., 2010). SGRBs are also found with greater offsets from their host galaxies (for well-localised SGRBs with known redshifts ~ 6 kpc on average) with some lying in the outskirts or outside the host altogether (Cenko et al., 2008; Rowlinson et al., 2010a; McBreen et al.,

2010). As has been mentioned, there is also a population of well-localised SGRBs which have no host galaxy detection down to deep limits and cannot be associated with any one galaxy in the field, termed "hostless" GRBs (Berger, 2010; Tunnicliffe et al., 2014). In Chapter 3, we discuss the likelihood that these GRBs are highly offset from galaxies at low redshift ($z < 1$), finding that this is the preferred explanation, over these GRBs residing within hosts at high redshift. Overall, for these GRBs the potential host galaxies in the field have typical offsets > 30 kpc where the galaxy redshift is known.

For LGRBs the detection of supernova provides proof of massive star association but for SGRBs the lack of a detected supernova and strong constraints in some cases is also particularly telling. In Chapter 4, we find a bright hypernova event such as SN 1998bw is ruled out in seven out of the nine GRBs with confirmed redshift.

It is clear that the population of detected GRBs is comprised of at least two, possibly more, unique channels. Two sets of progenitors capable of producing GRBs with large enough event rates and luminosities to be detectable are mergers of compact objects (double neutron star, or black hole - neutron star mergers) and rapidly spinning, hydrogen-stripped massive stars. These models are linked with SGRBs and LGRBs respectively. Since this thesis is largely concerned with SGRBs and their most likely progenitors, it is relevant to consider the creation, evolution and eventual merger of neutron star and neutron star - black hole binaries. In addition, due to potential contamination within the SGRB sample from LGRBs we also consider their creation and properties.

1.4 Neutron star binary and neutron star - black hole mergers

SGRBs are characterised by both their duration and their spectral properties. Their isotropic equivalent energies are of the order $E_{iso} \sim 10^{50}$ erg, lower than for their long counterparts ($E_{iso} \sim 10^{53}$ erg) (e.g. Amati 2006). Neutron star - neutron star (NS-NS) and neutron star - black hole (NS-BH) mergers were first suggested as a possible progenitor for GRBs by Paczyński (1986). The energy of the outflow produced, their presence in ageing populations and their potentially high space velocities make them good candidates for SGRBs. We outline the main features of these systems and their merger below.

1.4.1 Formation and evolution via primordial channel

Formation

There are several possible routes to create NS-NS and NS-BH binaries. The main formation channel begins with two massive progenitors in a binary pair (the primordial channel). The potential well of any set of binary objects can be described by the Roche potential (figures 1.3 and 1.4 show a rough approximation of the typical shape of this potential surface). This is the combination of the centrifugal and gravitational forces within the binary. The shape of the Roche potential is entirely determined by the binary mass ratio, q. There are five points in this potential with no net force, known as the Lagrange points, the most important of which lies between the two bodies and is termed L_1. The equipotential surfaces which pass through this point and around the stars are known as the Roche lobes (Paczyński, 1971). If a body expands to fill its Roche lobe mass transfer can occur through the L_1 point and spill onto the companion star (Kuiper, 1941).

In the binary system considered, the more massive star of the two (the primary star) is the first to evolve off the main sequence. It fills its Roche lobe beginning mass transfer onto its companion. Due to the relatively equal mass of the two bodies this mass transfer should be dynamically stable (Paczyński, 1971). As the primary star loses its hydrogen envelope it forms a helium star.

The initial mass of the primary determines the remnant produced when this star undergoes core collapse. If the main sequence mass of the star was $8\,M_\odot < M_p < 20 - 25\,M_\odot$ then the helium star will subsequently explode as a supernova leaving behind a neutron star remnant (New, 2003). For initial masses $M > 20 - 25\,M_\odot$ a black hole remnant can be formed. In the range $25\,M_\odot < M_p < 40\,M_\odot$ a supernova will still occur but this will be weak with $\sim 2\,M_\odot$ of material falling back onto the newly created neutron star, causing collapse to a black hole (New, 2003). For more massive stars with initial masses $> 40\,M_\odot$ no supernova occurs and a black hole will be formed by direct collapse (Fryer, 1999). Any supernova that does occur will impart a kick to the system both as a natural consequence of the anisotropy of the explosion in the rest frame of the binary and from any intrinsic anisotropy of the supernova itself. Providing the system remains bound this will provide a space velocity perhaps of $\sim 250 - 300\,\mathrm{km\,s^{-1}}$ on average (Bloom et al., 1999) (but also see the following sub-section).

When the secondary star evolves off the main sequence, as was the case with the primary before, it fills its Roche Lobe starting another mass transfer episode. However, due to the large discrepancy between the mass of the donor ($\sim 8 - 15 M_\odot$)

and the mass of the accretor ($M_{NS} \sim 1.4-3M_{\odot}$; $M_{BH} \gtrsim 3M_{\odot}$) the mass transfer is dynamically unstable (Belczynski et al., 2006), causing the Roche Lobe of the donor star to shrink. This causes a runaway effect where the mass transfer rate becomes so large the compact object cannot accrete the incoming matter (Belczynski et al., 2006). This causes a common envelope phase to occur where the matter surrounds the Roche Lobes of both stars in the binary (Kuiper, 1941).

This envelope of matter provides a drag on both objects, extracting orbital angular momentum and tightening the orbit of the binary. Eventually the envelope is ejected via the released orbital energy and the emerging system is a close binary consisting of the first compact object and a helium star (Fryer et al., 1999a). If the helium star does not fill its Roche lobe, it also explodes as a supernova imparting another kick to the system. The NS-NS or NS-BH system produced from this evolution has both a random space velocity and relatively tight orbit. This sequence of evolution to form both NS-NS and NS-BH binaries are shown in Figures 1.3 and 1.4.

In addition to the channel outlined above, it is also possible a population of highly compact binary systems could be produced. Before the supernova occurs, if the second helium star does fill its Roche Lobe, then a third period of mass transfer may be initiated, decreasing the orbital separation further (Belczyński and Kalogera, 2001; Belczynski et al., 2006). Only after this further tightening of the orbit does the helium star produce a supernova, forming the second compact object. It is unclear what fraction of binary systems will follow this channel to produce systems with these smaller orbital separations. However, some contribution of these shorter-lived binary systems could explain the preference for star-forming over elliptical host galaxies seen in the SGRB population discussed in section 1.3.

Evolution

The merger of the binary system will eventually occur after enough angular momentum has been lost via gravitational wave radiation. This depends on the orbital separation, a, such that:

$$\frac{da}{dt} \propto a^4 \tag{1.1}$$

(Peters, 1964). Hence, there will be a delay between the creation of the compact object binary and the eventual merger. Clearly, the length of this delay is strongly dependant on the initial orbital separation of the binary system after the final phase of common envelope evolution. For many of these systems this delay can be on the order of $10^7 - 10^{10}$ yrs (Bloom et al., 1999; Fryer et al., 1999a; Belczynski et al.,

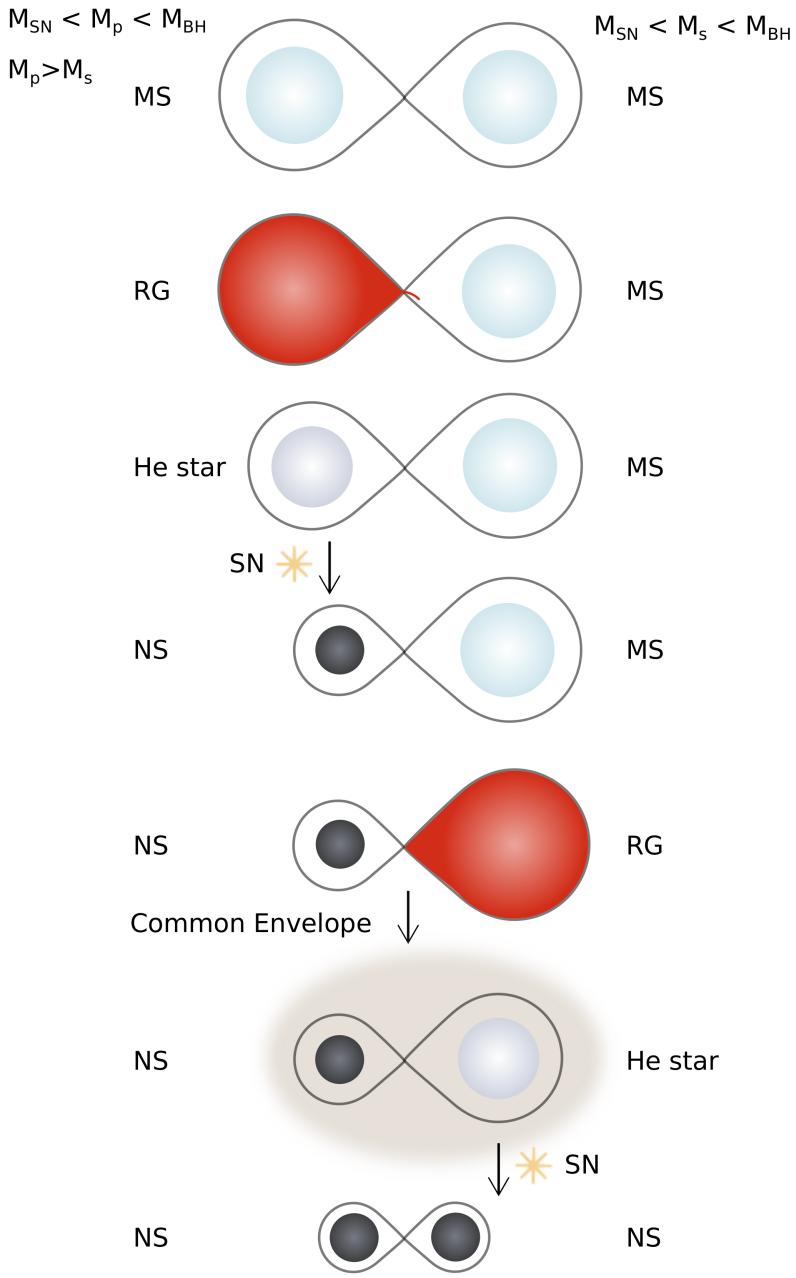

Figure 1.3: Evolution of two main sequence stars both with $8\,M_\odot \lesssim M \lesssim 25\,M_\odot$. The primary star with the larger mass (M_p) evolves off the main sequence first filling its Roche lobe and eventually producing a supernova with a neutron star remnant. When the secondary star evolves this causes a period of common envelope evolution decreasing the orbital separation. The common envelope is eventually ejected. The secondary star then explodes as a supernova creating a second neutron star leaving a close neutron star binary system. See also Fryer et al. (1999a)

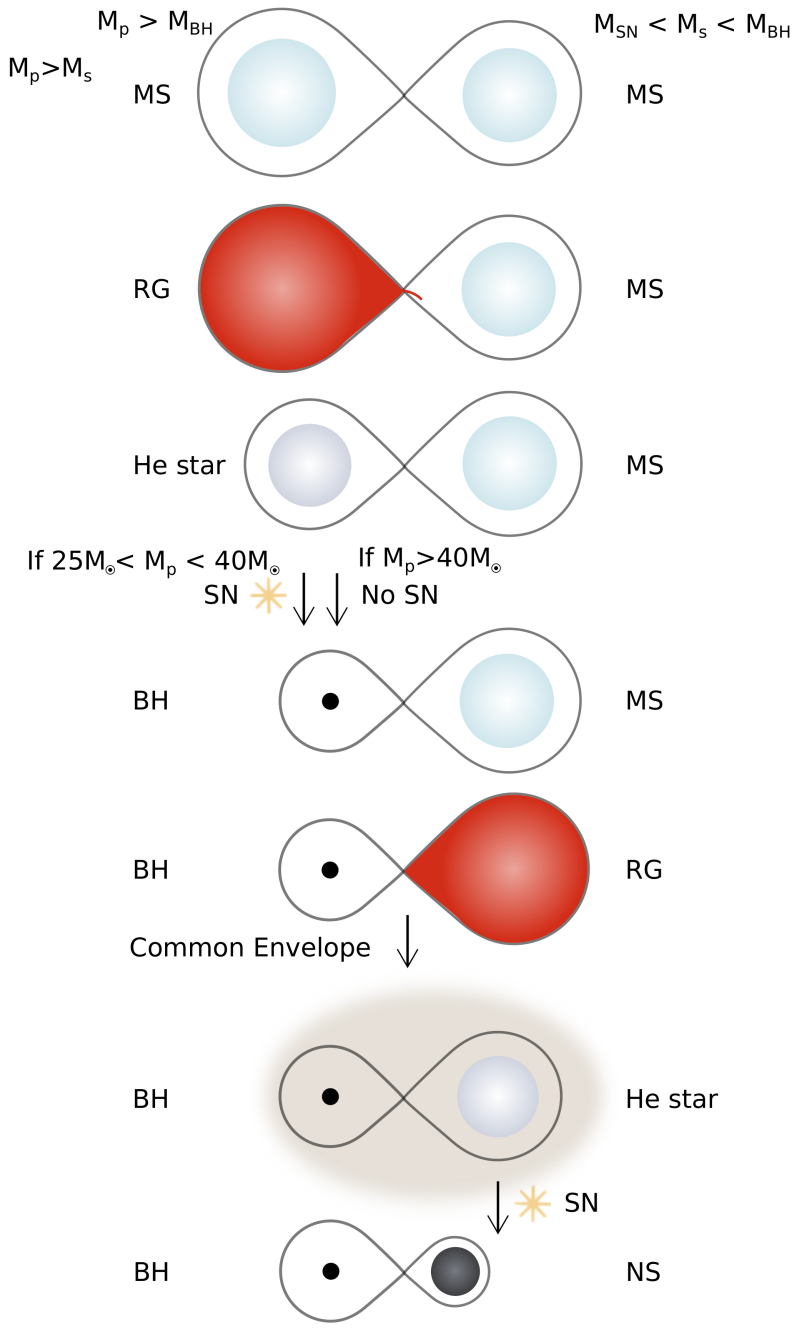

Figure 1.4: Evolution of two main sequence stars of differing initial masses: $M_p \gtrsim 25\,M_\odot$ and $8\,M_\odot \lesssim M_s \lesssim 25\,M_\odot$. As for the neutron star evolution shown in Figure 1.3, the primary star evolves off the main sequence first filling its Roche lobe. A supernova is produced only if the initial mass was $\lesssim 40\,M_\odot$, creating a black hole from fallback of material onto the neutron star remnant produced, otherwise the star collapses directly to a black hole. The secondary star, following the same sequence of evolution as in Figure 1.3, fills its Roche lobe causing a period of common envelope evolution resulting in a decreased orbital separation. After the common envelope is ejected, the secondary star explodes as a supernova, leaving a neutron star remnant. This leaves a neutron star -black hole binary system with a relatively tight orbit. See also Fryer et al. (1999a)

2006). Note, however, that for the systems which have undergone a second common envelope stage resulting in smaller orbital separations (Belczynski et al., 2006) this delay time would be significantly reduced with merger times of the order $10^3 - 10^6$ yrs.

For these binary systems the kicks imparted by each of the supernovae at the time of the neutron stars or black hole being formed give the system a potentially high space velocity. For neutron star binaries, based on the comparison between measured pulsar velocities and population synthesis, the distribution of the kicks is thought to be either bimodal or Maxwellian with the mean velocity around $\sim 250 - 300\,\mathrm{km\,s^{-1}}$ in two dimensions (Hansen and Phinney, 1997; Bloom et al., 1999; Hobbs et al., 2005). For the bimodal distribution the two peaks occur at $\sim 100\,\mathrm{km\,s^{-1}}$ and $\sim 600\,\mathrm{km, s^{-1}}$ with dispersions of $\sim 50\,\mathrm{km\,s^{-1}}$ and $\sim 150\,\mathrm{km\,s^{-1}}$ respectively (Fryer and Kalogera 1997; Fryer et al. 1999a; see also Arzoumanian et al. 2002). These measured kick distributions indicate that at least some proportion of the NS population has high space velocities. Overall, a bimodal kick distribution provides larger kicks on average compared with the Maxwellian values and this is a source of uncertainty when considering the spatial distribution of the binary systems at the point of merger (Church et al., 2011).

For an NS-NS system, two kicks will be imparted producing a random velocity overall. For the NS-BH systems, though those black holes formed from accretion-induced collapse of a neutron star will still receive a kick, it is possible that no kick will be imparted to a black hole formed from direct collapse, though this still under debate (e.g. Repetto et al. 2012). However, Church et al. (2011) claim that even omitting a black hole kick does not strongly affect the space velocity distribution for NS-BH binaries compared with NS-NS binaries since the properties are insensitive to the natal kick from the first supernova. The magnitude of the imparted kicks, and the resultant overall kick, is important for the location of the merger with respect to its host galaxy.

Both the merger time and the magnitude and direction of the received SN kicks influence the spatial distribution of the binary systems when they merge. For a significant delay combined with a potentially high space velocity it is expected that these systems will travel far from their original birth site before merging with the overall distance also dependant on the mass of the host galaxies themselves. Figure 1.5, adapted from Belczynski et al. (2006), shows the positions of the binary systems from population synthesis with respect to three different host galaxy types with high and low masses. For low mass galaxies in particular, it may be expected that binary mergers could be found over $> 30\,\mathrm{kpc}$ from their host centre for a non-negligible fraction of events (Bloom et al., 1999). We should note that any highly

compact systems would merge before travelling far from their birth site, though it is unlikely that this will account for a large proportion of the population.

This spatial distribution is consistent with what has been seen for SGRBs (Church et al., 2011). The presence of SGRBs in a variety of hosts is indicative of an old progenitor and, in addition, the lack of SGRBs found in star-forming regions combined with their sometimes high offsets from their hosts is consistent with the progenitor systems being kicked. For the "hostless" GRB population, if they are at high offset from a low redshift host then this is consistent with the distribution shown in Figure 1.5 where some NS-NS or NS-BH binaries should be found at high offsets from their host galaxies, to the point where it would no longer be possible to associate the SGRB with the host galaxy.

1.4.2 Formation and evolution via dynamical channel

An alternative formation channel for these binary systems is through dynamical interactions within globular clusters. This can occur through three (or more) body interactions where an existing compact binary, most likely a low mass X-ray binary containing a high mass compact object and a low mass main sequence companion, exchanges its lower mass companion for another compact object (Grindlay et al., 2006). In globular clusters, overall, the more massive stars slow down and amass in the cluster's core whereas the less massive stars speed up and spend more time in the cluster's outer regions (Davies, 1995). This is known as mass segregation. Because of the migration of the lower mass stars, through interactions, the loss in kinetic energy from the core can cause these clusters to undergo core collapse, causing the core to contract (Ashman and Zepf, 2008, pg. 29). The cores of these post-core-collapse globular clusters are thus very dense environments and so have more chance of creating these dynamically formed binaries.

Globular clusters are generally found out to $\sim 40\,\mathrm{kpc}$ from their host galaxies (Harris, 1996). Though no SGRBs have been found explicitly within globular clusters, this channel of NS-NS and NS-BH binary creation could account for some SGRBs seen at high offset (Salvaterra et al., 2008). However, the rate of these binary mergers is such that they could not account for all SGRBs observed (Grindlay et al., 2006; Salvaterra et al., 2008, 2010).

1.4.3 Merger and Jet Creation

When the binary system reaches the point of coalescence, the end point capable of producing a GRB will be a black hole surrounded by a hot torus of material. The

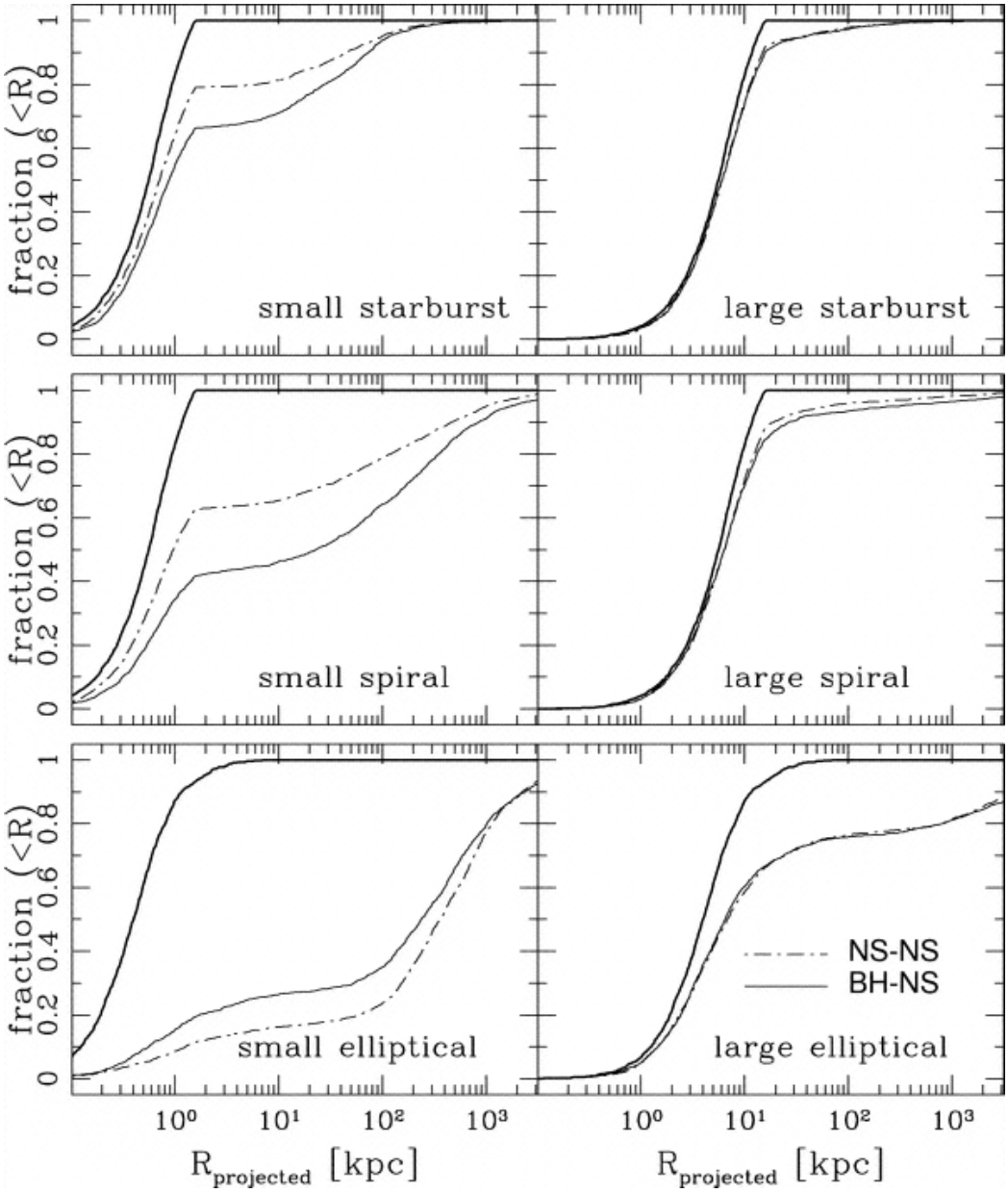

Figure 1.5: The distribution of NS-NS and NS-BH systems within their host galaxies, adapted from Belczynski et al. (2006). The solid thick black line shows the positions of the systems when they are initially created and the dot dash and thin lines show the positions of the NS-NS and NS-BH systems, respectively, when they merge. This distribution for low and high mass starburst, spiral and elliptical galaxies are shown. For low mass galaxies and elliptical galaxies, there is clearly a strong divergence between the initial and final positions for these systems. This distribution is also conservative as it contains a significant contribution from the ultra compact binary systems (differing for different host galaxies) though the proportion of these systems within the population is not well known.

main reservoirs of energy for launching the jets which create the GRB would be the binding energy of the disc and the spin energy of the black hole.

For an NS-NS binary the merger itself occurs very quickly, with two objects of roughly equal mass becoming a single object within 2 ms. As the two neutron stars merge they shed mass into spiral arms which then wrap around the central object to form a hot torus (Price and Rosswog, 2006). In some cases, though the total mass of this object exceeds that for a black hole (for a uniformly rotating object; Baumgarte et al. 2000), the differential rotation means it can be supported as a hypermassive neutron star (HMNS) for up to or perhaps beyond 50 ms (Shibata and Taniguchi, 2006). The HMNS collapses to a black hole after the angular momentum has been dissipated either by gravitational radiation or by magnetic effects such as magnetic braking, where any outgoing wind coupled to the magnetic field causes a drag extracting angular momentum. The delayed creation of the black hole over direct collapse can produce greater disc masses, and thus with a larger energy reservoir, these systems are more likely be able to create GRBs (Shibata and Taniguchi, 2006).

For an NS-BH merger, the ability of this system to launch relativistic jets is dependant on the tidal disruption of the neutron star. If the merger occurs directly, no accretion structure can be formed with any stripped matter falling directly into the black hole. The presence of tidal disruption, and a suitable disc mass, is sensitive to the mass ratio of the binary system as well as the spin of the neutron star (Rosswog et al., 2004). If the black hole is large enough (mass ratio $\lesssim 0.24$) this tidal disruption can occur within the black hole's innermost stable circular orbit (ISCO) in which case, though almost all of the mass will be within this radius, redistribution of the angular momentum can create spiral arms with enough matter outside the ISCO to form a disc (Faber et al., 2006). In addition, a neutron star without spin has a greater chance of forming a disc outside of the Schwarzchild radius (event horizon) (Rosswog et al., 2004).

A e^+- e^- γ fireball can be produced by the compressional heating and dissipation associated with accretion of matter from the disc onto the central object. The driving force leading to relativistic expansion may be due to the generation of large magnetic fields or by annihilation of $\nu\bar{\nu}$ (producing e^+e^- pairs) in the polar regions (Rosswog et al., 2003).

The energy deposited in the poles from $\nu\bar{\nu}$ annihilation is dependant on the neutrino luminosity generated by the hot torus surrounding the central object. For NS-NS systems this is around $E_{\nu\bar{\nu}} \sim 10^{50}$ erg with comparable values for NS-BH systems (Vedrenne and Atteia, 2009, pg. 451). This is consistent with the energies

seen for SGRBs.

There are various dynamo mechanisms suggested for the generation of the relativistic jets from strong magnetic fields (Thompson and Duncan, 1993; Kluźniak and Ruderman, 1998; Balbus and Hawley, 1998; Balbus, 2003), which would need to be of the order of 10^{15} G (Price and Rosswog, 2006). Fields of this magnitude could provide enough energy to power a GRB. Preceeding any dynamo action, Price and Rosswog (2006) suggested that the magnetic field could be amplified to this level from seed fields of 10^{12} G at the interface between the two neutron stars at merger. The shear between the two fluids can produce Kelvin-Helmholtz instabilities causing vortex rolls and amplifying the magnetic fields. Blobs of matter within the high field can float to the surface and break out producing a relativistic blastwave. Magnetic interactions between the infalling material and the spinning BH via the Blandford-Znajek process (magnetic fields threading the BH and extracting spin energy) (Blandford and Znajek, 1977) can also extract the magnetic energy and power the relativistic jet.

One factor, however, that must be considered when calculating the energies available in these systems to launch the relativistic jet is the level of baryon contamination in the polar regions. Initially after the merger the region along the rotation axis of the BH is clean of baryons due to the huge centrifugal forces (Vedrenne and Atteia, 2009, pg. 421). Any magnetic break out can also work to keep the region clean from baryons due to magnetic pressure. However, there is also a strong baryonic wind driven by the neutrino flux which could cause baryon pollution (Price and Rosswog, 2006). Hence, complex interactions between these two processes determine the outcome of the merger and whether or not this would prevent the launching of the jet.

Overall, potentially both NS-NS and NS-BH binary mergers are viable possibilities for the progenitors of SGRBs both in terms of energies and duration.

1.4.4 Associated sub-relativistic explosion: Kilonova

As well as the emission produced within the relativistic jets, radioactive material synthesised either within a tidal tail from the merger itself or within an outflow driven by the accretion disc can also produce emission (Li and Paczyński, 1998; Kulkarni, 2005; Metzger et al., 2008, 2010; Roberts et al., 2011). This type of transient accompanying a merger event is often referred to as a "kilonova".

The neutrino-driven outflow in the accretion disc can be produced at large radii, where the disc is thin and efficiently neutrino-cooled. The primary neutrino heating and cooling processes are due to neutrino and e^+- e^- pair capture onto

baryons respectively (Metzger et al., 2008). At a given height above the disc the temperature decreases and given the strong dependence of the neutrino cooling process on temperature ($\propto T^6$) there is a net heating and it is this heating which can drive the outflow (Metzger et al., 2008).

Both these non-relativistic outflows, the tidal tail and the disc wind, are dense enough to synthesise heavy isotopes. However the composition is neutron rich, though the electron fraction, Y_e ($Y_e = X_p/(X_n + X_p)$ and X_p and X_n are the proton and neutron mass fractions) is higher for the wind ($Y_e \sim 0.1 - 0.4$) than for the tidal tail ($Y_e \sim 0.03 - 0.1$) (Metzger et al., 2010). This means that little ^{56}Ni, the radioactive decay of which powers supernova, will be synthesised and instead an optical transient would be powered mainly by heavy elements produced by the r-process (rapid neutron capture). The r-process can only occur when the half-life of β-decay is long compared with the timescale for neutron capture with many successive neutron captures producing neutron-rich heavy isotopes (proton number, $N_P > 58$). Fission and β-decay of these heavy nuclei can produce radioactive heating which can power a transient (Metzger et al., 2010). Overall, the transient will most likely be powered by some combination of material produced within the disc wind and the tidal tail.

A transient powered by r-process material is likely to be fainter, shorter lived and peaking earlier than seen for normal supernova lightcurves, occurring on times scales of hours-days. Kasen et al. (2013) also consider the effect of opacity from the r-process elements, in particular the lanthanides ($58 < N_P < 70$) but taking Neodynium (Nd) as representative, where line blanketing in the optical can both redden the transient and extend its duration, making it dimmer at peak (Barnes and Kasen, 2013). This additional opacity is due to the complex valence structures of some rare elements produced in the r-process as well as a heterogeneous mixture of many elements with distinct lines (Kasen et al., 2013).

In chapter 4, we search for evidence of kilonovae within the optical lightcurves of SGRBs. When a high opacity is not considered, with ejecta masses $10^{-2}\,\mathrm{M}_\odot$ and velocities around $v \sim 0.1\,c$ the lightcurve would peak on timescales of ~ 1 day with $M_V \sim -15$ (Metzger et al., 2010). Within the SGRB lightcurves, there is at least one case where the presence of a kilonova is constrained at this optical brightness. With the current crude approximation of the higher opacity from r-process elements from Barnes and Kasen (2013), for the same ejecta mass and velocity parameters, find the peak time is on the order of ~ 1 week with peak magnitude in the R and B bands of $M_R \sim -13$ and $M_B \sim -11$ and with a more luminous peak in the infrared $M_H \sim -16$. These values are more consistent with what is seen in the SGRB

population and, in fact, a very red transient not seen in the optical lightcurve has been recently associated with a short GRB (Tanvir et al., 2013), indicative of this reddened kilonova.

1.5 GRBs from stellar collapse

The most often discussed model for the creation of LGRBs is that of the collapsar which involves the collapse of a hydrogen-stripped massive star into a black hole. More recently, however, there has also been much discussion of the protomagnetar model where the type of progenitor star collapses but rather than forming a black hole forms a rapidly-rotating magnetar (e.g. Metzger et al. 2011).

The overlap in duration space between short and long GRB populations (for example see Figure 1.2) makes it necessary to consider the progenitors of long GRBs as well as short if we are to disentangle the populations. Bromberg et al. (2013), for instance, have recently suggested, considering a pure LGRB collapsar sample, that up to 40% of an SGRB sample defined by the often-used two second divide could be comprised of collapsars (Bromberg et al., 2013). In chapters 4 and 5 we place constraints on the potential number of collapsar objects which could be within such an SGRB sample.

We discuss here the creation and properties of collapsars and protomagnetars, in particular their association with supernovae, to provide background for discussions later in this thesis. The collapsar model as a progenitor for LGRBs was first proposed by Woosley (1993) and the protomagnetar model by Usov (1992) and both are outlined below.

1.5.1 Collapsars

Formation and collapse

The collapsar model involves the collapse of a hydrogen-stripped massive star into a black hole. A large angular momentum in the system is also required to produce an accretion disc. Thus, the end point of a black hole with an accretion disc is very similar to the end product of the compact object mergers discussed in section 1.4.3.

A massive single star, during the course of its evolution, can lose its hydrogen envelope due to strong stellar winds. These winds are driven by radiation pressure from metal lines in the photosphere of the star (Chiosi and Maeder, 1986). The hydrogen-stripped star remaining is called a Wolf-Rayet star (Chiosi and Maeder, 1986). As a GRB progenitor, the loss of this envelope is important as it allows the

jet created to break out from the stellar surface. Too much baryonic matter and the jet would be quenched before it emerged. The star's initial mass determines whether it will collapse to form a black hole directly (Type I collapsar, $\gtrsim 40 M_{\odot}$) or whether the black hole will be formed by fallback of material onto a neutron star (Type II collapsar, $20 - 40 M_{\odot}$) (see MacFadyen et al. 2001). In order to form the accretion disc the collapsing star must have enough angular momentum to stop the material falling directly into the black hole (Fryer et al., 1999a).

Another way to form a collapsar is through a binary system comprised of a massive star, as before, and a smaller main sequence companion. In close binaries, when the primary star evolves off the main sequence, filling its Roche lobe, the subsequent common envelope evolution could strip its hydrogen envelope. After the common envelope has been expelled the helium core can collapse to a black hole with an accretion disc as before. Alternatively, two stars of comparable mass could evolve off the main sequence at the same time forming two helium stars and merging during the common envelope phase to form a massive helium core. The collapse of this core could, again, form a black hole (Fryer et al. 1999a; see also Fryer and Heger 2005).

Initially after the black hole has been formed the accretion rate is very high (MacFadyen and Woosley, 1999). This develops a favourable geometry for jet outflow. After several seconds the jet can be generated either by neutrino annihilation or MHD processes. The energy available for neutrino annihilation is typically greater than was seen for binary star mergers, on the order of $E_{\nu\bar{\nu}} \sim 1 - 14 \times 10^{50}$ erg (MacFadyen and Woosley, 1999). Since the black hole is at the centre of a core collapse event, the jet must also penetrate the stellar envelope causing a delay from jet creation to detection as a GRB (Woosley, 1993). This may place a lower limit on the duration a collapsar.

1.5.2 Proto-Magnetar Model

For the same initial Wolf-Rayet star progenitor, an alternative end state which could power a GRB would be a rapidly-rotating magnetar. When collapse of the star occurs, if the rotational energy of the proto-neutron star core exceeds the binding energy of the stellar envelope then, in principle, a neutron star remnant could be produced rather than a black hole (Dessart et al., 2008; Metzger et al., 2011; Dessart et al., 2012). Even for the more massive stars ($\gtrsim 40 M_{\odot}$), in this case enough material becomes unbound for fallback of material onto the core not to be sufficient to trigger collapse to a black hole. In addition, differential rotation within the neutron star can enhance initially weak magnetic fields to values up to $\sim 10^{15}$ G through various

magnetic effects including the magneto rotational instability and magnetic braking (Wheeler et al., 2000; Dessart et al., 2008)

Neutrinos heat the surface of the magnetar driving a wind. This wind is initially non-relativistic but as the proto-NS cools the magnetisation increases causing the wind to become relativistic (Metzger et al., 2011). Although the wind emission may be isotropic, collimation into a bipolar jet can occur by interaction of the wind from the magnetar with the surrounding star (Bucciantini et al., 2008). After $\sim 10\,\mathrm{s}$ the jet can break out of the stellar surface and produce the emission we see as a GRB.

As for the collapsar and binary merger models, this GRB emission can be powered by the fireball model (discussed in Section 1.6). However, it is also possible that the prompt and some part of the afterglow emission could be produced by magnetic dissipation i.e. dissipation of the jet's Poynting flux above the photosphere (Metzger et al., 2011). This depostion of energy can both accelerate the jet and increase the internal energy of the flow resulting in emission. Inverse Compton scattering of photons within the flow as well as synchrotron emission from the accelerated electrons could produce the power-law emission spectrum observed for GRBs (Metzger et al., 2011).

A maximum duration limit of $\sim 30 - 100\,\mathrm{s}$ could also potentially be set for GRBs driven by this mechanism. At this point the magnetisation becomes too large for the magnetic dissipation to continue to be effective, ending the prompt GRB phase (Metzger et al., 2011).

1.5.3 Associated supernova

In addition to the GRB, MacFadyen and Woosley (1999) also predicted that LGRBs should be associated with Type Ibc supernova (i.e. core collapse supernova with no hydrogen lines). Type II collapsars produce a weak supernova when the iron core collapses to a neutron star before delayed black hole formation but Type I collapsars directly collapse to a black hole with no associated supernova (MacFadyen et al., 2001). For the proto-magnetar model a supernova would naturally occur upon core collapse either powered by neutrinos or by a combination with magneto-rotational effects (Metzger et al., 2011).

A supernova can also be created from radioactive material generated after the black hole creation either from jet interaction with the stellar envelope or from a non-relativistic ($v \sim 0.1c$) viscosity-driven disc wind (MacFadyen and Woosley, 1999). The jet can displace the stellar material and the deposited energy can cause explosive nucleosynthesis. The composition of this and the disc wind is roughly equal

protons and neutrons (electron fraction $Y_e \sim 0.5$) meaning the right conditions exist to synthesise ^{56}Ni (Woosley and Bloom, 2006).

For detected supernovae associated with LGRBs the mass of synthesised ^{56}Ni measured is $\sim 0.5\,M_\odot$ (Iwamoto et al., 1998; Woosley et al., 1999; Lipkin et al., 2004; Soderberg et al., 2006b). This mass is on the upper end of that seen for Type Ibc supernova ($0.2 - 0.5\,M_\odot$) (Drout et al., 2011). SN 1998bw is normally used as an example of a canonical GRB-SN and Cano (2013) find that, on average, the bolometric luminosity of GRB-associated SN is consistent with this supernova (with scatter of $0.5 \times L_{\rm SN1998bw}$ where $L_{\rm SN1998bw} \sim 4 \times 10^{42}\,{\rm erg\,s^{-1}}$ at peak).

Since we would expect collapsars to be associated with these typically bright supernovae, constraints on the presence of a supernova in the lightcurve of an SGRB could provide strong evidence for its origin as a non-collapsar object. In chapter 4, the presence of supernovae within the lightcurves for a sample of SGRBs is constrained, and along with measures of the duration and hardness, can be used as a measure of the level collapsar contamination within a typical SGRB sample.

1.6 Prompt and afterglow emission

As has been discussed, the prompt emission properties are important for the classification of SGRBs based on their duration and hardness. In addition, throughout this thesis, the properties of SGRBs will be studied, in part based primarily on optical, infra-red and X-ray data of the afterglow emission. Below we outline how both the prompt and afterglow emission are thought to be generated along with the expected overall shape of the spectrum and lightcurve produced. The fireball model described in the following section is independant of the progenitor, as long as enough energy is provided, and is hence applicable to all progenitor models discussed in sections 1.4 and 1.5 (except perhaps for the proto-magnetar model).

1.6.1 Fireball model with internal and external shocks

To produce a GRB it is generally believed that an ultra-relativistic fireball of high energy photons is launched from some central engine. A small amount of entrained baryonic matter within the fireball can produce synchrotron emission via acceleration due to either internal (prompt emission) or external (afterglow emission) shocks (Rees and Meszaros, 1992).

An e^+- e^- γ fireball is formed at initial radius R_{in} due to the huge energies deposited by the compact object central engine. As the fireball expands adiabatically, the bulk Lorentz factor Γ initially increases linearly with radius until a saturation

radius (R_{sat}) is reached at which point the fireball coasts at a constant value Γ_{max}. Before R_{sat} is reached the e^+-e^- pairs within the fireball start to fall out of equilibrium, producing a quasi-thermal emission spectrum. However, the optical depth is still high enough that this emission cannot escape. It is only beyond the photospheric radius, R_{ph}, where the opacity $\tau_{ph} = 1$, that we can detect the non-thermal spectra produced first from internal shocks within the ejecta and then from the shock when the fireball decelerates due to coming into contact with the external medium surrounding the source.

The shocks which produce the GRB emission mainly accelerate the electrons associated with entrained baryonic matter. It is these accelerated electrons which then emit via synchrotron emission (and possibly inverse Compton scattering). Even a small amount of baryon loading ($\sim 10^{-7} - 10^{-5}\, M_\odot$) would mean that the baryonic matter would carry the bulk of the fireball energy. From repeated crossing of the shock, confined due to magnetic irregularities, the electrons at the shock front can be accelerated to very high energies resulting in an energy spectrum which is a power law distribution. We can define the electron energy spectrum based on Lorentz factor γ_e above a minimum Lorentz factor γ_m such that:

$$N(\gamma_e) \sim \gamma_e^{-p} \text{ for } \gamma_e > \gamma_m \tag{1.2}$$

Most electrons will be at $E_{min} = \gamma_m m_e c^2$, so γ_m can be seen as the characteristic γ. At higher frequencies there is a break in the spectrum known as the cooling break, $\nu_c \equiv \nu_c(\gamma_c)$, and is characterised by the regime where the electrons lose a significant fraction of their energy to radiation. The resultant synchrotron spectrum is shown in Figure 1.6, adapted from Sari et al. (1998), and is dependant on whether $\gamma_m > \gamma_c$ (fast cooling) or $\gamma_m < \gamma_c$ (slow cooling). For electrons with $\gamma > \gamma_c$ they cool rapidly emitting most of their energy at their synchrotron frequency.

The characteristic lightcurve produced for high frequency emission is shown in Figure 1.7, also adapted from Sari et al. (1998).

1.6.2 Prompt emission

The prompt emission is explained by internal shocks and is generally in the fast cooling regime. If the output of the central engine is time-varying then multiple shells of material with different bulk Lorentz factors can be produced (Narayan et al., 1992; Rees and Meszaros, 1994). When faster shells overtake slower ones a shock front will be created. The presence of many of these shocks could explain the complexity and variety seen in the γ-ray lightcurves of the GRB (e.g. Daigne and

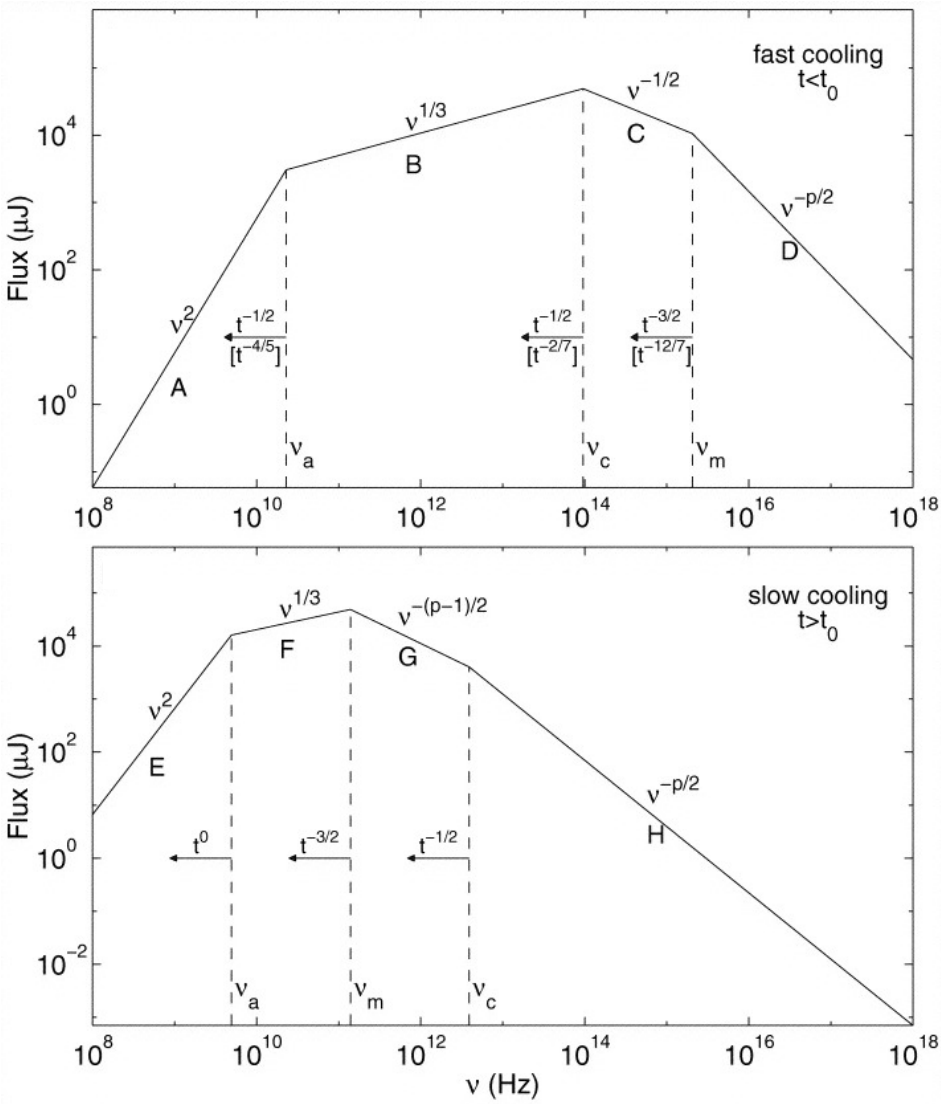

Figure 1.6: The synchrotron emission from shocked electrons in the ultra-relativistic jets of the GRB from Sari et al. (1998). The spectrum is characterised by two regimes: slow and fast cooling. The difference is based on the position of the cooling break ν_c above which the electrons lose significant energy from radiation. The top panel shows fast cooling, where $\nu_m > \nu_c$, where ν_m is the frequency associated with the characteristic Lorentz factor of the electron distribution, and the bottom panel shows slow cooling with $\nu_m < \nu_c$. The distribution will transition between these two regimes, most likely residing in the slow cooling regime for the majority of the afterglow emission. The lowest frequency emission is not dependant on the electron distribution and is affected by synchrotron self absorption, where the electrons re-absorb the synchrotron emission. This gives the regime below ν_a a blackbody profile with $F_\nu \propto \nu^2$. Above ν_a the flux density profile is $F_\nu \propto \nu^{1/3}$ where the emission is the sum of all the low energy tails of the electron distribution. At high frequencies the spectrum is dependant on the cooling regime and power-law index of electron distribution, p, as shown in the figure.

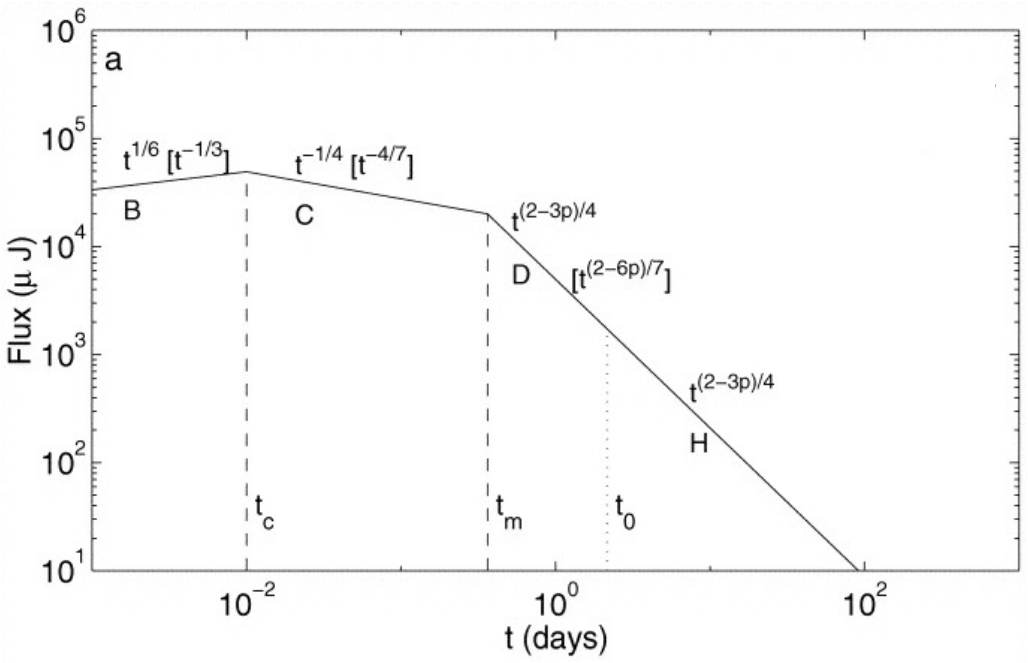

Figure 1.7: The canonical lightcurve produced for high frequency emission from the shocked electrons from Sari et al. (1998). The lightcurve seen is dependant on evolution of the break frequencies ν_m ($t_m \equiv t_m(\nu_m)$) and ν_c ($t_c \equiv t_c(\nu_c)$): the cooling break. Hence, a break seen in the lightcurve may be due to the evolution of the cooling break as it passes through the frequency regime being observed.

Mochkovitch 1998). The prompt emission itself reflects the activity of the central engine as well as the total duration telling us about its lifetime (Kobayashi et al., 1997).

1.6.3 Afterglow emission

Afterglow emission can be explained by external shocks when the fireball is decelerated by the external medium. As the shell expands more and more of the ISM is shocked and heated. Beyond the deceleration radius, $R > R_{dec}$, the shocked gas dominates, with the fireball reconverting the bulk kinetic energy into thermal energy (Kobayashi et al., 1999). Though two shocks are produced: the forward shock which propagates outwards into the external medium and the reverse shock which propagates into the ejecta, in the Standard Afterglow Model only the emission caused by the forward shock is considered. This is because the reverse shock is only mildly relativistic and most of the energy conversion takes place in the forward shock (Sari and Piran, 1995). However, it is predicted that the reverse shock will make a contribution to the afterglow emission producing a strong optical flash (Meszaros and Rees, 1997). When modelling the afterglow throughout this thesis the lightcurve and spectrum are treated as a series of power-laws, as shown in Figures 1.6 and 1.7, unless this is clearly a poor fit. However, we do also consider any deviations from this model such as flares.

1.7 Organisation of this thesis

Study of SGRBs has been greatly enhanced since the launch of initially *HETE-II* and now *f*. Rapid follow-up of these GRBs within orders of minutes-hours by the satellite itself and minutes-days from rapid ground based follow-up has allowed detection of X-ray and optical transients, providing sub-arcsecond localisation for a sample of $\sim$ 26 SGRBs up to the end of 2011. New data and analysis will be presented from sub-samples of this population, looking at host galaxy properties and afterglow lightcurves.

In addition, we address the issue of classification by considering a potential new population of "intermediate" GRBs emerging from studies of the γ-ray duration and hardness.

In Chapter 3, a population of well-localised SGRBs with no definitive host galaxy either at the position of the GRB to deep limits or from probabilistic arguments is considered. These SGRBs either present a population at high redshift or at high offset from galaxies at low redshift ($z < 1$). As well as presenting new

data with analysis of the lightcurves and potential host galaxies for four of these "hostless" GRBs, we look at the host galaxy offsets of the SGRB population as a whole, placing these bursts in context. We also compare the full sample of "hostless" GRBs to the distribution of galaxies on the sky with respect to random positions to test whether the potential host galaxies are simply a chance association.

In Chapter 4, the optically-localised SGRB population is considered as a whole (up to the end of 2011), compiling available data from the literature along with new data, to create consistent optical lightcurves. Fitting these lightcurves, and SEDs where possible, this data is then used to investigate physical properties of both the GRBs themselves and the surrounding medium. Within the lightcurves we search for achromatic jet breaks and accompanying optical thermal emission. We also place limits on the number of collapsars that could be masquerading as "short" GRBs within the population defined by a two second split in T_{90}.

In Chapter 5, we consider the issue of classification of GRBs, since overlap between the distinct progenitor systems around the two second divide undoubtedly produces contamination when attempting to define a cohesive sample. We split the population into duration bins; comparing their prompt emission, afterglow and host environment properties. In particular, we look around the two second divide, investigating the contamination of collapsars in the SGRB sample and the possibility of a new population of intermediate GRBs. Evidence for this intermediate population is found by looking at the distribution of the duration and hardness for several satellites including *BATSE*, *BeppoSAX* and *Swift* (Horváth, 1998; Horváth et al., 2008; Huja et al., 2009; Horváth, 2009; Horváth et al., 2010). Within the context of classification, we also present details of GRB 100816A, a GRB lying intermediate between the long and short populations. Its spectral hardness, host galaxy position and lack of associated supernova make it unusual for an LGRB and we investigate the possibility that this GRB is a mis-classified SGRB or a new kind of event entirely.

Chapter 2

Methods and Techniques

2.1 Overview of techniques used in this thesis

The main bulk of this thesis is comprised of analysis of optical and infra-red data from several world leading facilities including the Very Large Telescope (VLT) and the two Gemini telescopes: North and South. I will outline the basics of detection along with the necessary methods for general reduction and further calibration of this data.

2.1.1 Detectors

Charge Coupled Device (CCD)

The modern day workhorse of observational optical astronomy is the charge coupled device (CCD) which has allowed increased sensitivity and a linear response when compared with photographic plates. The detecting element of a CCD is comprised of a two dimensional array of individual pixels. Each pixel is essentially a light sensitive capacitor (Birney et al., 2006) comprised of metal-insulator-semiconductor junctions. Typically the semi-conductor is p-type meaning it has been doped to contain an excess of positive "holes". An applied positive voltage causes the migration of the positive holes away from the junction leaving a depletion region, setting up a potential well. Electrons within the depletion region can be excited from the valence band to the conduction band by any incoming photons. The positive "hole" produced migrates away from the depletion region leaving the excited electron behind. Hence each pixel stores the detection of incoming photons via the collection of photoelectrons within a potential well. The CCD itself can be read out by varying the voltage in such a way as to move the charge, column by column, out to the read-out register, which in itself is a column of pixels which have not been exposed to the

incoming radiation. The charge in each of the pixels in the readout register is then measured with an amplifier. This charge is passed onto an analog-to-digital converter. The output of this converter are analog to digital units (ADUs) or counts. Via the gain, the number of counts is directly related to the number of received photons taking account of introduced noise.

Infrared detectors

Infrared detectors work in a similar way to the CCD but require different materials in order to create the correct bandgap for excitation by the incident infra-red photons. Whereas CCDs are often silicon arrays, infrared detectors are typically created with InSb or HgCdTe. For instance, the four chips on the High Acuity Wide field K-band Imager (HAWK-I) on the VLT use HgCdTe (known as HAWAII arrays) (Kissler-Patig et al., 2008). For HgCdTe the detailed composition can be tuned over a large wavelength range to create the desired bandgap (Glass, 1999, pgs. 141–143).

The other main difference between CCDs and infra-red detectors is the separation of read out and detection into two layers. The read out layer uses silicon and is connected to the detector layer by small indium pillars known as "bumps" (Glass, 1999, pgs 145–148). This separation is necessary due to the difficulty of creating infrared sensitive material with effective charge transfer capabilities.

2.1.2 Imaging reduction

There are various sources of systematic and random noise which are introduced into the data during this process. These sources and the necessary calibrations we apply will be discussed below.

Bias frames

When calibrating a science image we first of all need to take account of the zero offset of the pixels. In addition to any zero offset which may exist a bias is also introduced by the amplifier. This is done in order to properly sample the readout noise. Readout noise is mainly introduced by the amplifier itself when collecting the charges from the pixels and is random rather than systematic. The best method of accounting for the bias depends on how uniform the bias pattern is across the CCD and how variable the pattern is throughout the night. The overall bias image of the CCD can be measured by taking zero second exposures, so that the total time is equal to the readout time. Multiple bias frames are often taken and can then be combined to find the median of these exposures. A bias frame samples the whole of

the image and hence is useful to measure bias patterns which persist. However, bias images will often be taken before the night has begun and not during and hence not simultaneous with the the science image. Another option is to measure the mean offset for each row using an overscan region where, for each image, either the final columns are read out multiple times or a physical unexposed region is read out. This will look like additional columns on the produced image. The benefit of using the overscan region is that the bias level can be measured concurrently with the image. Typically, over the course of the night an averaged stack of the initial bias frames are suitable for correcting for the zero offset in the science data though the overscan region can be used instead. Subtraction of the bias from your science image accounts for the zero point offset.

As well as accounting for the zero offset, bias frames can also be used to measure the read noise. Subtraction of one bias frame from a second (or an average of a set of bias frames from an additional bias), removes the bias offset and any non-uniformity leaving only the random noise in the frame. Measuring the variance of this bias difference frame allows measurement of the readout noise ($\sigma_R^2 = \sigma_{diff}^2/2$) noting that combining multiple bias frames increases the readout error by a factor of $\sqrt{N}$, where N is the number of frames.

Flat field frames

We must also account for both the variability of sensitivity between pixels and non-uniform illumination of the CCD. This can be achieved by imaging a uniformly illuminated field. For optical data, the most often used flat field is the twilight sky just after sunset and just before sunrise. At low zenith angle ($z \sim 20°$) the twilight sky is relatively flat and by moving the telescope between exposures and combining the frames using a median method the stars can be eliminated. Flat field frames can also be taken within the telescope dome using an illuminated screen. These are called dome flats. Twilight flats are often used in preference to dome flats when possible since the dome screens cannot be made as uniform as the twilight sky. Finally flat fields can be taken of the night sky if there are large areas of sky within an image by dithering and median combining. However, these images are low signal-to-noise. Hence, these are more likely to be used in the infra-red where the sky background is brighter. It should also be noted that since any flat frames is still an image of a field the bias must be subtracted. The flat frames can then be used to scale the image.

Dark frames

Within a CCD, in addition to photoelectrons, there will also be thermally excited electrons, which provide an unwanted background. This is known as dark current and scales exponentially with temperature such that $n \propto exp[-B/kT]$ where B is a constant (Birney et al., 2006). Though the current itself can be well modelled there is also a thermal noise component on top of this which scales as $\sqrt{n}$, hence it is beneficial to reduce this uncertainty as much as possible.

For the 8 m telescopes, in the optical regime the CCDs are cooled to around $-120°$C (for instance on the FOcal Reducer and low dispersion Spectrograph (FORS2) instrument on the VLT) whereas the near-infra red detectors are further cooled to around $\sim -200°$C. At these temperatures the dark current in the optical is typically $\sim 0.0006 e^-/px/s$ (Boffin, 2013, FORS User Manual) and in the near infra-red $\sim 0.10 - 0.15 e^-/px/s$ (Kissler-Patig et al. 2008; Carraro et al. 2011, HAWK-I User Manual). Hence dark current subtraction is important in the near infra-red region but for optical detectors it is negligible and attempting to remove it may add more noise to the data (Izzo et al., 2013, FORS2 Pipeline User Manual).

To correct for dark current a dark frame can be taken. Here the charge is allowed to accumulate for a duration equal to that of the science image but the CCD itself is never exposed. This dark frame can then be subtracted from the science image.

Background subtraction

The main reduction processes outlined above allow us to reduce the impact on our science images of error introduced by the CCD. However, there will also undoubtedly be a sky background level from scattered light within the camera, diffuse sources and the wings of bright objects. The background level and associated noise can be accounted for using sky apertures, as will be discussed in the next section. However, if there is a variable sky background, with gradients across the image, then it may still be prudent to remove this directly from the image before photometry is performed.

The method chiefly employed in this thesis to subtract the background is through use of the source extractor program, SExtractor (Bertin and Arnouts, 1996). To measure the varying background level, a grid is constructed across the whole frame separated into a set of meshes. The background is estimated using the clipped mean, from iterative clipping of the background histogram to 3σ, unless the field is particularly crowded (defined by a change in the standard deviation $> 20\%$) in

which case the mode is used instead (Da Costa, 1992; Bertin and Arnouts, 1996). The background map, which can then be applied to the image, is a bi-cubic spline interpolation of the grid created[1]. A median filter can also be applied to help reduce any overestimation on local scales due to bright sources. This is a sliding window of fixed width within which the median value is calculated for each window, smoothing out any unwanted extremes in the background map. The SExtractor program allows, amongst other things, the mesh and median filter sizes for background estimation to be specified and these values were chosen to best recreate the background seen in the processed images.

2.1.3 Photometry

Where possible our images were taken under photometric conditions, with no cloud cover and stable seeing. In addition, it is also preferable to take observations at low zenith angle, z, to reduce the atmospheric extinction (airmass).

Aperture Photometry

For measurement of the source magnitudes the main method applied in this thesis is aperture photometry. Here, a suitable aperture is chosen based on the point spread function (PSF) of unsaturated point sources in the field.

The main quantifiable sources of noise will be the read noise, sky background shot noise and source shot noise. Both the noise on the sky and on the source will be Poisson distributed. In units of detected electrons the Poisson noise is given by $\sqrt{n_{sky}}$ and $\sqrt{n_{source}}$ where n_{sky} and n_{source} are the number of detected events for the sky and source respectively. For counts (ADUs) this noise must be divided by the gain (i.e. $\sqrt{n/G}$). The gain, as discussed in section 2.1.1, provides the conversion between the measured counts (ADUs) in the image and the number of electrons (primarily photoelectrons) detected.

In our observations we are typically background limited, meaning the sky noise dominates. The noise, a combination of the sky and read noise, is well approximated by placing multiple apertures, with the same area as the source aperture, on the sky and measuring the variance between these apertures. Alternatively, an annulus around the source can be used to measure the variance of the sky pixel values. Combining this measured variance with the noise of the source will give us the overall error for the detection.

[1]Original interpolation details from Bertin and Arnouts 1996 have been updated in Bertin, SExtractor User Manual

In addition to these noise sources there are also many sources of systematic errors which could contribute. This includes mis-calculation of the bias level, bias structure or flat field, non-linearity near the point of saturation and interpolation errors introduced from placing a circular aperture on a grid of square pixels. However, most of these additional errors will be small with only the flat field error potentially adding any significant contribution to the noise already accounted for.

Zeropoint calibration

To produce absolute rather than relative photometry, the source magnitude can be calibrated from sources with known magnitude. One method of calibration is from the observation of a standard field containing bright primary standard stars. This can be done if the observations were taken under photometric conditions. Calibrating from a separate image in this way means any differences in exposure time and airmass must be taken into account. At angles from zenith less than $z < 60^\circ$ the airmass is well approximated by $X = \sec(z)$ (at $z = 0^\circ$, $X = 1$ and $z = 60^\circ$, $X \sim 2$) with second order terms becoming increasingly important at higher angles (Birney et al., 2006, pgs. 125-132). The extinction correction is dependant on wavelength with typical corrections in the range $0.02 - 0.16$ magnitudes per unit airmass for the wavelength range $7800 - 4700\,\text{Å}$[2]. The difference between the standard and science frame airmass values is often minimised and so this correction, especially for longer wavelength observations, is not normally significant.

If no standard calibration frames are available, or if the observations could not be taken under photometric conditions, secondary standard stars within the science images can be selected. These stars have been calibrated from the primary standard stars and are fainter with less accurate photometry. The calibrators chosen must be non-saturated, isolated point sources with magnitudes available in the appropriate filter within a photometry catalogue. Using secondary calibrators avoids any complications with different exposure times or airmass since they are within the same frame as the source. For optical observations the point sources selected were normally from the USNO or SDSS catalogues (Monet et al., 2003; Abazajian et al., 2009), where available in the field. For the near-infrared band observations the 2MASS catalogue was most often used (Skrutskie et al., 2006).

[2]Extinction values measured using the 0.6 m Bochum telescope at the La Silla site in Chile. Values available online at https://www.eso.org/sci/observing/tools/Extinction.html

Filter and magnitude systems

For calculation of fluxes as well as magnitudes we must also consider both the filter and the magnitude system being used to calibrate the standard stars. One consideration is whether the filter transmission as a function of wavelength between the observation and the standard stars differ, though this source of error is usually small. The standard broadband optical filters for the FORS instrument are based on the Johnson-Cousins $UBVRI$ system (Johnson and Morgan, 1953; Cousins, 1978) whereas the the Gemini telescopes follow the Sloan system with filters $g'r'i'z'$ (Fukugita et al., 1996). For calibration, when the magnitude of the standard stars is only known in the alternative filter set (e.g. $g'r'i'z'$ rather than $UBVRI$) a correction can be estimated using standard stellar conversions (e.g. Lupton et al. 2005).

The most frequently used magnitude systems are either based on the stellar spectrum of α-Lyrae (Vega) or on a constant flux per unit Hertz standard (AB). Conversion between these magnitude systems requires knowledge of the spectrum of Vega, sometimes causing a discrepancy if different spectra have been used or different interpolations of the spectrum used to calculate the conversion. In this thesis we try to achieve consistency through use of the astSED python code as part of the astLib package which bases its conversions on the Vega spectrum available from Bohlin and Gilliland (2004).

Chapter 3

Hostless short gamma-ray bursts

3.1 Introduction

As has been discussed in Chapter 1, the differing environments between SGRBs and LGRBs can tell us much about their progenitor systems. LGRBs are clearly linked to massive stars, residing in galaxies with a high star-formation rate, within the star forming regions. SGRBs, on the other hand, have distinct progenitors from LGRBs, sometimes appearing in galaxies with an established older population and sometimes found well outside star-forming regions.

In addition, for the majority of LGRBs at low redshift it has been possible to isolate the signature of a type Ic supernova, suggesting that their progenitors are Wolf-Rayet stars (Hjorth and Bloom, 2011, and refs therein). Deep searches in SGRBs fail to locate any supernova signatures, and offer further evidence that the progenitors of short bursts are not related to stellar core collapse (Bloom et al., 2006; Hjorth et al., 2005; Rowlinson et al., 2010a). The varied host demographics offer part of the picture, but the locations of the bursts on their hosts are also greatly diagnostic. It appears that SGRBs are scattered significantly on their hosts, occurring in typically fainter regions, and at larger offsets than their long cousins (Fruchter et al., 2006; Fong et al., 2010; Church et al., 2011). These properties can naturally be explained if the progenitor is a merger of two compact objects (e.g., NS-NS, collapsing to a black hole by accretion-induced collapse (AIC), or NS-BH) (Eichler et al., 1989; Fryer et al., 1999a; Bloom et al., 1999; Fong et al., 2010).

A key distinguishing factor between different intrinsically ancient progenitor populations, such as accretion-induced collapse (AIC) of white dwarfs to neutron

stars (Levan et al., 2006b; Metzger et al., 2007), and compact binary mergers, comes from the dynamics of the systems themselves. In a double compact object binary, a combination of natal kicks, and mass loss from the binary at the time of each supernova, can act to provide the systems with space velocities of several hundred $\mathrm{km\,s^{-1}}$ (e.g. Wong et al. 2010). Integrated over the lifetime of the binary of 10^7-10^{10} years this corresponds to distances of tens of kpc from their birth sites. For extremely high kicks, or relatively low mass host galaxies, the binary may escape the galactic potential of its host altogether. Hence, a population of SGRBs in intergalactic space would offer strong support for a binary merger model for their progenitors (Bloom and Prochaska, 2006; Berger, 2010).

However, determining the offset of a burst from its host is non-trivial when there is no obvious parent galaxy coincident with or close to the burst location. In these cases probabilistic methods based on the sky density of galaxies are often used to argue for a host association (e.g. Bloom et al. 2002, 2007; Levan et al. 2007; Berger 2010). However, the sky density is such that any random position on the sky is likely to be within a few arcseconds of a moderate redshift galaxy with $R < 25$. In other words, in many cases we cannot *strongly* identify the host galaxy (probability of $\lesssim 1\%$), which can often lead to mis-identifications. A second problem is that to the limits of our ground-based (or even *Hubble Space Telescope*) observations, we probe a reducing fraction of the galaxy luminosity function as we move to higher redshift. Hence there is a degeneracy between GRBs which have been kicked far, and hence are well offset, from relatively local hosts and those which lie within fainter galaxies at high redshifts. This problem is particularly acute if the high redshift galaxies host primarily old stellar populations, and hence exhibit only weak rest frame UV (observer-frame optical) emission.

In this sense the "hostless" problem for SGRBs in not that there are a lack of candidate hosts; in all lines of sight there will be plausible parent galaxies within a few tens of kpc. Frequently the probability of chance alignment with at least one of these is small, and may be suggestive of kicks to the SGRB progenitors (Berger, 2010). Instead, the problem in these hostless cases is the difficulty in determining uniquely the parent galaxy (from e.g. several with similar probabilities, or underlying larger scale structure). This means we are unable to make full use of the diagnostic information contained in the offset distribution and the properties of the hosts for improving our knowledge of SGRB progenitors.

Obtaining the redshift for the GRB using the afterglow would allow us to narrow our search to hosts within a small redshift range. However, for SGRBs the faintness of their afterglows (Kann et al., 2011) means that redshifts are difficult

to obtain in practice, and in nearly all cases to-date redshifts for SGRBs have been inferred from their presumed host galaxy rather than from the burst itself (e.g. Hjorth et al. 2005; Berger et al. 2005; Rowlinson et al. 2010a; Fong et al. 2011b). In fact, even accounting for the faint continuum, in some cases the lack of any absorption features also gives an indication that the burst is not in a dense interstellar medium (ISM) (Foley et al., 2005; Berger et al., 2010).

Based on the optically localised SGRB sample outlined in section 3.3.1, $\sim 70\%$ have apparently well-associated host galaxies, while the remainder are apparently hostless. This may offer evidence for kicks. Here, we present the discovery and subsequent observations of the optical afterglows and host limits of a further two hostless bursts, GRB 090305A (see also Berger 2010), GRB 091109B and deep limits of a third, GRB 111020A (see also Fong et al. 2012). We also present the host galaxy limits of a fourth GRB, GRB 110112A, and look for potential host galaxies in the field (see also Fong et al. 2013). These GRBs are all unambiguously of the short-hard class, with $T_{90} < 0.5\,\mathrm{s}$ and prompt emission which is spectrally hard. We consider the extent to which our current detection limits probe the galaxy luminosity function as a function of redshift, and what this implies for hostless GRBs more generally.

These hostless GRBs could reside within relatively high redshift (but so far unseen) host galaxies or have travelled far from their low redshift ($z < 1$) hosts, perhaps within the intergalactic medium (IGM). Clues to their origins may come from studies of the most likely hosts amongst the nearby galaxies on the sky. We present an alternative diagnostic tool developed by taking random positions and comparing them to the distribution of galaxies on the sky, thus reproducing the sort of analysis performed when looking for a SGRB host. From this we define probability of chance association (P_{chance}) and a radius within which we can confidently state a host association.

3.2 Observations and Analysis

3.2.1 GRB 090305A

Prompt and X-ray observations

GRB 090305A was detected by the Burst Alert Telescope (BAT) instrument on *Swift* (Barthelmy et al., 2005b) in 2009 on March 05 at 05:19:51 UT (Beardmore et al., 2009a). The GRB had a duration of $T_{90} = 0.4 \pm 0.1\,\mathrm{s}$ and a fluence $(15 - 150\,\mathrm{keV})$ of $7.5 \pm 1.3 \times 10^{-8}\,\mathrm{erg\,cm^{-2}}$ with the errors quoted at the 90% confidence level

(Krimm et al., 2009). For a GRB at $z = 0.5$ (a typical redshift for an SGRB) extrapolating this fluence to the $1 - 1000\,\mathrm{keV}$ range gives an isotropic equivalent energy of $E_{iso} = 4.5 \times 10^{50}\,\mathrm{erg}$.

The X-ray Telescope (XRT) on *Swift* (Burrows et al., 2005) began observations 103.4 s after the BAT trigger in photon counting (PC) mode but no X-ray afterglow was detected (Beardmore et al., 2009b). An optical afterglow was detected by the Gemini Multi-Object Spectrograph (GMOS) instrument on the Gemini-South telescope (Hook et al., 2004) at position $\alpha = 16^{\mathrm{h}}\,07^{\mathrm{m}}\,07.58^{\mathrm{s}}$, $\delta = -31^{\circ}\,33'\,22.1''$ (Cenko et al., 2009). Using the position provided by the Gemini observations and by relaxing the default screening criteria, the X-ray afterglow was identified with 99.99% confidence using the method of Kraft et al. (1991) for determining confidence limits with a low number of counts. The source was no longer detected when further XRT measurements were made 3.92 ks after the BAT trigger for 2.05 ks. Using all available data this gives a 3σ upper limit of $1.7 \times 10^{-3}\mathrm{count\ s^{-1}}$ indicating a decay slope of at least ~ 0.8 (Beardmore et al., 2009b). All BAT and XRT measurements and limits are shown in Figure 3.1.

Optical observations

We obtained multiple observations of the field of GRB 090305A using the Gemini South telescope. We reduced the data using the Gemini GMOS packages available for IRAF to produce bias subtracted, flat field corrected, and in the case of the i' band, fringe field subtracted images. The optical afterglow was detected in all bands with observations made ~ 35, ~ 55 and ~ 75 minutes after the GRB in the r', g', i' bands respectively. Further observations were made in the r' band ~ 95, ~ 125 and ~ 13000 minutes (~ 9.02 days) after the BAT trigger with the afterglow still detected in the first two epochs. The final Gemini epoch can be used to place a constraint on any host galaxy coincident with the GRB position, with the limit measured using an apeture equivalent to the full width at half maximum (FWHM) of the image. The r' band images are shown in Figure 3.2 with the optical transient (OT) and nearby source A indicated. Variation of the afterglow flux density, F, is described using $F \propto t^{-\alpha}\nu^{-\beta}$. The spectral fit using the r', g', i' band detections has an index of $\beta_O \sim 0.50$. The temporal fit to the r' band detections has slope of $\alpha_r = 0.52 \pm 0.03$, shown in Figure 3.1. We note that this could also be reasonably fit by a broken power law with a steep slope matching the X-ray observations. However, the broken power law fit is too overconstrained to determine whether this is a better fit than the single power law.

A final epoch of observations was made using the FORS2 instrument on the

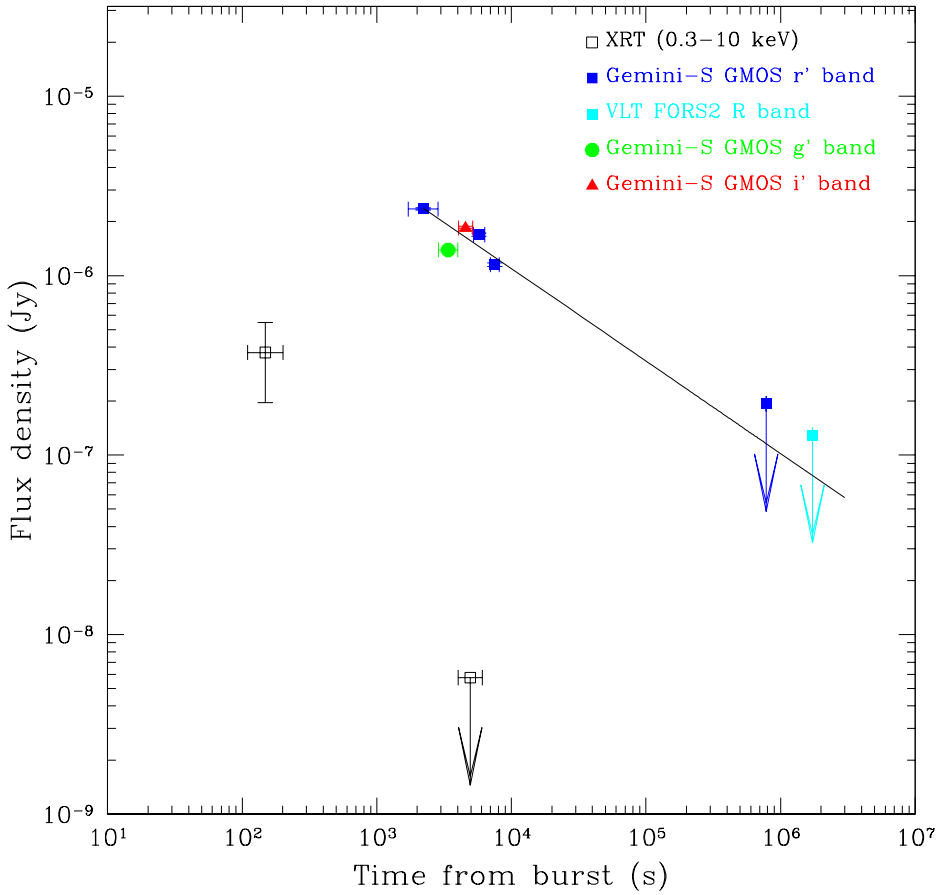

Figure 3.1: X-ray and optical light curve of GRB 090305A. The XRT measurements are shown as black open squares including the single XRT detection and late time upper limit (Evans et al., 2007). The Gemini South GMOS optical measurements and limit in the r', g' and i' bands are the blue filled squares, green circle and red triangle respectively. The VLT R band limit is shown as a cyan square. We have fit the r' band, where we have multiple detections, with a power law measuring a decay index of $\alpha_r = 0.52 \pm 0.03$.

Start of observations (UT)	Exposure time	ΔT (minutes)	Filter	Magnitude
Gemini South GMOS				
2009-03-05 05:47:23.5	$5 \times 180\,\mathrm{s}$	36.87	r'	22.98 ± 0.02
2009-03-05 06:07:00.6	$5 \times 180\,\mathrm{s}$	56.51	g'	23.54 ± 0.03
2009-03-05 06:26:41.5	$5 \times 180\,\mathrm{s}$	76.19	i'	23.28 ± 0.03
2009-03-05 06:46:21.2	$5 \times 180\,\mathrm{s}$	95.84	r'	23.33 ± 0.02
2009-03-05 07:07:20.5	$4 \times 500\,\mathrm{s}$	125.53	r'	23.75 ± 0.03
2009-03-16 05:37:04.7	$10 \times 150\,\mathrm{s}$	~ 13000	r'	> 25.69
VLT FORS2				
2009-03-25 05:08:06.8	$20 \times 240\,\mathrm{s}$	~ 28830	R	> 25.90

Table 3.1: A log of Gemini and VLT observations of GRB 090305A. Magnitudes quoted for the Gemini telescope are in the AB system and for the VLT are in the Vega system. ΔT is taken at the mid-point of the observations. All magnitudes have been corrected for Galactic extinction of $E(B-V) = 0.22$ (Schlegel et al., 1998).

VLT in the R band. This was a long exposure image but due to the proximity of a group of bright stars could only marginally improve on the Gemini limit. Details of all observations made are listed in Table 3.1.

3.2.2 GRB 091109B

Prompt and X-ray observations

GRB 091109B was detected by the BAT instrument on 2009 November 09 at 21:49:03 UT (Oates et al., 2009b). The *Suzaku* Wide-band All-sky Monitor (WAM), which also detected this GRB, measured an $E_{peak} = 1330^{+1120}_{-610}\,\mathrm{keV}$ showing the GRB is spectrally hard (Ohno et al., 2009). The GRB had a duration of $T_{90} = 0.3 \pm 0.03\,\mathrm{s}$ and a fluence $(15-150\,\mathrm{keV})$ of $1.9 \pm 0.2 \times 10^{-7}\,\mathrm{erg\,cm^{-2}}$ (Oates et al., 2009a). As for GRB 090305A, if we use a redshift of $z = 0.5$ and extrapolate this fluence to the $1-1000\,\mathrm{keV}$ range we measure an isotropic equivalent energy of $E_{iso} = 1.47 \times 10^{51}\,\mathrm{erg}$

The X-ray afterglow was detected by the XRT which began observing at 21:50:21.1 UT, 78.1 s after the BAT trigger (Oates et al., 2009b). The X-ray light curve shown in Figure 3.3, with data entirely taken in PC mode, can be fit by a power law with decay index $\alpha_X = 0.64^{+0.09}_{-0.08}$ (90% errors).

Optical observations

We obtained multiple observations of the GRB position in the R band using the FORS2 instrument and observations in the J and K band using the HAWK-I instrument both on the VLT. The data was reduced using the standard IRAF packages

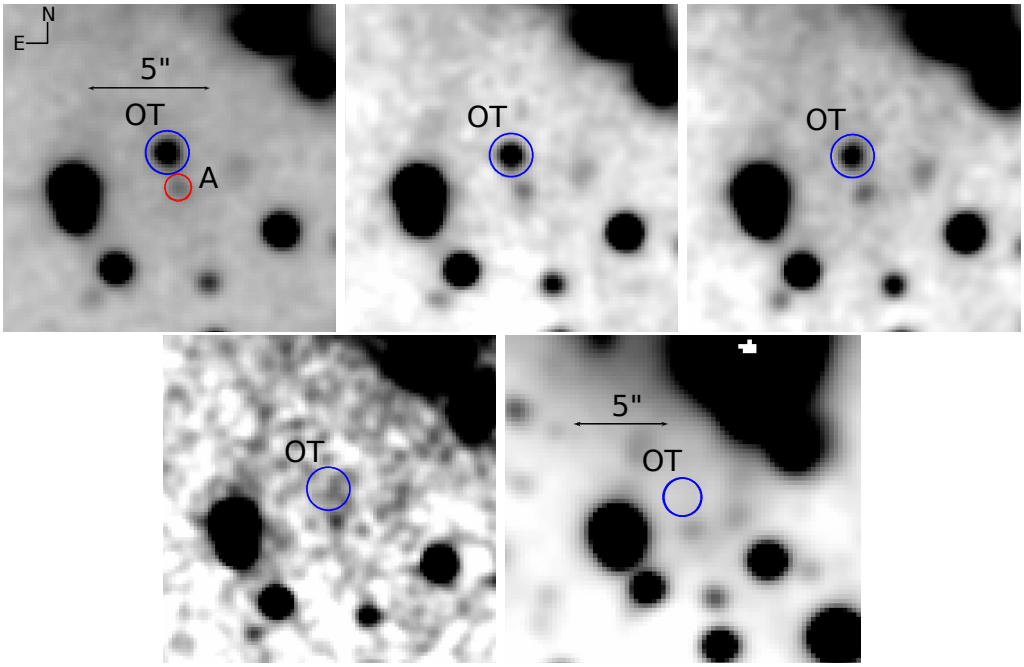

Figure 3.2: A finding chart for GRB 090305A. All images except the final image are from Gemini r' band observations and show the optical transient (OT - blue circle) fading. No coincident host galaxy is found from late time Gemini imaging at the GRB position. The potential host galaxy, source A, is identified in the first epoch image with a red circle. Due to the faintness of source A, it is not possible to determine whether it is extended. The final image is from our additional late time observation using the FORS2 instrument on the VLT and also shows the lack of a coincident host galaxy down to the limits of the image.

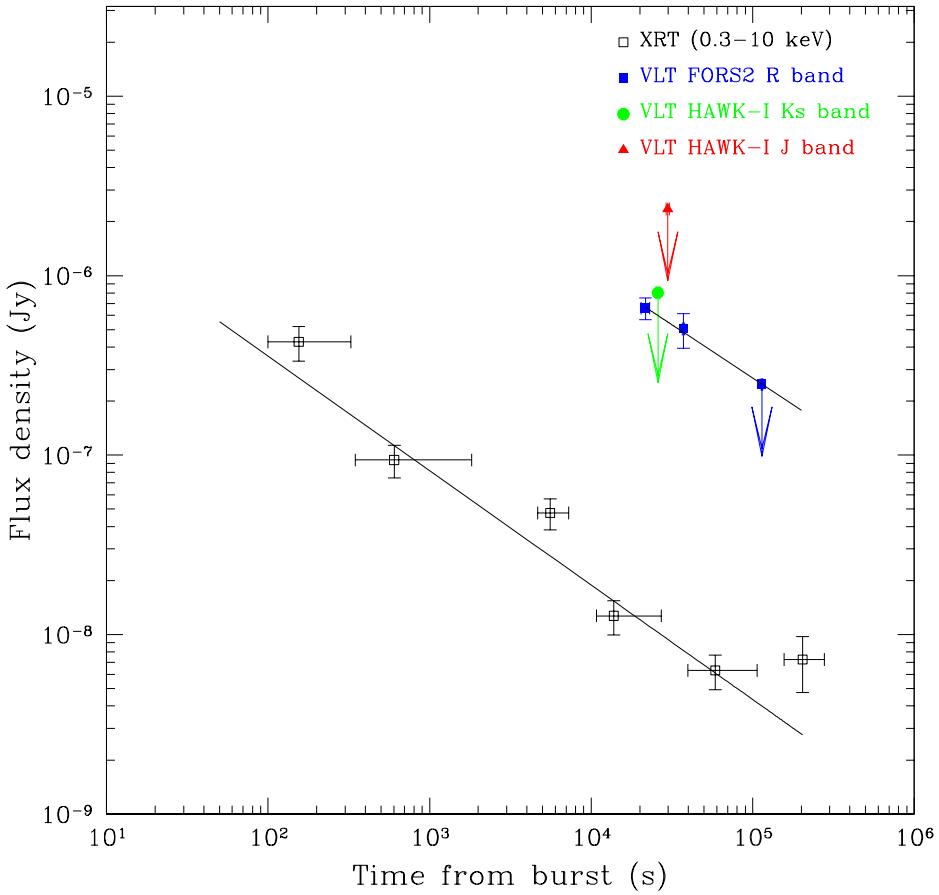

Figure 3.3: The XRT (Evans et al., 2007) and VLT optical light curves for GRB 091109B. The X-ray data is plotted as black open squares and the R band optical measurements and limits are plotted as blue filled squares. Additional J and K band limits from the HAWK-I instrument on the VLT are plotted as a red triangle and a green circle respectively. Both the X-ray and the R band data have been fit with power slopes giving decay indices of $\alpha_X = 0.64^{+0.09}_{-0.08}$ and $\alpha_R = 0.60 \pm 0.10$, consistent with each other.

Start of observations	Exposure time	ΔT (minutes)	Band	Magnitude
2009-11-10 03:28:37.800	8×300 s	361.56	R	24.13 ± 0.14
2009-11-10 04:53:49.091	$22 \times 10 \times 6$ s	431.95	K	> 22.23
2009-11-10 05:54:57.305	$22 \times 10 \times 6$ s	497.45	J	> 21.99
2009-11-10 07:59:36.965	4×300 s	621.39	R	24.42 ± 0.21
2009-11-11 05:10:38.044	8×300 s	1903.28	R	> 25.63

Table 3.2: A log of VLT FORS2 and HAWK-I observations of GRB 091109B. Magnitudes are in the Vega system and have been corrected for Galactic absorption of $E(B-V) = 0.17$ (Schlegel et al., 1998). ΔT is taken at the mid-point of the observations.

to produce bias subtracted and flat field corrected images.

We discovered an optical afterglow in the R band from two sets of R band observations taken on 2009 November 11 $\sim$ 360 minutes and $\sim$ 620 minutes after the BAT trigger with clear fading between the epochs. The position was $\alpha = 07^{\rm h}\,30^{\rm m}\,56.60^{\rm s} \pm 0.02$, $\delta = -54^\circ\,05'\,23.3'' \pm 0.3$, consistent with the revised X-ray position (Evans et al., 2009b). A third set of R band observations were taken on 2009 November 11, $\sim$ 1900 minutes ($\sim$ 1.32 days) after the start of the GRB and when the afterglow had faded allowing us to place a constraint on the magnitude of any underlying host galaxy. These images are shown in Figure 3.4 with the optical transient (OT) indicated in the image along with two potential host galaxies: nearby faint source A and bright galaxy, source B.

J and K band observations were also made on 2009 November 10, $\sim$ 495 minutes and $\sim$ 430 minutes after the GRB respectively. The transient was not detected in either band. The upper limit placed in the K band implies that the afterglow emission was unusually blue, with a practically flat SED, and therefore suggestive of low extinction. We note that this also unusual in the context of the afterglow model where we would expect a steeper slope of at least $\beta = 0.5$ (Sari et al., 1998). All observations, magnitudes and limits are listed in Table 3.2 and shown in Figure 3.3. The X-ray and optical temporal decay indices are $\alpha_X = 0.59 \pm 0.05$ and $\alpha_R = 0.60 \pm 0.10$, where this measured X-ray slope is consistent with that reported by Evans et al. (2009b).

3.2.3 GRB 110112A

Prompt and X-ray observations

Swift detected GRB 110112A with the BAT instrument on 2011 January 12 at 04:12:18 UT (Stamatikos et al., 2011). The duration of the GRB was $T_{90} = 0.5 \pm 0.1$ s

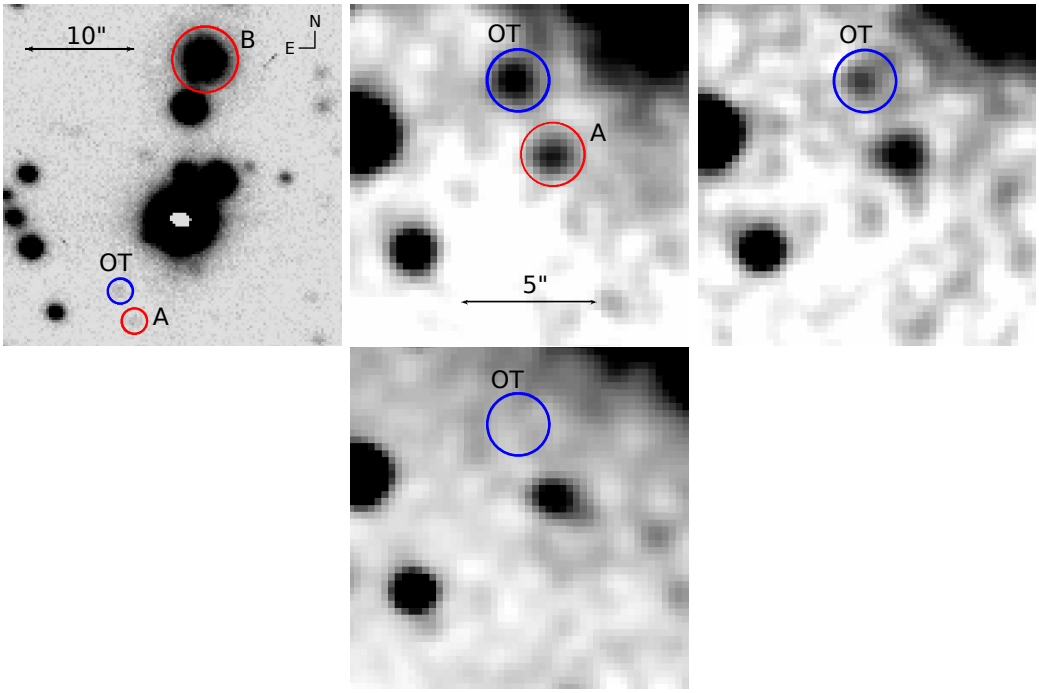

Figure 3.4: Finding chart for GRB 091109B. The images were taken in the *R_SPECIAL* filter on the VLT. The first 2 panels are from the first epoch and indicate the optical transient (OT), a nearby source (A) and a bright galaxy (B). The optical transient can clearly be seen to be fading across the three epochs. Other objects visible in the field appear to be foreground stars and not galaxies.

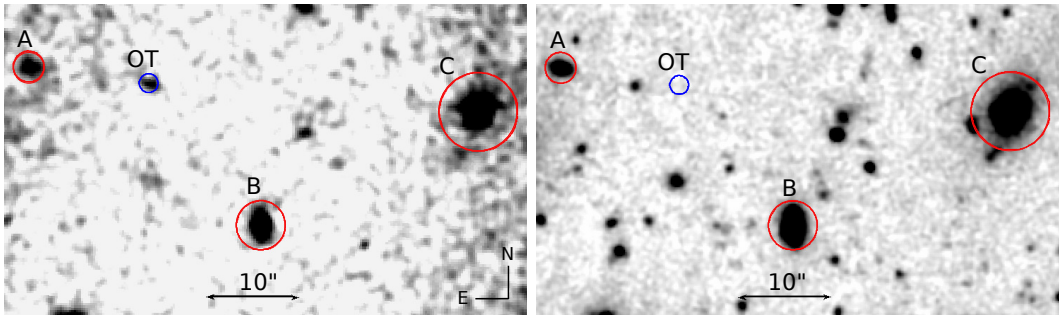

Figure 3.5: Finding chart for GRB 110112A. The images from the WHT ACAM instrument (left) and the Gemini-South GMOS instrument show the position of the optical transient (OT) and three potential host galaxies (A,B,C). These objects are clearly extended.

and it had a fluence ($15 - 150\,\mathrm{keV}$) of $3.0 \pm 0.9 \times 10^{-8}\,\mathrm{erg\,cm^{-2}}$ (Barthelmy et al., 2011). As for the previous GRBs, extrapolating this fluence to the $1 - 1000\,\mathrm{keV}$ range, using a redshift of $z = 0.5$, we measure an isotropic equivalent energy of $E_{iso} = 1.92 \times 10^{49}\,\mathrm{erg}$.

An X-ray afterglow was detected by the XRT which started observing 75.5 s after the BAT trigger (Stamatikos et al., 2011).

Optical observations

An optical transient was detected $\sim 15.4\,\mathrm{hrs}$ after the BAT trigger in the i' band using the ACAM (Auxiliary-port camera) on the William Herschel Telescope (WHT). This object was marginally coincident with the position for a candidate identified by Xin et al. (2011) with the Xinglong TNT telescope, whose brighter magnitudes implies fading (Levan et al., 2011). We took late-time imaging using the GMOS instrument at the Gemini-South telescope confirming this object as the afterglow of the GRB. The finding chart for the afterglow of GRB 110112A is shown in Figure 3.5. For further details of observations of GRB 110112A, see Fong et al. (2013).

3.2.4 GRB 111020A

Prompt and X-ray observations

GRB 111020A was detected by the BAT instrument on 2011 October 20 at 06:33:49 UT (Sakamoto et al., 2011b). The duration of the GRB was $T_{90} = 0.40 \pm 0.09\,\mathrm{s}$ and it had a fluence ($15 - 150\,\mathrm{keV}$) of $6.5 \pm 1.0 \times 10^{-8}\,\mathrm{erg\,cm^{-2}}$ (Sakamoto et al., 2011a). Extrapolating this fluence to the $1 - 1000\,\mathrm{keV}$ range, using a redshift of $z = 0.5$, we measure an isotropic equivalent energy of $E_{iso} = 1.77 \times 10^{50}\,\mathrm{erg}$.

The X-ray afterglow was detected by the XRT which started observing 72.8 s after the BAT trigger (Sakamoto et al., 2011b). The afterglow was also observed by the *Chandra* X-ray Observatory which placed the most precise position on the afterglow: $\alpha = 19^{\rm h}\,08^{\rm m}\,12.49^{\rm s} \pm 0.2$, $\delta = -38^\circ\,00'\,42.9'' \pm 0.2$ (Fong et al., 2012).

Optical and Infrared observations

Observing with the Gemini South telescope in the i' band Fong et al. (2011a) noted the presence of several point sources near to the X-ray afterglow position. However, with further imaging Fong and Berger (2011) later reported that none of these sources were fading between the epochs. Hence, no optical afterglow was observed for this GRB.

We obtained observations of GRB 111020A with the VLT, equipped with HAWK-I, in the J-band. We reduced this data using the HAWK-I recipes available for the ESO Recipe Execution Tool (esorex) to produce flat field corrected, dark and background subtracted images. Our observations started at 00:33 on October 21 2011, approximately 18 hours after the burst with a total exposure time of 44 minutes. We identify the same sources seen by Fong et al. (2012) (in particular G1, G2 and G3). In our imagery we label these objects A (G3), B (G2), and C (G1) in order of increasing offset from the GRB position. We note that only object C and perhaps B appears extended in our image with $0.4''$ seeing. We do not identify any additional sources which could be the IR afterglow of GRB 111020A to a limiting magnitude of $J = 23.6$ (3σ).

We obtained late time observations of the GRB position in the R band using the FORS2 instrument on the VLT. We reduced this data using the FORS recipes available for esorex to produce bias subtracted and flat field corrected images. This observation is shown in Figure 3.7 and the details of the observation are given in Table 3.3. Although no optical counterpart was found, due to the small error (sub-arcsecond) on the *Chandra* X-ray afterglow position we can still use this to accurately measure offsets from any potential host galaxies and to place deep limits at the position of the afterglow.

Additionally at this epoch we obtained FORS2 spectroscopy of a bright galaxy offset from the GRB position which is a plausible host (see section 2.5) shown in figure 3.6. The spectrum is significantly contaminated by light from a bright foreground star overlapping the galaxy and confused with its nucleus. However, in the outlying regions of the galaxy we identify a weak emission line at 6688 Å. Identifying this as H$-\alpha$ suggests at redshift of $z = 0.019$, or 81 Mpc.

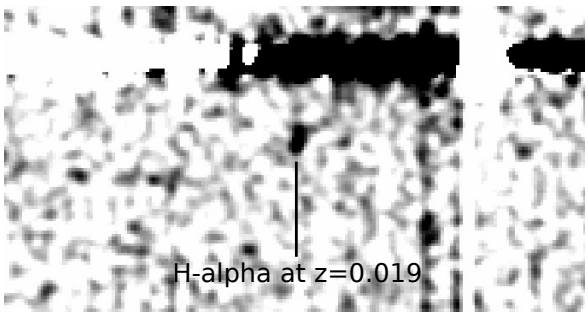

Figure 3.6: The VLT/FORS spectrum of the galaxy proximate to GRB 111020A. The source is significantly contaminated by an extremely bright foreground star sitting close to the location of the nucleus of the galaxy. We have attempted to remove this star by subtracting the median value across the wavelength range in each row from the spectrum. At an offset position, consistent with the disc of the galaxy we do observe an emission line at 6690Å. If this line is interpreted as Hα, the inferred redshift is $z = 0.019$

Start of observations	Exposure time	ΔT (days)	Band	Magnitude
2011-10-21 00:33:29.579	$44 \times 10 \times 6$ s	0.77213	J	> 23.6
2012-03-23 07:18:05.768	20×240 s	155.03	R	> 24.03

Table 3.3: A log of VLT HAWK-I and FORS2 observations of GRB 111020A in the J and $R\_SPECIAL$ filters. The HAWK-I observation was made at early times with no afterglow detected. Both observations allow us to place a constraint on any underlying host galaxy. The magnitudes quoted here are in the Vega system and have been corrected for Galactic absorption of $E(B-V) = 0.43$ (Schlegel et al., 1998). ΔT is taken at the mid-point of the observations.

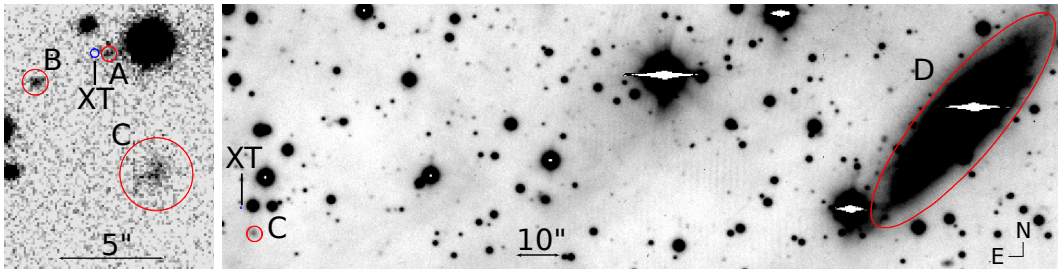

Figure 3.7: VLT observations for GRB 111020A. The early time J band image is shown on the left with three nearby objects (A,B,C) shown in relation to the position of the X-ray transient (XT) with no infra-red transient detected. Objects A, B, C are synonymous with objects G3, G2, G1 respectively identified in Fong et al. (2012). Though objects B (G2) and C (G3) show evidence for extension, the faintness of object A (G1), the object closest to the X-ray position, makes this difficult to determine and the afterglow is still clearly offset from this object. In the FORS $R_{SPECIAL}$ band image shown on the right of the 3 objects we only detect galaxy C. In addition, we detect, a nearby large spiral galaxy (labelled D).

3.2.5 Candidate host galaxies

For GRBs 090305A, 091109B, 110112A and 111020A there is no host galaxy coincident with the optical afterglow position down to deep limits. Hence, we investigate galaxies in the field around these SGRBs to determine if there are any strong host galaxy candidates.

GRB 090305A occurred in a region with a high density of sources meaning there are many field objects of the order of $5-8''$ away, none of which show evidence of extension. There is a faint object located $1.48''$ from the optical afterglow, shown in Figure 3.2 and labelled as source A. The magnitude of source A is $r'(AB) = 25.64 \pm 0.20$. Due to its faint magnitude it is not possible to determine with high confidence whether this object is extended.

For GRB 091109B we identified two extended objects which are potential host galaxies. The first is a faint object $\sim 3.0''$ from the GRB position marked in Figure 3.4 as source A with $R(Vega) = 23.82 \pm 0.10$. The object is not detected in the J and K band down to the limiting magnitude listed in Table 3.2. The second potential host, source B, is a spiral galaxy located $\sim 22.5''$ from the GRB position. Even though this is located much further from the GRB position than source A, it is much brighter with magnitudes $R(Vega) = 19.19 \pm 0.05$, $J(Vega) = 17.45 \pm 0.05$ and $K(Vega) = 16.16 \pm 0.05$.

GRB 110112A occured in a relatively clear region quite well offset from other objects in the field. We find 3 spiral galaxies which could potentially be host galaxies labelled as A, B and C in Figure 3.5. These objects have i' band AB magnitudes of 22.70 ± 0.07, 21.16 ± 0.04 and 20.17 ± 0.05 respectively with increasing offsets of $12.9''$, $19.3''$, $35.6''$.

In our images we identify four objects which could be candidate host galaxies for GRB 111020A, shown in Figure 3.7. Three of these objects are within $7''$ of the X-ray afterglow with the fourth being a large, extremely bright spiral galaxy at an offset of $166''$. The labels of A-D are with increasing offset from the afterglow position. This galaxy, labelled D in our image, has a magnitude $R(Vega) \sim 14.0$ with the uncertainity due to a number of saturated foreground stars obscuring the galaxy, making it difficult to make a precise measurement. Our measured redshift for the galaxy (if taken from the single line) is $z = 0.019$, corresponding to a projected separation of 60 kpc. At this redshift the absolute magnitude would be $M_R \sim -20.6$ ($\sim 0.5L^*$ for a spiral galaxy; Nakamura et al. 2003). Since this object was not within the field of view for our HAWK-I imagery we cannot use any colour information to check that the host galaxy properties are consistent with the inferred redshift but the absolute magnitude implied seems consistent with typical galaxy luminosities. The

3 objects nearby have offsets of 0.7″, 3.0″ and 6.8″ respectively, labelled as A, B, C in Figure 3.7 corresponding to galaxies G3, G2 and G1 in Fong et al. (2012). All these objects are detected in our HAWK-I data with magnitudes $J(Vega) = 22.00 \pm 0.09$, 21.41 ± 0.10 and 20.70 ± 0.08 respectively, but with only objects B, C showing evidence for extension. However, only object C is clearly detected in our FORS data with $R(Vega) = 21.34$ and object B marginally detected.

To give an indication of whether these galaxies are strong candidates to be the host we ask what is the probability, $P_{\rm chance}$, that an unrelated galaxy of the same magnitude or brighter would be found within the given offset. This approach has been considered extensively for LGRBs and SGRBs (e.g., Bloom et al., 2002; Levan et al., 2008; Berger, 2010). Here we use a simplified version based on the offset between the SGRB position and the given galaxy and compare this to the distribution of such offsets in a large sample of random sky positions, as described in section 3.3.3. For source A associated with GRB 090305A we measure a value of $P_{\rm chance} = 0.05$ which, though a low value, does not provide a firm host association. Similarly, for GRB 091109B sources A and B have values of $P_{\rm chance} = 0.08$ and 0.10 respectively. For GRB 110112A all three host candidates have relatively higher $P_{\rm chance}$ values of 0.55, 0.37 and 0.46 with galaxy B having the lowest $P_{\rm chance}$ value.

Looking at the objects we detect in the field of GRB 111020A, in both our R and J band data, we find $P_{\rm chance}$ values of 0.003, 0.05, 0.07 and 0.05 for objects A (G3), B (G2), C (G1) and D. If object A (G3) is indeed a galaxy then this object is strongly associated and hence the GRB could be classified as "hosted". However, we caution that this field is at low galactic latitude and that this object could be a faint star. In addition, this object does not show significant evidence for extension and so we do not conclusively rule out the other galaxies as potential hosts.

3.3 Identifying hostless SGRBs

3.3.1 A sample of SGRBs

We utilise a sample of all SGRBs detected up to the end of 2011. This includes bursts with $T_{90} < 2$ s, and those bursts which have been declared short bursts with extended emission by the *Swift* team in the GCN circulars archive. Since we are interested in host identifications we further cull this input list to require at least an XRT detection of the afterglow, since BAT-only positions are insufficient to identify hosts with moderate to high confidence unless they are extremely bright (e.g. Levan et al. 2008). In addition, since we are interested in the host galaxies of these SGRBs, we do not list XRT-localised SGRBs where a host galaxy search has not been reasonably

attempted. By these criteria the sample includes 40 GRBs: 33 SGRBs with $T_{90} < 2\,\mathrm{s}$ and 7 with extended emission. Of these GRBs 26 are well-localised (2 with *Chandra* detections) and 14 are localised using the XRT ($\gtrsim 1.4''$ error circle radius). Our complete host galaxy sample along with some basic properties of the GRBs is shown in Table 3.4 and 3.5.

The optically-localised SGRB sample given in Table 3.4 has also been subdivided into those with small and large offsets. To do this we use the methodology of Fruchter et al. (2006) to calculate the fraction of total galaxy light in regions of lower surface brightness than at the position of the GRB, F_{light}. Any burst with $F_{light} > 0$ must be within the host and $F_{light} = 0$ indicates it is not. We use values of F_{light} from Fong et al. (2010), supplementing these with our own values based on our VLT imaging of GRB 080905A and GRB 090510. In the few cases when no F_{light} measurement is available we assume the GRBs are on the light of their hosts, especially since these GRBs are at low offsets.

GRB	T_{90}[a] (s)	Fluence[a] (10^{-7}erg cm^{-2})	F_{light}	Host mag (r'(AB))[b]	z	Offset (arcsec)	Offset (kpc)	Ref
On-host GRBs								
SGRBs								
051221A	1.40 ± 0.20	11.6 ± 0.4	0.54-0.65	21.99 ± 0.09	0.55	0.12 ± 0.04	0.76 ± 0.25	[1]-[3]
060121	1.97 ± 0.06[c]	38.7 ± 2.7[c]		26.2 ± 0.3	> 4.0	0.119 ± 0.046	-	[4]-[7]
070429B	0.50 ± 0.10	0.63 ± 0.10		23.18 ± 0.10	0.9023	0.6	4.7	[8]-[10]
070707	0.8 ± 0.2[d]	$2.07^{+0.06}_{-0.32}$[d]		27.45 ± 0.13[e]	< 3.6	0.1 ± 0.3	-	[11],[12]
070724A	0.40 ± 0.04	0.30 ± 0.07	0.19	20.56 ± 0.03	0.46	0.71 ± 2.1	4 ± 12	[3],[13],[14]
071227	1.80 ± 0.00	2.2 ± 0.3	0.19	20.66[f]	0.38	2.9 ± 0.4	15.0 ± 2.2	[3],[15],[16]
081226A	0.4 ± 0.1	0.99 ± 0.18		25.79 ± 0.34		< 0.5		[17],[18]
090426	1.20 ± 0.30	1.8 ± 0.3		24.47 ± 0.15[g]	2.6	0.1	0.8	[19]-[21]
100117A	0.30 ± 0.05	0.93 ± 0.13		24.33 ± 0.10	0.92	0.6	-	[22],[23]
111117A	0.47 ± 0.09	1.40 ± 0.18		23.6	$1.3^{+0.3}_{-0.2}$	1.25 ± 0.20	10.5 ± 1.7	[24]-[26]
EE GRBs								
050709	0.07 ± 0.01[c]	3.03 ± 0.38[c]	0.00-0.09	21.46 ± 0.2[f]	0.1606	1.33	3.64	[7],[27]-[29]
050724	3 ± 1	6.3 ± 1.0	0.03-0.33	18.36 ± 0.03[f]	0.258	0.64 ± 0.02	2.57 ± 0.08	[28],[30]-[32]
051227	8 ± 2	2.3 ± 0.3	0.66	$25.78^{0.18}_{0.12}$		0.05 ± 0.02	< 0.7	[16],[33],[34]
061006	130 ± 10	14.3 ± 1.4	0.56-0.63	24.18 ± 0.09	0.436	0.3 ± 0.3	3.5	[16],[34],[35]

070714B	64 ± 5	7.2 ± 0.9	0.26	25.39 ± 0.23^{f}	0.9225	0.4	3.1	[10],[36]
Off-host GRBs								
SGRBs								
060313	0.70 ± 0.1	11.3 ± 0.5	0.00-0.04	25.21 ± 0.20^{e}		0.4	-	[34],[37]
080905A	1.00 ± 0.10	1.4 ± 0.2	0.00	18.4 ± 0.5^{f}	0.122	9	18.5	[38],[39]
090510	0.30 ± 0.10	3.4 ± 0.4	0.00	23.4 ± 0.07	0.9	1.2	9.4	[40]-[42]
Hostless SGRBs								
SGRBs								
061201	0.80 ± 0.10	3.3 ± 0.3	-	18.09^{h}	0.111	16.2	32.4	[7],[43],[44]
070809	1.30 ± 0.10	1.0 ± 0.1	-	21.8 ± 0.3^{f}	0.473	6.0	35.4	[45]-[47]
090305A	0.4 ± 0.1	0.75 ± 0.13	-	25.64 ± 0.20		1.5	-	[48]
090515	0.04 ± 0.02	0.2 ± 0.08	-	20.2 ± 0.1	0.403	14	75.2	[47],[49],[50]
091109B	0.27 ± 0.05	1.9 ± 0.2	-	23.93 ± 0.1^{e}		3.0	-	[51]
110112A	0.5 ± 0.1	0.30 ± 0.09	-	21.55 ± 0.13^{i}		19.3	-	[52]
111020A	0.40 ± 0.09	0.65 ± 0.10	-	21.19 ± 0.05^{j}		6.7	-	[53],[54]
EE GRBs								
080503	170 ± 40	20 ± 1	-	27.02 ± 0.2^{k}	< 4	0.8	< 6.6	[47],[55],[56]

Table 3.4: Host galaxy details for all well-localised SGRBs up to April 2012 (25 GRBs). The designation of on-host, off-host is described in the main text. The host galaxy listed is the one with the lowest $P_{\rm chance}$ value.
Footnotes: (*a*) T_{90} and Fluence are given in the $15-150$ keV energy band unless otherwise stated. (*b*) All magnitudes in this Table are in the AB magnitude system and have values corrected for Galactic absorption (Schlegel et al., 1998). Where we do not know the galaxy magnitude in the r' band a colour correction is made from the magnitude in the closest filter using the most appropriate of the four standard SED templates (Sbc, Scd, Ell, Im) from Coleman et al. (1980) and the galaxy redshift where known. When the galaxy type is not known the Sbc template is used and where the redshift is unknown we use $z = 0.5$. (*c*) *HETE-2* trigger. T_{90} and Fluence of GRB 060121 are given in the $30-400$ keV energy band. (*d*) *INTEGRAL* trigger. T_{90} and Fluence of GRB 070707 are given in the $20-200$ keV energy band. (*e*) For GRBs 070707, 060313 and 091109B no redshift for the most likely host galaxy is available. R band magnitudes for these galaxies are converted to r' band using the Sbc template at $z = 0.5$. (*f*) R band magnitude of the host galaxies of GRBs 071227, 050709, 050724, 070714B, 080905A, 070809 have been converted using the known redshift and an appropriate galaxy type. (*g*) We convert the V band of the host galaxy of GRB 090426 to the r' band using the Irr galaxy template. (*h*) $F606W$ band magnitude of the host galaxy of GRB 061201 with the lowest $P_{\rm chance}$ has been converted to the r' band using known redshift and the Sbc galaxy type. (*i*) i' band magnitude of the galaxy with the lowest $P_{\rm chance}$ for GRB 110112A has been converted using $z = 0.5$ and the Sbc galaxy template. (*j*) J band magnitude of the galaxy with lowest $P_{\rm chance}$ for GRB 111020A has been converted to the r' band using $z = 0.5$ and the Sbc galaxy type. (*k*) $F606W$ band magnitude of the galaxy of GRB 080503 with the lowest $P_{\rm chance}$ has been converted to the r' band using $z = 1$ and the Sbc galaxy type. References: [1] Cummings et al. (2005) [2] Soderberg et al. (2006a) [3] Berger (2009) [4] Donaghy et al. (2006) [5] Levan et al. (2006a) [6] de Ugarte Postigo et al. (2006) [7] Fong et al. (2010) [8] Markwardt et al. (2007) [9] Perley et al. (2007a) [10] Cenko et al. (2008) [11] McGlynn et al. (2008) [12] Piranomonte et al. (2008) [13] Ziaeepour et al. (2007b) [14] Berger et al. (2009) [15] Sato et al. (2007) [16] D'Avanzo et al. (2009) [17] Krimm et al. (2008) [18] Nicuesa Guelbenzu et al. (2012b) [19] Sato et al. (2009) [20] Levesque et al. (2010a) [21] Antonelli et al. (2009) [22] De Pasquale et al. (2010) [23] Fong et al. (2011b) [24] Mangano et al. (2012) [25] Margutti et al. (2012) [26] Cucchiara and Cenko (2011) [27] Villasenor et al. (2005) [28] Troja et al. (2008) [29] Prochaska et al. (2006) [30] Krimm et al. (2005) [31] Prochaska et al. (2005) [32] Berger et al. (2005) [33] Hullinger et al. (2005) [34] Berger et al. (2007b) [35] Schady et al. (2006) [36] Racusin et al. (2007) [37] Markwardt et al. (2006) [38] Pagani et al. (2008) [39] Rowlinson et al. (2010a) [40] Hoversten et al. (2009) [41] Rau et al. (2009) [42] McBreen et al. (2010) [43] Marshall et al. (2006) [44] Stratta et al. (2007) [45] Marshall et al. (2007) [46] Perley et al. (2008) [47] Berger (2010) [48] Krimm et al. (2009) [49] Barthelmy et al. (2009) [50] Rowlinson et al. (2010b) [51] Oates et al. (2009a) [52] Barthelmy et al. (2011) [53] Sakamoto et al. (2011a) [54] Fong et al. (2012) [55] Mao et al. (2008) [56] Perley et al. (2009a)

GRB	T_{90}[a] (s)	Fluence[a] (10^{-7}erg cm^{-2})	Host mag (r'(AB))[b]	z	Offset (arcsec)	Offset (kpc)	X-ray error radius (arcsec)	Ref
SGRBs								
050509B	0.13	0.23 ± 0.09	17.18 ± 0.05[c]	0.2248	17.7	63.4	3.4	[1]-[4]
050813	0.6 ± 0.1	1.24 ± 0.46	24.18 ± 0.07[c]	0.719	4.9	35.5	2.9	[5],[6]
051210	1.27 ± 0.05	0.83 ± 0.14	23.80 ± 0.15	$\gtrsim 1.4$	2.9	> 24.9	2.9	[7],[8]
060502B	0.09 ± 0.02	0.4 ± 0.05	19.17 ± 0.01[c]	0.287	17.1	73.3	4.36	[9],[10]
060801	0.5 ± 0.1	0.81 ± 0.10	23.20 ± 0.11	1.1304	2.1	17.6	1.5	[8],[11]
061217	0.212 ± 0.041	0.46 ± 0.8	23.33 ± 0.07	0.827	1.9	14.4	1.89	[8],[12]
070729	0.9 ± 0.1	1.0 ± 0.2	23.70 ± 0.25[d]		10.0	-	2.5	[4],[13]
090621B	0.14 ± 0.04	0.70 ± 0.10	21.76 ± 0.11[d]		11.5	-	5.1	[14],[15]
100206A	0.12 ± 0.03	1.4 ± 0.2	21.3 ± 0.3[d]		3.7	-	2.1	[16],[17]
100625A	0.33 ± 0.03	2.3 ± 0.2	~ 23		0.5	-	1.8	[18]-[20]
101219A	0.6 ± 0.2	4.6 ± 0.3	~ 24.2[e]	0.718	0.5	3.5	2.4	[21]-[24]
101224A	0.2 ± 0.01	0.58 ± 0.11	20.8 ± 0.2[f]		~ 0.5	-	3.2	[25]-[27]
111222A	0.32[g]	72 ± 7[g]	18.08 ± 0.01		0.48	-	2.9	[28],[29]
EE GRBs								
061210	85 ± 5	11 ± 2	21.00 ± 0.02	0.4095	2.9	15.6	1.8	[8],[30]

Table 3.5: Host galaxy details, where available, for XRT-localised SGRBs up to April 2012 (16 GRBs). The host galaxy listed is the one with the lowest $P_{\rm chance}$ value.
Footnotes: (*a*) As for Table 3.4, T_{90} and Fluence are given in the $15-150\,$keV energy band unless otherwise stated. (*b*) As for Table 3.4 all magnitudes in this table are in the AB magnitude system and have values corrected for Galactic absorption (Schlegel et al., 1998). Where we do not know the galaxy magnitude in the r' band a colour correction is made from the magnitude in the closest filter using the most appropriate of the four standard SED templates (Sbc, Scd, Ell, Im) from Coleman et al. (1980) and the galaxy redshift where known. When the galaxy type is not known the Sbc template is used. (*c*) R band magnitude of the host galaxies of GRBs 050509B, 050813, 060502B have been converted using the known redshift and the Ell galaxy type. (*d*) For GRBs 070729, 090621B and 100206A no redshift for the most likely host galaxy is available. R band magnitudes for these galaxies are converted to r' band using the Sbc template at $z = 0.5$. (*e*) The i' magnitude for the host of GRB 101219A has been converted to the r' band using the Sbc template at $z = 0.718$. (*f*) V band magnitude of the most likely host galaxy of GRB 101224A has been converted using the Sbc template at $z = 0.5$. (*g*) *INTEGRAL* trigger. T_{90} and Fluence of GRB 111222A are given in the $20\,$keV $-\,3\,$MeV energy band and were measured by the *Konus-Wind* instrument.
References: [1] Barthelmy et al. (2005a) [2] Bloom et al. (2006) [3] Fong et al. (2010) [4] Berger (2009) [5] Sato et al. (2005a) [6] Prochaska et al. (2006) [7] Sato et al. (2005b) [8] Berger et al. (2007b) [9] Sato et al. (2006a) [10] Bloom et al. (2007) [11] Sato et al. (2006b) [12] Ziaeepour et al. (2007a) [13] Guidorzi et al. (2007) [14] Curran et al. (2009) [15] Galeev et al. (2009) [16] Krimm et al. (2010a) [17] Miller et al. (2010) [18] Holland et al. (2010) [19] Levan and Tanvir (2010) [20] Tanvir and Levan (2010) [21] Krimm et al. (2010b) [22] Chornock et al. (2010) [23] Cenko et al. (2010) [24] Perley et al. (2010) [25] Krimm et al. (2011) [26] Nugent and Bloom (2010) [27] Xu et al. (2010) [28] Golenetskii et al. (2011) [29] Siegel and Grupe (2011) [30] Cannizzo et al. (2006)

3.3.2 Limitations of $P_{\rm chance}$

Probabilistic arguments of the sort outlined above have been used to argue for host galaxy associations for many *Swift* SGRBs (e.g. Prochaska et al. 2006; Kocevski et al. 2010; Rowlinson et al. 2010a; McBreen et al. 2010). However, $P_{\rm chance}$ is calculated as an independent quantity for each galaxy considered, meaning that for some SGRBs there are several galaxies with roughly similar $P_{\rm chance}$ values. This potentially produces a degeneracy in identification of candidate hosts between bright galaxies with large offsets and faint galaxies with small offsets (Berger, 2010), as seen for GRBs 091109B and 111020A.

If NS binary mergers are indeed responsible for the creation of SGRBs then we may expect larger offsets due to both the natal kick and the delay in merger time after creation (potentially $\sim 10^9$ yrs). Figure 3.8 shows typical NS binary merger sites with respect to a spiral host galaxy with $R(Vega) = 23$ at $z = 1$, slightly less luminous ($M_R \sim -22.5$) than the Milky Way (from Church et al. 2011). We include both the case of NS binary systems formed through a primordial channel and a dynamical channel within globular clusters (GCs), where a neutron star captures a companion through three-body interactions (Grindlay et al., 2006). We compare this with the $P_{\rm chance}$ values we would measure as a function of projected offset (in kpc) highlighting the areas where $P_{\rm chance}$ is 2% and 5%. This demonstrates that for NS binary mergers we would expect a significant fraction to merge at a point where we can no longer associate the resulting explosion with the host galaxy from which it originated (see also Berger 2010). This problem becomes even more acute when considering fainter galaxies. A lower luminosity galaxy at the same redshift will have significantly higher $P_{\rm chance}$ at moderate offsets, making a firm association difficult. Furthermore, the weaker potential for the galaxy means it will retain a smaller fraction of its binaries (e.g. Zemp et al., 2009). In other words, in any kicked scenario we would expect a significant fraction of bursts for which we cannot identify any host galaxy. The implications this could have for hostless GRBs are further discussed in section 3.4.2.

3.3.3 A diagnostic tool to help investigate short burst host associations

In the search for the hosts of apparently hostless GRBs, galaxies with the lowest $P_{\rm chance}$ are still often cited as the most likely host galaxies, even if there is no outstandingly good candidate (e.g. Stratta et al. 2007; Perley et al. 2009a; Berger 2010). This problem is compounded by the limitations of $P_{\rm chance}$ noted in section

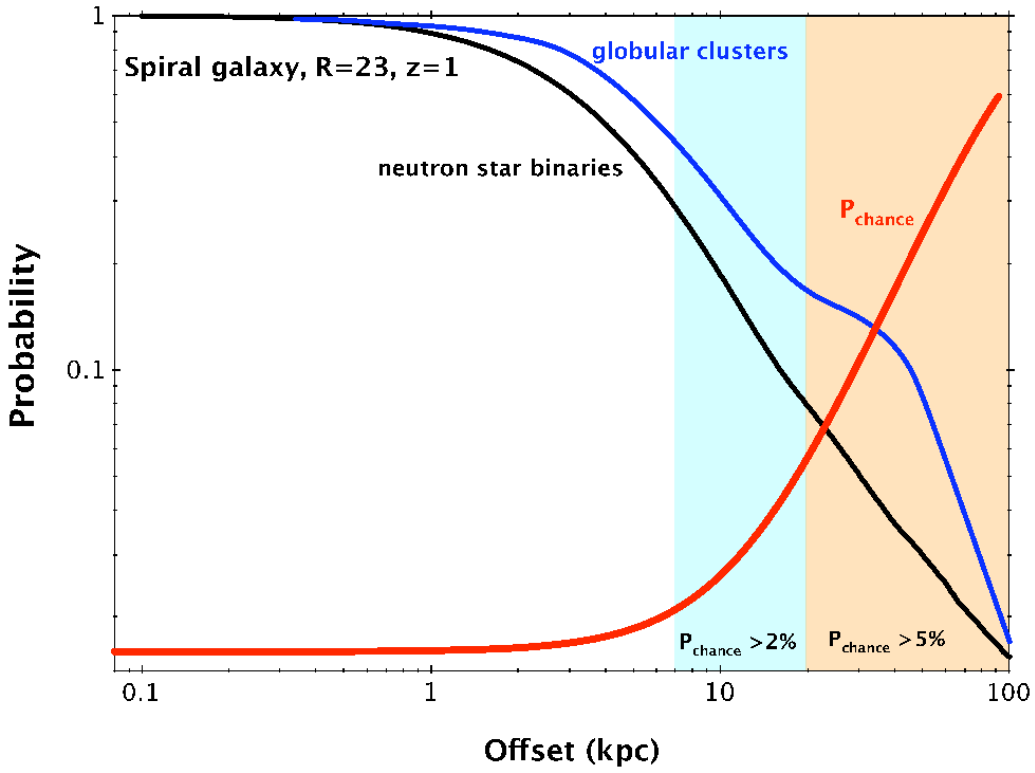

Figure 3.8: This plot shows the distribution of NS binary mergers with respect to a Milky Way-like spiral galaxy at $z = 1$. This is shown for both the primordial and the dynamical channel of NS binary formation. The value of $P_{\rm chance}$ we would expect for this galaxy at $R(Vega) = 23$ are also shown with the 2% and 5% $P_{\rm chance}$ areas highlighted.

3.2. To better assess this we took 15,000 random positions within the footprints of the Sloan Digital Sky Survey (SDSS) (Abazajian et al., 2009) and the Cosmological Evolution Survey (COSMOS) (Capak et al., 2007), and used the measured galaxy data available within these surveys to find the nearest galaxies brighter than a given magnitude. The galaxy magnitude range chosen was reflective of SGRB host galaxies, using SDSS data at the bright end ($15 - 22.5\,\mathrm{mag}$) and supplementing this with data from the Subaru telescope in the COSMOS survey at the faint end ($> 23\,\mathrm{mag}$). We applied a magnitude zero-point offset from the Subaru r^+ filter to SDSS r' of $r' = r^+ + 0.12$, determined by comparing magnitudes from a random sample of galaxies detected in both surveys.

The galaxy distribution is shown in Figure 3.9 along with the enclosing percentiles (1%, 5%, 10%, 15% and 50% percentiles) of the distribution, i.e. beyond the 1% line only 1% of the galaxies in the sample have magnitude $< r'$ and are at offset $<$ observed. Also shown are the putative host galaxies of the SGRB population. We would expect any well constrained host galaxy (by P_{chance} or similar probabilistic measure) to be an outlier to the main galaxy distribution and, indeed, we see that all strongly associated SGRB host galaxies lie below the 1% percentile line. For hostless GRBs, however, the proposed host galaxies lie closer to the background galaxy distribution.

We can use the division between GRBs strongly associated with their host galaxies and those considered hostless shown on Figure 3.9 to define an 'association radius', δx. For a galaxy of a given magnitude, this is the offset from the centre of the putative host galaxy within which we can say the GRB is strongly associated, specifically there is a less than 1% chance that an unrelated galaxy of this magnitude (or brighter) would appear within this distance. Conversely, if a GRB does not fall within this radius for *any* nearby galaxy then we chose to describe it as hostless. δx (in arcseconds) is given by Equation 3.1.

$$\delta x = 0.17 \times 10^{13}\, m_r^{-\gamma} \tag{3.1}$$

where m_r is the r' band AB magnitude of the suggested host galaxy and $\gamma = 8.84$ describes the best-fit power law dependence and is an empirical fit to the data. Hence, we can define a hostless SGRB where the position of the GRB (allowing for the error box) does not fall within the association radius of any nearby galaxies. The choice of association radius clearly depends on the minimum probability that one is prepared to accept (e.g. one could prescribe differing radii at different confidence

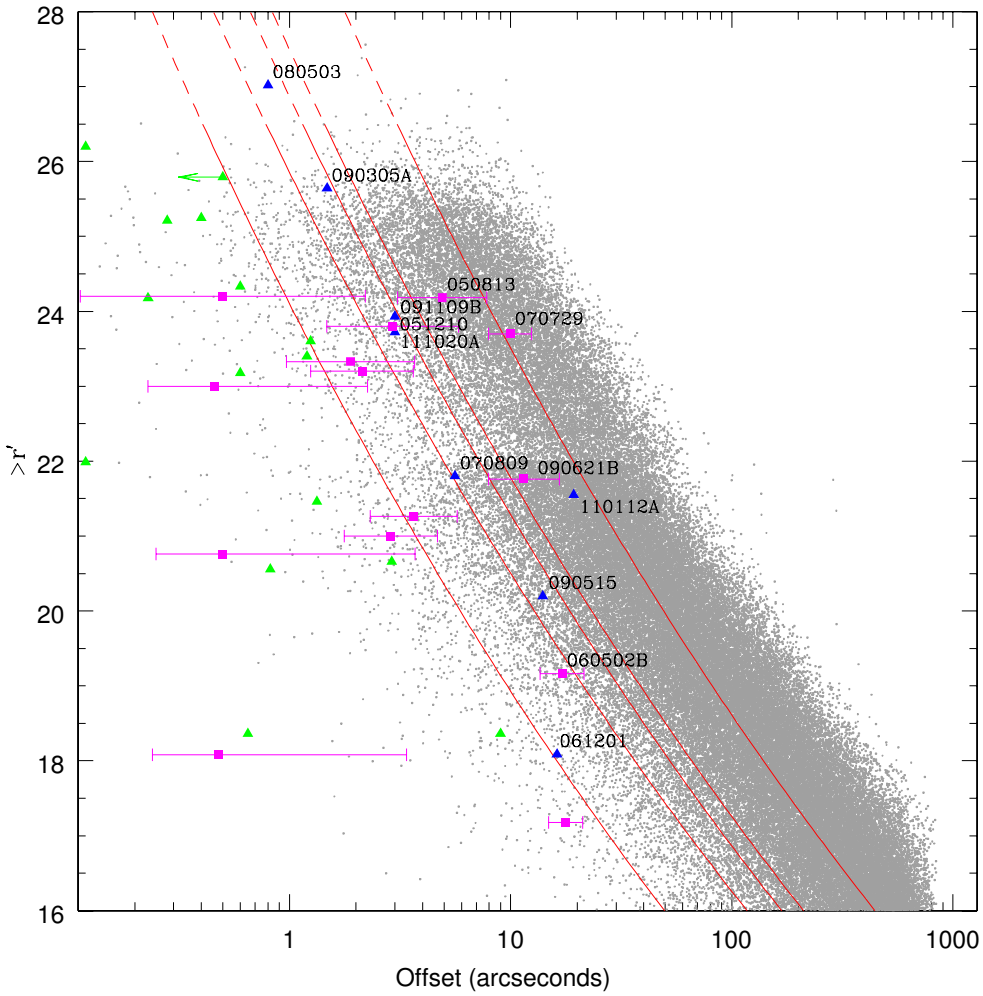

Figure 3.9: Using random positions in the Sloan Digital Sky Survey (SDSS) and the Subaru telescope in the Cosmological Evolution Survey (COSMOS) we have plotted the minimum offsets for galaxies brighter than a given r' AB magnitude for 15,000 random positions. The solid red lines are the 1%, 5%, 10%, 15% and 50% percentiles for this dataset, with the dotted lines showing the extrapolation of the fit beyond our dataset. We have plotted the galaxies with the lowest $P_{\rm chance}$ for all SGRBs with optical (or CXO) localisations (green and blue triangles) and for SGRBs with only *Swift*/XRT positions (magenta squares). The blue triangles represent galaxies in the field of hostless SGRBs, with only one galaxy being included for each GRB. All well-constrained host galaxies (green triangles) lie below the 1% percentile line.

levels). However, the 1% (3σ) contour is broadly applicable, and would suggest for our sample of ~ 20 SGRBs we may expect one to be falsely associated with a galaxy which is not its host. Using this approach we identify a total of seven (eight) hostless SGRBs, 061201, 070809, 080503, 090305A, 090515, 091109B, 110112A (and potentially 111020A).

We also note that 4 of the XRT-localised GRBs are potentially hostless: 050813, 060502B, 070729 and 090621B. For GRB 090621B, however, this may be due to the lack of a deep search thus far.

We can now compare the galaxies with the lowest $P_{\rm chance}$ values ($P_{\rm chance,min}$) for our seven (eight with our potential host of GRB 111020A) bursts to the distribution of random locations on the sky. This will allow us to ascertain if this sample of events, originate from the underlying galaxy distribution, as might be expected for local, but kicked SGRBs, or are essentially uncorrelated, as might be expected for SGRBs originating from higher redshift. To do this for each random location we identify the galaxy with the minimum $P_{\rm chance}$, and hence arrive at a distribution of $P_{\rm chance,min}$ for all random locations. The $P_{\rm chance}$ values can be calculated using the percentile lines themselves. The percentiles are calculated by binning the magnitude distribution ($\Delta m = 0.1$ increment) and calculating the offset value for each percentile within each bin. The lines for multiple percentiles are calculated using the same formulaic form as Equation 3.1. $P_{\rm chance}$ itself is then based on these percentile lines. This is shown graphically in Figure 3.10. The $P_{\rm chance}$ values for the galaxies considered have been given in section 3.2.5. Note that although $P_{\rm chance,min}$ is strictly a function of the galaxy magnitude range considered, the span of galaxies covered by our joint SDSS/COSMOS analysis is fairly representative of the typical range accessible in our GRB host fields. The Kolmogorov-Smirnov (KS) test probability that the hostless SGRB positions are drawn from an underlying random distribution of the sky is $P_{KS} = 0.19$, which is not a rejection of this statement.

Interestingly, as can also be seen in Figure 3.10, comparison between the $P_{chance,min}$ distributions of the hostless GRBs and the random sample with $P_{\rm chance}$ calculated from the method of Bloom et al. (2002) ($P_{\rm chance,B}$) would give a rejection ($P_{KS} = 0.01$). Bloom et al. (2002) assume the surface distribution of galaxies is uniform, ignoring the clustering of galaxies, and defining $P_{\rm chance,B}$ as

$$P_{\rm chance,B} = 1 - \exp(-\eta) \tag{3.2}$$

where η is the expected number of galaxies in a circle with effective radius r given by $\eta = \pi r^2 \sigma(\leq m)$. $\sigma(\leq m)$ is the mean surface density of galaxies brighter than magnitude m in the R band and is based on deep optical galaxy surveys

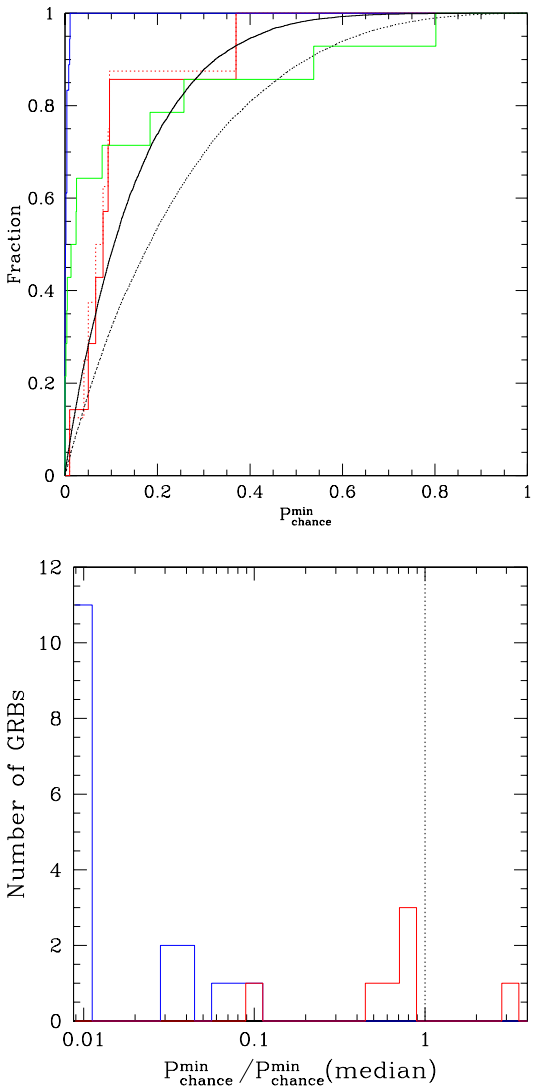

Figure 3.10: The upper plot shows the cumulative distribution of $P_{\rm chance,min}$ for a set of 15,000 random positions within the SDSS and COSMOS footprints (black line). For comparison, the $P_{\rm chance,min}$ values calculated using the method of Bloom et al. (2002) (dotted black line) are included. This is clearly distinct from the $P_{\rm chance}$ values calculated with the method outlined in the text. Also shown is the cumulative distribution of $P_{\rm chance,min}$ for the well-localised SGRBs with a host galaxy (blue), hostless SGRBs (red) and the *Swift*/XRT only detected SGRBs (green). The dotted red line is the hostless sample with the inclusion of a our identified galaxy (galaxy B) for GRB 111020A, but this is uncertain due to the presence of another object close-by which could be a faint star as explained in the text. The lower plot shows a histogram of the ratios of the $P_{\rm chance,min}$ values to the median of the random galaxy distribution, for all the well-localised SGRBs in our sample. As for the upper plot the hostless GRBs are shown in red and the other well-localised GRBs in blue. A KS test of these distributions compared to the random positions does not show that these populations are statistically distinct. However, looking at the median values does show that a significant fraction (6/7) of secure hostless cases the $P_{chance,min}$ values are less than the median value for the random galaxy distribution.

(Hogg et al., 1997; Beckwith et al., 2006). There is clearly a distinction between this $P_{\rm chance,B}$ calculation for the random sample and the method we have developed especially given the stronger rejection when compared with the hostless $P_{chance,B,min}$ values. This could be due to the assumption of unformity and may reflect that the clustering of galaxies may be more significant on the scales we consider here.

In figure 3.10 in addition to direct comparison we also compare the $P_{\rm chance,min}$ values for the hostless GRBs to the median of the random galaxy distribution, looking only at galaxies above the limiting magnitude placed on each individual hostless GRB. In this case we find that in 6/7 secure hostless cases (i.e. excluding GRB 111020A) the $P_{\rm chance,min}$ value is less than the median. Only in the case of GRB 110112A do we find that the $P_{\rm chance,min}$ value is greater than the median. For a random sky distribution we would expect to sample this distribution evenly and the binomial probability of 6/7 (7/8) events lying at less than the median is 0.0547 (0.0313), suggestive that we are observing SGRBs from local structure in their fields.

Hence, these results provide some evidence that we are observing SGRBs that are correlated with large scale structure on the sky, even if the individual host galaxy that we identify with $P_{chance,min}$ is not the true host. This may reflect that these bursts are kicked from relatively low redshift, and relatively luminous galaxies. However, it is also possible that we are observing these SGRBs from moderately massive structures at higher redshift, and hence the low values for $P_{chance,min}$ are actually reflecting other cluster members. Early estimates from Berger et al. (2007a) put the percentage of SGRBs in clusters at $\sim 20\%$ (e.g. Bloom et al. 2006; Levan et al. 2008), though further studies of this nature have yet to be published. Hence this possibility is not necessarily unlikely.

Furthermore, the galaxies identified with lowest $P_{\rm chance}$ in these cases are likely to be relatively massive, such galaxies are more likely to retain any dynamically kicked systems within their haloes. In contrast, lower mass galaxies have a much larger escape fraction, and are more likely to create a population of hostless SGRBs (see also Bloom et al. 2002; Fryer et al. 1999a). Alternatively, the relative offsets from the galaxies with lowest $P_{\rm chance}$ is broadly consistent ($< 50\,$kpc) with the presence of globular cluster systems within these hosts in at least some cases. In this case it may be that we are observing a population of dynamically formed binaries within these globular clusters, and that, given the typically large distances we cannot directly observe the host cluster (e.g. Grindlay et al. 2006; Salvaterra et al. 2008; Church et al. 2011).

3.4 Discussion

By considering the locations of SGRBs relative to random locations on the sky we have shown that even those SGRBs for which it is most difficult to unambiguously identify a host are likely to be at moderate redshift ($z \leq 1$). However, it is possible that rather than observing the hosts themselves, we instead are tracing larger scale structure.

3.4.1 Constraints on the possibility of high-redshift host galaxies

We can use the 3σ point source detection limits at the locations of the hostless GRBs in our sample to place constraints on the possibility of a coincident host galaxy. For increasing redshift we can determine the minimum galaxy luminosity, L_{lim} as a fraction of L^* (the characteristic luminosity of the knee of the Schechter luminosity function; Schechter, 1976), we would be able to detect in a given filter. To do this we used an evolving Schechter galaxy luminosity function where the number density of galaxies per unit luminosity, $\phi(L)$, is given by Equation 3.3.

$$\phi(L)dL = \phi^* \left(\frac{L}{L^*}\right)^{\alpha} \exp\left(-\frac{L}{L^*}\right) \frac{dL}{L^*} \tag{3.3}$$

Using L_{lim} we can determine the probability of detection of a galaxy, P_{detect}, as given in Equation 3.4

$$P_{detect} = \int_{L_{low}}^{L_{lim}} L\phi(L)dL \Big/ \int_{L_{low}}^{\infty} L\phi(L)dL \tag{3.4}$$

where we define $M_{low} = -10$ as the magnitude corresponding to a suitable lower limit on galaxy luminosities. This definition of P_{detect} given in Equation 3.4 is made under the simplifying assumption that the likelihood of a galaxy producing an SGRB is proportional to its luminosity.[1] Specifically, P_{detect} describes the fraction of the luminosity-weighted luminosity function that we probe with increasing redshift. To perform this analysis we used the templates for Sbc, Elliptical (Ell) and Irregular (Irr) galaxies from Coleman et al. (1980) and considered magnitudes in the SDSS r' band. We note that the templates used are based on agregates of observed local galaxies and so includes typical levels of extinction appropriate for the galaxy type. In addition, we have neglected the effect of surface brightness dimming, but we expect this to be a small effect for these sources which are only marginally resolved.

For increasing redshift we use a simple linear evolution of the luminosity function, investigating the magnitudes in the SDSS r' band up to $z = 4$. We use

[1] But see also Belczynski et al. (2006)

a value of $M_r^* = -21.48$ at $z = 0$ from Montero-Dorta and Prada (2009) and an adapted value for $M_r^* = -22.88$ at $z = 2.0$ from Ilbert et al. (2005), using $r'(AB) = R(AB) + 0.06$ (Sbc), $= R(AB) + 0.06$ (Ell) and $= R(AB) + 0.04$ (Irr) appropriate for the galaxy templates used (Coleman et al., 1980). Similarly we also evolved α from $\alpha_{z=0} = -1.26$ at $z = 0$ (Montero-Dorta and Prada, 2009) to $\alpha_{z=2} = -1.53$ at $z = 2$ (Ilbert et al., 2005).[2]

Figure 3.11 shows this analysis using the detection limits determined for all the hostless GRBs in our sample. We use our measured deepest r' limits placed on GRB 090305A, 091109B (both adapted from the VLT R band limits) and 110112A (extrapolated from the Gemini North i' band). We have also included published limits for GRBs 061201, 070809, 080503, 090515 and 111020A (Perley et al., 2009a; Berger, 2010; Fong et al., 2012) again adapted to the r' band where necessary. There is a deeper limiting magnitude for GRB 111020A from Fong et al. (2011a) and hence this value is used here rather than our reported limit.

Looking at the redshift range thought to be typical for SGRBs ($z < 1$) we find for at least six of the bursts we uncover $\sim 85\%$ of the integrated galaxy luminosity for the Irr galaxy type, $\sim 73\%$ Sbc galaxy type and 55% for the Ell galaxy type. In addition, the extremely deep limit placed on GRB 080503 means that even for the Ell galaxy type we uncover 88% of the integrated galaxy luminosity.

This analysis suggests that it is unlikely that the hostless SGRBs are simply cases of faint, but coincident, hosts in the redshift range for $z < 1$, though this case is less strong for Ell galaxies. Higher redshifts, however, up to e.g., $z \sim 4$, are not ruled out by observations of the afterglows or the limits on coincident host galaxies. In addition, detection of the afterglow of GRB 091109B in the R band and GRB 090305A in the g' band allows us to place upper redshift limits of $z \lesssim 5$ and $z \lesssim 3.5$, respectively.

Though the majority of SGRBs have been found at redshifts in the range $0.1-0.9$ there is some evidence indicating the existence of a higher redshift population. GRB 090426 has the highest confirmed redshift ($z = 2.609$) of a GRB with $T_{90} < 2\,\mathrm{s}$ (Levesque et al., 2010a; Thöne et al., 2011). However, there remains considerable discussion as to its nature with its host galaxy, environment and spectral properties being more suggestive of a massive star progenitor than a compact binary merger despite its short duration (Antonelli et al., 2009; Levesque et al., 2010a; Xin et al., 2010; Thöne et al., 2011). There is potential evidence for other SGRBs at high redshift with indications for a $z > 4.0$ host for GRB 060121 (Levan et al., 2006a; de

[2]The minimum galaxy luminosity detectable with our detection limits, L_{lim}, is determined using the *python* astSED module as part of the astLib package.

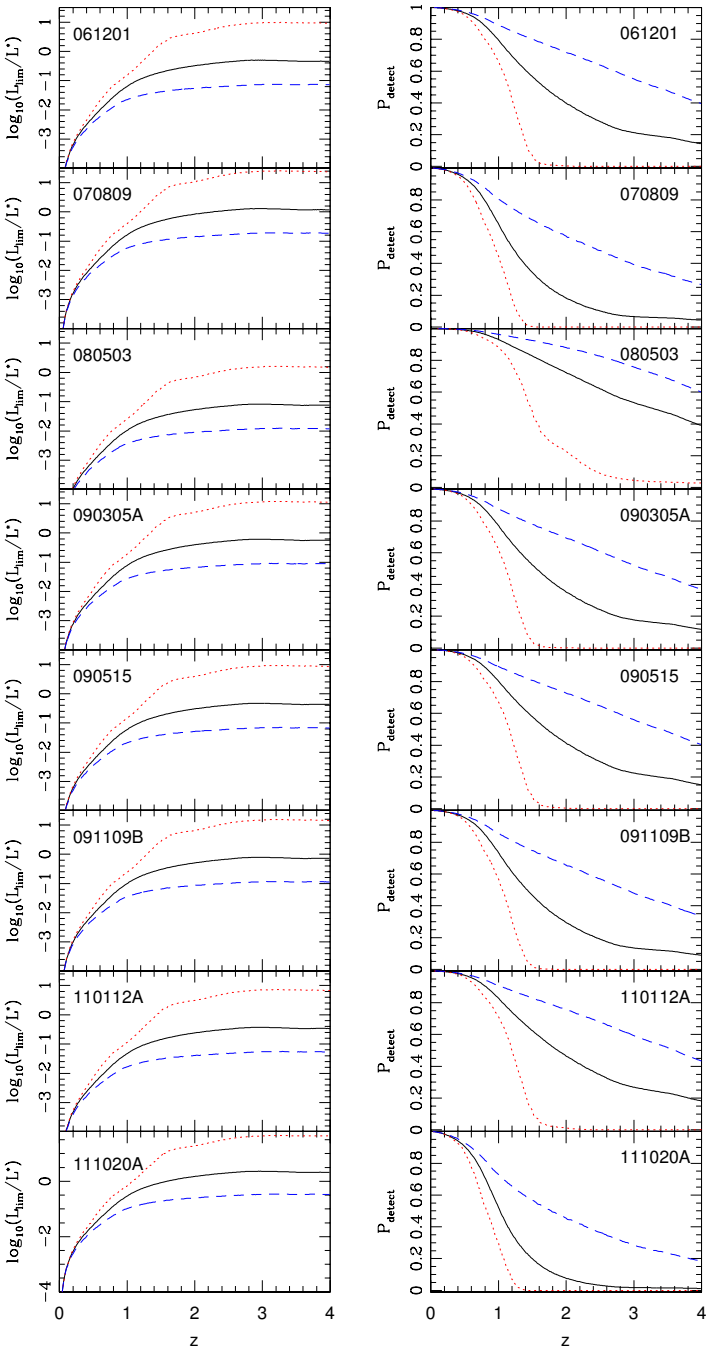

Figure 3.11: The set of panels on the left hand side show the minimum luminosity galaxy, L_{lim}, we could detect as a function of redshift in the SDSS r' band and based on the deepest available magnitude limits of all the hostless GRBs in our sample. Each of these panels contains this evolution for an Sbc (black, solid line), Ell (red, dotted line) and Irr (blue, dashed line) galaxy. This includes a simple linear evolution of the luminosity function with redshift. Using these L_{lim} values, we then plot the fraction of the integrated luminosity we probe at increasing redshift in the right hand set of panels (P_{detect}). This is again shown for the three types of galaxies we consider here.

Ugarte Postigo et al., 2006), beyond the redshift detection limits we have placed for a fainter galaxy, and the faint, possibly high redshift hosts of GRB 060313 ($z \lesssim 1.7$) (Schady and Pagani, 2006) and GRB 051227 (Berger et al., 2007b). In particular, GRB 070707 ($z < 3.6$), has a very faint coincident host at $R \sim 27$ (Piranomonte et al., 2008). These results may indicate that hostless GRBs are a window onto a higher redshift population. However, some hostless SGRBs have been probed to deep limits, especially GRB 080503 with a limit of F606W > 28.5 from *HST* (Perley et al., 2009a). If the delay-time distribution for SGRB progenitors is long, then we would expect to preferentially see them at lower redshift. Under the binary neutron star model a significant component will be created around the peak of the Universal star formation rate and so will merge in a time $\sim 10^9$ yrs after this era (O'Shaughnessy et al., 2008).

A further constraint on the high redshift scenario can be obtained simply by contrasting the properties of the long and short host populations. To first order, LGRBs should trace the global star formation rate (allowing for plausible biases introduced by metallicity, which could increase the high-z, low-Z rate). In contrast, SGRBs (assuming they have a stellar progenitor), trace the star formation rate convolved with a delay time distribution. In other words, in general we would expect the SGRB redshift distribution to be skewed towards lower redshifts, than for the LGRBs. The samples of Fruchter et al. (2006); Savaglio et al. (2009); Svensson et al. (2010) all measured $15 - 20\%$ of the optically localised LGRB host galaxies have $R > 26.5$. However, the TOUGH survey (The optically unbiased GRB host survey) (Hjorth et al., 2012) find this value to be 30%. To these same limits $\sim 30\%$ of SGRBs are "hostless" meaning that from this comparison we cannot draw a strong conclusion either way. However, we find the limits outlined above and coupled with the fact we see more clustering of the hostless GRBs towards galaxies at low redshift than we would expect compared to random galaxies suggestive for a low redshift origin.

3.4.2 The low redshift scenario

The apparent preference for hostless SGRB sight lines to lie close to bright galaxies, with low $P_{\rm chance}$ relative to random positions on the sky, offers support for models in which we are observing the hostless SGRBs to arise from systems kicked from their hosts at high velocities (several hundred $\mathrm{km\,s^{-1}}$), and most likely with significant time between their creation and explosion as a GRB ($\sim 10^9$ yrs). For the seven secure hostless GRBs in our sample, using $z = 0.5$ where the redshift is unknown, the average offset is ~ 42 kpc with offsets ranging from $\lesssim 6.6$ kpc to ~ 118 kpc.

We consider this our preferred explanation of the hostless SGRBs and consider the implications here.

For the limited sample of (12) SGRBs with optical positions, confidently identified host galaxies and measured redshifts, the physical offsets shown in Table 3.4 are mostly relatively low (e.g. 051221A, 050724, 070714B), with an overall mean of ≈ 6 kpc. There are some, however, which are further from their host galaxy centres either in the outskirts (e.g. 080905A, 071227) or outside of the host galaxy (e.g. 070429B, 090510). For the hostless SGRBs physical offsets > 30 kpc are measured for the suggested host galaxies with confirmed redshifts (e.g. 061201, 070809, 090515) (Fong et al., 2010; Berger, 2010; Rowlinson et al., 2010b) and $\gtrsim 6$ kpc for the cases with only an upper limit on the redshift (e.g. 080503) (Perley et al., 2009a).

Within the considerable uncertainties, the measured SGRB offset distribution (assuming the galaxy with the lowest $P_{\rm chance}$ is the host in the hostless cases) does appear broadly consistent with predictions for the positions of NS-NS and NS-BH binary mergers using host galaxies of mass comparable to the Milky Way (Fong et al., 2010) and using estimated galaxy masses for the SGRBs (Church et al., 2011). However, in some individual cases, the offsets from the galaxies with the lowest $P_{\rm chance}$ are surprisingly large given these predictions, including hostless GRBs 060121, 070809 and XRT-localised 060502B (Church et al., 2011).

Larger offsets would also be a natural product of neutron star binary progenitors formed via a dynamical channel within globular clusters (GCs) where a neutron star captures a companion through three-body interactions (Grindlay et al., 2006). For GRBs 061201 and 070809 Salvaterra et al. (2010) suggested that their bright afterglows preclude a location in the IGM and suggested the dynamical channel as the most likely solution. However, SGRBs with optical afterglows have been detected outside their host galaxies, most likely within a low density medium if not within the IGM, meaning at least in some cases that the afterglow can be detected (Berger, 2011). Indeed, for the hostless GRBs presented here, along with GRB 090515 (Rowlinson et al., 2010b), their faint afterglows could be in line with their being embedded within the IGM, with detection being possible since they are at low redshift.

Another important consideration is that lower mass host galaxies, due to their shallower potential wells and therefore lower escape velocities, should typically exhibit larger burst offsets due to unbound binaries. For dwarf galaxies we would expect a non-negligible fraction of binary mergers to be found > 30 kpc from their host centres (Bloom et al., 2002). Using an evolving galactic potential, the merger sites may be even more diffusively distributed with respect to their host galaxies and

may occur out to a few Mpc for lighter halos (Zemp et al., 2009). Particularly given that for dwarf galaxies, even at moderate redshifts ($z \sim 1$), their intrinsic faintness would make them more difficult to detect, this means that it would be more difficult to associate such a SGRB with its low mass host galaxy and so these cases would appear as being hostless. In this case it could be that these fainter galaxies are within the halo of a larger galaxy and this is the reason we're seeing a suggested association with larger galaxies at low redshift.

3.4.3 Implications for co-incident gravitational waves

The prime means by which an unambiguous association between SGRBs and compact object binaries may be determined is the observation of a simultaneous gravitational wave signal (Phinney, 1991; Abadie et al., 2010). Such signals should be detectable to next generation GW detectors to distances of $\sim 500\,\mathrm{Mpc}$ NS-NS and $\sim 1\,\mathrm{Gpc}$ NS-BH (Abadie et al., 2010). To date, relatively few of the detected SGRBs fall within this horizon (formally only the lowest $z = 0.105$, GRB 080905A Rowlinson et al. 2010a is consistent with NS-NS or NS-BH detection), suggesting in common with independant analysis (e.g. Abbott et al. 2010) that simultaneous detections with *Swift* and GW detectors will be rare. One possibility which could increase the event rate would be if the hostless SGRBs were in fact kicked from local structures within the horizon of the new advanced detectors. Our observations suggest that in general this is not the case, most of the candidate host galaxies are too faint to lie within this volume, and there are not many bright galaxies within several arcminutes (corresponding to projected distances of several hundred kpc at a distance of 100 Mpc) of the GRB positions.

In the case of GRB 111020A there is an apparently local galaxy with low P_{chance}. This galaxy, at an apparent distance of $\sim 80\,\mathrm{Mpc}$ is comfortably within the threshold for GW detection with next generation instrumentation, although in this case the energy release of the burst of $E_{iso} \sim 10^{46}$ ergs would be far lower than typical for SGRBs, while the offset from the host would strongly disfavour events akin to soft-gamma repeaters (Hurley et al., 2005; Tanvir et al., 2005). In addition, for the rest of the hostless SGRB sample we searched the NASA extragalactic database (NED)[3] (Schmitz et al., 2011) for any bright, low redshift host within $10'$ of the GRB position. Galaxy 2MASX J13350593-2206302 (also designated 6dFGS gJ133506.0-220631 in the 6dFGS catalog) is detected within $50''$ of GRB 070809 with magnitude $R = 15.38$ (Jones et al., 2004, 2009). With redshift $z = 0.042783$ (Paturel et al., 2003) this galaxy is within 190 Mpc, again within the GW detection volume. These

[3]http://ned.ipac.caltech.edu/

situations are rather similar to the more poorly constrained case of GRB 050906 (Levan et al., 2008) whose γ-ray only position places it close on the sky to IC 328, and whose energy (if associated with IC 328) would be similar.

These results suggest that we should expect to see a handful of SGRBs within the GW horizon per year (all sky), but also imply that the hostless SGRBs likely contribute no more to this population than those with optically identified hosts.

3.5 Conclusions

We have looked at the afterglow properties of three apparently hostless SGRBs: GRB 090305A, GRB 091109B and GRB 111020A. The former, in particular, had a very faint X-ray counterpart, only identified due to the detection of the optical afterglow within the BAT error circle. In addition, redshift limits of $z \lesssim 5$ and $z \lesssim 3.5$ for GRBs 091109B and 090305A can be placed due to their detection in the R and g' band respectively.

Deep optical observations at the GRB position after the afterglow had faded allows us to put constraints on any coincident host galaxy, specifically the 3σ limiting magnitude for GRB 090305A is $r'(AB) > 25.69$, for GRB 091109B the limits are $R(Vega) > 25.80$, $K(Vega) > 22.23$ and $J(Vega) > 21.99$ and for GRB 111020A is $R(Vega) > 24.23$ (a deeper limit of $i'(AB) > 24.4$ has also be placed by Fong et al. 2012). Although r' band observations make elliptical galaxies in particular difficult to detect at higher redshifts, use of a deep limit in the K band would even the chances of detecting any type of host galaxy. Using the deepest limiting magnitudes for GRBs 090305A and 091109B we find that out to $z = 1$ we uncover $\sim 75\%$ of the integrated galaxy luminosity for an Sbc type galaxy, $\sim 85\%$ for an Irr galaxy and 55% for an Ell galaxy. This means that any undetected host galaxy would have to occupy the low mass end of the galaxy luminosity function. GRB 111020A which, even using the deepest limit available from Fong et al. 2012, has a shallower limit, would uncover $\sim 50\%$ (Sbc galaxy). It is unclear as to the status of GRB 111020A as a hostless burst due to the presence of an unresolved object $0.7''$ from its position which would have $P_{\rm chance} < 0.01$[4]. However, for other GRBs considered here as well as no coincident host detection, we also find no host that can be confidently identified using $P_{\rm chance}$ values ($< 1\%$).

These GRBs represent a growing population of optically localised SGRBs with no obvious host galaxy. We have considered two possible origins for these

[4]This case is also complicated by the relatively low Galactic latitude, which means that foreground stars significantly outnumber background galaxies in our images.

hostless SGRBs. The first is that they originate from a higher redshift, and so far unseen population of SGRBs, while the second is that they lie at lower redshift, and are kicked from local, and relatively bright host galaxies.

To address these issues we developed a diagnostic to assess the significance of the association of any given galaxies with a SGRB, and compared the properties of the sample of bursts with those of random positions on the sky. These results suggest that hostless SGRBs as a population have a correlation with structure at small angular scales, more so that "average" random lines of sight. This perhaps offers evidence that the hostless SGRBs are in fact associated either with these bright galaxies, or with fainter galaxies associated with the same large scale structure. In this case the offsets are either as a result of large scale natal kicks to the progenitors, or of their dynamical formation within globular clusters.

We note that a similar study by Berger (2010) concluded that large offsets of $15 - 70\,\mathrm{kpc}$ from relatively low redshift galaxies are their preferred explanation. They found for a high redshift solution the constraints on any underlying host galaxy implied a bimodal population of SGRBs with peaks at $z \sim 0.5$ and $z \sim 3$. They also allow for a minor contribution from NS binary mergers in globular clusters. Our work broadly agrees with the results considered by Berger (2010), although critically extends it to consider the true distribution of galaxies on the sky (rather than average number counts), utilizing this comparison to make statistical statements on the population as a whole.

Ultimately, if hostless GRBs are present at low redshift, deeper observations of their locations will continue to yield null detections of their host galaxies. However, for bursts associated with structure at lower redshift we may be able to ascertain if they are hosted within globular clusters via deep observations with either the Hubble Space Telescope (to $z < 0.1$) or the James Webb Space Telescope (to $z < 0.2$). Such a detection could offer strong evidence for the origin of SGRBs in compact binary mergers.

Chapter 4

A sample study of the optical afterglow of short gamma-ray bursts

4.1 Introduction

The sample of well-localised short GRBs is substantially smaller than for their long cousins, due to their short duration, making them more difficult to detect, smaller event rate and generally fainter afterglows (Kann et al., 2011). Their greater spectral hardness also means the BAT instrument on the *Swift* telescope is less attuned to their detection compared to the *BATSE* instrument due to its softer spectral band.

It is thus important to consolidate all the detections to date and to perform sample studies on the population as whole. We compile a sample consisting of all optically localised SGRBs from 2005 to the end of 2011 and combine all available optical data from the GCN circulars, all published material and our own data. For this sample we apply an upper limit on the duration of $T_{90} = 2\,\mathrm{s}$ (or, for GRBs with an initial hard pulse followed by extended emission, an initial pulse duration of $T_{90} = 2\,\mathrm{s}$) (Kouveliotou et al., 1993) but we also investigate claims that a split of $0.8\,\mathrm{s}$ for the *Swift* telescope would be more appropriate (Bromberg et al., 2011, 2013). Detailed studies of individual bursts and some sample studies have been produced previously (in particular Kann et al. 2011) but here we analyse all available optical and XRT data using a consistent method, fitting the lightcurves and SEDs where possible. The data points and fits are then used to investigate many of the global and local properties within the sample. In particular:

- We search for jet breaks and place limits on jet opening angles.

- We look for the presence of extinction by considering the optical to X-ray spectral slope and looking for suppressed optical emission with respect to the fireball model (Jakobsson et al., 2004; van der Horst et al., 2009). For completeness in this analysis we include SGRBs with optical upper limits (and X-ray lightcurves) as well as those with optical detections.

- We look for evidence of predicted mini-supernova or kilonova produced from radioactive material associated with the merger of neutron stars (Li and Paczyński, 1998), placing constraints on the brightness of these events in the optical band.

- Using late time detections we also place constraints on any associated supernova. Considering the proposed $T_{90} = 0.8\,\mathrm{s}$ divide for collapsar - non-collapsar events we use these constraints to determine the maximum fraction of collapsar events which could be present within our optically localised sample.

4.2 Analysis

4.2.1 Sample construction

The sample includes all GRBs from 2005-2011 inclusive with at least one optical afterglow detection and with $T_{90} < 2\,\mathrm{s}$. This sample is mainly comprised of GRBs detected by *Swift* by also includes those SGRBs which fit this criteria detected by *HETE-II* and *INTEGRAL*. The γ-ray emission of some "short" GRBs is comprised of a short hard peak, known as the initial pulse complex (IPC), followed by low level, softer extended emission. Hence, we have also included all those GRBs where the IPC is $< 2\,\mathrm{s}$ (Norris and Bonnell, 2006; Norris et al., 2010b). Norris et al. (2010b) determined the presence of extended emission by sampling a time interval around the pulse (up to 200 seconds before and 400 seconds after), testing within varying time bins for a change from high to low level intensity. If no change was detected it was assumed there was no extended emission. The duration of the IPC, given in Table 4.1, is measured by Norris et al. (2010b) as occurring over an interval where the intensity is above $1/e$ times the IPC peak intensity.

The total sample considered here contains 24 GRBs. The optical sample has been constructed from all available data for the GRBs within published material as well as from the Gamma-ray Coordinates Network (GCN) circulars. We have also included some previously unpublished material for GRB 060313 mainly in the R band and GRB 051221A in the Ks band. Table 4.1 shows the full list of GRBs included in this sample. All GRBs detected by the BAT instrument from the launch

of *Swift* to the end of 2011 are shown in Figure 4.1 with the GRBs in our sample highlighted.

4.2.2 Lightcurve and SED fitting

The lightcurves for these GRBs have been constructed from all available afterglow measurements in all bands. Vega to AB magnitude conversion (as well as flux calculations) have been performed making using of the astSED python module which is part of the astLib package.[1] Within the literature, conversion between magnitude systems can differ, creating discrepancies between magnitude and flux values published. Though this difference may be small we have aimed to be consistent in our conversions by making use of this code. All bands have been extrapolated to the R filter using a power law spectrum of the form $F_\nu \propto \nu^{-\beta_O}$. To measure the optical spectral slope, β_O, where the colour data is available a spectral energy distribution (SED) has been constructed for each GRB and a representative β value chosen to scale the points. Where this is not possible the β_O value has been inferred from the β_X (Evans et al., 2009a).[2] Assuming a synchrotron spectrum and that both the X-ray and optical emission originate from the same source β_O should be between β_X and $\beta_X - 0.5$ depending on the position of the cooling break (van der Horst et al., 2009). Hence we infer a value of $\beta_0 = \beta_X - 0.25$ ensuring the errors are > 0.25 to cover our lack of certainty of the absolute β_O slope compared with β_X. In the case of GRB 070809 the shallow X-ray power law index of $\beta_X = 0.22$ means we cannot use this to infer a sensible β_O value. Using a value of $p = 2.2$ for the spectral index of the synchrotron electron distribution as a canonical value (e.g. Achterberg et al. 2001) implies a measured optical slope, assuming the frequency considered is above the cooling break and hence giving a slope of $\beta = (p-1)/2$, of $\beta = 0.6$ as suggested by Kann et al. (2011). The β values which can be used to extrapolate all bands to the R band are given in Table 4.2.

[1] Using the version 0.4.0 available from http://astlib.sourceforge.net/

[2] Photon index (Γ_X) measurements available from http://www.swift.ac.uk/xrt_spectra/

GRB	T_{90} (s)	$T_{90}(IPC)$ (s)	Fluence (10^{-7}erg cm^{-2})	HR
GRB 050709	0.07^{a}	-	3.03 ± 0.38^{a}	
GRB 050724	96	0.384	6.3 ± 1.0	1.05
GRB 051221A	1.4	-	11.6 ± 0.4	1.52
GRB 051227	114.6	0.832	2.3 ± 0.3	1.54
GRB 060121	1.97^{a}	-	38.7 ± 2.7^{a}	
GRB 060313	0.74	-	11.3 ± 0.5	2.49
GRB 061006	129.9	0.448	14.3 ± 1.4	1.20
GRB 061201	0.76	-	3.3 ± 0.3	2.30
GRB 070429B	0.47	-	0.63 ± 0.10	1.28
GRB 070707	0.8^{b}	-	$2.07^{+0.06\ b}_{-0.32}$	
GRB 070714B	64	1.152	7.2 ± 0.9	1.52
GRB 070724A	0.4	-	0.30 ± 0.07	1.10
GRB 070809	1.3	-	1.0 ± 0.1	1.27
GRB 071227	1.8	-	2.2 ± 0.3	0.98
GRB 080503	170	0.128	20 ± 1	1.06
GRB 080905A	1.0	-	1.4 ± 0.2	2.31
GRB 081226A	0.4	-	0.99 ± 0.18	1.52
GRB 090305A	0.4	-	0.75 ± 0.13	2.22
GRB 090426	1.4	-	1.8 ± 0.3	1.12
GRB 090510	0.3	-	3.4 ± 0.4	1.92
GRB 090515	0.036	-	0.2 ± 0.08	1.49
GRB 091109B	0.27	-	1.9 ± 0.2	2.45
GRB 100117A	0.3	-	0.93 ± 0.13	2.17
GRB 110112A	0.5	-	0.30 ± 0.09	0.91

Table 4.1: The sample of short GRBs comprising of all GRBs with T_{90} or with $T_{90}(IPC) \leq 2$ s. T_{90} values are measured by the BAT instrument on the *Swift* telescope in the 15−150 keV band unless explicitly stated otherwise. The Hardness Ratio (HR) is measured as the ratio between the fluence in the $50-100$ keV and $25-50$ keV bands over the entire T_{90} duration of the GRB. In this case for GRBs with extended emission they appear softer than if the IPC component alone was considered.
Footnotes: (*a*) *HETE-2* trigger. T_{90} and Fluence are given in the $30-400$ keV energy band (GRB 050709; Villasenor et al. 2005, GRB 060121; Donaghy et al. 2006). (*b*) *INTEGRAL* trigger. T_{90} and Fluence are given in the $20-200$ keV energy band (GRB 070707; McGlynn et al. 2008).

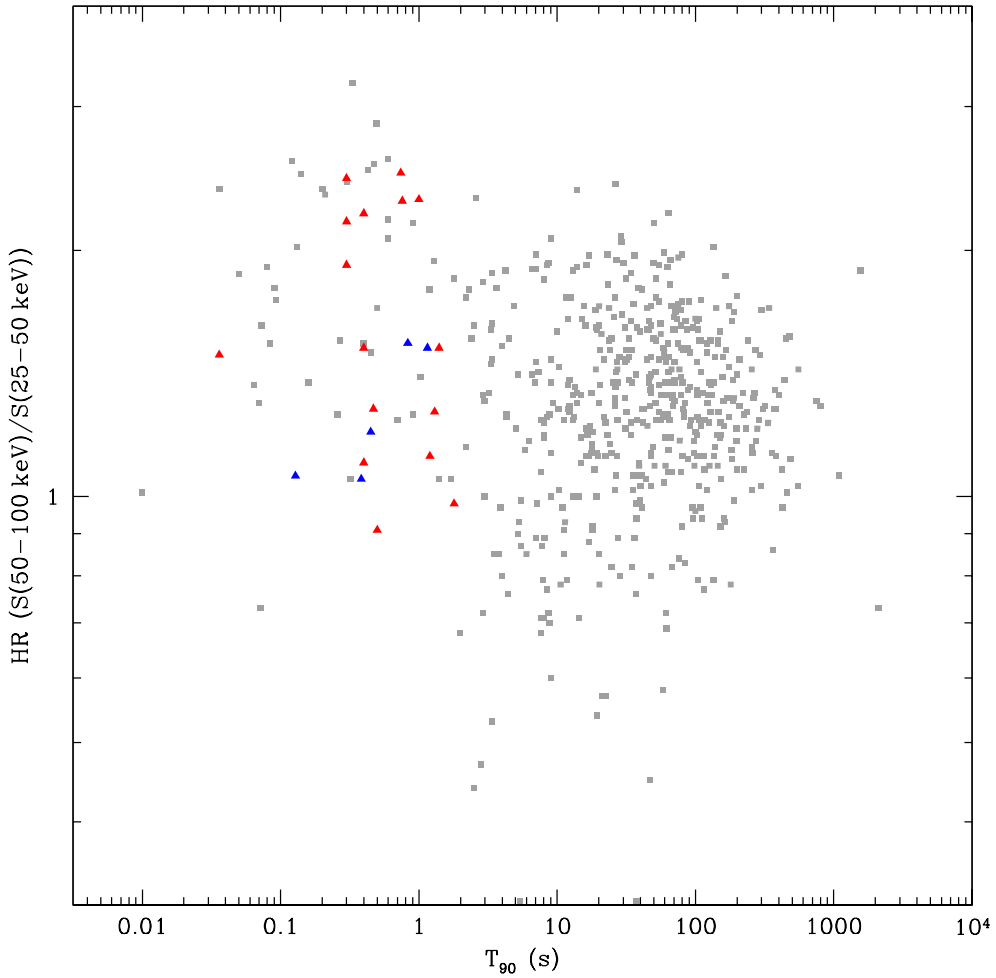

Figure 4.1: T_{90} versus Hardness Ratio plot for all GRBs detected by the BAT instrument on *Swift* from its launch to the end of 2011. From our sample of optically localised GRBs, those detected by the BAT are shown in the plot (triangles) and the bursts with and without extended emission are shown as blue and red points respectively. For the GRBs with extended emission the hardness ratio is shown for the entire BAT detection whereas the T_{90} is for the initial pulse complex only. For comparison the rest of the population is also shown (grey squares).

GRB	β_O	Bands	Time from trigger (hrs)	Time range (s)	Refs[a]
SED fits					
GRB 050709	1.14 ± 0.67	K', $F814W$	136.09 - 136.24	540	[1]
GRB 050724	$0.97^{+0.05}_{-0.06}$	V, Ks, R, I	11.41 - 11.81	1447	[2],[3]
GRB 051221A[b]	$1.05^{+0.30}_{-0.42}$	K, r, i	26.66 - 27.22	2010	[4], *this work*
	$0.03^{+0.79}_{-1.86}$	z, i, r	50.98 - 51.64	2368	[4]
GRB 060121	2.3 ± 0.14	R, Ks	7.25 - 7.45	713	[5],[6]
GRB 060313	$1.0^{+0.27}_{-0.35}$	I, R, $UVW2$[c]	1.46 - 1.52	206	[7], *this work*
GRB 070714B	$0.62^{+0.57}_{-0.43}$	v, $UVM2$[c], $UVW1$[c], $UVW2$[c]	0.87 - 1.12	872	[8]
GRB 070724A	2.16 ± 0.16	i, Ks	2.33 - 2.83	1814	[9]
GRB 081226A	$2.9^{+1.33}_{-1.82}$	g, r, i, z	1.13	0	[10]
GRB 090305A	$0.85^{+0.48}_{-0.50}$	g, r, i	1.27 - 1.34	243	[10]
GRB 090426	$0.83^{+0.07}_{-0.07}$	g, r, i, z, J, H	14.65	0	[11]
GRB 090510	$1.8^{+1.34}_{-1.12}$	r, z, g, i	6.32 - 6.42	384	[12]
β_0 **derived from** β_X **fits**					
GRB 051227	$1.01^{+0.51}_{-0.44}$	-	-	-	
GRB 061006	$1.06^{+0.64}_{-0.56}$	-	-	-	
GRB 061201	$0.94^{+0.45}_{-0.41}$	-	-	-	

GRB 070429B	$1.75^{+1.0}_{-1.0}$	-	-	-
GRB 070707	$2.05^{+3.5}_{-1.0}$	-	-	-
GRB 070809	(0.6)	-	-	-
GRB 071227	$0.65^{+0.48}_{-0.35}$	-	-	-
GRB 080503	$1.28^{+0.42}_{-0.19}$	-	-	-
GRB 080905A	$0.28^{+0.29}_{-0.27}$	-	-	-
GRB 090515	$1.28^{+1.24}_{-0.44}$	-	-	-
GRB 091109B	$0.81^{+0.54}_{-0.41}$	-	-	-
GRB 100117A	$1.36^{+0.51}_{-0.40}$	-	-	-
GRB 110112A	$0.92^{+0.40}_{-0.25}$	-	-	-

Table 4.2: The β_0 values used to extrapolate all colours into the R band when constructing the lightcurves. Where there is available colour and temporal information an SED has been constructed (11 GRBs). The time range over which the detections within the SED are taken is indicated. In the cases where the measurements are simultaneous the time range is given as 0. For the GRBs where sufficient colour data was not available the β_0 value is based on the measured β_X value from the XRT spectra using $\beta_0 = \beta_X - 0.25$ (see the text for more information). Footnotes: (a) The references here are for the data used to construct the SED. (b) In the case of GRB 051221A β_O showed evolution. To not bias our lightcurve results we did not use scaled values. (c) Non-standard filters $UVW1$, $UVM2$ and $UVW2$ are available on the UVOT instrument on the *Swift* telescope with central wavelengths 2600Å, 2246Å and 1928Å respectively (Poole et al., 2008).
References: [1] Fox et al. (2005) [2] Malesani et al. (2007) [3] Berger et al. (2005) [4] Soderberg et al. (2006a) [5] Levan et al. (2006a) [6] de Ugarte Postigo et al. (2006) [7] Roming et al. (2006) [8] Landsman et al. (2007) [9] Berger et al. (2009) [10] Nicuesa Guelbenzu et al. (2012b) [11] Nicuesa Guelbenzu et al. (2011) [12] Nicuesa Guelbenzu et al. (2012a)

Some afterglow measurements contain a significant contribution from underlying host galaxies. In these cases we have attempted to correct for this using the known host galaxy magnitude (or magnitude of the host galaxy at the afterglow position) in the given passband or extrapolating using the galaxy type and redshift, if necessary. In some cases, it was not appropriate to combine the available bands into an extrapolated lightcurve. In these cases we have indicated the bands included in the stated lightcurve fit. The fits are based on the power law lightcurve of the form $F_t \propto t^{-\alpha_O}$ with best fits given in Table 4.3. All the lightcurves with data points extrapolated to the R band and in the observer frame are shown in Figure 4.2.

From looking at Figure 4.2 it is clear that the sample of SGRB optical lightcurves is diverse. The range of decay slopes is wide sometimes showing a plateau before a steeper break occurs. The sample also suffers from a variety of sampling durations over the full decay slope making it difficult to characterise behaviour in some cases. Overall, however, in all but a few cases the lightcurves are reasonably well fit with a series of power laws, though there may be some additional small scale variation in the more well sampled cases. There are a few cases however where additional components are clearly required.

For GRB 050724 an additional outburst must be added at ~ 12.5 hrs (lasting ~ 13 mins) to fit the data. This is approximately coincident with a flare in the X-ray lightcurve. This peaks at ~ 15.9hrs but lasts for ~ 7 hrs (Malesani et al., 2007). Malesani et al. (2007) suggested that this is related to late-time activity of the central engine. However, it is interesting that there is no strong evidence for outbursts in the other optical lightcurves, meaning perhaps GRB 050724 was unusual in this behaviour.

In addition, the lightcurve of GRB 080503 shows a rise and then a steeper decay not well fit by a set of power laws. Although GRB 080503 is a burst with extended prompt emission the optical lightcurve was also extremely faint (Perley et al., 2009a). Perley et al. (2009a) suggest this late peak could be due to an off-axis jet or a refreshed shock. It is again interesting that behaviour such as this is not seen in any of the other SGRB lightcurves.

The lightcurves of GRBs 060313 and 070714B show evidence for a plateau period before a steeper decay. This plateau characterises the early part of the lightcurve before the break which occurs a few thousand seconds after the trigger. Overall, within the sample, 13 of the 24 GRBs show some evidence for a break, be it a late time upper limit showing steepening or where the lightcurve is well sampled enough to see the break. We consider in section 4.2.3 whether any of these breaks

GRB	Bands	α_1	T_{break} (s)	α_2	Refs
GRB 050709	all	1.50	850000	2.75	[1],[2]
GRB 050724[a]	all	1.60	204000	3.87	[3]-[6]
GRB 051221A	R,r'	0.64	37370	1.23	[7]-[10]
	K	0.46	-	-	*this work*
GRB 051227	all	2.20	-	-	[11, 12]
GRB 060121	all	0.71	-	-	[13]-[15]
GRB 060313	all	-0.06	6904	0.93	[12],[16]-[20], *this work*
GRB 061006	I	> 0.26	-	-	[11]
GRB 061201	all	0.97	-	-	[21]
GRB 070429B[b]	all	-1.82	2330	> 1.79	[22]-[24]
GRB 070707	all	0.68	130000	3.08	[25]
GRB 070714B	all	-0.04	3147	1.15	[26]-[29]
GRB 070724A	all	> 0.60	-	-	[30],[31]
GRB 070809	all	0.73	-	-	[32],[33]
GRB 071227	all	0.98	-	-	[34],[11]
GRB 080503[c]	all	-0.24	128000	0.99	[35]
GRB 080905A	all	0.40	79480	1.01	[36]
GRB 081226A	r'	1.27	-	-	[37]
GRB 090305A	all	0.61	-	-	[37], *this work*
GRB 090426	all	0.26	3740	2.31	[38]-[46]
GRB 090510	all	0.70	39250	1.23	[47]-[51]
GRB 090515	all	0.06	111400	> 0.15	[52]
GRB 091109B	all	0.50	38000	> 1.00	*this work*
GRB 100117A	r'	1.65	-	-	[53],[37]
GRB 110112A	i'	> 0.56	-	-	[54], *this work*

Table 4.3: Fits to the lightcurve sample. All bands have been extrapolated to the R band unless the bands have been explicitly stated. A negative slope indicates a rise in the lightcurve. Footnotes: (a) The fit to GRB 050724 also includes a fit to an outburst at early times. (b) The rise quoted here, based on early time UVOT points, is not likely a physical rise but an issue with the scaling to the optical points. (c) GRB 080503 is clearly not best fit by a decaying power law. The lightcurve shows a consistent rise, not indicative of flaring behaviour, before steeping falling off. References: [1] Fox et al. (2005) [2] Hjorth et al. (2005) [3] Wiersema et al. (2005) [4] Cobb and Bailyn (2005) [5] Malesani et al. (2007) [6] Berger et al. (2005) [7] Roming et al. (2005) [8] Wren et al. (2005) [9] Boettcher and Joshi (2005) [10] Soderberg et al. (2006a) [11] D'Avanzo et al. (2009) [12] Berger et al. (2007b) [13] Hearty et al. (2006) [14] de Ugarte Postigo et al. (2006) [15] Levan et al. (2006a) [16] Cobb (2006a) [17] Cobb (2006b) [18] Thöne et al. (2006) [19] Nysewander et al. (2006) [20] Roming et al. (2006) [21] Stratta et al. (2007) [22] Holland et al. (2007) [23] Antonelli et al. (2007) [24] Perley et al. (2007a) [25] Piranomonte et al. (2008) [26] Landsman et al. (2007) [27] Covino et al. (2007) [28] Perley et al. (2007b) [29] Graham et al. (2009) [30] Berger et al. (2009) [31] Kocevski et al. (2010) [32] Perley et al. (2007d) [33] Perley et al. (2007c) [34] Cucchiara and Sakamoto (2007) [35] Perley et al. (2009a) [36] Rowlinson et al. (2010a) [37] Nicuesa Guelbenzu et al. (2012b) [38] Yoshida et al. (2009) [39] Oates and Cummings (2009) [40] Kinugasa et al. (2009) [41] Mao et al. (2009) [42] Rumyantsev et al. (2009) [43] Xin et al. (2010) [44] Thöne et al. (2011) [45] Antonelli et al. (2009) [46] Nicuesa Guelbenzu et al. (2011) [47] Kuin and Hoversten (2009) [48] Marshall and Hoversten (2009) [49] Olofsson et al. (2009) [50] Olivares et al. (2009) [51] Nicuesa Guelbenzu et al. (2012a) [52] Rowlinson et al. (2010b) [53] Fong et al. (2011b) [54] Xin et al. (2011)

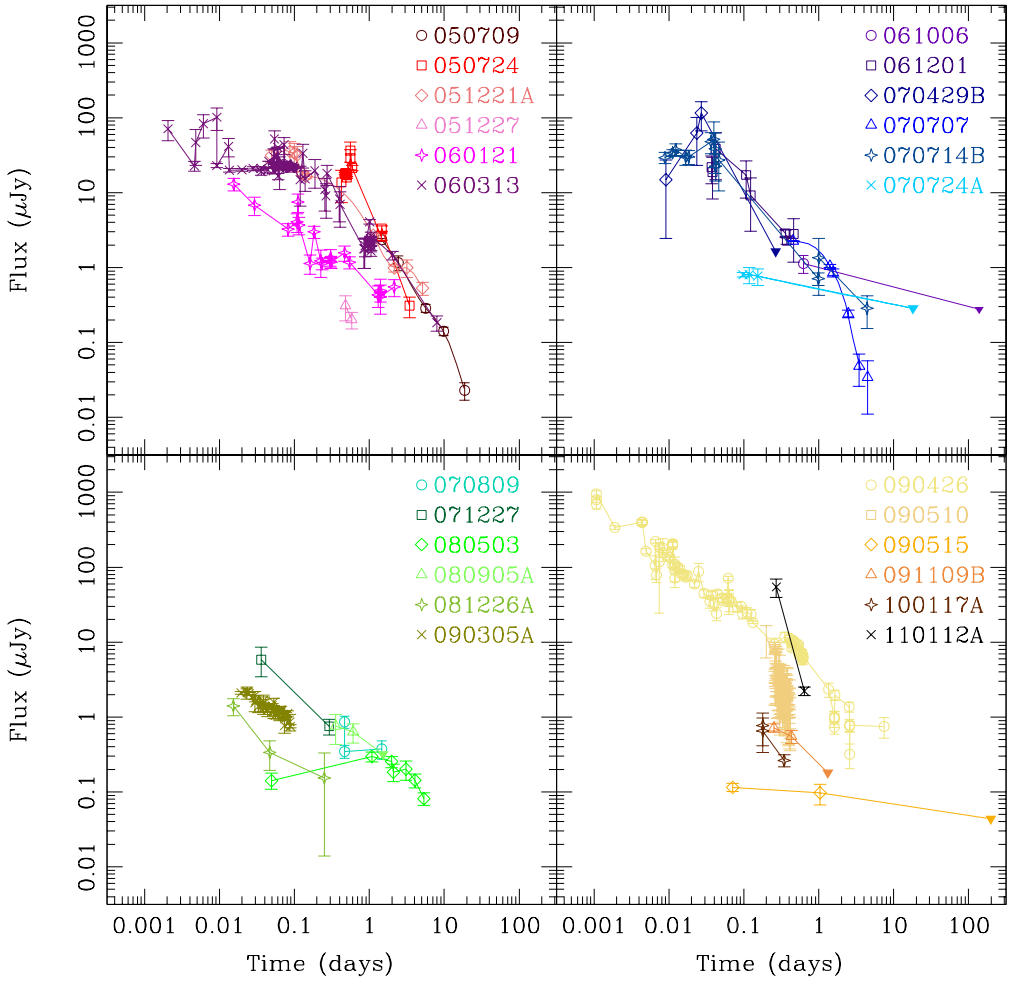

Figure 4.2: The set of R band extrapolated lightcurves for all GRBs in the sample separated into four panels. Upper limits are shown as triangles where they are constraining of the best fit. These values are in the observer frame. The lightcurve for each GRB is a different colour with symbols indicated on each of the panels.

may be evidence for a jet.

4.2.3 Constraints on jet breaks

The highly-relativistic collimated outflow from a GRB will be strongly beamed (with beaming angle Γ^{-1} where Γ is the bulk Lorentz factor of the material in the jet) so that initially $\Gamma^{-1} < \theta_j$ where θ_j is the jet half opening angle. As Γ decreases and, due to lateral expansion, the jet eventually reaches the point where $\Gamma \sim \theta_j^{-1}$ we, as the observer, see the edge of the emission. At this point we should see an achromatic break: a jet break. Depending on the external medium, the decay index of the lightcurve should alter by $\delta\alpha \sim 0.75$ (medium dominated by the contribution from the stellar wind of the progenitor) to $\delta\alpha = 0.5$ (uniform medium), with the latter expected for SGRBs (Granot, 2007).

Breaks such as this have been seen for some LGRBs (e.g. Frail et al. 2001; Bloom et al. 2003; Tanvir et al. 2010a). However, it is also known that breaks can occur for other reasons such as migration of the cooling break. Hence, for breaks in the lightcurve, as well as considering the change in slope it is also important to ensure the break is achromatic in order to determine whether it is, in fact, a jet break.

To constrain the presence of jet breaks in the SGRB sample we looked for simultaneous breaks in both the optical and the X-ray lightcurves. To do this we have looked at the *Swift* XRT data within the $0.3 - 10\,\mathrm{keV}$ band (Evans et al., 2007)[3] for the subset of GRBs in the sample with breaks in the optical lightcurves. This sample is given in Table 4.4. As well as the break times we also consider the change in the lightcurve slope in both the overall optical lightcurve and the X-ray lightcurves. For those lightcurves where a simultaneous break may be present we also looked at the individual filters to look for further evidence of simultaneous break points.

Within this sample there are two GRBs which may show simultaneous breaks: GRBs 060313 and 051221A. We also further consider the lightcurve of GRB 090426 which has been purported as having a jet break in the literature (Nicuesa Guelbenzu et al., 2011).

GRB 060313 shows a simultaneous break between the optical and the X-ray lightcurve. The R band (only) and X-ray lightcurves and their best fits are plotted in Figure 4.3. However, the steepening of this break in the optical band of $\delta\alpha_O = 0.99^{+0.44}_{-0.46}$ is potentially greater than we would expect for a jet break, though the large error does not preclude this being the case. In the R band lightcurve there

[3]Available from http://www.swift.ac.uk/xrt_curves/

GRB	$\Delta\alpha_0$	$T_{break,O}$ (s)	$\Delta\alpha_X$	$T_{break,X}$ (s)	X-ray data range (s)
GRB 050709	1.25	$850100^{+696500}_{-201100}$	-	-	$100 - 1391040$
GRB 050724	2.26	$203600^{+81200}_{-127700}$	5.23	491^{+28}_{-23}	$80 - 181680$
GRB 051221A	0.59	37374^{+63450}_{-22530}	1.37	24216^{+4648}_{-2782}	$96 - 997400$
GRB 060313	0.99	$6904^{+175.4}_{-154.5}$	0.86	7736^{+971}_{-1494}	$88 - 192320$
GRB 070429B	3.61	2333^{+2077}_{-1221}	-	-	$522 - 1492$
GRB 070707	2.40	129700^{+}_{-}	-	-	$45070 - (447240)$
GRB 070714B	1.20	3147^{+9820}_{-1192}	1.03	753^{+304}_{-128}	$69 - 87840$
GRB 080503	1.23	$128300^{+51050}_{-117700}$	3.45	227^{+6}_{-7}	$82 - 1403$
GRB 080905A	0.62	79479^{+79220}_{-21520}	1.77	584^{+273}_{-226}	$116 - 887$
GRB 090426	0.53	39252^{+1254}_{-1353}	-[a]	-[a]	$124 - 436890$
GRB 090510	2.05	3740^{+4042}_{-1585}	1.46	1469^{+161}_{-177}	$100 - 23006$
GRB 090515	> 0.09	$111400^{+16940000}_{-105300}$	9.7	162^{+3}_{-3}	$72 - 284$
GRB 091109B	> 0.51	38000^{+76200}_{-16310}	-	-	$155 - 203630$

Table 4.4: A subset of GRBs within the sample with breaks in the optical lightcurves. Here we compare breaks (if present) in the X-ray lightcurves to those in the optical to look for simultaneity. There are two examples where this may be the case: GRBs 060313 and 051221A. However, we also note that in 5/12 cases above the XRT data does not extend far enough to constrain the break seen in the optical lightcurve.
Footnotes: (a) For GRB 090426 the presence of a break in the X-ray lightcurve is not significant over a single power law but the data points do not extend far enough to properly constrain the non-detection of a break. We consider the lightcurve of this GRB further in the text.

is a plateau (with perhaps a slight rise) before the break. The change in the slopes is also not consistent between the X-ray and the optical. It is therefore unclear whether this break is related to the expansion of the jet.

In the combined R and r' band lightcurve for GRB 051221A there is a break coincident with the end of a plateau period in the XRT data. However, this break is not evident in the K band. This data, along with the best fits to the lightcurve can be seen in Figure 4.4. Burrows et al. (2006) also claim evidence for a jet break in the lightcurve of GRB 051221A. However, they place this at 354 ks based on a late time break in their data taken with the ACIS (Advanced CCD Imaging Spectrometer) instrument on the *Chandra* satellite. We cannot constrain this break in the optical lightcurve since it does not extend far beyond the suggested late time X-ray break point. From our investigation, we do not find convincing evidence of a jet break.

For GRB 090426 though there could be a simultaneous break with the optical data in the X-ray lightcurve, the F-test probability of chance improvement from the single power law to the inclusion of a break is 38%. Hence, adding a break is not a significant improvement on the simpler model. However, the X-ray lightcurve data does not extend far into the regime of the optical lightcurve with only one detection beyond the optical break point. Looking at the lightcurves in the individual filters we found breaks in the R and g' band lightcurves at ~ 39300 s. Both the X-ray and optical data can be seen in Figure 4.5. Hence, though Nicuesa Guelbenzu et al. (2011) suggest the presence of a jet break from looking at the multiple individual optical bands, the low significance of a break in the X-ray lightcurve suggests that this break is most likely not a jet break.

Overall, in the sample of 24 optically localised GRBs we do not find a convincing case for a jet break. The sparcity of detections in some cases makes this unsurprising as it is often difficult to constrain the presence of breaks. However, even for those lightcurves which are well sampled many of the breaks do not appear to be achromatic. We therefore promote caution when claiming to have found jet breaks in the optical or X-ray only for GRBs as the causes for these breaks to be more widespread than simply in cases of jet breaks.

Using the last detection in our lightcurves we can place constraints on the jet opening angle, θ_j, given in Table 4.5. This was calculated using the relation in Equation 4.1 from Frail et al. (2001).

$$\theta_j(radians) = 0.057 \times {t_j}^{3/8} \times \left(\frac{1+z}{2}\right)^{-3/8} \left[\frac{E_{iso}(\gamma)}{10^{53}\,\mathrm{ergs}}\right]^{-1/8} \left(\frac{\eta_\gamma}{0.2}\right)^{1/8} \left(\frac{n}{0.1\,\mathrm{cm}^{-3}}\right)^{1/8} \tag{4.1}$$

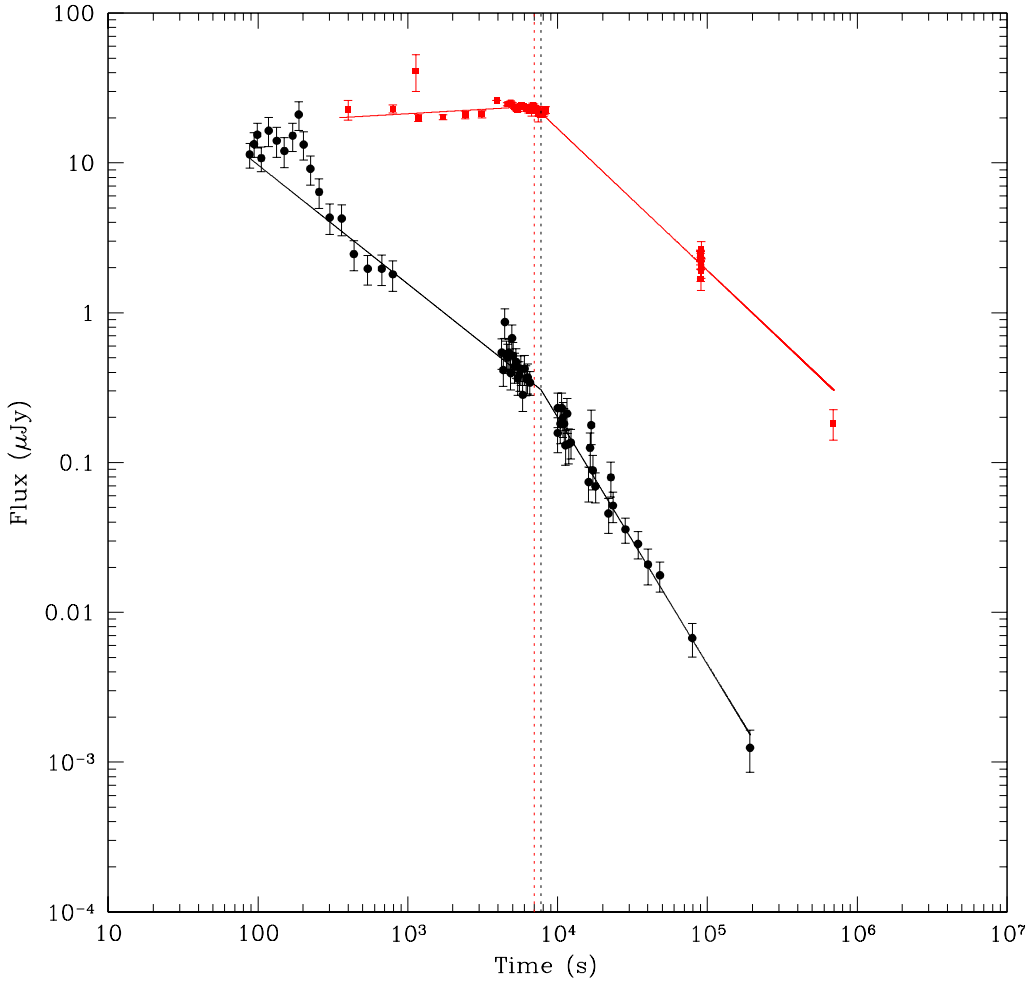

Figure 4.3: The R band (red squares) and X-ray (black, circles) lightcurves for GRB 060313. The best fit power law model is also shown for both sets of data. The break points of the lightcurves are marked with vertical red and black lines respectively. The R band lightcurve shows a steep decay after a plateau phase whereas the X-ray shows a steepening with a smaller change in $\Delta\alpha$.

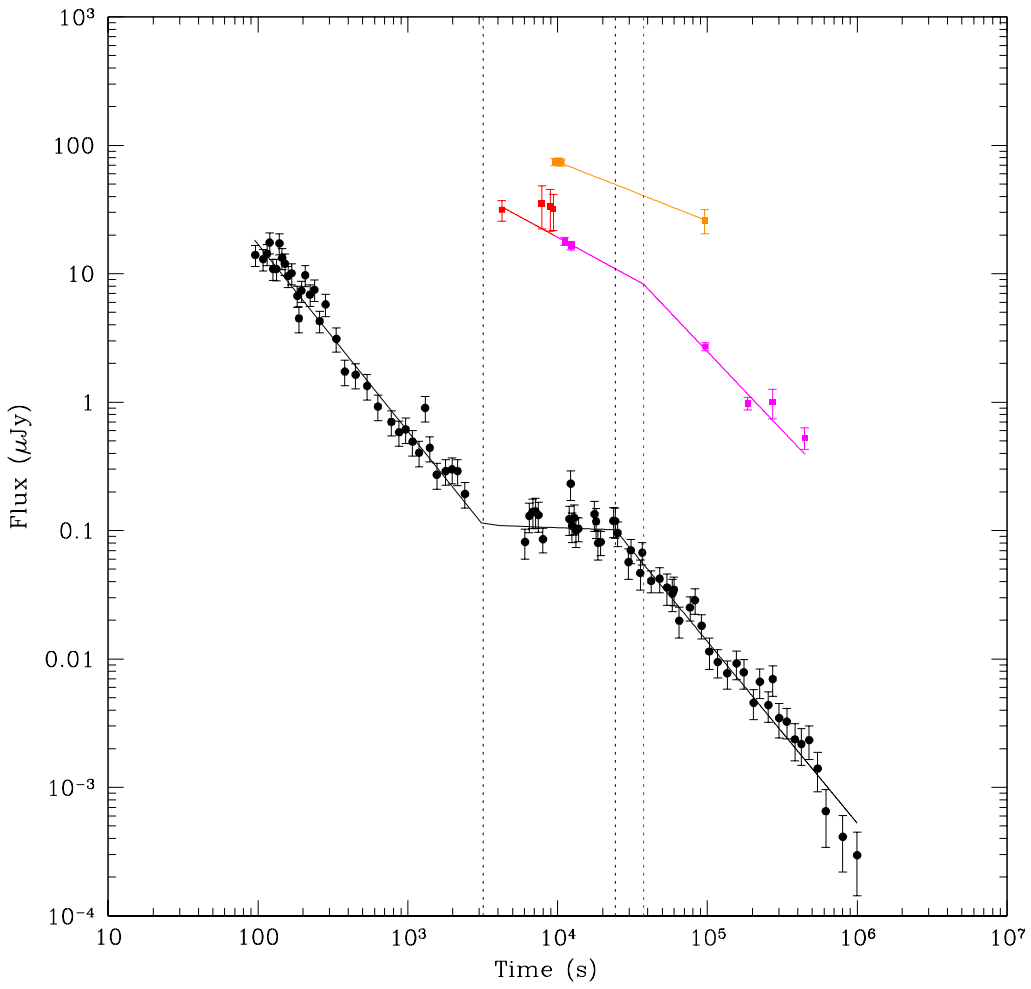

Figure 4.4: The R band (red squares), r' band (magenta squares), K band (offset by -1.0 mag, orange squares) and X-ray (black circles) lightcurves for GRB 051221A.

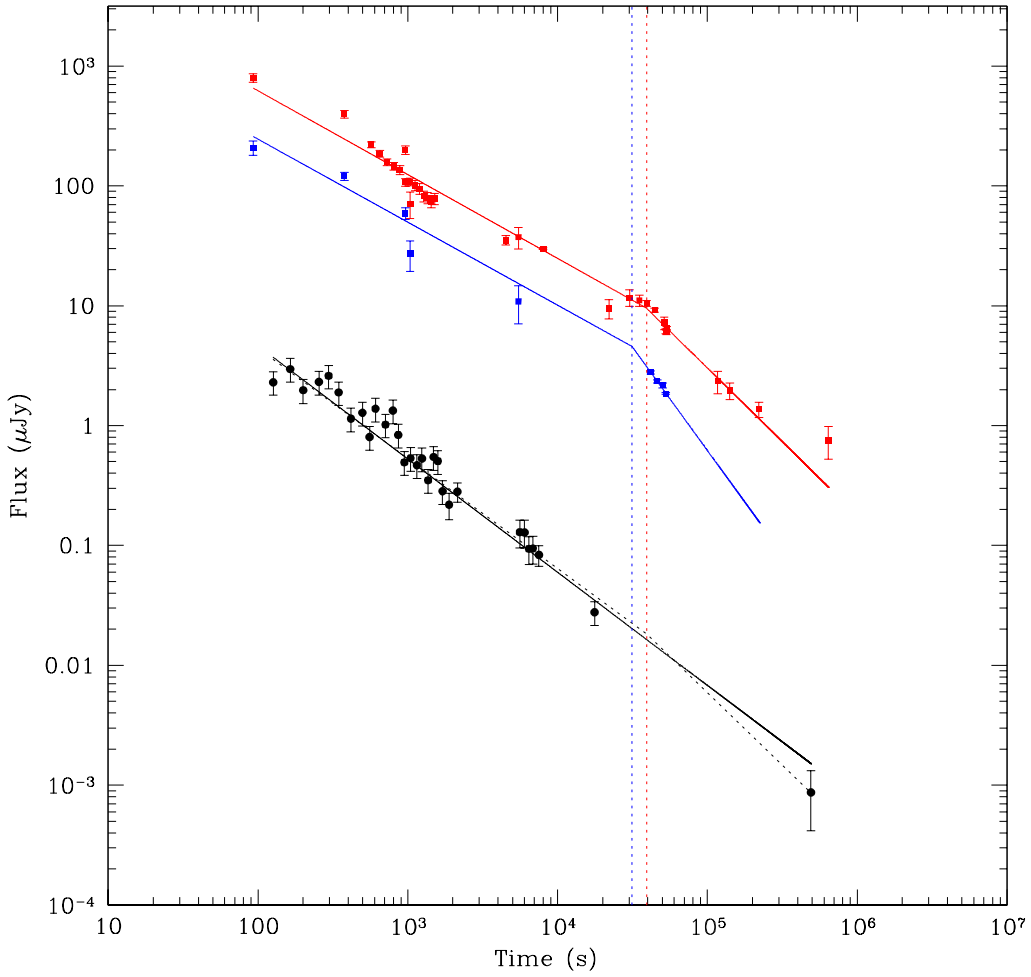

Figure 4.5: The R band (red squares), g' band (offset by +1.0 mag, blue squares) and X-ray (black circles) lightcurves for GRB 090426. The best fit power law model is also shown for the data sets (solid lines). For the X-ray data both the single and broken power law (dotted line) fits are shown. The power law with a break is not a significant improvement on the fit with no break. There is a simultaneous break in the R and the g' bands with the break point indicated.

where $E_{iso}(\gamma)$ is the isotropic equivalent energy released in γ-rays, n is the mean circumburst density of the material at the site of the GRB and η_γ is the efficiency of the fireball in converting the energy from the ejecta into γ-rays. For SGRBs, n is typically between $10^{-4} - 1\,\mathrm{cm}^{-3}$ and is usually lower than for LGRBs (Fong et al., 2013). In our calculations, we adopt a value of $n = 10^{-2}\,\mathrm{cm}^{-3}$. η_γ is proposed to be around 0.2 as the fireball process is efficient at producing γ-rays (Frail et al., 2001).

From Table 4.5 the mean lower limit for θ_j is $> 5.8^\circ$ with a standard deviation of 4.1°. This is conservative compared with LGRB beaming angles mean of $\sim 8.5^\circ$ using the sample of Bloom et al. (2003). The lower limit is also close to the measured jet opening angles in the literature of $\sim 4 - 8^\circ$ for GRB 051221A (Burrows et al., 2006) and $\sim 3 - 8^\circ$ for GRB 111020A (Fong et al., 2012), both measured using late time *Chandra* data. This suggests a wide range of jet angles for short GRBs, especially with some high lower limits of $> 21.8^\circ$ for GRB 050709 and $> 25^\circ$ for GRB 050724 (Burrows et al., 2006).

The indication that some GRBs may have wide jets has implications for the detection of gravitational waves from merger events, both for the confirmation of electromagnetic counterparts and for the numbers of potential events that can be detected. On the one hand a wide jet increases the likelihood that a gravitational wave detection will be accompanied by γ-ray emission especially since the gravitational waves themselves favour face on emission. On the other hand, if merger events are accompanied with wide jets then this means the true event rate will not be much higher than observed making the probability of detection smaller. Overall, constraining the jet opening angle will help us to determine the detection fraction of gravitational wave events and the possibility of detecting a simultaneous GRB-event.

4.2.4 Constraints on extinction

Using the optical and XRT data available we calculated, the optical to X-ray spectral index, β_{OX} for our sample. For this analysis, we also included those GRBs with X-ray lightcurves and optical upper limits to derive limits on their associated β_{OX} values. Jakobsson et al. (2004) propose that a GRB is optically subluminous with respect to the fireball model, termed "dark", if $\beta_{OX} < 0.5$. In its simplest form, the fireball model states that we expect the electron energy distribution to have a power law index $p \geq 2$ (Sari et al., 1998). The photon spectral index is dependant on this value and, depending on the position of the cooling break, we would expect this to be $(p-1)/2$ or $p/2$ meaning any value less than this must be caused by something outside the realms of the model. More sophisticated definitions of "darkness" have also been proposed, for example van der Horst et al. (2009) define a cutoff of $\beta_{OX} <$

GRB	z	$E_{iso}(\gamma)$ (ergs)	t_j (days)	θ_j (degrees)
050709	0.1606	8.51×10^{49}	> 19.0	$> 21.78^{a}$
050724	0.257	2.4×10^{50}	> 3.5	$> 9.87^{b}$
051221A	0.5464	2.57×10^{51}	> 5.2	$> 7.88^{c}$
051227	(0.5)	6.7×10^{50}	> 0.58	> 4.16
060121	4.6	2.19×10^{53}	> 2.1	> 2.01
	1.7	4.07×10^{52}	> 2.1	> 3.26
060313	(0.5)	8.5×10^{51}	> 8.0	> 8.10
061006	0.4377	1.74×10^{51}	> 0.62	> 3.85
061201	(0.5)	3.2×10^{51}	> 0.46	> 3.14
070429B	0.9023	1.35×10^{50}	> 0.027	> 1.47
070707	(0.5)	9.3×10^{50}	> 4.5	> 8.61
070714B	0.9224	1.1×10^{52}	> 4.4	> 5.71
070724A	0.4571	2.45×10^{49}	> 0.15	> 3.86
070809	(0.5)	7.3×10^{49}	> 1.5	> 7.76
071227	0.381	5.62×10^{50}	> 0.29	> 3.38
080503	(0.5)	8.7×10^{51}	> 5.4	> 6.95
080905A	0.1218	2.29×10^{49}	> 0.6	> 7.21
081226A [d]	(0.5)	2×10^{50}	> 0.25	> 3.53
090305A	(0.5)	4.5×10^{50}	> 0.088	> 2.15
090426 [e]	2.609	4.2×10^{51}	> 7.4	$> 6.18^{f}$
090510	0.903	4.07×10^{52}	> 0.41	> 2.00
090515	(0.5)	1.5×10^{49}	> 1.0	> 8.32
091109B	(0.5)	1.38×10^{51}	> 0.43	> 3.40
100117A	0.915	9.12×10^{50}	> 0.34	> 3.00
110112A [d]	(0.5)	1.89×10^{49}	> 0.64	> 6.75

Table 4.5: Constraints on the jet opening angle, θ_j, from our non-detection of a jet break and using the last optical lightcurve detection. $E_{iso}(\gamma)$ is bolometric and taken from Kann et al. (2011) unless otherwise stated.
Footnotes: (a) Fox et al. (2005) give a jet opening angle of 14° based on the break in the optical lightcurve. However, we see no coincident break in the X-ray lightcurve and so have not classed it as a jet break. (b) This lower limit is consistent with the lower limit from Grupe et al. (2006) of $> 25°$ from late time *Chandra* observations of the X-ray afterglow taken 3 weeks after the GRB. (c) The upper end of the opening angle range given by Burrows et al. (2006) of $\sim 4 - 8°$ is consistent with our lower limit. The proposed jet break occured in late time *Chandra* observations of the X-ray afterglow and outside of the range of our optical measurements. (d) The $E_{iso}(\gamma)$ value for GRBs 081226A and 110112A are in the *Swift* BAT $15 - 150$ keV energy band (e) $E_{iso}(\gamma)$ is taken from Levesque et al. (2010a) (f) Nicuesa Guelbenzu et al. (2011) give the opening angle for a single jet as 4.8° based on the simultaneous break in the optical and near infra-red lightcurves. However, due to no convincing break being evident in the X-ray lightcurve we do not class this as a jet break.

$\beta_X - 0.5$ to allow for values of $p < 2$ which can be reconciled by introducing a high energy-cutoff in the electron energy distribution, and this interpretation therefore allows for GRBs with unusually shallow X-ray spectral indices. Here we consider both criteria for darkness.

There are many possible explanations for bursts which appear dark by either of the above criteria. A small subset are likely to be at high redshift, where the Lyman-α break has moved through the optical (e.g. Tanvir et al. 2009; Cucchiara et al. 2011), while for the majority of LGRBs it appears likely that dust extinction is the prime cause (Perley et al., 2009b; Greiner et al., 2011), although numerous other mechanisms (e.g. Inverse Compton in the X-ray, low circumburst density) remain plausible in individual cases (Li et al., 2002; Sari et al., 1998).

The β_{OX} slope was calculated using interpolated data from the X-ray lightcurve and the most constraining optical measurement or upper limit available. The X-ray lightcurve was fit and interpolated to the same mid-time as the optical measurements. When multiple optical observations were available, and within the time period of the X-ray observations, we used measurements taken 2000 s after the BAT trigger to eliminate the contribution at early times by either reverse shocks or from the prompt emission. The results of this analysis for the optically-detected SGRB sample are given in Table 4.6 and for the X-ray detected sample in Table 4.7.

There are six potentially dark GRBs in Table 4.6. Interestingly, two of these GRBs are "hostless": GRBs 061201 and 070809. As discussed in Chapter 3 of this thesis, "hostless" GRBs have no clearly identifiable host galaxy down to deep optical limits. Though this potential evidence for extinction could then be indicative of an unseen underlying host galaxy, we must add the following caveats. Though GRB 070809 has $\beta_{OX} = 0.45 \pm 0.05$, qualifying it as a dark GRB by the Jakobsson et al. (2004) criterion, the shallow X-ray spectral index of $\beta_X = 0.22^{+0.14}_{-0.11}$ means it is not dark according to the definition of van der Horst et al. (2009) where $\beta_{OX} < \beta_X - 0.5$. GRB 061201 does qualify as dark by both criteria and so could be seen as a genuine dark GRB. The remaining four dark GRBs are 060121, 060313, 070429B and 081226A. These GRBs all reside at a low offset from their host galaxies and so this could be evidence for extinction. In addition, GRB 060121 is purported to be at high redshift ($z \gtrsim 4.0$) meaning this optical extinction could be due to Lyman-α absorption (Levan et al., 2006a; de Ugarte Postigo et al., 2006).

For the sample of seventeen X-ray detected SGRBs with optical upper limits given in Table 4.7 six are potentially dark. Three of these GRBs: GRBs 051210, 100625A and 111117A have known host galaxy candidates within their XRT error circles (Berger et al., 2007b; Fong et al., 2013; Sakamoto et al., 2013). In addi-

GRB	Filter	Mid-time of observation	β_X	β_{OX}
Dark GRB - $\beta_{OX} < 0.5$				
060121	R	7128	$1.28^{+0.17}_{-0.16}$	0.30 ± 0.03
061201	U	3283	$1.19^{+0.28}_{-0.26}$	0.36 ± 0.13
070809	g'	40356	$0.22^{+0.14}_{-0.11}$	0.45 ± 0.05
Dark GRB - $\beta_{OX} < \beta_X - 0.5$				
060313	R	2419	$1.21^{+0.11}_{-0.11}$	0.49 ± 0.06
070429B	V	2029	$2.0^{+0.6}_{-0.6}$	1.14 ± 0.10
081226A	r'	4070	$2.27^{+1.24}_{-0.32}$	0.98 ± 0.09
Dark GRB - $\beta_{OX} \geq 0.5$				
050709	R	126000	$1.24^{+0.22}_{-0.22}$	1.26 ± 0.06
050724	R	41800	$0.67^{+0.13}_{-0.12}$	0.78 ± 0.02
051221A	r'	11120	$1.07^{+0.12}_{-0.11}$	0.76 ± 0.03
051227	R	41363	$1.26^{+0.32}_{-0.27}$	0.70 ± 0.05
061006	I	53753	$1.31^{+0.40}_{-0.35}$	0.73 ± 0.04
070707	R	388907	$2.3^{+2.2}_{-0.6}$	> 0.48
070714B	R	85052	$0.86^{+0.23}_{-0.09}$	0.91 ± 0.13
070724A	K_s	10195	$0.64^{+0.23}_{-0.22}$	0.72 ± 0.03
071227	R	25104	$0.90^{+0.30}_{-0.22}$	0.92 ± 0.06
080503	g	4247	$1.53^{+0.26}_{-0.12}$	1.5 ± 0.12
080905A	R	52806	$0.53^{+0.18}_{-0.17}$	> 0.71
090305A	r'	2014	-	0.72
090426	V	7048	$1.04^{+0.09}_{-0.09}$	0.86 ± 0.04
090510	r'	22299	$0.75^{+0.07}_{-0.07}$	1.00 ± 0.06
090515	R	7911	$1.53^{+0.77}_{-0.27}$	< 4.8
091109B	R	21694	$1.06^{+0.34}_{-0.26}$	0.60 ± 0.04
100117A	r'	15480	$1.61^{+0.32}_{-0.25}$	> 1.2
110112A	i'	55560	$1.17^{+0.25}_{-0.10}$	0.97 ± 0.03

Table 4.6: Table of β_{OX} for the optically detected SGRB sample. The β_X values are taken from Evans et al. (2009a) where we have used, in order of preference: PC mode LT (Late Time) and PC mode TA (Time Averaged) values. The only exception to this choice is if the errors on the late time values are significantly higher than for the time averaged values, in which case we use the value with smaller error. All errors are at the 1σ level.

GRB	Filter	Mid-time of observation	β_X	β_{OX}	Refs
Dark GRB - $\beta_{OX} < 0.5$					
100625A	I	992	$1.40^{+0.40}_{-0.15}$	> 0.48	[1]
100702A	J	364	$1.5^{+0.44}_{-0.3}$	> 0.35	[2]
111117A	u	262	$1.2^{+0.25}_{-0.3}$	> 0.44	[3]
Dark GRB - $\beta_{OX} < \beta_X - 0.5$					
051210	R	63	$2.1^{+0.4}_{-0.3}$	> 0.88	[4]
080919	Ks	699	$1.9^{+0.6}_{-0.4}$	> 0.93	[2]
090621B	R	3180	$2.7^{+0.7}_{-1.0}$	> 1.05	[5]
Dark GRB - $\beta_{OX} \geq 0.5$					
050509B	r'	7797	$0.88^{+0.64}_{-0.34}$	> 0.83	[6]
060801	v	373	$0.68^{+0.12}_{-0.11}$	> 0.50	[7]
061210	u	254800	$1.86^{+1.26}_{-0.61}$	> 1.08	[8]
070714A	v	867	$1.2^{+0.3}_{-0.2}$	> 0.80	[9]
080123	$UVW2$	7379	$1.6^{+0.5}_{-0.4}$	> 1.02	[10]
080426	I	27000	$0.8^{+0.3}_{-0.3}$	> 0.98	[11]
080702A	v	379	$1.0^{+0.4}_{-0.4}$	> 0.98	[12]
081024A	R	135	$0.7^{+0.4}_{-0.3}$	> 1.24	[13]
101219A	u	404	$0.53^{+0.16}_{-0.15}$	> 0.61	[14]
111020A	J	66712	$0.8^{+0.31}_{-0.3}$	> 0.57	[15]
111121A	$UVW2$	750	$0.88^{+0.14}_{-0.13}$	> 0.84	[16]

Table 4.7: Table of β_{OX} for a sample of twelve X-ray detected SGRBs. This includes SGRBs where the X-ray lightcurve best fit can be determined and excludes any SGRBs with only an upper limit on the X-ray decay. As for table 4.6 the β_X values are taken from Evans et al. (2009a). All errors are at the 1σ level. References: [1] Suzuki et al. (2010) [2] Nicuesa Guelbenzu et al. (2012b) [3] Oates and Mangano (2011) [4] Jelinek et al. (2005) [5] Galeev et al. (2009) [6] Bloom et al. (2006) [7] Brown and Racusin (2006) [8] Cucchiara et al. (2006) [9] Chester and Grupe (2007) [10] Cucchiara and Ukwatta (2008) [11] de Ugarte Postigo et al. (2008) [12] de Pasquale (2008) [13] Melandri et al. (2008) [14] Kuin and Gelbord (2010) [15] Tunnicliffe et al. (2014) [16] Kuin et al. (2011)

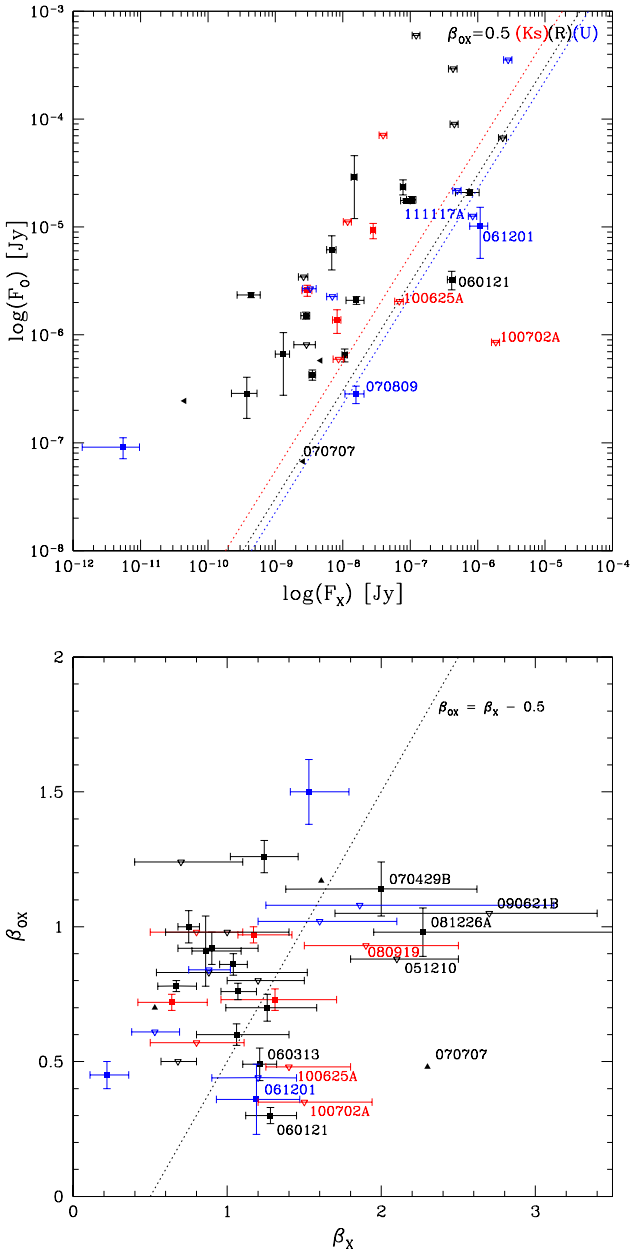

Figure 4.6: The upper plot shows the X-ray flux plotted against optical (black)/infra-red (red)/ultra-violet (blue) flux measured for the SGRB afterglows in our sample (the X-ray flux having been found by interpolating the light curve to the same epoch as the corresponding UV/optical/IR observation). In addition, the SGRBs X-ray detections and optical upper limits are shown as open triangles. The lines representing $\beta_{OX} = 0.5$ for three different wavelengths are shown (cf. Jakobsson et al., 2004). From left to right these lines represent Ks band (red line; $\nu \sim 1.39 \times 10^{14}$Hz), R band (black line; $\nu \sim 4.50 \times 10^{14}$Hz) and the U band (blue line; $\nu \sim 8.18 \times 10^{14}$Hz). Bursts to the right of these lines in the corresponding colour are dark. The triangles represent limits on the values. The lower plot shows the spectral indices β_X vs β_{OX}. The colours are the same as in the first plot. Here the line representing $\beta_{OX} = \beta_X - 0.5$ is shown (c.f. van de Horst et al, 2009). Any GRBs which fall into the dark regime on either plot are labelled.

tion, the subarcsecond localisation with the *Chandra* telescope for GRB 111117A (Sakamoto et al., 2013) shows that this GRB is at a low offset from its host galaxy. Although no host galaxy has yet been identified for the remaining three GRBs extensive investigation at the position of the GRB and in the surrounding regions has not been undertaken. Hence, for all GRBs in the sample the sub-luminous optical upper limit could be evidence for extinction, as for the optically localised sample. Overall, for the sample of 36 GRBs (24 with optical detections and 12 with optical upper limits) 30% are potentially dark GRBs.

4.2.5 Constraints on associated kilonova

Many models of NS-NS and NS-BH mergers, the models often proposed as the progenitors of SGRBs, predict that, as well as the GRB and its subsequent afterglow, there should also be associated thermal emission. This emission is powered by the radioactive decay of heavy elements produced by the r-process within strong winds from the accretion disc (e.g. Li and Paczyński 1998; Kulkarni 2005; Metzger et al. 2008, 2010; Metzger and Berger 2012) or within a tidal tail from the merger itself (Kasen et al., 2013; Barnes and Kasen, 2013). Low ejected mass means that the lightcurve will be dimmer and faster evolving than a typical supernova and hence is often termed a kilonova (Metzger and Berger, 2012).

Metzger and Berger (2012) state that for typical values of ejecta masses $M_{ej} = 10^{-2} M_{\odot}$ the associated kilonova would peak at a visual magnitude of $M_V = -15$ in the rest frame, reaching maximum light around 1 day after the merger and initial GRB emission. However, Barnes and Kasen (2013) suggest that the high opacity from the r-process elements will cause line blanketing in the optical, peaking at $M_R = -13$, with most of the emission in the infra-red. This opacity also produces a broader bolometric lightcurve peaking over longer timescales (a few days to a week) (Kasen et al., 2013; Barnes and Kasen, 2013).

Within the sample of SGRBs investigated here we have looked for any evidence of a kilonova by searching for a rise from $0.5 - 5$ days post-GRB. There is no clear indication for additional thermal emission within the optical lightcurves and we can thus use our fits to place upper limits on any kilonova emission. When the optical lightcurve spans the peak of the kilonova emission, around 1 day in the rest frame, we can use our lightcurve fits to interpolate and to place consistent constraints around this time period. For many GRBs, however, the optical lightcurve is not detected over this time period and in these cases we have used the most constraining detection or upper limit. These values are given in Table 4.8.

Since the kilonova emission should be quasi-thermal, to calculate the upper

limits given in Table 4.8 we have used a blackbody spectrum at $T = 10000K$ to extrapolate the limit from the lightcurve to the V band in the rest frame (Metzger and Berger, 2012). Where the redshift is not known we use $z = 0.5$ as a typical redshift for a SGRB (e.g. Kann et al. 2011). We also only consider detections and upper limits after 0.25 days (based on limits of Barnes and Kasen 2013) in the rest frame since, depending on the initial ejecta mass and velocity, high opacity before this time would mean we would not expect to detect the emission and limits cannot be placed.

To explore the full parameter space we plotted the GRB lightcurves in the r' band rest frame (as before assuming $z = 0.5$ when no redshift is available) and compared them to the the optical kilonova lightcurves adapted from Metzger and Berger (2012) and Barnes and Kasen (2013).

Figure 4.7 demonstrates that in the majority of cases at the peak time of the kilonova the optical emission is still dominated by the afterglow. However, there are seven good examples of the lightcurve constraining the brightest kilonova which are labelled in the figure. The most constraining limit placed on a kilonova is by GRB 080905A. In this case any associated kilonova emission would be a factor of ~ 43 times less luminous in the r' band than the brightest kilonova limit and ~ 4 times fainter than predicted in the standard scenario both from Metzger and Berger (2012). Interestingly, even the deep constraint from GRB 080905A is consistent with the fainter R band lightcurve predicted by Barnes and Kasen (2013). This suggests the contribution of higher opacity from r-process elements may be significant and it may be prudent to conduct future kilonova searches in the infra-red.

4.2.6 Constraints on supernova

For this sample selection we have utilised the oft-used two second divide first proposed by Kouveliotou et al. (1993) in relation to the *BATSE* instrument on board the CGRO telescope. However, this division is based on the spectral response of *BATSE* which is considerably harder than the BAT instrument on the *Swift* satellite. Using the duration distribution of GRBs detected by *Swift*, Bromberg et al. (2013) have proposed a Collapsar - non-Collapsar split based on a flattening in the distribution at short times. They propose that this flattening is due to the minimum time for the jet created by accretion onto the black hole at the centre of the massive collapsed star to break out of the stellar envelope. It should be noted that this non-collapsar - collapsar model for the GRB population does not take account of the proto-magnetar model, which may be the progenitor of a significant proportion of LGRBs (Metzger et al., 2011; Dessart et al., 2012). However, the proto-magentar

GRB	z	Time (rest frame) (days)	Upper limit on M_V (AB)	νL_ν ($10^{42}\,\mathrm{erg\,s^{-1}}$)
Extrapolated fits to 1 day				
GRB 050709	0.1606	1.000	-16.6	1.09
GRB 050724	0.257	1.000	-17.8	3.23
GRB 051221A	0.5464	1.000	-18.7	7.49
GRB 060313	(0.5)	1.000	-18.4	5.63
GRB 070707	(0.5)	1.000	-17.9	3.56
GRB 070714B	0.9224	1.000	-18.4	5.32
GRB 080503	(0.5)	1.000	-16.7	1.12
GRB 090426	2.609	1.000	-22.0	158
Most constraining upper limits or detections				
GRB 051227	(0.5)	1.458	< -16.1	< 0.466
GRB 060121	1.7	13.33	< -17.4	< 2.28
	4.1	0.951	< -23.3	< 481
GRB 061006	0.4377	1.331	< -18.2	< 4.46
GRB 061201	(0.5)	2.261	< -17.6	< 2.65
GRB 070429B	0.9023	0.663	< -20.0	< 23.5
GRB 070724A	0.4571	0.636	< -16.5	< 0.976
GRB 070809	(0.5)	0.976	< -16.6	< 1.06
GRB 071227	0.381	2.441	< -17.2	< 1.78
GRB 080905A	0.1218	1.355	< -13.5	< 0.0601
GRB 081226A	(0.5)	18.83	< -16.1	< 0.672
GRB 090305A	(0.5)	6.019	< -16.2	< 0.748
GRB 090510	0.903	-	-	-
GRB 090515	(0.5)	0.694	-15.3	0.324
GRB 091109B	(0.5)	0.881	< -16.0	< 0.630
GRB 100117A	0.915	-	-	-
GRB 110112A	(0.5)	0.429	-18.9	8.63

Table 4.8: The limits on a kilonova detection in the V band for all GRBs in the sample. The peak brightness time for the most common kilonova is taken as 1 day in the rest frame. For those GRBs with data covering this time period the lightcurve fit is used to interpolate the V band absolute magnitude at that time. When the data does not extend to 1 day we used the most constraining upper limits or detections closest to this time to put an upper limit on a kilonova detection. An early time cutoff of 0.25 days in the rest frame has been applied as it is likely that little emission will escape before this time due to the opacity of the ejecta. For GRBs 090510 and 100117A no data is available after this cutoff and hence no upper limit has been given. When the redshift is unknown $z = 0.5$ is used as a common SGRB redshift.

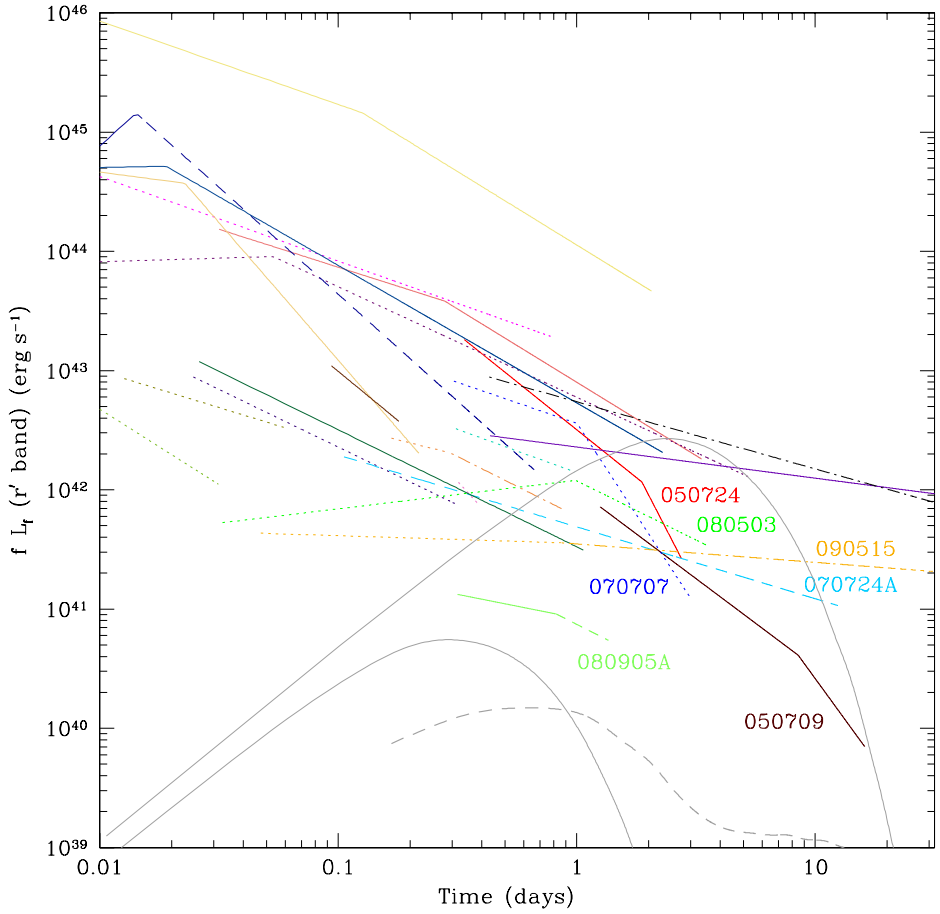

Figure 4.7: The fits to the lightcurves of the GRBs in the sample in the rest frame. To show the typical expected brightness of a kilonova in the r' band we have also plotted the kilonova limits adapted from Metzger and Berger (2012) (grey, solid lines) and from Barnes and Kasen (2013) (grey, dashed line). The limits from Metzger and Berger (2012) represent a range of plausible kilonova models spanning the expected range of ejecta mass ($M_{ej} \sim 10^{-3} - 0.1\,M_{\odot}$) and velocity ($\beta \approx 0.1 - 0.3$) based on the work of Metzger et al. (2010). The limits from Barnes and Kasen (2013), adapted from the R band, are calculated with ejecta mass $M_{ej} = 10^{-2} M_{\odot}$ and velocity $\beta = 0.1$ and include additional opacity from r-process elements (particularly the lanthanides) dimming the R band lightcurve and causing reddening to the infra-red (see also Kasen et al. 2013) The GRB lightcurves are also shown and are colour coded in the same way as Figure 4.2. The lightcurves of GRBs with known redshifts are shown as solid lines and upper limits as dashed lines. Where the redshift is unknown $z = 0.5$ has been used and these lightcurves are shown as dotted lines for the fits and dot-dash lines for upper limits. To scale to the rest frame r' band we have used the beta values from Table 4.2. Seven GRBs are reasonably constraining of the brightest kilonova but only GRB 080905A places a deeper constraint on the presence of a greater range of possible kilonova lightcurves. None of the lightcurves reach the limit placed by Barnes and Kasen (2013).

model is still subject to the same constraints placed on the collapsar model at short durations since the GRB still have to emerge from within a stellar envelope. Hence, we would expect the contribution of this population to be more significant at longer durations and the fit to any plateau based on minimum time constraints for any GRBs from stellar collapse should not be strongly skewed. Based on the fit to the plateau, Bromberg et al. (2013) calculate the probability of an object at a given duration being a non-collapsar, f_{NC}, and using $f_{NC} = 0.5$ place a division at 0.8 s. They also suggest that 40% of GRBs with durations below 2 s are collapsars. In order to investigate this claim we divided the GRB sample into those above and below $T_{90} = 0.8$ s (or, for those with extended emission, $T_{90}(IPC) \geq 0.8$ s) and searched for the presence of a supernova. In our sample nine GRBs are above this new proposed duration threshold (given in Table 4.9). We did not detect any characteristic rise in the lightcurves suggestive of supernova emission and so we can use our data to place constraints.

All limits have been scaled to the rest frame R band using spectra available for SN 1998bw (Patat et al., 2001).[4] As shown in Patat et al. (2001) there is clear spectral evolution over the course of the supernova and hence we attempted to match the spectrum used to the time of of the upper limits as closely as possible and where the spectral range of the available spectra allowed. As for section 4.2.5 where the redshift is not known we use $z = 0.5$. Limits on the R band absolute magnitudes are given in Table 4.9. We also include the f_{NC} values individually calculated by Bromberg et al. (2013) for all traditional short GRBs in the sample using, where possible, both the duration and spectral hardness information. Due to ambiguity in the duration of GRBs with extended emission no probabilities were given. Figure 4.8 show the rest frame R band supernova constraints along with the R band lightcurve of SN 1998bw from Galama et al. (1998). We also include the lightcurve for SN 2002ap which was a SN 1998bw-like event but represents the faint end possible for these types of supernova (Gal-Yam et al., 2002).

[4]Data obtained using the The Online Supernova Spectrum Database (SUSPECT) available at http://suspect.nhn.ou.edu

GRB	z	Time (rest) (days)	M_R (AB)	$L_R/L_{R,\mathrm{SN1998bw}}$	M_V (AB)	$L_V/L_{V,\mathrm{SN1998bw}}$	f_{NC}
SGRBs with $T_{90} \geq 0.8\,\mathrm{s}$							
GRB 051221A	0.5464	5.26	> -18.08	1.92	> -17.40	0.79	$0.18^{+0.08}_{-0.11}$
GRB 060121	~ 4.0	1.06	-	-	-	-	$0.17^{+0.14}_{-0.15}$
GRB 070707	(0.5)	5.03	> -15.68	0.14	> -15.03	0.056	$0.84^{+0.02}_{-0.03}$
GRB 070809	(0.5)	0.976	-18.07	2.67	-17.42	1.40	$0.09^{+0.13}_{-0.05}$
GRB 071227	0.381	15.4	> -18.07	0.44	> -17.65	0.24	$0.71^{+0.15}_{-0.59}$
GRB 080905A	0.1218	15.6	> -13.37	0.006	> -13.47	0.005	$0.88^{+0.07}_{-0.11}$
GRB 090426	2.609	7.42	-	-	-	-	$0.10^{+0.15}_{-0.06}$
GRBs with extended emission with $T_{90}(IPC) \geq 0.8\,\mathrm{s}$							
GRB 051227	(0.5)	61.5	> -17.44	1.01	> -16.83	0.68	
GRB 070714B	0.9224	4.40	-19.51	10.21	-18.79	3.82	
SGRBs with $T_{90}(IPC) < 0.8\,\mathrm{s}$							
GRB 050709	0.1606	29.9	> -11.24	0.001	> -11.00	0.001	$0.92^{+0.02}_{-0.03}$
GRB 060313	(0.5)	5.34	-17.30	0.58	-16.66	0.23	$0.92^{+0.05}_{-0.08}$
GRB 061201	(0.5)	10.9	> -17.46	0.30	> -16.97	0.16	$0.92^{+0.05}_{-0.08}$
GRB 070429B	0.9023	0.592/42.00 [a]	> -20.97		> -20.86	16.52	$0.32^{+0.26}_{-0.15}$

GRB 070724A	0.4571	12.5	-15.16	0.033	> -14.73	0.018	$0.37^{+0.26}_{-0.17}$
GRB 081226A	(0.5)	18.8	> -17.34	0.22	> -16.85	0.12	$0.60^{+0.36}_{-0.24}$
GRB 090305A	(0.5)	13.3	> -17.19	0.21	> -16.70	0.11	$0.96^{+0.02}_{-0.36}$
GRB 090510	0.903	0.214	-21.04		-20.32		$0.97^{+0.01}_{-0.29}$
GRB 090515	(0.5)	0.694/132 [a]	-17.04		> -16.32	1.41	$0.94^{+0.03}_{-0.07}$
GRB 091109B	(0.5)	0.881	> -17.28	1.29	> -16.64	0.69	$0.97^{+0.01}_{-0.03}$
GRB 100117A	0.915						$0.97^{+0.01}_{-0.03}$
GRB 110112A	(0.5)	132	> -16.35	1.39	> -15.75	0.84	$0.30^{+0.26}_{-0.15}$
GRBs with extended emission with $T_{90}(IPC) < 0.8\,\mathrm{s}$							
GRB 050724	0.257	25.8	> -16.11	0.084	> -15.74	0.058	
GRB 061006	0.4377	96.3	> -17.79	2.90	> -17.25	1.88	
GRB 080503	(0.5)	6.09	> -15.40	0.085	> -14.76	0.035	

Table 4.9: The most constraining limits placed on an accompanying supernova either with upper limits or when a detection was made with no noticeable rise. For comparison we also include the ratio between the luminosity of the limit to the of SN 1998bw, $L_{SN1998bw}$, at the stated rest frame time (Galama et al., 1998). No value is given when the limit is outside the SN measured range. For GRBs 090426 and 060121 the redshifts are such that we cannot place a meaningful limit and are included here to demonstrate their presence in the appropriate subsample. We also include the probability of the GRB being a non-collapsar object, f_{NC} from Bromberg et al. (2013). For GRBs with extended emission no f_{NC} is assigned.
Footnotes: (a) For GRBs 070429B and 090515 the most constraining limits in the R and V band were at different times.

In figure 4.8 six out of the twelve GRBs with known redshift are constraining of a hypernova event such as SN 1998bw and five of these GRBs discount fainter associated supernovae such as SN 2002ap. Cano (2013) finds that most LGRB-associated SN have luminosities equivalent to SN 1998bw with scatter of $\sim 0.5 \times L_{SN\,1998bw}$ and hence these limits are constraining of the majority of measured collapsar supernovae. The limit of GRB 050709 is particularly strong, due to follow-up with the ACS instrument on the Hubble Space Telescope (HST). Of the five GRBs above the proposed duration split with a well-constrained redshift three of these events constrain a SN 1998bw-like event and perhaps in two cases a fainter such event. The limit of GRB 080905A very strongly constrains the non-detection of an associated supernova ~ 200 times fainter than SN 1998bw (in line with the limit reported by Rowlinson et al. 2010a) and is comparable to the limits placed on long GRBs 060505 and 060614 which occured at low redshift (Fynbo et al., 2006).

Setting unknown redshifts in our sample to $z = 0.5$, we find that 15 of the 24 GRBs constrain a bright associated supernova, allowing for a maximum of 38% of the sample being associated with collapsar events. If we also use the f_{NC} values for the sample, where these values are available (19 GRBs, excluding GRBs with extended emission) and assuming all GRBs with $f_{NC} > 0.5$ are non-collapsar objects, we find a maximum collapsar percentage of 21%. However, though a redshift of $z = 0.5$ is suitable for a typical SGRB event if the GRBs are collapsars then for GRBs with unknown redshift this assumption would be incorrect and we would expect the redshift to be higher ($< z > \sim 2.2$; Jakobsson et al. 2012), severely weakening the supernova constraints. Hence to check that the validity of this constraint we consider the limited sample of GRBs with measured redshift and f_{NC} values, finding the maximum percentage of GRBs which could have associated supernovae to be 22% (7/9 events likely to be non-collapsar objects), consistent with the number inferred above. This suggests that the 37% collapsar contamination suggested by the f_{NC} values in our sample is too high, with supernova constraints on three of the GRBs below the $f_{NC} < 0.5$ threshold. Of these three GRBs, in particular, GRBs 051221A and 070724A have a well-constrained redshift and the latter also has a strong supernova constraint. Also comparing, for example, the positions of the SGRBs within their host galaxies, a sample defined as $T_{90} < 2\,\mathrm{s}$ is clearly distinct from a LGRB sample (Fong et al., 2010). As we will discuss in Chapter 5, this same distribution containing only GRBs with $0.8\,\mathrm{s} < T_{90} \leq 2.0\,\mathrm{s}$ is still distinct from the LGRB sample, also suggesting the level of contamination is perhaps not as high as proposed. However, it should be noted that since this sample is optically localised it does not include a large proportion of GRBs and is not necessarily representative

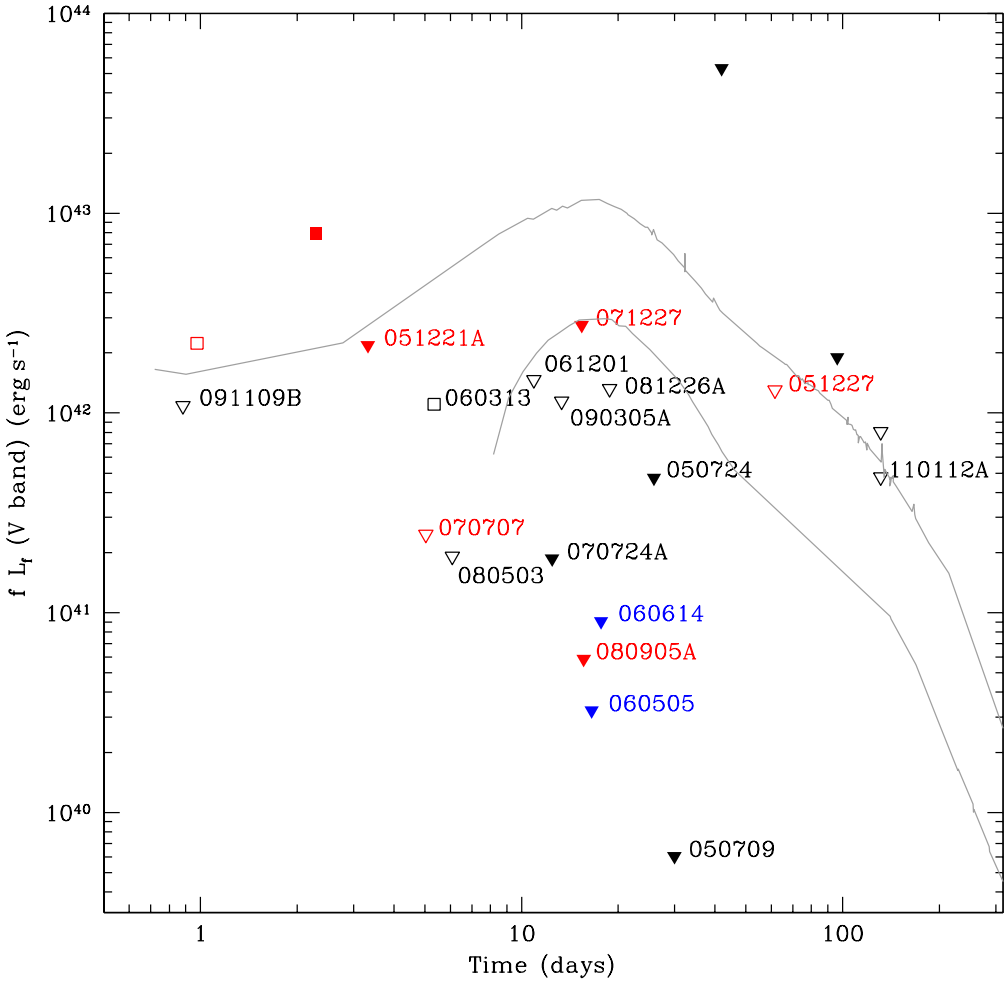

Figure 4.8: The limits placed on any associated supernova in the rest frame V band either with upper limits (triangles) or when no supernova was seen in the detections (squares). Closed and open symbols represent known and unknown redshift, with unknown redshift set to $z = 0.5$. The subset of GRBs with T_{90} (or $T_{90}(IPC)$) above and below the 0.8 s division are shown as red and black points respectively. For comparison we plot the V band lightcurve of SN 1998bw, which accompanied GRB 980425 and the lightcurve of SN 2002ap. The lightcurve for SN 1998bw peaked around 16 days (post GRB trigger) with an absolute magnitude of $M_V = -19.35 \pm 0.05$. SN 2002ap reached an absolute magnitude of -17.7. Since this supernova did not accompany a GRB but is SN 1998bw-like, the offset time used from the GRB was estimated to be the same as for SN 1998bw. We also include the upper limits (blue triangles) for low redshift SN-less LGRBs 060505 and 060614 (Fynbo et al., 2006). These limits are clearly deeper than the majority of GRBs in this sample but are comparable to the limit of GRB 080905A and not as deep as for GRB 050709.

of the whole SGRB sample.

4.3 Conclusions

We have investigated a sample of 24 SGRBs combining those with and without extended emission. Using fitted SEDs, where possible, and extrapolating an optical slope from the X-ray slope where not, we have combined all the optical data into an extrapolated R band lightcurve for each short GRB. In some cases due to either a clear evolution of the β_O slope, or no improvement in the overall lightcurve by combining the data we have investigated single band lightcurves instead. There is great diversity in the optical lightcurve slopes with many containing breaks. Except for GRBs 050724 and 080503, which show flaring activity and rising behaviour respectively, the optical lightcurves are all reasonably well fit with a set of power laws.

We find an achromatic break in the lightcurve of GRB 060313 between the optical and X-ray lightcurves. However the change in slope in the optical lightcurve is particularly steep, making it unlikely that this is a jet break. In the lightcurve of GRB 090426 though there is a consistent break between optical bands, in particular r' and g' there is no significant evidence for a break in the X-ray lightcurve, though this lightcurve does not extend far beyond the optical break, making it difficult to constrain. Overall, we do not find significant evidence of a jet break in any of the lightcurves of our sample, though in six cases the X-ray data does not overlap with the optical break.

Adding a sample of SGRBs with optical upper limits to the sample with optical detections, 12/36 SGRBs show evidence for suppression of optical emission from comparison of their flux with available X-ray data. Interestingly, within this sample are two GRBs with no clear host galaxy down to deep optical limits ("host-less" GRBs). The remaining optically detected SGRBs are embedded within their host galaxies and in the case of GRB 060121 this optical suppression may be an indication of high redshift.

Using the optical detections or limits interpolated to or closest to 1 day after the GRB we can constrain the presence of thermal emission from an NS-NS or NS-BH merger (kilonova). Looking at the fitted lightcurves for the GRBs in our sample and comparing with the canonical kilonova brightness in the optical from Metzger and Berger (2012), in seven cases (assuming a redshift of $z = 0.5$ for three) we can constrain a optically bright associated kilonova. In the case of GRB 080905A any associated thermal emission must be ~ 43 times fainter than the brightest kilonova

and ~ 4 times fainter than the standard scenario. Detecting this emission is difficult due to the lightcurve still being dominated by the afterglow for many SGRBs at the peak brightness of the kilonova.

Within the sample we also placed constraints on associated supernova, paying attention in particular to GRBs with $T_{90} > 0.8$ s, ostensibly a more suitable duration division for SGRBs detected by *Swift*. We did this by looking at the late time upper limits (and sometimes detections) around 17 days after the GRB. For the five GRBs in this subsample with measured redshifts (of nine GRBs in total), the limits on three of these events constrain a SN1998bw like transient, with the deepest limit in this subsample coming from GRB 080905A of > 100 times fainter than SN 1998bw, which is comparable to the deep limits of GRB 060614 and GRB 060505 (Fynbo et al., 2006). For the sample of GRBs with known redshift, ostensibly, combining our supernova limits with the probabilities of a GRB being a non-collapsar object, f_{NC}, we find a maximum of 22% of the GRBs could have been collapsar objects.

Chapter 5

Classification of γ-ray bursts: a population study and the case of GRB 100816A

5.1 Introduction

As has been discussed extensively throughout this thesis, gamma-ray bursts can be nominally split into two categories of long and short GRBs. The importance of this distinction lies in the fact that these populations have disparate progenitors and are not simply the manifestation of the same physical process. In chapters 3 and 4, samples of SGRBs have been collated utilising the often-used 2.0 s duration division between the classes, based on the original GRB sample observed by *BATSE*. However, overlap between the classes means consideration of other properties; the spectral hardness, lag (Norris and Bonnell, 2006) and the nature of the GRB host galaxy can also be important for classification (e.g. Levan et al. 2007). In addition, as was also discussed in chapter 4, based on the *Swift* data, which has a softer spectral response than *BATSE* had, Bromberg et al. (2013) have suggested a duration split at 0.8 s would be more appropriate for *Swift* SGRBs (see also (Bromberg et al., 2011)).

The importance of correctly classifying GRBs is twofold; firstly the true duration distribution of a class provides a direct handle on the lifetime of the central engine within the progenitor, and hence on the progenitor itself. Secondly, an observational selection effect is that longer lasting bursts tend to yield high fluences, and a greater chance of detailed study (e.g. Gehrels et al. 2009; Nysewander et al. 2009). Hence, the key task of unveiling the progenitors of SGRBs may be much

easier if we can isolate both a clean sample, and one of moderate size.

In addition to the main progenitor classes (collapsars and compact object mergers) often associated with short and long GRBs we may expect to see some contribution from other events capable of producing GRB-like transients such as giant flares from magnetars within local galaxies (Tanvir et al., 2005; Levan et al., 2006b), massive white dwarf - neutron star or black hole mergers (Fryer et al., 1999b; King et al., 2007) producing longer lived objects ($> 100\,$s) (Thompson et al., 2009) or even the end point in the lives of hydrogen-rich supergiants as opposed to the hydrogen-stripped Wolf-Rayet progenitors for traditional collapsars (Levan et al., 2013). The observed diversity within the GRB population may suggest this is already the case with some individual outliers having properties deviating from both expectations and other, similar, events. Within the *Swift* sample GRBs 060614 and 060505 (Della Valle et al., 2006; Fynbo et al., 2006; Gehrels et al., 2006) are two examples of ostensibly long GRBs (i.e. $T_{90} > 2.0\,$s) but with no accompanying supernova to deep limits, perhaps suggesting collapsar objects accompanied by particularly weak supernova (from a small ^{56}Ni yield, maybe due fall-back BH formation rather than direct collapse) (Fryer et al., 2006; Tominaga et al., 2007; Kochanek et al., 2008), examples of mis-classified short GRBs (Xu et al., 2009) or a different progenitor entirely. Clearly the wealth of potential progenitors for gamma-ray bursts means that some proportion of the population may not fit into a two-category designation.

Looking at the duration distribution of GRBs from multiple GRB telescopes, there are suggestions of a third group of GRBs of intermediate duration, and spectra typically softer than both long and short GRBs (Horváth, 1998; Horváth et al., 2008; Řípa et al., 2009; Horváth, 2009). This putative third group contributes a much smaller fraction of the total population than either long or short bursts, but its contribution could be significant around the notional two second divide. This is especially true for bursts detected by *Swift*, since its energy response relative to *BATSE* means it tends to detect bursts with a rather softer spectral shape. In essence this can dramatically change the selection function of different burst types.

Isolation of individual intermediate GRBs has been attempted by de Ugarte Postigo et al. (2011), exploring the multi-dimensional parameters space of bursts with intermediate duration to assess if any obvious differences emerge relative to the expected properties of LGRBs and SGRBs. de Ugarte Postigo et al. (2011) conclude that, within their sample, the majority of such bursts are consistent with lying within either of the classical long or short populations (the majority within the long group).

Hence, the issue of classification is a complex one. In this chapter we attempt to probe this issue by considering a sample of GRBs split using a set of duration cuts. We consider, in particular, the region around the two second divide looking at "short" GRBs both below 0.8 and 2.0 seconds and GRBs of intermediate duration up to 10.0 seconds. For these samples we look at:

- The prompt emission properties. Looking at the E_{peak}-E_{iso} relation followed by long but not by short GRBs (Amati et al., 2002).
- The X-ray and R-band afterglow properties sampled at a given time in the rest frame.
- The environment within the host galaxy.

Into this mix we also consider the particular case of GRB 100816A, a hard burst of intermediate duration (3 s) with good γ-ray, X-ray and optical followup. We locate the burst well offset from a bright galaxy at $z = 0.8$, and discuss the nature of the burst in comparison with the populations of both long, short and potentially intermediate GRBs. We place constraints on any accompanying supernova at the burst position and find the emission would have to be ~ 3 times fainter than a hypernova such as SN1998bw. Within the context of the population as a whole, the afterglow and environment properties of GRB 100816A align it with the SGRB population. However, looking at its prompt emission it is consistent with the E_{iso}-E_{peak} relation normally only seen for LGRBs. If GRB 100816A is a short GRB then not only does it add another well-studied example to the SGRB sample but also represents the first measured absorption redshift within an afterglow spectrum, providing confirmation of the redshift rather than relying on the association of an SGRB with its host galaxy. It is unlikely that this GRB is associated with a collapsar event due to its lack of coincident supernova and its position within its host galaxy.

Though, we see a trend of more collapsar contamination as we look at GRBs with increasing T_{90}, the case of GRB 100816A, a hard GRB at the long end of the short distribution, also demonstrates that there are still objects which do not fit the simple divide between short and long GRBs. Overall, comparing factors beyond simple hardness and duration, we do not find any strong evidence for a distinct third population sitting near the two second divide, but it also likely that any population at this duration has a contribution too small compared to the short and long populations to identify its unique properties.

5.2 GRB 100816A: Observations and Analysis

5.2.1 High energy observations

GRB 100816A was first detected by *Swift* at 00:37:51 on 16 August 2010 (Oates et al., 2010), and was also recorded by both Fermi (Fitzpatrick, 2010a,b) and Konus-Wind (Golenetskii et al., 2010). Its duration was $T_{90} = 2.9 \pm 0.6\,\mathrm{s}$ in the $15 - 150\,\mathrm{keV}$ band. *Fermi* measured the duration as $2.04 \pm 0.23\,\mathrm{s}$ in the $50 - 300\,\mathrm{keV}$ band, closer to the *BATSE* spectral energy range for which the $T_{90} = 2.0\,\mathrm{s}$ division was first measured, though Bromberg et al. (2013) suggest the SGRB split for *Fermi* should be placed at 1.7 s. For both duration measures, GRB 100816A sits near the short-long GRB T_{90} boundary. In addition, the burst is spectrally hard, with a best fit peak energy of $E_p = 170.7 \pm 79.7\,\mathrm{keV}$, based on the *Swift* observations (Markwardt et al., 2010), consistent with those obtained by Konus-Wind ($E_p = 148^{+41}_{-26}\,\mathrm{keV}$) and Fermi ($E_p = 146.30 \pm 3.44\,\mathrm{keV}$). In addition, looking at the difference in photon arrival times for different BAT bands, GRB 100816A has a small lag measurement of $10 \pm 25\,\mathrm{ms}$ in the (100-350) - (25-50) keV range (Norris et al., 2010a). Its total fluence of $(2 \pm 0.1) \times 10^{-6}\,\mathrm{ergs\,cm^{-2}}$ places it at the bright end of the *Swift* SGRB fluence distribution, and central in the distribution for LGRBs.

5.2.2 XRT and UVOT observations

A prompt slew of the telescope yielded detections with both the X-ray and Ultraviolet-Optical Telescopes (XRT and UVOT). The XRT starting observing 89 s after the BAT trigger, obtaining 4.4 ks of data. We downloaded the pre-reduced XRT lightcurve and fit the data (Evans et al., 2007).[1] Looking at the X-ray data from 200 s onwards, at the end of the flaring activity, we fitted the lightcurve with a power law with slope $\alpha_X = 1.08^{+0.03}_{-0.03}$. Fitting a broken power law with a break around 800 s does improve the fit but an F-test value of 12.6% shows this is not strongly significant. This is shown in Figure 5.1.

The XRT early time spectrum formed from Window Timing (WT) mode data can be fit with an absorbed power-law spectrum with photon index $2.16^{+0.22}_{-0.21}$, consistent with the index of the later time spectrum from Photon Counting (PC) mode data (Littlejohns and Oates, 2010). The best fitting absorption column of $1.4^{+0.5}_{-0.4} \times 10^{21}\,\mathrm{cm^{-2}}$ is in excess of the Galactic value of $4.5 \times 10^{20}\,\mathrm{cm^{-2}}$ (Kalberla et al., 2005). Using the detected Gemini points described in section 5.2.3 we measured the optical to X-ray slope of $\beta_{OX} \sim 0.57$, consistent with the canonical GRB

[1] From the XRT repository available online at http://www.swift.ac.uk/xrt_curves/

afterglow model (Sari et al., 1998).

The UVOT started observing the GRB position 91 s after the BAT trigger. The optical afterglow was detected with high significance in the *white* and U band filters and marginally in V, B and $UVW1$ (Oates et al., 2010). In order to characterise the decay of the lightcurve measured by UVOT we downloaded the pre-reduced UVOT data.[2] Using the HEASOFT UVOT data analysis tools to both detect objects in the field (using SExtractor) and calibrate them, we extracted the two U band epochs where the source was detected, details in Table 5.1, finding a power law index of $\alpha_U = 1.09 \pm 0.12$.

5.2.3 Optical observations

We observed the afterglow of GRB 100816A with the GMOS instrument on the Gemini North telescope, beginning at 11:34 UT, approximately 11 hours after the burst. The afterglow was well detected, as was the apparent host galaxy (Tanvir et al., 2010b). A log of our Gemini observations is given in Table 5.1 and the finding chart is shown in Figure 5.2.

Spectroscopic data were reduced in the standard fashion using the Gemini IRAF packages to create a flattened, cosmic-ray cleaned and wavelength calibrated spectrum covering the wavelength range 4000–6700Å. The resulting data are of low signal to noise, but the trace from both afterglow and host galaxy can be seen within the spectrum. Within the afterglow spectrum we see signatures of MgII (2797/2803 Å) and FeII (2600Å), at a common redshift of $z = 0.8035$, which matches the redshift obtained from emission lines from the X-shooter spectrograph on the Very Large Telescope (VLT) (Tanvir et al., 2010b) and we adopt it as the redshift of GRB 100816A.

In addition to our spectroscopic observations we also obtained imaging observations in the r' and i' band over several epochs (see Table 5.1). This photometric data was reduced using the Gemini IRAF packages to produce bias subtracted, flat-field corrected images. The afterglow is clearly detected in our early epochs, but no source is seen in difference imaging between the final two epochs as can be seen in Figure 5.3. To assess the depth of this subtraction we populated the images with artificial stars with a PSF matched to that of isolated objects within the field, and subsequently attempted to recover these in new subtractions. Though the depth of the subtraction image is measured as $r'(AB) > 25.85$, both epochs involved in

[2] From http://www.swift.ac.uk/swift_portal/

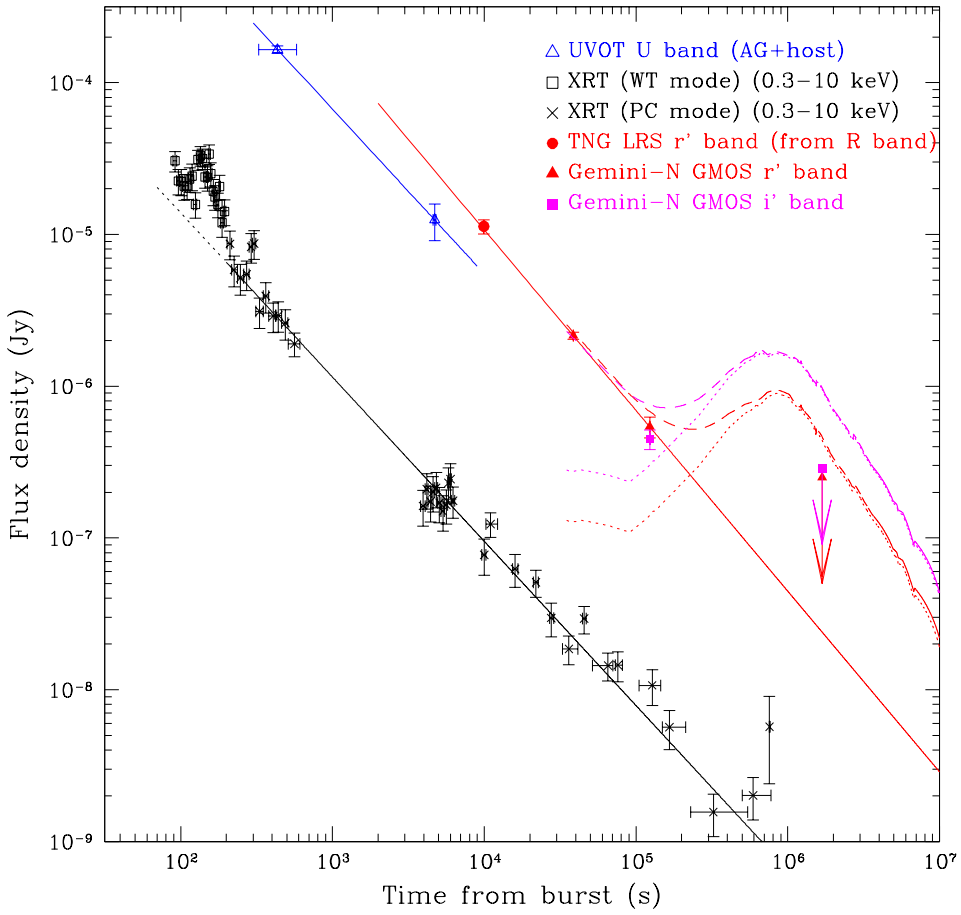

Figure 5.1: The X-ray and optical lightcurve of GRB 100816A. The X-ray lightcurve is shown with black points with open squares and crosses respectively for points measured in Window Timing (WT) and Photon Counting (PC) modes. The lightcurve shows early time flaring superimposed on a power law. Fitting the data from 200 s onwards yields a best fit single power law with $\alpha_X = 1.08^{+0.03}_{-0.03}$. The black, broken line shows this power law extended to earlier times. The GMOS r' and i' band afterglow measurements are also shown as red triangles and magenta squares. The best fit power law is shown for the r' of $\alpha_r = 1.19$ (solid line), with the contribution a supernova with the shape and magnitude of SN1998bw would make to the lightcurve (dotted line) and the lightcurve produced from the combination of the two (dotted line). The constraint on any accompanying supernova was placed from subtraction between the epochs at 6.6 and 19.5 days. At these epochs the contribution of any SN is non-negligible and hence the limit has been scaled based on the difference in contributions between the epochs. The upper limit on the i' band decays faster than -0.67. Assuming the same power law slope for the i' band as the r' band the limit placed on any accompanying SN must be $\lesssim 1.9$ times (r' band) and $\lesssim 3.4$ times (i' band) fainter than a SN1998bw-like hypernova. The TNG r' band point, scaled from R band, is also shown (red, filled circle) and is consistent with the fit to the r' band GMOS points.

the subtraction could have contributions from any underlying supernova (as can be seen in Figure 5.1). Using the difference between the combined afterglow and supernova fluxes for a SN1998bw-like transient we can scale the measured depth and place a limit on any underlying supernova at 19.5 days of $r'(AB) > 25.4$ and and $i'(AB) > 25.3$, ~ 1.9 times and ~ 3.4 times fainter than SN1998bw respectively. In addition, this limit is also fainter than the vast majority of supernova associated with GRBs (Hjorth and Bloom, 2011; Cano, 2013).

Along with the X-ray and UVOT U band lightcurves, the i' and r' band optical lightcurves for GRB 100816A are shown in Figure 5.1. To compare with our Gemini r' lightcurve we also plot the measured TNG LRS afterglow point measured at earlier times, calibrated from SDSS stars in the field.[3] The host-afterglow complex was not resolved in the TNG images and so a host contribution was subtracted using measured magnitudes from the Gemini imagery. The TNG image was also in the R band and so was scaled to the appropriate r' band using a power law SED and a representative spectral slope based on the canonical afterglow model (Achterberg et al., 2001) of -0.6 from Kann et al. (2011). The TNG point is consistent with our Gemini r' band measured slope. The best fit r' band slope is $\alpha_r = 1.19 \pm 0.15$ and an upper limit can be placed on the i' band slope of $\alpha_i > 0.67$. In addition to the afterglow we also show the lightcurves combined with the contribution we would see for a supernova with the magnitude and shape of SN 1998bw at $z = 0.8035$ (Galama et al., 1998). The SN lightcurve has been scaled to the r' and i' bands using the appropriate spectra closest to the measured time period from Patat et al. (2001).[4]

Host galaxy

Our X-shooter spectroscopy of the host galaxy shows emission lines of $H\alpha$, $H\beta$, OII (3727 Å), NII (6548/6583 Å) and OIII (5007 Å) and the H and K absorption lines of CaII identified at redshifts $z = 0.8034$ and $z = 0.8049$ (Tanvir et al., 2010b). This is possibly indicative of either an interacting system or velocity components within the galaxy itself (Tanvir et al., 2010b).

The presence of emission lines in the spectra tells us that it is actively star forming. Considering the late time Gemini imaging in the r' and i' bands we measure a galaxy magnitude of $r' = 22.44 \pm 0.02$ and $i' = 21.41 \pm 0.01$. At $z = 0.8035$ these bands span the Balmer break, the relative strength of which can inform us about the age of the stellar population, with older populations displaying a stronger break.

[3] Available from the TNG public archive at http://ia2.oats.inaf.it/index.php/tngarchive/tng

[4] Making use of the SUSPECT SN spectrum archive available at http://bruford.nhn.ou.edu/ suspect/index1.html

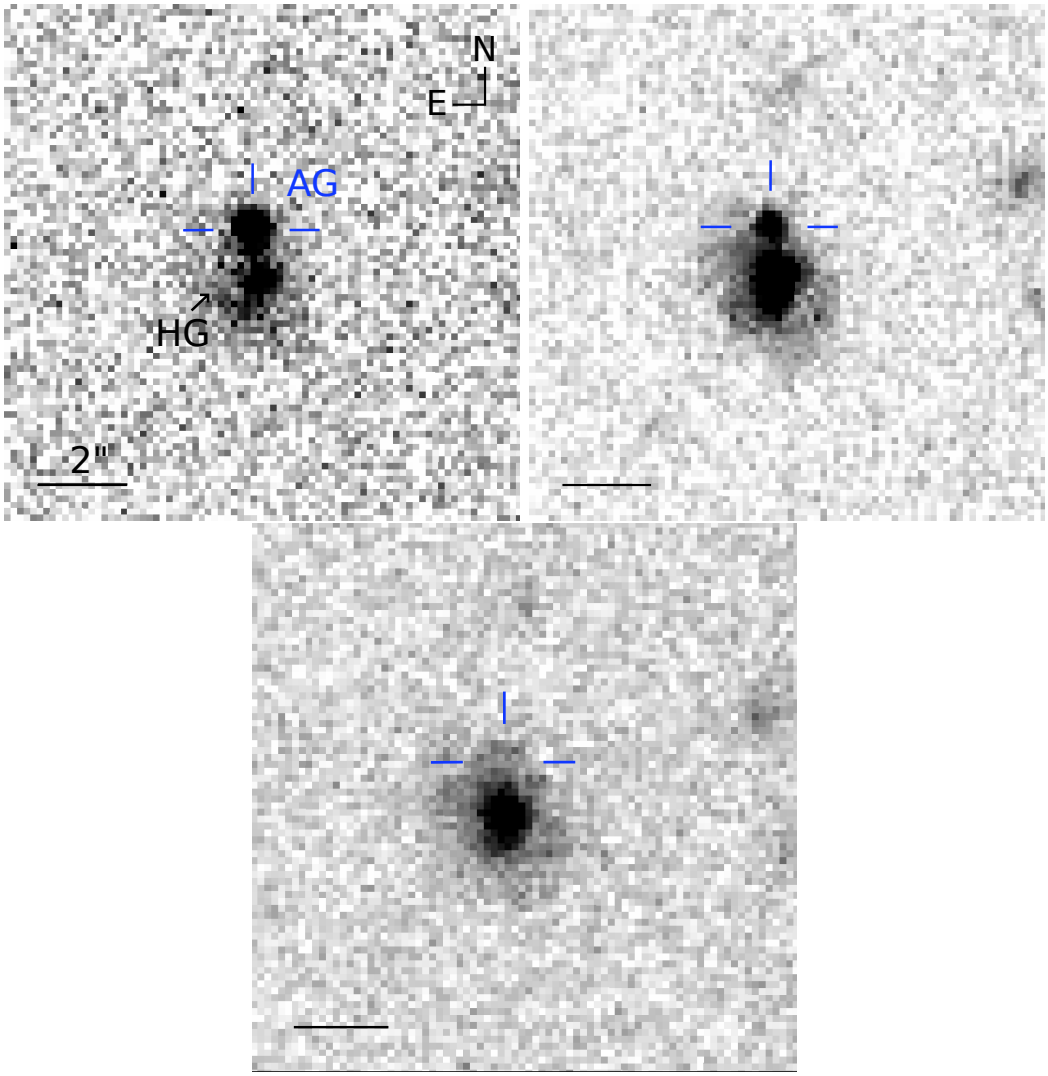

Figure 5.2: The finding chart for GRB 100816A. These images were taken by the GMOS instrument on the Gemini North telescope in the r' band. The afterglow (AG) was detected on the north side of its host galaxy (HG), indicated in the first panel. The third panel shows the reference epoch of observation which was the deepest exposure at ~ 6.6 days after the GRB. This image was used as the reference when subtracting from the other epochs to both measure the afterglow magnitude and to place limits on any associated supernova emission.

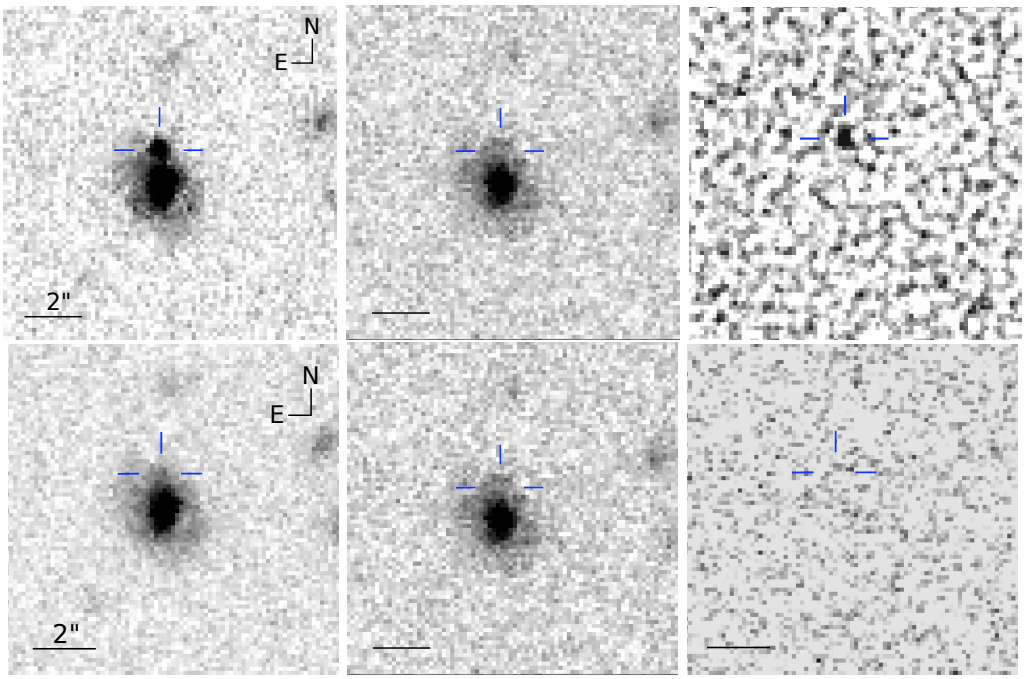

Figure 5.3: Two sets of subtraction images for GRB 100816A. As for Figure 5.2 these images were taken in the r' band by the GMOS instrument. The top line shows the the subtraction of the second epoch image (at ~ 1.4 days) along with the reference image (at ~ 6.6 days). The top right panel (final in the sequence) shows the residual from this subtraction from which we can measure the magnitude of the afterglow. The bottom line of images shows the result to the subtraction used to place a constraint on any associated supernova. The series shows the imaging taken at ~ 19.5 days, when we would expect the supernova to peak, the same reference image before and the result of the subtraction. No object is present at the GRB position down to a 3σ limit of $r' > 25.9$ in the subtraction image.

Date	Time	ΔT (days) (midtime)	Filter / Grism	Exposure (s)	Mag	Object
UVOT observations						
2010-08-16	00:43	0.0050347	U	240	18.38 ± 0.06	Host+AG
2010-08-16	01:54	0.054526	U	190	21.2 ± 0.30	Host+AG
TNG LRS observation						
2010-08-16	03:22	0.11500	R	180	21.3 ± 0.1	AG
Gemini North GMOS observations						
2010-08-16	11:27	0.44653	r'	120	23.10 ± 0.06	AG
2010-08-16	11:34	0.47881	B600	4x1000	-	-
2010-08-17	10:42	1.42478	r'	3x180	24.60 ± 0.17	AG
2010-08-17	10:54	1.43295	i'	3x180	24.80 ± 0.16	AG
2010-08-22	14:30	6.58274	r'	5x120		-
2010-08-22	14:45	6.59291	i'	5x120		-
2010-09-04	12:02	19.48535	r'	5x240	> 25.85	-
2010-09-04	12:27	19.50241	i'	5x240	> 25.91	-

Table 5.1: A log of optical observations of GRB 100816A. All magnitudes quoted here are in the AB magnitude system and have been corrected for Galactic Extinction of $E(B-V) = 0.09$ (Schlegel et al., 1998). The UVOT magnitudes have not been corrected for the contribution of the host galaxy but it is expected the afterglow will dominate at this time. The magnitudes in the Gemini images have been measured using image subtraction with the images at ~ 6.6 days in the r' and i' bands were used as reference images.

The strength of the break is indicative of either an Sbc or Scd galaxy (based on the models of Coleman et al. 1980), consistent with the evidence that the host galaxy is star-forming but also demonstrating that this galaxy is not strongly blue. However, even though the host galaxy is star-forming, GRB 100816A resides in a faint region, as can be seen in Figures 5.2 and 5.3. In addition, this is consistent with the HST infra-red imagery from Fruchter et al. (in prep.) demonstrating that this region is genuinely faint and not just at a high optical depth due to a large volume of dust. This shows that GRB 100816A is not strongly associated with the star-formation within the host itself.

5.3 Discussion

5.3.1 Comparison sample definition

To consider the GRB population as a whole, and to put the properties of GRB 100816A in context, we consider prompt, afterglow and host properties of a sample of GRBs split into four duration bins. When we consider duration we use either T_{90} of the entire prompt emission or, where the structure of the emission is composed of a short,

hard spike known as the initial pulse complex (IPC) followed by softer extended emission, the T_{90} of the IPC only.

These are set out as follows:

- Set S1: $T_{90} \leq 0.8\,\mathrm{s}$. This is the split proposed by Bromberg et al. (2013) as appropriate for the division of SGRBs detected by *Swift*. This is based on the point at which the "average" hardness burst has a 50% probability of being a non-collapsar object, i.e. $f_{NC} = 0.5$.

- Set S2: $0.8 < T_{90} \leq 2.0\,\mathrm{s}$. This encompasses the remainder of GRBs often classed as short. Defining this duration bin allows us to probe any differences between this population and that of Set S1.

- Set I: $2.0 < T_{90} \leq 10.0\,\mathrm{s}$. This time bin should exclude the majority of the SGRB population and allows us to probe an intermediate duration.

- Set L: $T_{90} > 10.0\,\mathrm{s}$. This longest time bin encompasses the remainder of the GRB population, primarily composed of LGRBs.

Within these duration cuts (combining Sets S1 and S2 for SGRBs) we hope to discriminate between the bulk of the short, intermediate and long samples.

Previous population studies of this sort, especially when considering an intermediate population, use more complex definitions based on the two-dimensional phase space of duration and hardness (see e.g. Horváth 1998; Horváth et al. 2010; de Ugarte Postigo et al. 2011). These splits are based on multi-variate fits in hardness and duration, using the combination of three overlapping Gaussian distributions (Horváth et al., 2010), producing probabilities that each individual GRB belong to one of the three classes (de Ugarte Postigo et al., 2011).

We choose to use these simpler duration cuts since we do not wish to bias our results based on those of previous studies. An intermediate class has been claimed within the population based on duration alone (Horváth, 1998, 2002; Horváth et al., 2008). In the case of GRB 100816A we wish to determine whether or not this GRB shares properties with other intermediate GRBs and, since it is harder than the bulk of the population, we do not wish to exclude any GRBs which may be similar. We note that some other intermediate samples, where hardness ratio is a factor, GRB 100816A would lie on the short-intermediate boundary (e.g. de Ugarte Postigo et al. 2011) but still has enough ambiguity for us to not classify this GRB with any great certainty before we perform this further analysis.

Except for the sample used in the analysis of section 5.3.4, where we look at the positions of the GRBs within the host galaxies, each of our samples is a

subset of all GRBs detected by *Swift* from its launch to the end of 2011. Though we require a *Swift* detection, in some cases we also make use of detections made by other telescopes, with details highlighted in the text.

5.3.2 Constraints from the prompt emission

Figure 5.4 shows the duration-hardness distribution for the complete sample of *Swift* GRBs (up to the end of 2011) with the four duration bins outlined in section 5.3.1 highlighted. We also highlight GRB 100816A, showing that it is particularly hard for its duration. Figure 5.4 shows that some GRBs within the intermediate duration bin (Set I) are typically softer than even the GRBs within the long duration bin (Set L). The mean values, however, are consistent due to the large scatter in the distributions with $< \log(HR) >= 0.060$ (Set I) and $< \log(HR) >= 0.11$ with standard deviations, σ, of 0.19 and 0.11 respectively. Additionally, though the two short duration bins (S1 and S2) clearly contain some harder GRBs compared to long and intermediate samples the mean hardness ratios for both samples are consistent with the rest of the population with values of $< \log(HR) >= 0.23$ ($\sigma = 0.15$) and $< \log(HR) >= 0.15$ ($\sigma = 0.14$).

However, the cumulative distribution of the hardness ratios for the four duration bins, shown in figure 5.5, demonstrates that Sets S1, I and L are is distinct. Performing a Kolmogorov Smirnov (KS) test to check the likelihood of two samples being drawn from the same underlying distribution we find a strong rejection between Set I and both Sets S1 and L with values of $KS = 0.0002$ and 0.0004 respectively as well as a very strong rejection between Sets S1 and L ($KS = 5.2 \times 10^{-7}$). However, the KS test values between the hardness ratio of Set S2 and any other distribution show no rejection of the samples being drawn from the same underlying distribution with values of $KS = 0.16$, 0.26 and 0.36 when compared with the S1, I and L populations.

With a hardness ratio of $\log(HR) = 0.26$, GRB 100816A is clearly an outlier in the intermediate distribution, more similar to the SGRBs. In addition, we see no significant spectral lag between the hard and soft photons for GRB 100816A (Norris et al., 2010a). This fact is also consistent with SGRB behaviour as a positive spectral lag, where the hard photons arrive before the soft, is sometimes seen for LGRBs but not for SGRBs (Norris et al., 2000, 2005; Yi et al., 2006).

As well as looking at the population as a whole, Bromberg et al. (2013) also consider the collapsar distribution as a function of hardness by using the prompt emission photon index, Γ, to split the sample into soft, intermediate hardness and hard bins. In the *Swift* sample, for the GRBs with the hardest spectrum the duration

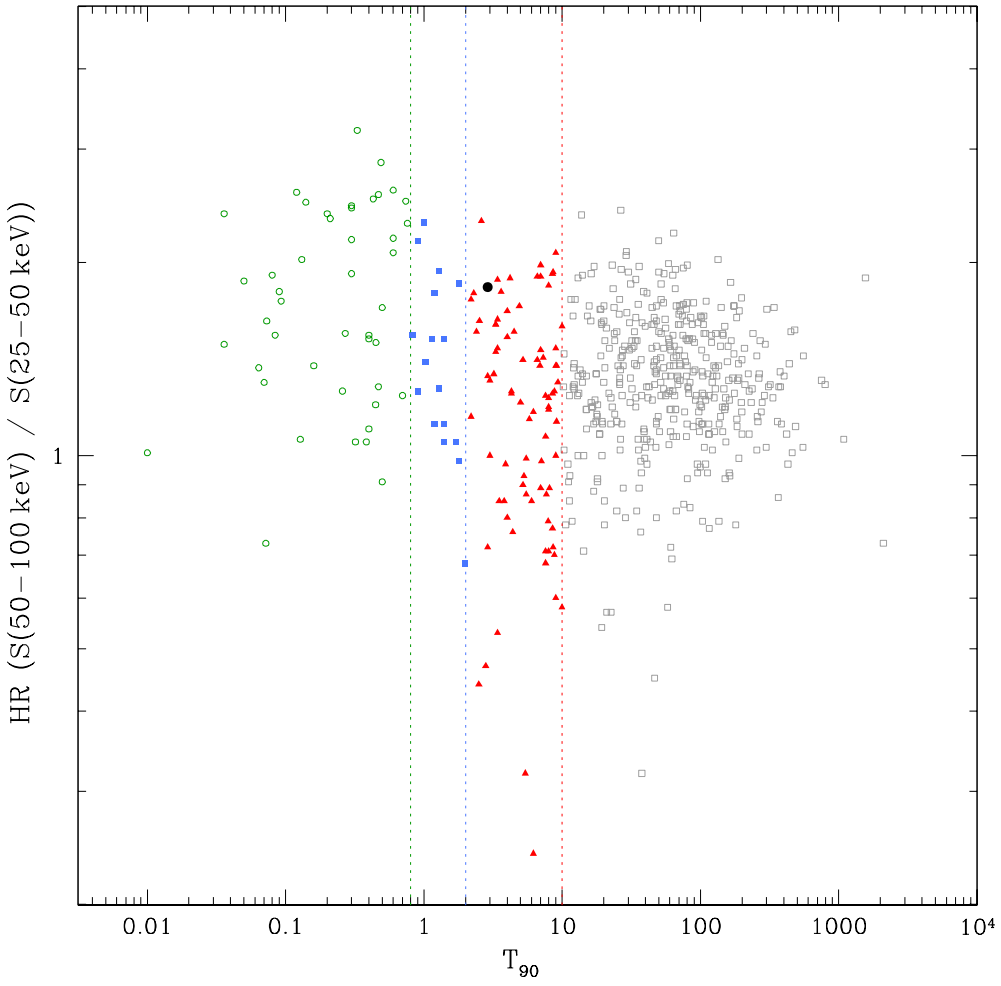

Figure 5.4: The *Swift* duration against hardness ratio for all GRBs in our sample. The hardness ratio is measured using the fluence from $50 - 100$ keV band and the $25 - 50$ keV band both measured by the BAT. The GRBs have been separated into the four durations bins with sets S1 (green, open circles), S2 (blue, closed squares), L (grey, open squares) and I (red, closed triangles) as described in the text. In addition, GRB 100816A is highlighted (black circle) and is clearly among the hardest GRBs of that duration.

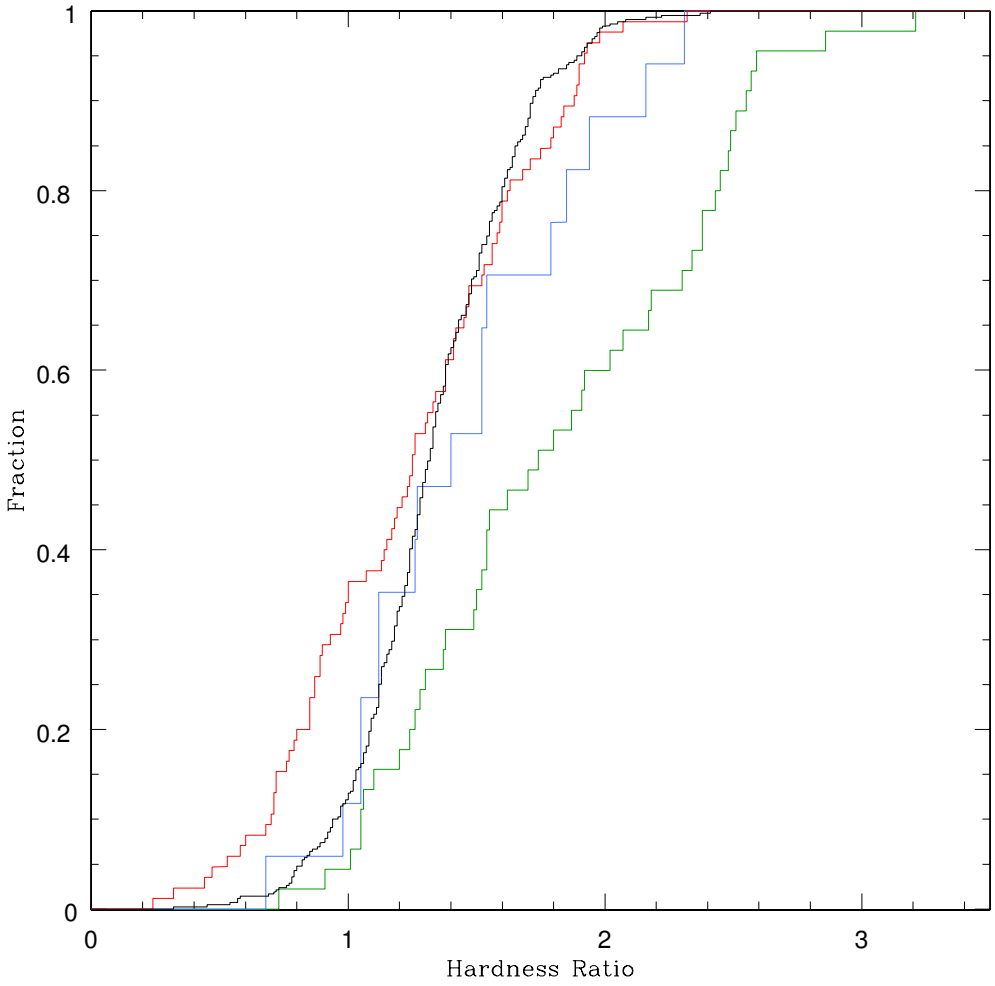

Figure 5.5: The *Swift* hardness ratio for the four duration bins: Set S1 (green), S2 (blue), I (red) and L (black). The hardness ratio distribution of Set I is clearly distinct from Set S1 and L as are Sets S1 and L. The distribution of Set S2, however, is not distinct from any of the other duration bins.

at which $f_{NC} = 0.5$ is $T_{90} = 2.8^{+1.5}_{-1.0}$ s. In addition, for the *Fermi* sample of hard GRBs, at $T_{90} = 2.0$ s the probability of being a non-collapsar object is as high as $f_{NC} \sim 0.8$. This means that for hard GRBs, any proposed cutoff between collapsar and non-collapsar objects is at a much higher duration than when considering the population average. In the case of GRB 100816A, even though, for the average across the population, its *Swift* duration does not exclude it as a collapsar object, its *Fermi* duration of 2.04 ± 0.23 s and its hard spectral index means, by this measure, the probability of being a non-collapsar object is very high. This also suggests there may be additional hard GRBs excluded from most non-collapsar samples due to their longer duration which, by the measure of Bromberg et al. (2013), would also have a significant probability of not being a collapsar.

Another property of the prompt emission to consider is the correlation in the LGRB population between the isotropic equivalent energy, E_{iso}, and the E_{peak} value in the rest frame, $E_{peak,src}$ (Amati et al., 2002). This has been shown to hold for intermediate GRBs (de Ugarte Postigo et al., 2011) but SGRBs are clear outliers (Amati et al., 2002). To look at this relation we considered a sample of GRBs, in addition to being detected by *Swift* BAT instrument, detected by the *Fermi* Gamma-Ray Burst Monitor (GBM), due to its wide energy coverage (typically $10-1000$ keV). The combination of information from two detectors gives us knowledge of the fluence and accurate determination of the $E_{peak}(obs)$ as well as the possibility of a redshift to determine values in the source frame of the GRB. We also expanded this sample to include GRBs between 2005 and the launch of the *Fermi* satelitte (end of 2008) using $E_{peak,src}$ and E_{iso} values from de Ugarte Postigo et al. (2011). This is shown in Figure 5.6. In our sample we see no distinction between sets S1 and S2 with all SGRBs being outliers to the distribution. GRB 100816A, though perhaps a little harder than for the average long GRB, is not distinct from the main bulk of Set L. It is also, however, among the lowest energy GRBs with its E_{iso} less than for the bulk of the LGRB population. Of the small number of intermediate bursts within the intermediate sample (Set I) all but one follow the Amati relation. The outlier is GRB 060505, a GRB with no associated supernova to deep limits.

Though Set I is softer on average than Set L, the consistency of the intermediate sample with the Amati relation shows the prompt emission properties in the rest frame are similar to that of the long population. As a SGRB, it would be unusual for GRB 100816A to follow the Amati relation but otherwise its prompt properties are consistent with the SGRB population.

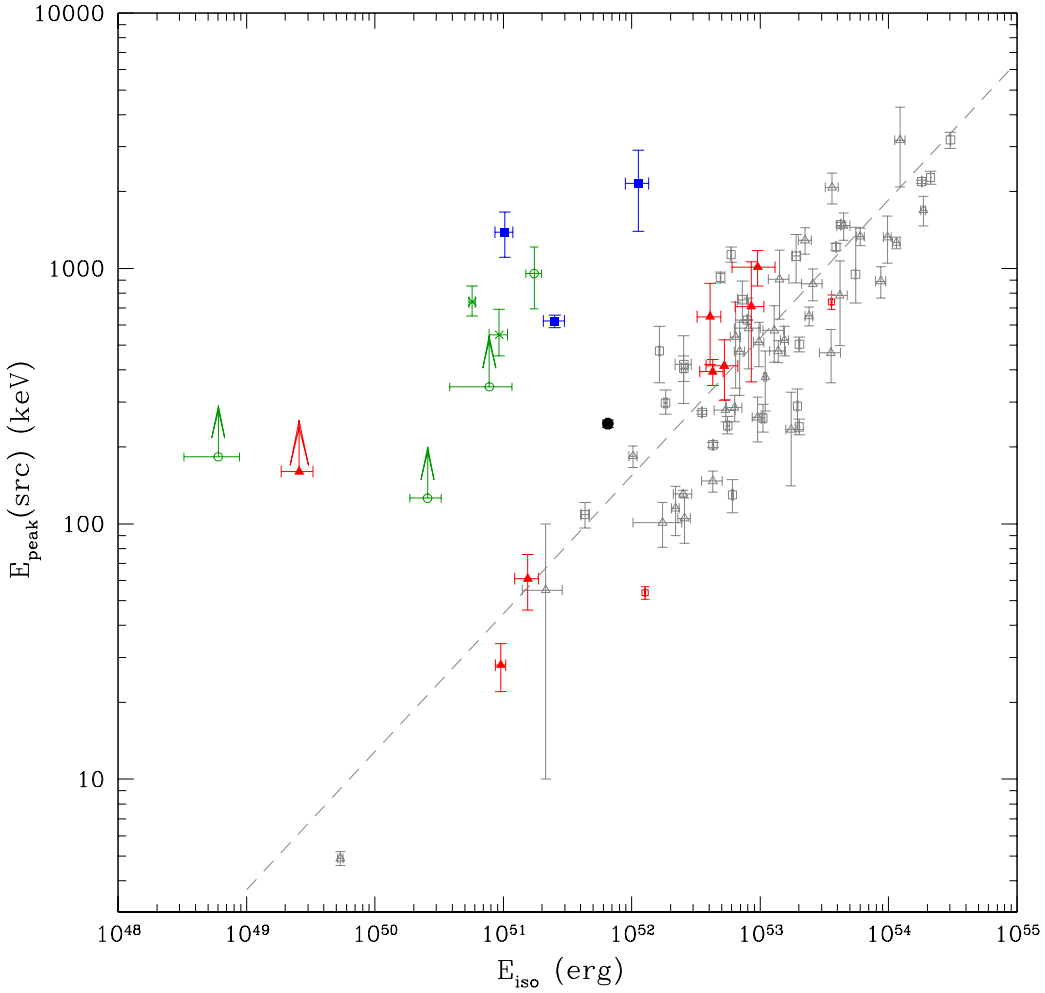

Figure 5.6: The E_{iso} vs $E_{peak}(src)$ distribution for Set L (grey squares and triangles), I (red triangles), S1 (green circles) and S2 (blue squares). Both Set L and the majority of Set I follow the Amati relation with both Sets S1 and S2 being clearly distinct. GRB 100816A, shown as a black circle, is consistent with the long GRB population. All but one of the small sample of intermediate GRBs follow the Amati relation, the outlier being GRB 060505.

5.3.3 Constraints from the afterglow

To consider the rest frame X-ray afterglow properties for our sample of GRBs we looked at the XRT afterglow luminosity measured at 11 hr in the rest frame. The sample is comprised of all GRBs with an XRT detection up to the end of 2011 with known redshift, combing samples from Evans et al. (2009a) and the *Swift* GRB table available online,[5] also making use of the table of measured spectral and temporal slopes.[6] The observed flux could be converted to unabsorbed flux at 11 hr in the rest frame using the spectral fits available on the *Swift* XRT details available online with details of the fitting procedures available in Evans et al. (2007, 2009a).[7] Using the X-ray spectral slope β_X the X-ray luminosity was then calculated using Equation 5.1 (Ghisellini et al., 2009).

$$L_X = \frac{4\pi d_L^2}{(1+z)^{1-\beta_X}} f_X \tag{5.1}$$

This equation converts observer frame $0.3 - 10$ keV fluxes to rest frame $0.3 - 10$ keV luminosities, assuming there is no spectral break between the bands. Figure 5.7 shows the comparison of the X-ray afterglow luminosity. The mean X-ray luminosities for our four duration cuts are as follows: $< \log(L_X) >= 42.87$ ($\sigma = 0.63$, S1), 43.86 ($\sigma = 0.63$, S2), 44.49 ($\sigma = 0.74$, I) and 44.67 ($\sigma = 0.86$, L). Though de Ugarte Postigo et al. (2011) found that their sample of intermediate GRBs had a significantly different distribution of X-ray afterglows than the long GRBs, with the afterglows generally being fainter both at early (100 s) and later (10^4 s) times, we do not find this to be strongly the case in out sample. GRB 100816A itself, as can be seen in Figure 5.7, is bright compared to the short GRB population but is fairly typical of the long and intermediate samples.

We have also looked at the R band afterglow Vega magnitude at 1 day in the rest frame of the GRB after the burst trigger for a sample of GRBs from Kann et al. (2010) and Kann et al. (2011) with known redshift. These magnitudes have been extrapolated to a common redshift of $z = 1$. In Figure 5.8 it can be seen that the shortest duration bin (S1) is clearly fainter with a mean magnitude $R = 24.5 \pm 2.8$ compared to long GRBs where $R = 19.8 \pm 1.6$. However, it should be noted that since this sample requires an optical detection it does not include the sample of LGRBs which are optically sub-luminous with respect to their X-ray fluxes (Jakobsson et al., 2004; van der Horst et al., 2009), showing non-detections even sometimes when their

[5] http://swift.gsfc.nasa.gov/docs/swift/archive/grb_table.html/
[6] Available at http://www.swift.ac.uk/xrt_live_cat/
[7] http://www.swift.ac.uk/xrt_spectra/

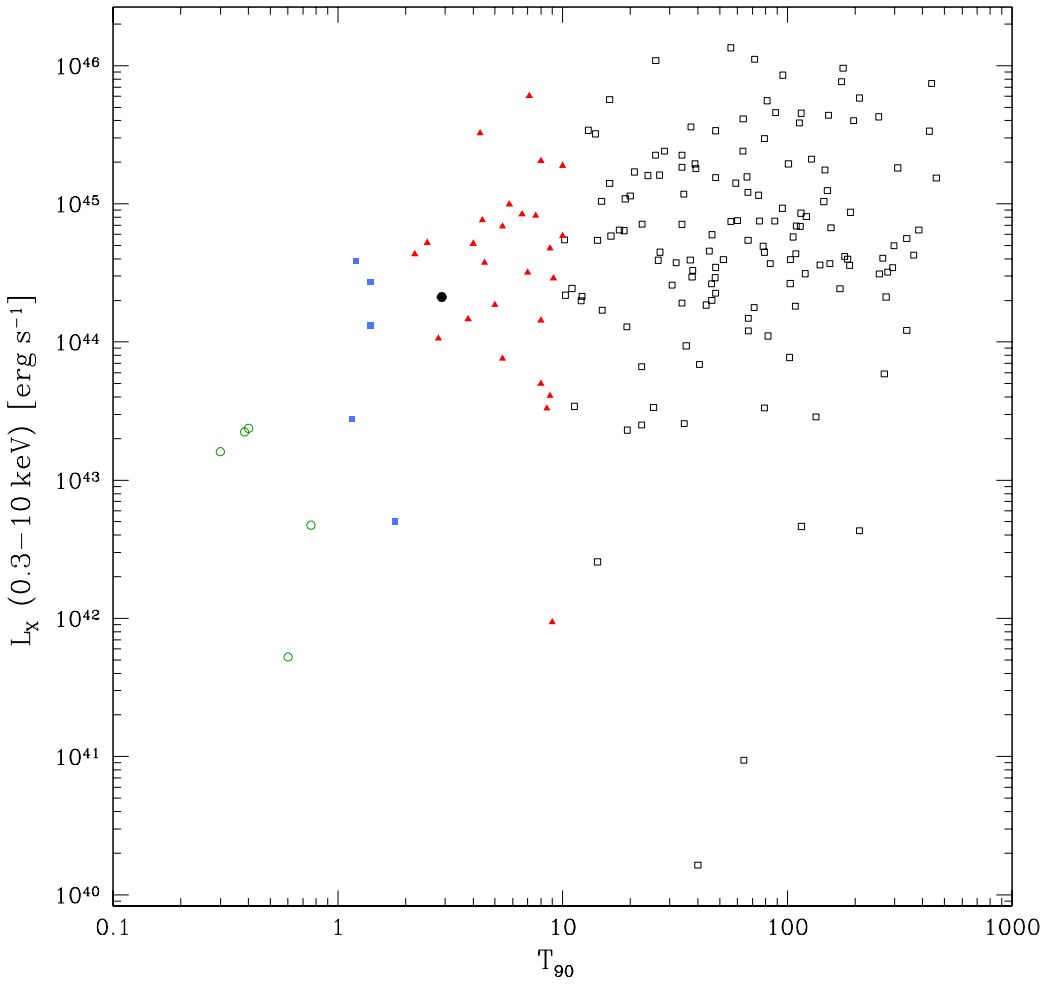

Figure 5.7: XRT luminosity at 11 hrs (rest frame) for four duration bins: Sets S1 (green, open circle), S2 (blue, closed squares), I (red, closed triangles) and L (grey, open squares). GRB 100816A, shown as a black circle, has a high luminosity compared to the sample of short GRBs but is fairly typical for the long and intermediate samples. The X-ray luminosity is in the $0.3 - 10$ keV energy band in the rest frame.

X-ray afterglows can be fairly bright (e.g. D'Elia and Stratta 2011). The faintness of any optical afterglow, however, might not be due to intrinsic property of the GRB but may in part be explained by highly dust-obscured local environments (Perley et al., 2009b). Though the mean magnitude for the GRBs within the Set I is less than for Set L, $R = 21.51$, these GRBs are fairly scattered with a standard deviation of $\sigma = 3.11$ mag. In fact, the distribution of the GRBs at the intermediate duration do not show a cohesive sample and they are fairly evenly scattered between the short, as is the case for GRB 100816A, and long populations.

5.3.4 Constraints from the host galaxy

Using high resolution imaging, the position of a GRB (or other transient object) within its host galaxy with respect to the star-forming regions can be characterised by measuring F_{light}: the cumulative fraction of total host galaxy light at the burst position (Fruchter et al., 2006). This distribution has been shown to be widely disparate between LGRBs and SGRBs, with LGRBs strongly correlated with the light of their host but SGRBs having a tendancy to occur in fainter regions (Fong et al., 2010; Svensson et al., 2010).

Figure 5.9 shows the normalised cumulative distribution of a set of F_{light} values for the four duration bins. The samples for the long and intermediate GRBs are comprised of bursts from the sample of Fruchter et al. (2006) supplemented with data from Svensson et al. (2010). For both short GRB bins, F_{light} values were compiled from Fong et al. (2010) and Fong and Berger (2013). We also added additional measurements to the intermediate sample, given in Table 5.2, from analysis of available HST and Gemini data, increasing the sample from five GRBs to ten. Performing a Kolmogorov Smirnov (KS) test to check the likelihood of two samples being drawn from the same underlying distribution we find a strong rejection between the S1 sample and both the intermediate and long duration bins with values of 0.002 and 0.00005. Interestingly, there is also a strong rejection between the S2 sample and the long duration bin ($P_{KS} = 0.005$). To characterise the maximum level of collapsar contamination this implies we constructed an artificial sample comprising 40% of randomly selected GRBs from the long sample and 60% from the S1 sample ($3:5$ GRB ratio to match the 8 GRBs in S2 sample). We do this 10,000 times and then perform KS tests between these distributions and that of the long GRBs. By doing this we aim to mimic the behaviour a sample with 40% collapsar contamination, as suggested by Bromberg et al. (2013), would have and to test how likely this would be to produce the same KS test rejection as seen for the S2 and long samples. We find in only 4% of the cases do we recover $KS \leq 0.005$, suggesting a 40% collapsar

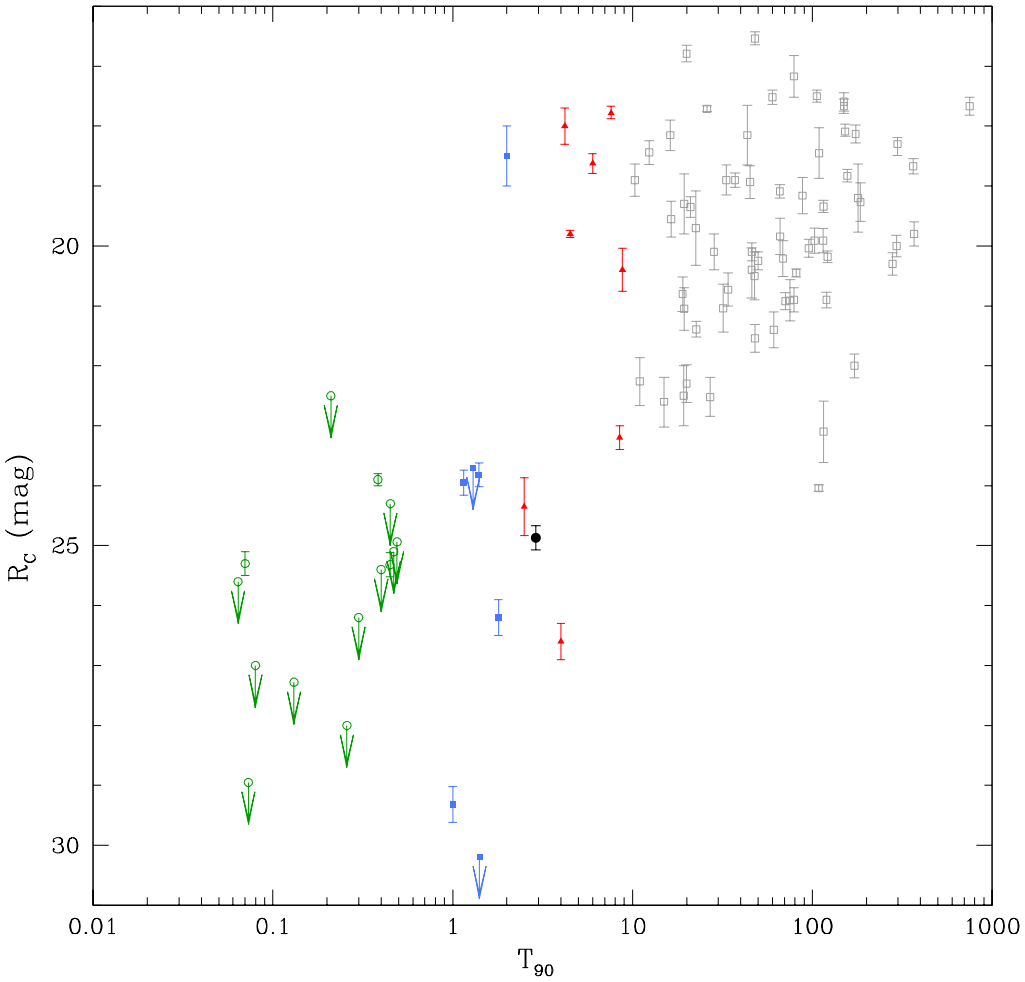

Figure 5.8: The optical afterglow R band magnitude at 1 day (rest frame) extrapolated to redshift $z = 1$. The majority of the GRBs within the two short duration bins (S1 and S2) are consistent with each other and consistent with being fainter than the long GRB detected population. However, we should note that there are some long GRBs which are optically sub-luminous in comparison with their X-ray afterglows but this is often purported as being due to dust extinction local to the GRB position or a result of high redshift rather than an intrinsic property of the GRB. The intermediate population is highly scattered but there are some of these GRBs, including GRB 100816A, which are outliers from the GRBs within the long duration bin.

GRB	Telescope	Instrument	Filter	F_{light}
051016B	*HST*	WFC3	$F160W$	0.92
060912A	*HST*	WFC3	$F160W$	0.53
080520	*HST*	WFC3	$F160W$	0.87^a
071020	Gemini	GMOS-N	r'	0.62
100816A	Gemini	GMOS-N	r'	0.29

Table 5.2: Calculated F_{light} values for GRBs within the intermediate duration cut where appropriate data is available. These images were taken at times when the afterglow no longer contributes to the host galaxy light (in some cases years after the GRB). The F_{light} value was calculated by masking out all pixels in the image unrelated to the host galaxy, using SExtractor to define its extent. Summing the remaining pixels within the image and normalising, the F_{light} value at the well-localised position of the GRB can then be extracted. Footnotes: (*a*) F_{light} from Tibbets-Harlow et al. (in prep.)

contamination would be unlikely to produce this level of rejection. We must also add, however, that this is a rough estimate since we cannot assume the S1 sample is comprised purely of non-collapsar objects. However, looking at the f_{NC} values for individual objects in the S2 sample suggests a potential contamination of up to 60% meaning 40% distribution tested here is conservative and, hence, overall these two uncertainties will act against each other. Comparing the S2 and intermediate sample, the KS test does not strongly reject these two distributions being drawn from the same population ($P_{KS} = 0.08$). The long and intermediate samples clearly have a very similar distribution, both showing a strong association with the bright regions of their host galaxies.

Figure 5.10 shows the distribution of F_{light} values compared to their GRB duration. As can also be seen in Figure 5.9, the mean F_{light} value increases from the shortest to the longest duration bin. For GRB 100816A, though its host galaxy is star-forming, the GRB itself is well offset from the centre as can be seen in Figures 5.2 and 5.3. This is reflected in its VLT R band F_{light} value of 0.29, with an even lower value from infra-red *HST* data of 0.12 (Fruchter et al., in prep.), which is clearly an outlier from both the long and intermediate duration bins with mean values of 0.78 ($\sigma = 0.22$) and 0.73 ($\sigma = 0.24$). The low F_{light} value is more typical of the S1 and S2 samples with means of 0.17 ($\sigma = 0.21$) and 0.29 ($\sigma = 0.31$)

5.4 Conclusions

We have considered a sample of *Swift* detected GRBs split into four duration bins, attempting to characterise behaviour around the two second duration divide. We

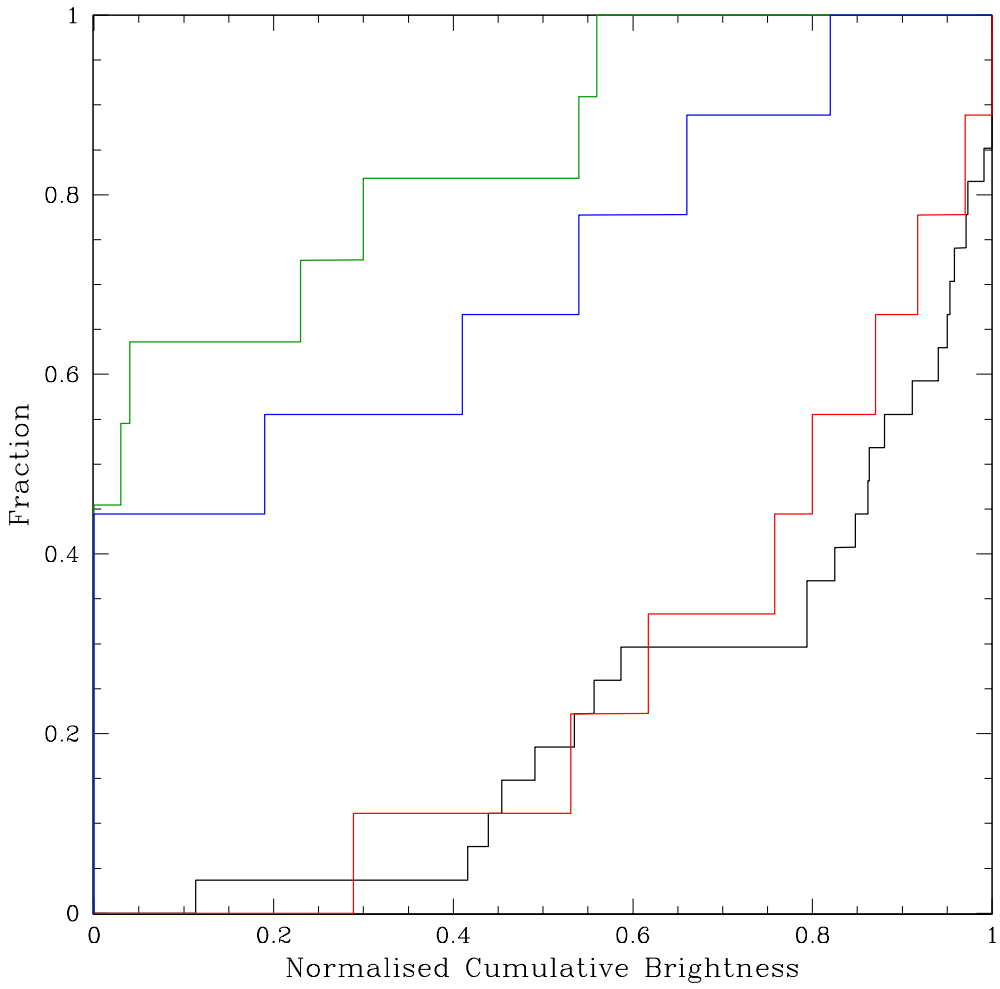

Figure 5.9: A cumulative distribution of F_{light} values for the S1 (green), S2 (blue), I (red) and L (black) GRB samples. F_{light} represents the fraction of the host galaxy light at the position of the GRB and is representative of the preference for the GRB to reside in star-forming regions. In this sample, both the long and intermediate GRBs clearly occur most often in star forming regions whereas both S1 and S2 samples show the opposite and preferentially lie in the fainter regions of their host galaxies (or even offset from the host entirely).

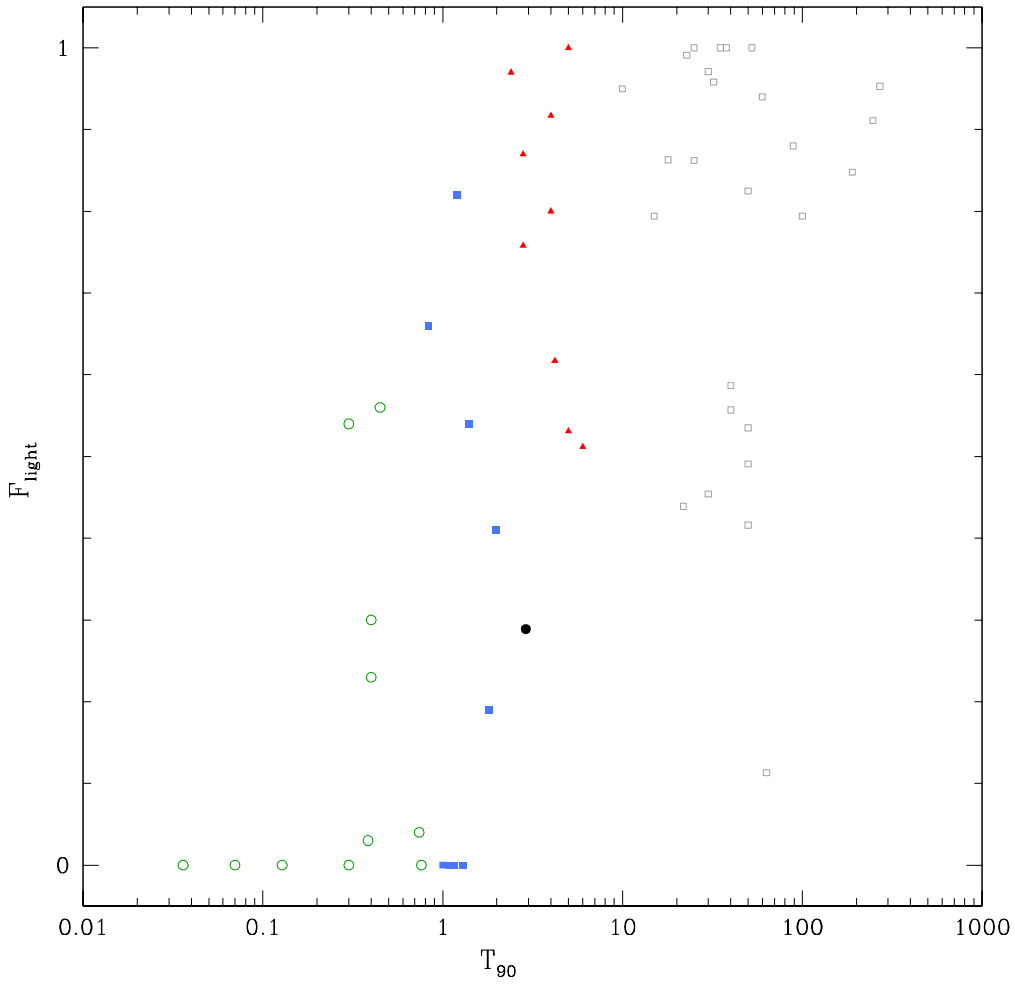

Figure 5.10: Plot of T_{90} versus F_{light} for the four GRB samples. There is a clear increase with T_{90} in the mean F_{light} across the four duration bins though there is significant scatter. Both the L and I samples clearly favour the brightest regions of their galaxies. GRB 100816A is an outlier to the rest of the GRBs at that duration. There is also a slight increase in $< F_{light} >$ from the S1 to the S2 sample though the samples are consistent with each other.

T_{90} bin (s)	$< \log_{10}(HR) >$	$< \log_{10}(L_X) >$ (erg)	$< R(1\,\mathrm{day}) >$ (Vega mag)	$< F_{light} >$
$T_{90} \leq 0.8$	0.23 (0.15)	42.87 (0.63)	24.84 (0.67)	0.17 (0.21)
$0.8 < T_{90} \leq 2.0$	0.15 (0.14)	43.86 (0.70)	24.36 (3.54)	0.29 (0.31)
$2.0 < T_{90} \leq 10.0$	0.06 (0.19)	44.49 (0.74)	21.51 (3.11)	0.73 (0.22)
$T_{90} > 10.0$	0.11 (0.11)	44.70 (0.85)	19.78 (1.61)	0.78 (0.24)
GRB 100816A	0.26	44.32	24.87	0.29

Table 5.3: A summary of the mean values within each of the duration bins considered. The standard deviation of each of these values is also given in brackets. For comparison, we have also included the measured values for GRB 100816A.

consider the sub-sample of GRBs both below and above the duration cut of 0.8 s which has been suggested by Bromberg et al. (2013) as a more suitable short divide for *Swift* GRBs, looking for any bulk differences in behaviour due to contamination for collapsar-like objects. We also consider the suggestion of a third class of intermediate GRB by looking at duration cuts between 2.0 and 10.0 s, comparing to the bulk of the LGRB population with $T_{90} > 10.0$ s. It is interesting to note that the intermediate sample lies on the plateau of the GRB duration distribution (1-10 seconds) as measured by Bromberg et al. (2011), suggesting this is perhaps a regime where the distribution of collapsars falls as the contribution of merger events starts to increase. The summary of results from the samples considered is given in Table 5.3.

Overall there is a clear distinction between the shortest ($T_{90} \leq 0.8$ s, Set S1) and the longest duration bin ($T_{90} \leq 10.0$ s, Set L) for both the X-ray and optical afterglow magnitudes and the distribution of the GRBs on their host galaxies. The distinction is less clear when considering the second short bin between $0.8 < T_{90} \leq 2.0$ (Set S2) and the intermediate duration bin $2.0 < T_{90} \leq 10.0$ (Set I). The properties of Set I are typically consistent with those of Set L and, for the afterglow magnitudes, is not distinct from the S2 sample. However, when considering F_{light}, the cumulative fraction of the light of the host galaxy at the position of the GRB, though a KS test does not strongly reject these samples being drawn from the same underlying population ($P_{KS} = 0.08$), the mean F_{light} values the intermediate and S2 distributions are significantly different. For the afterglow magnitudes and F_{light} values, across the four samples the mean of the distributions considered systematically increase. This suggests, in particular for the S2 sample, that the sample starts as a fairly pure "short" GRB sample with increasing contamination from collapsar events as we reach and exceed the two second divide. The level of

contamination, however, is difficult to determine but from supernova constraints placed in chapter 4 may be not as high as the 40% suggested by Bromberg et al. (2013) especially considering the F_{light} distribution where the majority of the GRBs in S2 still occur in fainter regions than the LGRBs and the KS test results shows these distributions are distinct ($P_{KS} = 0.005$). Indeed, we find that in only 4% of cases do we have the same level of rejection when considering a non-collapsar sample with 40% collapsar contamination.

Considering the case of GRB 100816A this event seems a lot more consistent with the short GRB population than the long. Its F_{light} value in particular is a clear outlier to both the intermediate and long samples, showing a clear correlation with both of the SGRB samples. In addition, we place a constraint on any associated supernova of ~ 3 times fainter than a SN1998bw-like hypernova event, meaning any supernova present would have to be fainter than the bulk of the LGRB population (Cano, 2013; Hjorth and Bloom, 2011). One peculiarity is that GRB 100816A is consistent with the Amati relation (the correlation between E_{iso} and $E_{peak,src}$ values) which, while typical for a LGRB, is unusual for a SGRB and, indeed, the SGRBs in our sample are all clear outliers to the Amati relation for LGRBs. In addition, we also find that GRB 060505, within the intermediate duration bin, is an outlier to the Amati relation and coupled with the fact there is a strong constraint on any accompanying supernova (Fynbo et al., 2006) could indicate this GRB is also not of a collapsar origin. It is therefore clear that some events do not conform to a simple division in duration. Indeed, the hardness cuts performed by Bromberg et al. (2013) on the sample demonstrate that when the prompt emission spectrum is hard, they expect to see a significant proportion of non-collapsar events out to longer durations and perhaps even beyond the two second divide. On balance, it is likely that GRB 100816A is a disguised SGRB but it is still possible that this object represents a new event distinct from a NS-NS/NS-BH merger or a traditional collapsar event.

If there is a distinct progenitor represented by an intermediate class then attempts to localise a unique sample, whether using simple duration cuts or other factors such as hardness ratio (e.g. (de Ugarte Postigo et al., 2011)), are too contaminated with objects from the other two progenitor systems to really be able to distinguish. It is therefore important to continue to search for an elusive signature event indicative of a new class of object, potentially within the intermediate class.

Chapter 6

Conclusions

The primary focus of this thesis has been the identification and study of short γ-ray bursts (SGRBs), looking principally at properties of their lightcurves and host galaxies (or lack thereof) through use of optical and near infra-red data. This work compares simple expectations of compact object mergers to the SGRB population in terms of their location with respect to their putative host galaxies and through the presence of kilonovae. In addition, we constrain the presence of interlopers within the SGRB population from collapsar objects or potentially a third class of intermediate GRBs. Overall, through this work we strive to identify the progenitors of SGRBs, paving the way for a deeper understanding both for their intrinsic properties as a population, including lifetimes and kick velocities, and any associated emission of interest to other related fields such as gravitational wave searches and r-process transients.

6.1 Summary of results

6.1.1 SGRB host environments: "hostless" GRBs

The diversity of SGRB host galaxies and their positions within them are often cited as evidence for progenitors from older populations, in particular compact object binaries. Within the SGRB population, the "hostless" GRBs, those with no coincident host galaxy to deep limits and no strongly associated galaxy by probabilistic measures, can provide an additional test to this hypothesis by perhaps providing evidence for strong kicks if they reside at low redshift, as we would expect for at least some proportion of compact object mergers (Hansen and Phinney, 1997; Arzoumanian et al., 2002; Hobbs et al., 2005).

From sampling the distribution of galaxies on the sky with respect to random

positions, using multiple surveys to cover the full magnitude range, we find that the hostless GRBs are moderately closer to galaxies nearby in projection than we would expect for a random distribution, although less so than one would see from considerations of classical measurements of P_{chance}. Some of these galaxies are known to be at low redshift ($z < 1$), with the brightness of others suggestive of a low redshift origin. In addition, from the deepest limits placed at the positions of two of the hostless GRBs we find that we would have expected at $z = 1$ to uncover $\sim 75\%$ of the integrated galaxy luminosity for an Sbc type galaxy, $\sim 85\%$ for an Irr galaxy and 55% for an Ell galaxy. If they lie at $z = 1$, both these facts together point to a low redshift origin being more likely. Whether the GRBs are correlated with the nearby galaxies identified, with fainter satellite galaxies associated with a cluster, or are residing within globular clusters remains unclear. The presence of two hostless GRBs close to very low redshift galaxies within the horizon of the upgraded gravitational wave detectors also presents the possibility of future simultaneous detections of a SGRB event and a gravitational wave detection.

6.1.2 SGRB lightcurves

Of the 24 optically localised GRBs detected up to the end of 2011 classified as "short" (by either the measure of $T_{90} \leq 2\,\mathrm{s}$ or $T_{90}(IPC) \leq 2\,\mathrm{s}$) we found no evidence of the collimated emission of the jet. Though there were breaks detected within multiple optical lightcurves, for most of these GRBs this was not accompanied by a simultaneous break in their X-ray lightcurve (or vice versa), implying that many breaks seen are not achromatic and hence are not associated with the widening of the GRB jet. On average, the lower bound placed on the jet opening angle, θ_j, is $\gtrsim 6^\circ$ comparable with the LGRB average of $\sim 8.5^\circ$ and so demonstrating that the jets from compact object mergers are no narrower than collapsars. Suggested jet break angles for SGRBs in the literature, measured at late times in the X-ray lightcurve by the *Chandra* satellite, are $\sim 4 - 8^\circ$ for GRB 051221A (Burrows et al., 2006) and $\sim 3 - 8^\circ$ for GRB 111020A (Fong et al., 2012), although these lack evidence of achromatic behaviour. Additionally the presence of some high lower limits ($> 20^\circ$) implies that the jet opening angle for some compact objects is wide. For gravitational wave searches this increases the possibility of detection of a simultaneous electromagnetic counterpart for these events but also implies that the measured rate of SGRBs may be close to the true rate of compact object mergers reducing the possibility of object detection.

In addition, within the SGRB optical lightcurves there is no evidence for associated thermal emission and in seven cases we can rule out the brightest kilonova

predicted by Metzger et al. (2010). For the strongest kilonova constraint, that of GRB 080905A, we can rule out a substantial portion of the parameter space suggested by Metzger and Berger (2012). This is in line with the recent predictions by Kasen et al. (2013) that opacity by r-process elements in the ejecta may cause substantially more reddening that previously predicted, making an R band transient not only fainter but also peaking later, with more of the emission re-emitted in the infra-red. Since these r-process transients are expected to be less collimated (if at all) than the jetted afterglow emission, it has been suggested that these transients may be more suitable for gravitational wave followup (Metzger and Berger, 2012). However, the lack of an optical detection from the sample of SGRBs investigated suggests that these surveys would need to be targeted towards the infra-red in order to detect these transients, increasing the complexity of the searches.

6.1.3 GRB classification: short and intermediate GRBs

Though it is clear that the GRB population as a whole is comprised of multiple progenitor systems, it is not always clear how best to classify them. Some authors (e.g. Zhang et al. 2009) have suggested a complex classification system based on multiple measured and intrinsic properties such as associated supernovae, environment, energy properties and host galaxies in addition to duration and spectral hardness. However, many of these classification schemes require detailed information for each individual GRB which in many cases, especially for the shorter lived fainter GRBs, is simply not available.

The simpler two second divide, more often used to define SGRBs, was based on number statistics measured by the *BATSE* instrument on the CGRO telescope and not the currently used *Swift* telescope with a softer spectral response function. Bromberg et al. (2013) suggest that a division at 0.8 s would include a sample with 20% contamination from collapsar objects as opposed to 40% for a sample defined by the two second divide. In particular, the sample from chapter 4 does contain at least two GRBs which are more likely to be collapsars than merger events: GRBs 090426 and 060121, as evidenced, in particular, by their host galaxy environments and emission properties (Levan et al., 2006a; Antonelli et al., 2009; Levesque et al., 2010a).

However, from both constraints on a bright accompanying supernova and high probabilities of an object being a non-collapsar ($f_{NC} > 0.5$), we find a maximum collapsar contamination of $\sim 22\%$ when considering the limited sample of SGRBs with measured redshifts. In addition, when looking at the GRB positions with respect to the brightest regions of the host galaxy (F_{light}) for the sample of

GRBs between $0.8 < T_{90} < 2.0\,\mathrm{s}$, the possibility of this sample being drawn from the same underlying population as the long population is strongly rejected. From a rough test of a non-collapsar sample with 40% contamination from randomly drawn collapsar objects we find the same level of rejection only 4% of the time. Considering the prompt emission and afterglow properties, the mild increase in luminosities from the shortest GRBs to this higher duration sample indicates there is some contamination from collapsar objects but this is unlikely to be as high as previously suggested. This is encouraging for the creation of clean samples of SGRBs with a larger sample size especially when deriving overall SGRB properties.

The case of GRB 100816A also adds an interesting prospect to the study of SGRBs. This GRB is traditionally long ($T_{90} = 2.9 \pm 0.6\,\mathrm{s}$, *Swift*) but its spectral hardness, afterglow properties and, in particular, host environment all suggest it is more consistent with being a non-collapsar object. In addition, even though the prompt emission properties show this GRB is compatible with the E_{iso} - $E_{peak,src}$ relation, applicable to LGRBs but not to SGRBs, it has a particularly low isotropic equivalent energy for an LGRB. The association of this GRB with the SGRB population is actually consistent with the result of Bromberg et al. (2013) if we also consider its spectral hardness. For the hardest GRBs, the duration splits suggested by Bromberg et al. (2013) are much higher than when considering the population as a whole. For instance when examining the *Fermi* duration distribution at $T_{90} \sim 2\,\mathrm{s}$ the probability of being a non-collapsar object is as high as $f_{NC} \sim 0.8$, suggesting GRB 100816A, with a *Fermi* duration of $T_{90} = 2.04 \pm 0.23\,\mathrm{s}$, is most likely a non-collapsar object. This opens up the interesting question of additional objects at this longer duration which may also be non-collapsar objects and should be part of the "short" class of GRBs.

Contemplating these results in the context of future classification schemes, we posit that the host galaxy characteristics, both in terms of galaxy properties and position within the host, and the hardness could be more telling than the duration. Though the population does have a peak at shorter durations, GRBs with extended emission do demonstrate that these objects are capable of producing longer duration GRBs in some form and that considering this population of objects as "short" is perhaps causing some objects to be misclassified. A classification scheme based on hardness, or at least combining duration with hardness, would perhaps prove more fruitful at producing a complete sample while still keeping the sample as clean as possible. The host galaxy properties and, in particular, F_{light} values are also particularly telling. The strong preference of SGRBs for low F_{light} could prove as a useful way to determine whether a GRB is a non-collapsar object especially when

coupled with host galaxy properties not consistent with the LGRB population.

From the suggestion of a separate population of intermediate GRBs, the sample considered here (defined as GRBs with $2.0\,\mathrm{s} < T_{90} \leq 10.0\,\mathrm{s}$) did not show any significant difference from the LGRB population. This suggests that, if this class is significant, overlap from both the short and long classes are not allowing a clean sample to be determined. However, there are likely to be additional objects other than neutron star mergers and collapsars capable of producing GRB-like objects such as massive white dwarf - neutron star or white dwarf - black hole mergers and it could perhaps be the case that these are represented by this intermediate population.

6.2 Future prospects

The progenitors often proposed for SGRBs are neutron star binary (NS-NS) or neutron star - black hole (NS-BH) mergers. For a "smoking gun" confirmation of such a merger event we would need to detect an unmistakable signal. Two such detectable events could be the signature of a kilonova or a unique gravitational wave pattern. Since, our constraints on kilonova emission in the SGRB sample rule out the brightest kilonovae in the r' band it is prudent to focus these searches in the infra-red where we are perhaps more likely to detect an r-process transient (Kasen et al., 2013). Indeed, for recently detected short GRB 130603B at $z = 0.356$, the first SGRB with an absorption redshift measured from the afterglow emission, deep infra-red searches have been performed using the $F160W$ and $F606W$ bands on the WFC and ACS instruments respectively on the *HST* (Berger et al., 2013; Tanvir et al., 2013). Tanvir et al. (2013) have shown that the GRB is accompanied by a rebrightening in the infra-red not seen in the optical, indicative of a kilonova. This gives strong support for the compact object merger model.

An open question is whether both NS-NS and NS-BH systems are represented in the SGRB population. Their differing evolution, merger dynamics and, in particular, total system rest masses ($10M_\odot$ compared with $3M_\odot$) means we may expect NS-BH binaries to be more energetic, have longer durations and perhaps even have a different distribution of kilonovae properties. In addition, it has been suggested that NS-BH binaries may actually have larger offsets than NS-NS binaries, depending on the kick distribution considered (Church et al., 2011). Hence one avenue for investigation could be to obtain deeper observations of the "hostless" GRBs, to confirm or deny the existance of a host galaxy at high redshift, and thus to help unveil the true SGRB distribution. In addition to studies of the energetics

and durations, this may help to distinguish between these progenitors.

Another question is whether all compact object mergers should have a detectable kilonova in the infra-red and what range of properties we can expect. These r-process transients may contribute a significant fraction of many of the heavy elements in the Universe, the abundances of which cannot be simply accounted for by e.g. supernovae (Woosley and Weaver, 1995), and understanding this process better will help to constrain this fraction.

Some of the "hostless" GRBs in our sample could have occured within the upgraded gravitational wave detector horizon of $\sim 500\,\mathrm{Mpc}$ for a NS-NS and $\sim 1\,\mathrm{Gpc}$ for NS-BH mergers, providing interesting prospects for potential future detections when these facilities come online. Simultaneous detection of an electromagnetic counterpart, as well as providing information about the source, significantly improves this localisation (subarcsecond precision for an optical transient). Any followup needs to cover a large field of view in addition to achieving the necessary depth for detection. For compact object binary mergers detection of kilonova, rather than the optical afterglow of an SGRB, may prove a better prospect especially since the emission from the kilonova will be less collimated than for the afterglow and hence would be detectable to higher degrees off-axis of the jet than for the afterglow (Metzger and Berger, 2012). However, having to focus the search in the infra-red rather than the optical will make this more challenging especially since it is difficult to probe the infra-red emission as deeply as the optical. As has been discussed, wider jets could increase the possibility of a simultaneous detection between gravitational waves and the SGRB collimated emission (prompt or afterglow), though this would also lower the expected rate of these objects. Constraints on the beaming angles of SGRBs would help us to understand the gravitational wave detection rates we can expect from their progenitors. For the next generation of gravitational wave detectors and beyond (e.g. Einstein telescope; Punturo et al. 2010) simultanous detection of SGRBs and gravitational waves also presents the possiblity of accurate determination of the Hubble constant, through measurements of both the luminosity distance and the redshift of compact binary mergers for multiple systems (Nissanke et al., 2013).

Some associated properties of SGRBs could also allow for their use as cosmological probes. If, as has been suggested, their locations are strongly correlated with galaxy clusters (Berger et al., 2007a; Levan et al., 2008) then detection of an SGRB could be used as a marker for the likely presence of a mass overdensity or large scale structure. Additionally, if some SGRBs do reside at high offset from their host galaxies then they could also provide useful probes of the intergalactic

medium. The capability of the LAT instrument on the *Fermi* satellite to detect high energy γ-ray emission ($> 1\,\mathrm{GeV}$) has also allowed tests of Lorentz invariance violation to be performed for one SGRB, GRB 090510 (Abdo et al., 2009). With the lack of intrinsic spectral lag seen at lower prompt emission energies for SGRBs and the range of γ-ray energies, these objects are excellent test beds for this type of analysis and high energy detections of more of these objects in the future will allow further probing of this fundamental property of light.

For detailed SGRB studies to continue it must be ensured that these objects are localised to sub-arcsecond positions, providing host galaxy information, environment properties and improving the possibility of an associated redshift. As well as optical localisations providing this level of precision, recent X-ray afterglow follow-up with the *Chandra* satellite (Fong et al., 2012; Margutti et al., 2012; Sakamoto et al., 2013), has also given excellent positional information potentially providing a more complete well-localised sample in the future.

The continued study of SGRBs offers opportunity not only to learn more about the evolution and final end point of compact object mergers but also as potential gravitational wave sources, mutliple potential probes and for the study of rare transients and how their production contributes to the makeup of the Universe. With the recent detection of an r-process transient along with the upcoming upgraded gravitational wave detectors, with the strong possibility of a simultaneous detection of an SGRB with a gravitational wave signal, this is an exciting time to be working in the field with a wealth of information still to be uncovered, questions to be answered and many new discoveries still to be made.

Bibliography

J. Abadie et al. TOPICAL REVIEW: Predictions for the rates of compact binary coalescences observable by ground-based gravitational-wave detectors. *Classical and Quantum Gravity*, 27(17):173001, September 2010. doi: 10.1088/0264-9381/27/17/173001.

K. N. Abazajian et al. The Seventh Data Release of the Sloan Digital Sky Survey. *ApJS*, 182:543, June 2009. doi: 10.1088/0067-0049/182/2/543.

B. P. Abbott et al. Search For Gravitational-wave Bursts Associated with Gamma-ray Bursts using Data from LIGO Science Run 5 and Virgo Science Run 1. *ApJ*, 715:1438–1452, June 2010. doi: 10.1088/0004-637X/715/2/1438.

A. A. Abdo et al. A limit on the variation of the speed of light arising from quantum gravity effects. *Nature*, 462:331–334, November 2009. doi: 10.1038/nature08574.

A. Achterberg et al. Particle acceleration by ultrarelativistic shocks: theory and simulations. *MNRAS*, 328:393–408, December 2001. doi: 10.1046/j.1365-8711.2001.04851.x.

L. Amati. The $E_{p,i}$-E_{iso} correlation in gamma-ray bursts: updated observational status, re-analysis and main implications. *MNRAS*, 372:233–245, October 2006. doi: 10.1111/j.1365-2966.2006.10840.x.

L. Amati et al. Intrinsic spectra and energetics of BeppoSAX Gamma-Ray Bursts with known redshifts. *AAP*, 390:81–89, July 2002. doi: 10.1051/0004-6361:20020722.

L. A. Antonelli et al. GRB070429B: VLT observations. *GRB Coordinates Network*, 6372:1, 2007.

L. A. Antonelli et al. GRB 090426: the farthest short gamma-ray burst? *AAP*, 507: L45–L48, December 2009. doi: 10.1051/0004-6361/200913062.

Z. Arzoumanian, D. F. Chernoff, and J. M. Cordes. The Velocity Distribution of Isolated Radio Pulsars. *ApJ*, 568:289–301, March 2002. doi: 10.1086/338805.

Keith. M. Ashman and Stephen. E. Zepf. *Globular Cluster Systems*. Cambridge Astrophysics Series, 2008.

S. A. Balbus. Enhanced Angular Momentum Transport in Accretion Disks. *ARAA*, 41:555–597, 2003. doi: 10.1146/annurev.astro.41.081401.155207.

S. A. Balbus and J. F. Hawley. Instability, turbulence, and enhanced transport in accretion disks. *Reviews of Modern Physics*, 70:1–53, January 1998. doi: 10.1103/RevModPhys.70.1.

J. Barnes and D. Kasen. Effect of a High Opacity on the Light Curves of Radioactively Powered Transients from Compact Object Mergers. *ApJ*, 775:18, September 2013. doi: 10.1088/0004-637X/775/1/18.

S. Barthelmy et al. GRB 050509b: Swift-BAT refined analysis of the short hard burst. *GRB Coordinates Network*, 3385:1, 2005a.

S. D. Barthelmy, T. Sakamoto, and M. Stamatikos. GRB 110112A: Swift-BAT refined analysis. *GRB Coordinates Network*, 11557:1, 2011.

S. D. Barthelmy et al. The Burst Alert Telescope (BAT) on the SWIFT Midex Mission. *SSR*, 120:143–164, October 2005b. doi: 10.1007/s11214-005-5096-3.

S. D. Barthelmy et al. GRB 090515: Swift-BAT refined analysis. *GRB Coordinates Network*, 9364:1, 2009.

T. W. Baumgarte, S. L. Shapiro, and M. Shibata. On the Maximum Mass of Differentially Rotating Neutron Stars. *ApJL*, 528:L29–L32, January 2000. doi: 10.1086/312425.

A. P. Beardmore et al. GRB 090305: Swift detection of a short burst. *GRB Coordinates Network*, 8932:1, 2009a.

A. P. Beardmore et al. GRB 090305: Swift-XRT refined analysis. *GRB Coordinates Network*, 8937:1, 2009b.

S. V. W. Beckwith, M. Stiavelli, A. M. Koekemoer, J. A. R. Caldwell, H. C. Ferguson, R. Hook, R. A. Lucas, L. E. Bergeron, M. Corbin, S. Jogee, N. Panagia, M. Robberto, P. Royle, R. S. Somerville, and M. Sosey. The Hubble Ultra Deep Field. *AJ*, 132:1729–1755, November 2006. doi: 10.1086/507302.

M. C. Begelman, P. Meszaros, and M. J. Rees. Gamma-ray bursts from blast waves around Galactic neutron stars. *MNRAS*, 265:L13–L16, November 1993.

K. Belczyński and V. Kalogera. A New Formation Channel for Double Neutron Stars Without Recycling: Implications for Gravitational Wave Detection. *ApJL*, 550:L183–L187, April 2001. doi: 10.1086/319641.

K. Belczynski et al. A Study of Compact Object Mergers as Short Gamma-Ray Burst Progenitors. *ApJ*, 648:1110–1116, September 2006. doi: 10.1086/505169.

E. Berger. The Host Galaxies of Short-Duration Gamma-Ray Bursts: Luminosities, Metallicities, and Star-Formation Rates. *ApJ*, 690:231–237, January 2009. doi: 10.1088/0004-637X/690/1/231.

E. Berger. A Short Gamma-ray Burst "No-host" Problem? Investigating Large Progenitor Offsets for Short GRBs with Optical Afterglows. *ApJ*, 722:1946–1961, October 2010. doi: 10.1088/0004-637X/722/2/1946.

E. Berger. The environments of short-duration gamma-ray bursts and implications for their progenitors. *NAR*, 55:1–22, January 2011. doi: 10.1016/j.newar.2010.10.001.

E. Berger, W. Fong, and R. Chornock. An r-process Kilonova Associated with the Short-hard GRB 130603B. *ApJL*, 774:L23, September 2013. doi: 10.1088/2041-8205/774/2/L23.

E. Berger et al. The afterglow and elliptical host galaxy of the short γ-ray burst GRB 050724. *Nature*, 438:988–990, December 2005. doi: 10.1038/nature04238.

E. Berger et al. Galaxy Clusters Associated with Short GRBs. I. The Fields of GRBs 050709, 050724, 050911, and 051221a. *ApJ*, 660:496–503, May 2007a. doi: 10.1086/512664.

E. Berger et al. A New Population of High-Redshift Short-Duration Gamma-Ray Bursts. *ApJ*, 664:1000–1010, August 2007b. doi: 10.1086/518762.

E. Berger et al. Discovery of the Very Red Near-Infrared and Optical Afterglow of the Short-Duration GRB 070724A. *ApJ*, 704:877–882, October 2009. doi: 10.1088/0004-637X/704/1/877.

E. Berger et al. GRB 100117A: Gemini north spectroscopy. *GRB Coordinates Network*, 10346:1, 2010.

D. Bersier et al. Evidence for a Supernova Associated with the X-Ray Flash 020903. *ApJ*, 643:284–291, May 2006. doi: 10.1086/502640.

E. Bertin. SExtractor v2.13 User Manual. User Manual for SExtractor (Draft).

E. Bertin and S. Arnouts. SExtractor: Software for source extraction. *AAPS*, 117: 393–404, June 1996.

D. Scott Birney, Guillermo Gonzalez, and David Oesper. *Observational Astronomy*. Cambridge University Press, 2nd. edition, 2006.

R. D. Blandford and R. L. Znajek. Electromagnetic extraction of energy from Kerr black holes. *MNRAS*, 179:433–456, May 1977.

J. S. Bloom and J. X. Prochaska. Constraints on the Diverse Progenitors of GRBs from the Large-Scale Environments. In S. S. Holt, N. Gehrels, & J. A. Nousek, editor, *Gamma-Ray Bursts in the Swift Era*, volume 836 of *American Institute of Physics Conference Series*, pages 473–482, May 2006. doi: 10.1063/1.2207943.

J. S. Bloom, S. G. Djorgovski, S. R. Kulkarni, and D. A. Frail. The Host Galaxy of GRB 970508. *ApJL*, 507:L25–L28, November 1998. doi: 10.1086/311682.

J. S. Bloom, S. Sigurdsson, and O. R. Pols. The spatial distribution of coalescing neutron star binaries: implications for gamma-ray bursts. *MNRAS*, 305:763–769, May 1999. doi: 10.1046/j.1365-8711.1999.02437.x.

J. S. Bloom, S. G. Djorgovski, and S. R. Kulkarni. The Redshift and the Ordinary Host Galaxy of GRB 970228. *ApJ*, 554:678–683, June 2001. doi: 10.1086/321398.

J. S. Bloom, S. R. Kulkarni, and S. G. Djorgovski. The Observed Offset Distribution of Gamma-Ray Bursts from Their Host Galaxies: A Robust Clue to the Nature of the Progenitors. *AJ*, 123:1111–1148, March 2002. doi: 10.1086/338893.

J. S. Bloom, D. A. Frail, and S. R. Kulkarni. Gamma-Ray Burst Energetics and the Gamma-Ray Burst Hubble Diagram: Promises and Limitations. *ApJ*, 594: 674–683, September 2003. doi: 10.1086/377125.

J. S. Bloom et al. Closing in on a Short-Hard Burst Progenitor: Constraints from Early-Time Optical Imaging and Spectroscopy of a Possible Host Galaxy of GRB 050509b. *ApJ*, 638:354–368, February 2006. doi: 10.1086/498107.

J. S. Bloom et al. A Putative Early-Type Host Galaxy for GRB 060502B: Implications for the Progenitors of Short-Duration Hard-Spectrum Bursts. *ApJ*, 654: 878–884, January 2007. doi: 10.1086/509114.

M. Boettcher and M. Joshi. GRB 051221A: MDM optical observations. *GRB Coordinates Network*, 4392:1, 2005.

H. M. J. Boffin. Very Large Telescope Paranal Science Operations FORS User Manual. User Manual for the FORS instrument on the VLT, February 2013.

R. C. Bohlin and R. L. Gilliland. Hubble Space Telescope Absolute Spectrophotometry of Vega from the Far-Ultraviolet to the Infrared. *AJ*, 127:3508–3515, June 2004. doi: 10.1086/420715.

M. S. Briggs et al. BATSE Observations of the Large-Scale Isotropy of Gamma-Ray Bursts. *ApJ*, 459:40, March 1996. doi: 10.1086/176867.

O. Bromberg et al. New insights on the duration distribution of long GRBs from Collapsars. *arxiv:1112.5949*, December 2011.

O. Bromberg et al. Short versus Long and Collapsars versus Non-collapsars: A Quantitative Classification of Gamma-Ray Bursts. *ApJ*, 764:179, February 2013. doi: 10.1088/0004-637X/764/2/179.

P. J. Brown and J. L. Racusin. GRB060801: Swift/UVOT upper limits. *GRB Coordinates Network*, 5385:1, 2006.

N. Bucciantini et al. Relativistic jets and long-duration gamma-ray bursts from the birth of magnetars. *MNRAS*, 383:L25–L29, January 2008. doi: 10.1111/j.1745-3933.2007.00403.x.

D. N. Burrows et al. The Swift X-Ray Telescope. *SSR*, 120:165–195, October 2005. doi: 10.1007/s11214-005-5097-2.

D. N. Burrows et al. Jet Breaks in Short Gamma-Ray Bursts. II. The Collimated Afterglow of GRB 051221A. *ApJ*, 653:468–473, December 2006. doi: 10.1086/508740.

S. Campana et al. The association of GRB 060218 with a supernova and the evolution of the shock wave. *Nature*, 442:1008–1010, August 2006. doi: 10.1038/nature04892.

J. K. Cannizzo et al. Swift report on GRB 061210. *GCN Report*, 20.1, 2006.

Z. Cano. A new method for estimating the bolometric properties of Ibc supernovae. *MNRAS*, 434:1098–1116, September 2013. doi: 10.1093/mnras/stt1048.

P. Capak et al. The First Release COSMOS Optical and Near-IR Data and Catalog. *ApJS*, 172:99–116, September 2007. doi: 10.1086/519081.

Giovanni Carraro et al. Very Large Telescope HAWK-I User Manual. User Manual for the HAWK-I instrument on the VLT, March 2011.

S. B. Cenko et al. GRBs 070429B and 070714B: The High End of the Short-Duration Gamma-Ray Burst Redshift Distribution. *arxiv:0802.0874*, February 2008.

S. B. Cenko et al. GRB090305: GMOS-s candidate optical afterglow. *GRB Coordinates Network*, 8933:1, 2009.

S. B. Cenko et al. GRB 101219A: further gemini-south imaging. *GRB Coordinates Network*, 11468:1, 2010.

M. Chester and D. Grupe. GRB 070714A: Swift/UVOT Upper limits. *GRB Coordinates Network*, 6633:1, 2007.

C. Chiosi and A. Maeder. The evolution of massive stars with mass loss. *ARAA*, 24:329–375, 1986. doi: 10.1146/annurev.aa.24.090186.001553.

R. Chornock et al. GRB 101219A: Magellan NIR observations. *GRB Coordinates Network*, 11469:1, 2010.

R. P. Church, A. J. Levan, M. B. Davies, and N. Tanvir. Implications for the origin of short gamma-ray bursts from their observed positions around their host galaxies. *MNRAS*, 413:2004–2014, May 2011. doi: 10.1111/j.1365-2966.2011.18277.x.

B. E. Cobb. GRB 060313, SMARTS optical/IR observations. *GRB Coordinates Network*, 4869:1, 2006a.

B. E. Cobb. GRB 060313, SMARTS optical counterpart? *GRB Coordinates Network*, 4872:1, 2006b.

B. E. Cobb and C. D. Bailyn. GRB 050724, SMARTS optical/IR afterglow observations. *GRB Coordinates Network*, 3694:1, 2005.

G. D. Coleman, C.-C. Wu, and D. W. Weedman. Colors and magnitudes predicted for high redshift galaxies. *ApJS*, 43:393–416, July 1980. doi: 10.1086/190674.

E. Costa et al. Discovery of an X-ray afterglow associated with the γ-ray burst of 28 February 1997. *Nature*, 387:783–785, June 1997. doi: 10.1038/42885.

A. W. J. Cousins. VRI Photometry of E and F Region Stars. *Monthly Notes of the Astronomical Society of South Africa*, 37:8, 1978.

S. Covino et al. GRB070714B: TNG NIR observations. *GRB Coordinates Network*, 6635:1, 2007.

A. Cucchiara and S. B. Cenko. GRB 111117A: Gemini host observation. *GRB Coordinates Network*, 12567:1, 2011.

A. Cucchiara and T. Sakamoto. GRB071227: Swift/UVOT refined analysis. *GRB Coordinates Network*, 7150:1, 2007.

A. Cucchiara and T. N. Ukwatta. GRB 080123: Swift/UVOT refined analysis. *GRB Coordinates Network*, 7207:1, 2008.

A. Cucchiara, J. Cannizzo, and E. Berger. GRB061210: Swift/UVOT observations. *GRB Coordinates Network*, 5924:1, 2006.

A. Cucchiara et al. A Photometric Redshift of z $\sim$ 9.4 for GRB 090429B. *ApJ*, 736: 7, July 2011. doi: 10.1088/0004-637X/736/1/7.

J. Cummings et al. GRB 051221: refined analysis of the Swift-BAT short hard burst. *GRB Coordinates Network*, 4365:1, 2005.

P. A. Curran et al. Swift report on GRB 090621B. *GCN Report*, 224.1, 2009.

G. S. Da Costa. Basic Photometry Techniques. In S. B. Howell, editor, *Astronomical CCD Observing and Reduction Techniques*, volume 23 of *Astronomical Society of the Pacific Conference Series*, page 90, 1992.

F. Daigne and R. Mochkovitch. Gamma-ray bursts from internal shocks in a relativistic wind: temporal and spectral properties. *MNRAS*, 296:275–286, May 1998. doi: 10.1046/j.1365-8711.1998.01305.x.

P. D'Avanzo et al. The optical afterglows and host galaxies of three short/hard gamma-ray bursts. *AAP*, 498:711–721, May 2009. doi: 10.1051/0004-6361/200811294.

M. B. Davies. The binary zoo: the calculation of production rates of binaries through 2+1 encounters in globular clusters. *MNRAS*, 276:887–905, October 1995.

M. de Pasquale. Swift/UVOT observation of GRB080702A. *GRB Coordinates Network*, 7932:1, 2008.

M. De Pasquale, C. Markwardt, and B. Sbarufatti. Swift report on GRB 100117A. *GCN Report*, 269.1, 2010.

A. de Ugarte Postigo et al. GRB 060121: Implications of a Short-/Intermediate-Duration γ-Ray Burst at High Redshift. *ApJL*, 648:L83–L87, September 2006. doi: 10.1086/507868.

A. de Ugarte Postigo et al. GRB080426: observations from CAHA. *GRB Coordinates Network*, 7644:1, 2008.

A. de Ugarte Postigo et al. Searching for differences in Swift's intermediate GRBs. *AAP*, 525:A109, January 2011. doi: 10.1051/0004-6361/201015261.

V. D'Elia and G. Stratta. GRB 100614A and GRB 100615A: two extremely dark gamma-ray bursts. *AAP*, 532:A48, August 2011. doi: 10.1051/0004-6361/201116505.

M. Della Valle et al. An enigmatic long-lasting γ-ray burst not accompanied by a bright supernova. *Nature*, 444:1050–1052, December 2006. doi: 10.1038/nature05374.

L. Dessart, E. O'Connor, and C. D. Ott. The Arduous Journey to Black Hole Formation in Potential Gamma-Ray Burst Progenitors. *ApJ*, 754:76, July 2012. doi: 10.1088/0004-637X/754/1/76.

L. Dessart et al. The Proto-Neutron Star Phase of the Collapsar Model and the Route to Long-Soft Gamma-Ray Bursts and Hypernovae. *ApJL*, 673:L43–L46, January 2008. doi: 10.1086/527519.

S. G. Djorgovski et al. GRB 970228: redshift and properties of the host galaxy. *GRB Coordinates Network*, 289:1, 1999.

T. Q. Donaghy et al. HETE-2 Localizations and Observations of Four Short Gamma-Ray Bursts: GRBs 010326B, 040802, 051211 and 060121. *ArXiv Astrophysics e-prints*, May 2006.

M. R. Drout et al. The First Systematic Study of Type Ibc Supernova Multi-band Light Curves. *ApJ*, 741:97, November 2011. doi: 10.1088/0004-637X/741/2/97.

D. Eichler et al. Nucleosynthesis, neutrino bursts and gamma-rays from coalescing neutron stars. *Nature*, 340:126–128, July 1989. doi: 10.1038/340126a0.

P. A. Evans et al. An online repository of Swift/XRT light curves of γ-ray bursts. *AAP*, 469:379–385, July 2007. doi: 10.1051/0004-6361:20077530.

P. A. Evans et al. Methods and results of an automatic analysis of a complete sample of Swift-XRT observations of GRBs. *MNRAS*, 397:1177–1201, August 2009a. doi: 10.1111/j.1365-2966.2009.14913.x.

P. A. Evans et al. GRB 091109B: enhanced Swift-XRT position. *GRB Coordinates Network, Circular Service, 151, 1 (2009)*, 151:1, 2009b.

J. A. Faber et al. Black Hole-Neutron Star Binary Merger Calculations: GRB Progenitors and the Stability of Mass Transfer. In J.-M. Alimi and A. Füzfa, editors, *Albert Einstein Century International Conference*, volume 861 of *American Institute of Physics Conference Series*, pages 622–629, November 2006. doi: 10.1063/1.2399634.

X. L. Fan, J. Yin, and F. Matteucci. The nature of long-GRB host galaxies from chemical abundances. *AAP*, 521:A73, October 2010. doi: 10.1051/0004-6361/201015293.

G. Fitzpatrick. GRB 100816A: Fermi GBM observation. *GRB Coordinates Network*, 11124:1, 2010a.

G. Fitzpatrick. GRB 100816A: Fermi GBM observation (correction to GCN 11124). *GRB Coordinates Network*, 11128:1, 2010b.

R. J. Foley et al. GRB 051227: Keck spectroscopy. *GRB Coordinates Network*, 4409:1, 2005.

W. Fong and E. Berger. GRB 111020A: gemini-south additional observations and limit on an optical afterglow. *GRB Coordinates Network*, 12470:1, 2011.

W. Fong, E. Berger, and D. B. Fox. Hubble Space Telescope Observations of Short Gamma-Ray Burst Host Galaxies: Morphologies, Offsets, and Local Environments. *ApJ*, 708:9–25, January 2010. doi: 10.1088/0004-637X/708/1/9.

W. Fong, E. Berger, and D. Fox. GRB 111020A: gemini-south i-band observations. *GRB Coordinates Network*, 12467:1, 2011a.

W. Fong et al. The Optical Afterglow and z = 0.92 Early-type Host Galaxy of the Short GRB 100117A. *ApJ*, 730:26, March 2011b. doi: 10.1088/0004-637X/730/1/26.

W. Fong et al. A Jet Break in the X-Ray Light Curve of Short GRB 111020A: Implications for Energetics and Rates. *ApJ*, 756:189, September 2012. doi: 10.1088/0004-637X/756/2/189.

W. Fong et al. Demographics of the Galaxies Hosting Short-duration Gamma-Ray Bursts. *ApJ*, 769:56, May 2013. doi: 10.1088/0004-637X/769/1/56.

W.-f. Fong and E. Berger. The Locations of Short Gamma-ray Bursts as Evidence for Compact Object Binary Progenitors. *ArXiv e-prints*, July 2013.

D. B. Fox et al. The afterglow of GRB 050709 and the nature of the short-hard γ-ray bursts. *Nature*, 437:845–850, October 2005. doi: 10.1038/nature04189.

D. A. Frail et al. A search for the radio counterpart to the 1994 March 1 gamma-ray burst. *ApJL*, 437:L43–L46, December 1994. doi: 10.1086/187678.

D. A. Frail et al. Beaming in Gamma-Ray Bursts: Evidence for a Standard Energy Reservoir. *ApJL*, 562:L55–L58, November 2001. doi: 10.1086/338119.

A. S. Fruchter et al. Long gamma-ray bursts and core-collapse supernovae have different environments. *Nature*, 441:463–468, May 2006. doi: 10.1038/nature04787.

A. S. Fruchter et al. in prep.

C. Fryer and V. Kalogera. Double Neutron Star Systems and Natal Neutron Star Kicks. *ApJ*, 489:244, November 1997. doi: 10.1086/304772.

C. L. Fryer. Mass Limits For Black Hole Formation. *ApJ*, 522:413–418, September 1999. doi: 10.1086/307647.

C. L. Fryer and A. Heger. Binary Merger Progenitors for Gamma-Ray Bursts and Hypernovae. *ApJ*, 623:302–313, April 2005. doi: 10.1086/428379.

C. L. Fryer, S. E. Woosley, and D. H. Hartmann. Formation Rates of Black Hole Accretion Disk Gamma-Ray Bursts. *ApJ*, 526:152–177, November 1999a. doi: 10.1086/307992.

C. L. Fryer, P. A. Young, and A. L. Hungerford. Explosive Nucleosynthesis from Gamma-Ray Burst and Hypernova Progenitors: Direct Collapse versus Fallback. *ApJ*, 650:1028–1047, October 2006. doi: 10.1086/506250.

C. L. Fryer et al. Merging White Dwarf/Black Hole Binaries and Gamma-Ray Bursts. *ApJ*, 520:650–660, August 1999b. doi: 10.1086/307467.

M. Fukugita et al. The Sloan Digital Sky Survey Photometric System. *AJ*, 111: 1748, April 1996. doi: 10.1086/117915.

J. P. U. Fynbo et al. No supernovae associated with two long-duration γ-ray bursts. *Nature*, 444:1047–1049, December 2006. doi: 10.1038/nature05375.

A. Gal-Yam, E. O. Ofek, and O. Shemmer. Supernova 2002ap: the first month. *MNRAS*, 332:L73–L77, June 2002. doi: 10.1046/j.1365-8711.2002.05535.x.

A. Gal-Yam et al. A novel explosive process is required for the γ-ray burst GRB 060614. *Nature*, 444:1053–1055, December 2006. doi: 10.1038/nature05373.

T. J. Galama et al. An unusual supernova in the error box of the γ-ray burst of 25 April 1998. *Nature*, 395:670–672, October 1998. doi: 10.1038/27150.

A. Galeev et al. GRB 090621B: RTT150 optical observations. *GRB Coordinates Network*, 9549:1, 2009.

N. Gehrels, E. Ramirez-Ruiz, and D. B. Fox. Gamma-Ray Bursts in the Swift Era. *ARAA*, 47:567–617, September 2009. doi: 10.1146/annurev.astro.46.060407.145147.

N. Gehrels et al. A short γ-ray burst apparently associated with an elliptical galaxy at redshift z = 0.225. *Nature*, 437:851–854, October 2005. doi: 10.1038/nature04142.

N. Gehrels et al. A new γ-ray burst classification scheme from GRB060614. *Nature*, 444:1044–1046, December 2006. doi: 10.1038/nature05376.

G. Ghisellini et al. A unifying view of gamma-ray burst afterglows. *MNRAS*, 393: 253–271, February 2009. doi: 10.1111/j.1365-2966.2008.14214.x.

I. S. Glass. *Handbook of Infrared Astronomy*. Cambridge University Press, 1999.

S. Golenetskii et al. Konus-wind observation of GRB 100816A. *GRB Coordinates Network*, 11127:1, 2010.

S. Golenetskii et al. Konus-wind observation of GRB 111222A. *GRB Coordinates Network*, 12715:1, 2011.

J. F. Graham et al. GRB 070714B—Discovery of the Highest Spectroscopically Confirmed Short Burst Redshift. *ApJ*, 698:1620–1629, June 2009. doi: 10.1088/0004-637X/698/2/1620.

J. Granot. The Structure and Dynamics of GRB Jets. In *Revista Mexicana de Astronomia y Astrofisica, vol. 27*, volume 27 of *Revista Mexicana de Astronomia y Astrofisica Conference Series*, pages 140–165, March 2007.

J. Greiner et al. The nature of "dark" gamma-ray bursts. *AAP*, 526:A30, February 2011. doi: 10.1051/0004-6361/201015458.

J. Grindlay, S. Portegies Zwart, and S. McMillan. Short gamma-ray bursts from binary neutron star mergers in globular clusters. *Nature Physics*, 2:116–119, February 2006. doi: 10.1038/nphys214.

D. Grupe et al. Jet Breaks in Short Gamma-Ray Bursts. I. The Uncollimated Afterglow of GRB 050724. *ApJ*, 653:462–467, December 2006. doi: 10.1086/508739.

C. Guidorzi et al. Swift report on GRB 070729. *GCN Report*, 77.1, 2007.

B. M. S. Hansen and E. S. Phinney. The pulsar kick velocity distribution. *MNRAS*, 291:569, November 1997.

W. E. Harris. Globular Clusters in the Milky Way (Harris, 1996). *VizieR Online Data Catalog*, 7195:0, November 1996.

F. Hearty et al. GRB 060121: probable detection of NIR afterglow. *GRB Coordinates Network*, 4604:1, 2006.

J. Hjorth and J. S. Bloom. The Gamma-Ray Burst - Supernova Connection. *arXiv:1104.2274*, April 2011.

J. Hjorth et al. A very energetic supernova associated with the γ-ray burst of 29 March 2003. *Nature*, 423:847–850, June 2003. doi: 10.1038/nature01750.

J. Hjorth et al. The optical afterglow of the short γ-ray burst GRB 050709. *Nature*, 437:859–861, October 2005. doi: 10.1038/nature04174.

J. Hjorth et al. The Optically Unbiased Gamma-Ray Burst Host (TOUGH) Survey. I. Survey Design and Catalogs. *ApJ*, 756:187, September 2012. doi: 10.1088/0004-637X/756/2/187.

G. Hobbs et al. A statistical study of 233 pulsar proper motions. *MNRAS*, 360: 974–992, July 2005. doi: 10.1111/j.1365-2966.2005.09087.x.

D. W. Hogg, M. A. Pahre, J. K. McCarthy, J. G. Cohen, R. Blandford, I. Smail, and B. T. Soifer. Counts and colours of faint galaxies in the U and R bands. *MNRAS*, 288:404–410, June 1997.

S. T. Holland, M. de Pasquale, and C. B. Markwardt. GRB 070429B: possible UVOT detection of an optical afterglow. *GRB Coordinates Network*, 7145:1, 2007.

S. T. Holland et al. Swift report on GRB 100625A. *GCN Report*, 289.1, 2010.

I. M. Hook et al. The Gemini-North Multi-Object Spectrograph: Performance in Imaging, Long-Slit, and Multi-Object Spectroscopic Modes. *PASP*, 116:425–440, May 2004. doi: 10.1086/383624.

I. Horváth. A Third Class of Gamma-Ray Bursts? *ApJ*, 508:757–759, December 1998. doi: 10.1086/306416.

I. Horváth. A further study of the BATSE Gamma-Ray Burst duration distribution. *AAP*, 392:791–793, September 2002. doi: 10.1051/0004-6361:20020808.

I. Horváth. Classification of BeppoSAX's gamma-ray bursts. *APSS*, 323:83–86, September 2009. doi: 10.1007/s10509-009-0039-1.

I. Horváth, Z. Bagoly, L. G. Balázs, A. de Ugarte Postigo, P. Veres, and A. Mészáros. Detailed Classification of Swift 's Gamma-ray Bursts. *ApJ*, 713:552–557, April 2010. doi: 10.1088/0004-637X/713/1/552.

I. Horváth et al. Classification of Swift's gamma-ray bursts. *AAP*, 489:L1–L4, October 2008. doi: 10.1051/0004-6361:200810269.

E. A. Hoversten et al. Swift report on GRB 090510. *GCN Report*, 218.1, 2009.

D. Huja, A. Mészáros, and J. Řípa. A comparison of the gamma-ray bursts detected by BATSE and Swift. *AAP*, 504:67–71, September 2009. doi: 10.1051/0004-6361/200809802.

D. Hullinger et al. GRB 051227: refined analysis of the Swift-BAT burst. *GRB Coordinates Network*, 4400:1, 2005.

K. Hurley, P. Li, M. Sommer, A. Smette, C. Kouveliotou, G. Fishman, T. Cline, M. Boer, M. Niel, J. Laros, R. Klebesadel, and E. Fenimore. The optical and X-ray content of the 1992 May 1 gamma-ray burst error box. *ApJS*, 92:655–657, June 1994. doi: 10.1086/192035.

K. Hurley et al. An exceptionally bright flare from SGR 1806-20 and the origins of short-duration γ-ray bursts. *Nature*, 434:1098–1103, April 2005. doi: 10.1038/nature03519.

O. Ilbert et al. The VIMOS-VLT deep survey. Evolution of the galaxy luminosity function up to z = 2 in first epoch data. *AAP*, 439:863–876, September 2005. doi: 10.1051/0004-6361:20041961.

K. Iwamoto et al. A hypernova model for the supernova associated with the γ-ray burst of 25 April 1998. *Nature*, 395:672–674, October 1998. doi: 10.1038/27155.

C. Izzo, L. de Bilbao, and J. M. Larsen. FORS Pipeline User Manual. User Manual for the FORS pipeline, April 2013.

P. Jakobsson et al. Swift Identification of Dark Gamma-Ray Bursts. *ApJL*, 617: L21–L24, December 2004. doi: 10.1086/427089.

P. Jakobsson et al. The Optically Unbiased GRB Host (TOUGH) Survey. III. Redshift Distribution. *ApJ*, 752:62, June 2012. doi: 10.1088/0004-637X/752/1/62.

M. Jelinek et al. GRB 051210: FRAM early limit. *GRB Coordinates Network*, 4319: 1, 2005.

H. L. Johnson and W. W. Morgan. Fundamental stellar photometry for standards of spectral type on the revised system of the Yerkes spectral atlas. *ApJ*, 117:313, May 1953. doi: 10.1086/145697.

D. H. Jones et al. The 6dF Galaxy Survey: samples, observational techniques and the first data release. *MNRAS*, 355:747–763, December 2004. doi: 10.1111/j.1365-2966.2004.08353.x.

D. H. Jones et al. The 6dF Galaxy Survey: final redshift release (DR3) and southern large-scale structures. *MNRAS*, 399:683–698, October 2009. doi: 10.1111/j.1365-2966.2009.15338.x.

P. M. W. Kalberla et al. The Leiden/Argentine/Bonn (LAB) Survey of Galactic HI. Final data release of the combined LDS and IAR surveys with improved stray-radiation corrections. *AAP*, 440:775–782, September 2005. doi: 10.1051/0004-6361:20041864.

D. A. Kann et al. The Afterglows of Swift-era Gamma-ray Bursts. I. Comparing pre-Swift and Swift-era Long/Soft (Type II) GRB Optical Afterglows. *ApJ*, 720: 1513–1558, September 2010. doi: 10.1088/0004-637X/720/2/1513.

D. A. Kann et al. The Afterglows of Swift-era Gamma-Ray Bursts. II. Type I GRB versus Type II GRB Optical Afterglows. *ApJ*, 734:96, June 2011. doi: 10.1088/0004-637X/734/2/96.

D. Kasen, N. R. Badnell, and J. Barnes. Opacities and Spectra of the r-process Ejecta from Neutron Star Mergers. *ApJ*, 774:25, September 2013. doi: 10.1088/0004-637X/774/1/25.

A. King, E. Olsson, and M. B. Davies. A new type of long gamma-ray burst. *MNRAS*, 374:L34–L36, January 2007. doi: 10.1111/j.1745-3933.2006.00259.x.

K. Kinugasa et al. GRB 090426: GAO 150cm telescope optical observation. *GRB Coordinates Network*, 9292:1, 2009.

M. Kissler-Patig et al. HAWK-I: the high-acuity wide-field K-band imager for the ESO Very Large Telescope. *AAP*, 491:941–950, December 2008. doi: 10.1051/0004-6361:200809910.

R. W. Klebesadel, I. B. Strong, and R. A. Olson. Observations of Gamma-Ray Bursts of Cosmic Origin. *ApJL*, 182:L85, June 1973. doi: 10.1086/181225.

W. Kluźniak and M. Ruderman. The Central Engine of Gamma-Ray Bursters. *ApJL*, 508:L113–L113, November 1998. doi: 10.1086/311732.

S. Kobayashi, T. Piran, and R. Sari. Can Internal Shocks Produce the Variability in Gamma-Ray Bursts? *ApJ*, 490:92, November 1997. doi: 10.1086/512791.

S. Kobayashi, T. Piran, and R. Sari. Hydrodynamics of a Relativistic Fireball: The Complete Evolution. *ApJ*, 513:669–678, March 1999. doi: 10.1086/306868.

D. Kocevski et al. Limits on radioactive powered emission associated with a short-hard GRB 070724A in a star-forming galaxy. *MNRAS*, 404:963–974, May 2010. doi: 10.1111/j.1365-2966.2010.16327.x.

C. S. Kochanek et al. A Survey About Nothing: Monitoring a Million Supergiants for Failed Supernovae. *ApJ*, 684:1336–1342, September 2008. doi: 10.1086/590053.

C. Kouveliotou et al. Identification of two classes of gamma-ray bursts. *ApJL*, 413: L101–L104, August 1993. doi: 10.1086/186969.

R. P. Kraft, D. N. Burrows, and J. A. Nousek. Determination of confidence limits for experiments with low numbers of counts. *ApJ*, 374:344–355, June 1991. doi: 10.1086/170124.

H. Krimm et al. GRB050724: refined analysis of the Swift-BAT possible short burst. *GRB Coordinates Network*, 3667:1, 2005.

H. A. Krimm et al. GRB 081226A: Swift-BAT refined analysis. *GRB Coordinates Network*, 8735:1, 2008.

H. A. Krimm et al. GRB 090305, Swift-BAT refined analysis. *GRB Coordinates Network*, 8936:1, 2009.

H. A. Krimm et al. Swift report on GRB 100206A. *GCN Report*, 271.1, 2010a.

H. A. Krimm et al. GRB 101219A: Swift-BAT refined analysis. *GRB Coordinates Network*, 11467:1, 2010b.

H. A. Krimm et al. Swift report on GRB 101224A. *GCN Report*, 312.1, 2011.

N. P. M. Kuin and J. M. Gelbord. GRB 101219A: Swift/UVOT upper limits. *GRB Coordinates Network*, 11472:1, 2010.

N. P. M. Kuin and E. A. Hoversten. GRB 090510: UVOT refined analysis. *GRB Coordinates Network*, 9342:1, 2009.

N. P. M. Kuin, S. Oates, and V. D'Elia. GRB 111121A: Swift/UVOT upper limits. *GRB Coordinates Network*, 12584:1, 2011.

G. P. Kuiper. On the Interpretation of β Lyrae and Other Close Binaries. *ApJ*, 93: 133, January 1941. doi: 10.1086/144252.

S. R. Kulkarni. Modeling Supernova-like Explosions Associated with Gamma-ray Bursts with Short Durations. *arXiv:astro-ph/0510256*, October 2005.

D. Q. Lamb. The Distance Scale to Gamma-Ray Bursts. *PASP*, 107:1152, December 1995. doi: 10.1086/133673.

W. Landsman, F. E. Marshall, and J. Racusin. Swift/UVOT detection of GRB070714B. *GRB Coordinates Network*, 6689:1, 2007.

C. N. Leibler and E. Berger. The Stellar Ages and Masses of Short Gamma-ray Burst Host Galaxies: Investigating the Progenitor Delay Time Distribution and the Role of Mass and Star Formation in the Short Gamma-ray Burst Rate. *ApJ*, 725:1202–1214, December 2010. doi: 10.1088/0004-637X/725/1/1202.

A. J. Levan and N. R. Tanvir. GRB 100625A: Gemini candidate afterglow. *GRB Coordinates Network*, 10887:1, 2010.

A. J. Levan, N. R. Tanvir, and D. Baker. GRB 110112A: WHT candidate afterglow/host galaxy. *GRB Coordinates Network*, 11559:1, 2011.

A. J. Levan et al. The Faint Afterglow and Host Galaxy of the Short-Hard GRB 060121. *ApJL*, 648:L9–L12, September 2006a. doi: 10.1086/507625.

A. J. Levan et al. Short gamma-ray bursts in old populations: magnetars from white dwarf-white dwarf mergers. *MNRAS*, 368:L1–L5, May 2006b. doi: 10.1111/j.1745-3933.2006.00144.x.

A. J. Levan et al. A case of mistaken identity? GRB060912A and the nature of the long-short GRB divide. *MNRAS*, 378:1439–1446, July 2007. doi: 10.1111/j.1365-2966.2007.11879.x.

A. J. Levan et al. On the nature of the short-duration GRB 050906. *MNRAS*, 384: 541–547, February 2008. doi: 10.1111/j.1365-2966.2007.11953.x.

A. J. Levan et al. A new population of ultra-long duration gamma-ray bursts. *arxiv:1302.2352*, February 2013.

E. M. Levesque et al. GRB090426: the environment of a rest-frame 0.35-s gamma-ray burst at a redshift of 2.609. *MNRAS*, 401:963–972, January 2010a. doi: 10.1111/j.1365-2966.2009.15733.x.

E. M. Levesque et al. The Host Galaxies of Gamma-Ray Bursts. I. Interstellar Medium Properties of Ten Nearby Long-Duration Gamma-Ray Burst Hosts. *AJ*, 139:694–711, February 2010b. doi: 10.1088/0004-6256/139/2/694.

L.-X. Li and B. Paczyński. Transient Events from Neutron Star Mergers. *ApJL*, 507:L59–L62, November 1998. doi: 10.1086/311680.

Z. Li, Z. G. Dai, and T. Lu. Overall temporal synchrotron emissions from relativistic jets: adiabatic and radiative breaks. *MNRAS*, 330:955–964, March 2002. doi: 10.1046/j.1365-8711.2002.05141.x.

Y. M. Lipkin et al. The Detailed Optical Light Curve of GRB 030329. *ApJ*, 606: 381–394, May 2004. doi: 10.1086/383000.

O. M. Littlejohns and S. R. Oates. GRB100816A Swift-XRT refined analysis. *GRB Coordinates Network*, 11114:1, 2010.

R. H. Lupton et al. Dissecting the Milky Way with SDSS - I: Stellar Overdensities. In *American Astronomical Society Meeting Abstracts*, volume 37 of *Bulletin of the American Astronomical Society*, page 133.08, December 2005.

A. I. MacFadyen and S. E. Woosley. Collapsars: Gamma-Ray Bursts and Explosions in "Failed Supernovae". *ApJ*, 524:262–289, October 1999. doi: 10.1086/307790.

A. I. MacFadyen, S. E. Woosley, and A. Heger. Supernovae, Jets, and Collapsars. *ApJ*, 550:410–425, March 2001. doi: 10.1086/319698.

D. Malesani et al. SN 2003lw and GRB 031203: A Bright Supernova for a Faint Gamma-Ray Burst. *ApJL*, 609:L5–L8, July 2004. doi: 10.1086/422684.

D. Malesani et al. Multicolor observations of the afterglow of the short/hard GRB 050724. *AAP*, 473:77–84, October 2007. doi: 10.1051/0004-6361:20077868.

V. Mangano et al. Swift report on GRB 111117A. *GCN Report*, 363.1, 2012.

J. Mao, G. Cha, and J. Bai. GRB 090426: YNAO-GMG observations. *GRB Coordinates Network*, 9285:1, 2009.

J. Mao et al. Swift report on GRB 080503. *GCN Report*, 138.1, 2008.

R. Margutti et al. The Afterglow and Environment of the Short GRB 111117A. *ApJ*, 756:63, September 2012. doi: 10.1088/0004-637X/756/1/63.

C. Markwardt et al. GRB 060313: refined analysis of the Swift-BAT bright short hard burst. *GRB Coordinates Network*, 4873:1, 2006.

C. B. Markwardt et al. Swift report on GRB 070429B. *GCN Report*, 51.1, 2007.

C. B. Markwardt et al. GRB 100816A, Swift-BAT refined analysis. *GRB Coordinates Network*, 11111:1, 2010.

F. E. Marshall and E. A. Hoversten. GRB 090510: Swift/UVOT detection of a candidate optical afterglow. *GRB Coordinates Network*, 9332:1, 2009.

F. E. Marshall et al. Swift report on GRB 061201. *GCN Report*, 18.1, 2006.

F. E. Marshall et al. Swift report on GRB 070809. *GCN Report*, 80.1, 2007.

S. McBreen et al. Optical and near-infrared follow-up observations of four Fermi/LAT GRBs: redshifts, afterglows, energetics, and host galaxies. *AAP*, 516:A71, June 2010. doi: 10.1051/0004-6361/200913734.

S. McGlynn et al. GRB 070707: the first short gamma-ray burst observed by INTEGRAL. *AAP*, 486:405–410, August 2008. doi: 10.1051/0004-6361:20079295.

C. A. Meegan et al. Spatial distribution of gamma-ray bursts observed by BATSE. *Nature*, 355:143–145, January 1992. doi: 10.1038/355143a0.

A. Melandri et al. GRB 081024: faulkes telescope north optical observations. *GRB Coordinates Network*, 8402:1, 2008.

A. Melandri et al. The optical SN 2012bz associated with the long GRB 120422A. *AAP*, 547:A82, November 2012. doi: 10.1051/0004-6361/201219879.

P. Meszaros and M. J. Rees. Gamma-Ray Bursts: Multiwaveband Spectral Predictions for Blast Wave Models. *ApJL*, 418:L59, December 1993. doi: 10.1086/187116.

P. Meszaros and M. J. Rees. Optical and Long-Wavelength Afterglow from Gamma-Ray Bursts. *ApJ*, 476:232, February 1997. doi: 10.1086/303625.

P. Meszaros, M. J. Rees, and H. Papathanassiou. Spectral properties of blast-wave models of gamma-ray burst sources. *APJ*, 432:181–193, September 1994. doi: 10.1086/174559.

B. D. Metzger and E. Berger. What is the Most Promising Electromagnetic Counterpart of a Neutron Star Binary Merger? *ApJ*, 746:48, February 2012. doi: 10.1088/0004-637X/746/1/48.

B. D. Metzger, T. A. Thompson, and E. Quataert. Proto-Neutron Star Winds with Magnetic Fields and Rotation. *ApJ*, 659:561–579, April 2007. doi: 10.1086/512059.

B. D. Metzger, A. L. Piro, and E. Quataert. Time-dependent models of accretion discs formed from compact object mergers. *MNRAS*, 390:781–797, October 2008. doi: 10.1111/j.1365-2966.2008.13789.x.

B. D. Metzger et al. Electromagnetic counterparts of compact object mergers powered by the radioactive decay of r-process nuclei. *MNRAS*, 406:2650–2662, August 2010. doi: 10.1111/j.1365-2966.2010.16864.x.

B. D. Metzger et al. The protomagnetar model for gamma-ray bursts. *MNRAS*, 413:2031–2056, May 2011. doi: 10.1111/j.1365-2966.2011.18280.x.

M. R. Metzger, S. G. Djorgovski, S. R. Kulkarni, C. C. Steidel, K. L. Adelberger, D. A. Frail, E. Costa, and F. Frontera. Spectral constraints on the redshift of the optical counterpart to the γ-ray burst of 8 May 1997. *Nature*, 387:878–880, June 1997. doi: 10.1038/43132.

A. A. Miller et al. GRB 100206A: pre-explosion imaging and host candidate. *GRB Coordinates Network*, 10377:1, 2010.

D. G. Monet et al. The USNO-B Catalog. *AJ*, 125:984–993, February 2003. doi: 10.1086/345888.

A. D. Montero-Dorta and F. Prada. The SDSS DR6 luminosity functions of galaxies. *MNRAS*, 399:1106–1118, November 2009. doi: 10.1111/j.1365-2966.2009.15197.x.

O. Nakamura, M. Fukugita, N. Yasuda, J. Loveday, J. Brinkmann, D. P. Schneider, K. Shimasaku, and M. SubbaRao. The Luminosity Function of Morphologically Classified Galaxies in the Sloan Digital Sky Survey. *AJ*, 125:1682–1688, April 2003. doi: 10.1086/368135.

R. Narayan, B. Paczyński, and T. Piran. Gamma-ray bursts as the death throes of massive binary stars. *ApJL*, 395:L83–L86, August 1992. doi: 10.1086/186493.

K. C. B. New. Gravitational Waves from Gravitational Collapse. *Living Reviews in Relativity*, 6:2, March 2003.

A. Nicuesa Guelbenzu et al. GRB 090426: Discovery of a jet break in a short burst afterglow. *AAP*, 531:L6, July 2011. doi: 10.1051/0004-6361/201116657.

A. Nicuesa Guelbenzu et al. The late-time afterglow of the extremely energetic short burst GRB 090510 revisited. *AAP*, 538:L7, February 2012a. doi: 10.1051/0004-6361/201118416.

A. Nicuesa Guelbenzu et al. Multi-color observations of short GRB afterglows: 20 events observed between 2007 and 2010. *AAP*, 548:A101, December 2012b. doi: 10.1051/0004-6361/201219551.

S. Nissanke et al. Determining the Hubble constant from gravitational wave observations of merging compact binaries. *arxiv:1307.2638*, July 2013.

J. Norris et al. GRB 100816A: Swift-BAT spectral lag results. *GRB Coordinates Network*, 11113:1, 2010a.

J. P. Norris and J. T. Bonnell. Short Gamma-Ray Bursts with Extended Emission. *ApJ*, 643:266–275, May 2006. doi: 10.1086/502796.

J. P. Norris, G. F. Marani, and J. T. Bonnell. Connection between Energy-dependent Lags and Peak Luminosity in Gamma-Ray Bursts. *ApJ*, 534:248–257, May 2000. doi: 10.1086/308725.

J. P. Norris, N. Gehrels, and J. D. Scargle. Threshold for Extended Emission in Short Gamma-ray Bursts. *ApJ*, 717:411–419, July 2010b. doi: 10.1088/0004-637X/717/1/411.

J. P. Norris et al. Long-Lag, Wide-Pulse Gamma-Ray Bursts. *ApJ*, 627:324–345, July 2005. doi: 10.1086/430294.

P. E. Nugent and J. S. Bloom. GRB 101224A: pre-event imaging from DeepSky; detection of a source in the XRT error circle. *GRB Coordinates Network*, 11491: 1, 2010.

M. Nysewander, A. S. Fruchter, and A. Pe'er. A Comparison of the Afterglows of Short- and Long-duration Gamma-ray Bursts. *ApJ*, 701:824–836, August 2009. doi: 10.1088/0004-637X/701/1/824.

M. Nysewander et al. GRB 060313: PROMPT observations. *GRB Coordinates Network*, 4878:1, 2006.

S. R. Oates and J. R. Cummings. GRB090426 Swift/UVOT observations. *GRB Coordinates Network*, 9265:1, 2009.

S. R. Oates and V. Mangano. GRB 111117A: Swift/UVOT upper limits. *GRB Coordinates Network*, 12569:1, 2011.

S. R. Oates, K. L. Page, P. A. Evans, and C. B. Markwardt. Swift report on GRB 091109B. *GCN Report*, 259.1, 2009a.

S. R. Oates et al. GRB 091109B: Swift detection of a short burst. *GRB Coordinates Network, Circular Service, 148, 1 (2009)*, 148:1, 2009b.

S. R. Oates et al. GRB 100816A: Swift detection of a possibly short burst with optical afterglow. *GRB Coordinates Network*, 11102:1, 2010.

M. Ohno et al. GRB 091109B: Suzaku WAM observation of the prompt emission. *GRB Coordinates Network, Circular Service, 10168, 1 (2009)*, 168:1, 2009.

F. Olivares et al. GRB 090510: GROND observations. *GRB Coordinates Network*, 9352:1, 2009.

G. Olofsson et al. GRB 090510: NOT afterglow confirmation. *GRB Coordinates Network*, 9338:1, 2009.

R. O'Shaughnessy, K. Belczynski, and V. Kalogera. Short Gamma-Ray Bursts and Binary Mergers in Spiral and Elliptical Galaxies: Redshift Distribution and Hosts. *ApJ*, 675:566–585, March 2008. doi: 10.1086/526334.

B. Paczyński. Evolutionary Processes in Close Binary Systems. *ARAA*, 9:183, 1971. doi: 10.1146/annurev.aa.09.090171.001151.

B. Paczyński. Gamma-ray bursters at cosmological distances. *ApJL*, 308:L43–L46, September 1986. doi: 10.1086/184740.

B. Paczyński. How Far Away Are Gamma-Ray Bursters? *PASP*, 107:1167, December 1995. doi: 10.1086/133674.

C. Pagani et al. Swift report on GRB 080905A. *GCN Report*, 162.1, 2008.

F. Patat et al. The Metamorphosis of SN 1998bw. *ApJ*, 555:900–917, July 2001. doi: 10.1086/321526.

G. Paturel et al. The provisional DENIS I-band catalog of galaxies revisited. *AAP*, 405:1–3, July 2003. doi: 10.1051/0004-6361:20030535.

D. A. Perley, J. S. Bloom, M. Modjaz, D. Poznanski, and C. C. Thoene. GRB 070429B: probable host galaxy and redshift. *GRB Coordinates Network*, 7140:1, 2007a.

D. A. Perley, J. S. Bloom, C. Thoene, and N. R. Butler. GRB 070714B: Keck observations. *GRB Coordinates Network*, 6652:1, 2007b.

D. A. Perley, C. C. Thoene, and J. S. Bloom. GRB 070809: confirmation of optical transient. *GRB Coordinates Network*, 6774:1, 2007c.

D. A. Perley, C. C. Thoene, J. Cooke, J. S. Bloom, and E. Barton. GRB 070809: Keck imaging. *GRB Coordinates Network*, 6739:1, 2007d.

D. A. Perley, J. S. Bloom, M. Modjaz, A. A. Miller, J. Shiode, J. Brewer, D. Starr, and R. Kennedy. GRB 070809: putative host galaxy and redshift. *GRB Coordinates Network*, 7889:1, 2008.

D. A. Perley et al. GRB 080503: Implications of a Naked Short Gamma-Ray Burst Dominated by Extended Emission. *ApJ*, 696:1871–1885, May 2009a. doi: 10.1088/0004-637X/696/2/1871.

D. A. Perley et al. The Host Galaxies of Swift Dark Gamma-ray Bursts: Observational Constraints on Highly Obscured and Very High Redshift GRBs. *AJ*, 138: 1690–1708, December 2009b. doi: 10.1088/0004-6256/138/6/1690.

D. A. Perley et al. GRB 101219A: gemini-south observations. *GRB Coordinates Network*, 11464:1, 2010.

Philip Carl Peters. *Gravitational radiation and the motion of two point masses.* PhD thesis, California Institute of Technology, February 1964.

E. S. Phinney. The rate of neutron star binary mergers in the universe - Minimal predictions for gravity wave detectors. *ApJL*, 380:L17–L21, October 1991. doi: 10.1086/186163.

E. Pian et al. An optical supernova associated with the X-ray flash XRF 060218. *Nature*, 442:1011–1013, August 2006. doi: 10.1038/nature05082.

S. Piranomonte et al. The short GRB 070707 afterglow and its very faint host galaxy. *AAP*, 491:183–188, November 2008. doi: 10.1051/0004-6361:200810547.

T. S. Poole et al. Photometric calibration of the Swift ultraviolet/optical telescope. *MNRAS*, 383:627–645, January 2008. doi: 10.1111/j.1365-2966.2007.12563.x.

D. J. Price and S. Rosswog. Producing Ultrastrong Magnetic Fields in Neutron Star Mergers. *Science*, 312:719–722, May 2006. doi: 10.1126/science.1125201.

J. X. Prochaska et al. GRB 050724: secure host redshift from Keck. *GRB Coordinates Network*, 3700:1, 2005.

J. X. Prochaska et al. The Galaxy Hosts and Large-Scale Environments of Short-Hard Gamma-Ray Bursts. *ApJ*, 642:989–994, May 2006. doi: 10.1086/501160.

M. Punturo et al. The Einstein Telescope: a third-generation gravitational wave observatory. *Classical and Quantum Gravity*, 27(19):194002, October 2010. doi: 10.1088/0264-9381/27/19/194002.

J. Racusin, L. Barbier, and W. Landsman. Swift report on GRB 070714B. *GCN Report*, 70.1, 2007.

J. L. Racusin et al. Jet Breaks and Energetics of Swift Gamma-Ray Burst X-Ray Afterglows. *ApJ*, 698:43–74, June 2009. doi: 10.1088/0004-637X/698/1/43.

A. Rau, S. McBreen, and T. Kruehler. GRB090510: VLT/FORS2 spectroscopic redshift. *GRB Coordinates Network*, 9353:1, 2009.

M. J. Rees and P. Meszaros. Relativistic fireballs - Energy conversion and time-scales. *MNRAS*, 258:41P–43P, September 1992.

M. J. Rees and P. Meszaros. Unsteady outflow models for cosmological gamma-ray bursts. *ApJL*, 430:L93–L96, August 1994. doi: 10.1086/187446.

S. Repetto, M. B. Davies, and S. Sigurdsson. Investigating stellar-mass black hole kicks. *MNRAS*, 425:2799–2809, October 2012. doi: 10.1111/j.1365-2966.2012.21549.x.

L. F. Roberts et al. Electromagnetic Transients Powered by Nuclear Decay in the Tidal Tails of Coalescing Compact Binaries. *ApJL*, 736:L21, July 2011. doi: 10.1088/2041-8205/736/1/L21.

P. Roming et al. GRB 051221A: detection at 251nm with swift UVOT. *GRB Coordinates Network*, 4390:1, 2005.

P. W. A. Roming et al. GRB 060313: A New Paradigm for Short-Hard Bursts? *ApJ*, 651:985–993, November 2006. doi: 10.1086/508054.

S. Rosswog, E. Ramirez-Ruiz, and M. B. Davies. High-resolution calculations of merging neutron stars - III. Gamma-ray bursts. *MNRAS*, 345:1077–1090, November 2003. doi: 10.1046/j.1365-2966.2003.07032.x.

S. Rosswog, R. Speith, and G. A. Wynn. Accretion dynamics in neutron star-black hole binaries. *MNRAS*, 351:1121–1133, July 2004. doi: 10.1111/j.1365-2966.2004.07865.x.

A. Rowlinson et al. Discovery of the afterglow and host galaxy of the low-redshift short GRB 080905A. *MNRAS*, 408:383–391, October 2010a. doi: 10.1111/j.1365-2966.2010.17115.x.

A. Rowlinson et al. The unusual X-ray emission of the short Swift GRB 090515: evidence for the formation of a magnetar? *MNRAS*, 409:531–540, December 2010b. doi: 10.1111/j.1365-2966.2010.17354.x.

V. Rumyantsev, K. Antoniuk, and A. Pozanenko. GRB 090426: optical observations. *GRB Coordinates Network*, 9312:1, 2009.

T. Sakamoto et al. GRB 111020A: Swift-BAT refined analysis. *GRB Coordinates Network*, 12464:1, 2011a.

T. Sakamoto et al. GRB 111020A: Swift detection of a short burst. *GRB Coordinates Network*, 12460:1, 2011b.

T. Sakamoto et al. Identifying the Location in the Host Galaxy of the Short GRB 111117A with the Chandra Subarcsecond Position. *ApJ*, 766:41, March 2013. doi: 10.1088/0004-637X/766/1/41.

R. Salvaterra et al. Short Gamma-ray bursts: a bimodal origin? *MNRAS*, 388: L6–L9, July 2008. doi: 10.1111/j.1745-3933.2008.00488.x.

R. Salvaterra et al. On the offset of short gamma-ray bursts. *MNRAS*, 406:1248–1252, August 2010. doi: 10.1111/j.1365-2966.2010.16752.x.

R. Sari and T. Piran. Hydrodynamic Timescales and Temporal Structure of Gamma-Ray Bursts. *ApJL*, 455:L143, December 1995. doi: 10.1086/309835.

R. Sari, T. Piran, and R. Narayan. Spectra and Light Curves of Gamma-Ray Burst Afterglows. *ApJL*, 497:L17, April 1998. doi: 10.1086/311269.

G. Sato et al. GRB 050813: Swift-BAT refined analysis. *GRB Coordinates Network*, 3793:1, 2005a.

G. Sato et al. GRB 051210: Swift-BAT refined analysis of a short burst. *GRB Coordinates Network*, 4318:1, 2005b.

G. Sato et al. GRB 060502B: refined analysis of the Swift-BAT short burst. *GRB Coordinates Network*, 5064:1, 2006a.

G. Sato et al. GRB 060801: refined analysis of the Swift-BAT short hard burst. *GRB Coordinates Network*, 5381:1, 2006b.

G. Sato et al. Swift-BAT refined analysis of short GRB 071227. *GRB Coordinates Network*, 7148:1, 2007.

G. Sato et al. GRB 090426: Swift-BAT refined analysis. *GRB Coordinates Network*, 9263:1, 2009.

S. Savaglio, K. Glazebrook, and D. Le Borgne. The Galaxy Population Hosting Gamma-Ray Bursts. *ApJ*, 691:182–211, January 2009. doi: 10.1088/0004-637X/691/1/182.

P. Schady and C. Pagani. GRB 060313: Swift/UVOT observations. *GRB Coordinates Network*, 4877:1, 2006.

P. Schady et al. Swift report on GRB 061006. *GCN Report*, 6.1, 2006.

B. E. Schaefer et al. Rapid searches for counterparts of GRB 930131. *ApJL*, 422: L71–L74, February 1994. doi: 10.1086/187215.

P. Schechter. An analytic expression for the luminosity function for galaxies. *ApJ*, 203:297–306, January 1976. doi: 10.1086/154079.

D. J. Schlegel, D. P. Finkbeiner, and M. Davis. Maps of Dust Infrared Emission for Use in Estimation of Reddening and Cosmic Microwave Background Radiation Foregrounds. *ApJ*, 500:525, June 1998. doi: 10.1086/305772.

M. Schmitz et al. The NASA/IPAC Extragalactic Database (NED): Enhanced Content and New Functionality. In *American Astronomical Society Meeting Abstracts #217*, volume 43 of *Bulletin of the American Astronomical Society*, page #344.08, January 2011.

M. Shibata and K. Taniguchi. Merger of binary neutron stars to a black hole: Disk mass, short gamma-ray bursts, and quasinormal mode ringing. *PRD*, 73(6): 064027, March 2006. doi: 10.1103/PhysRevD.73.064027.

M. H. Siegel and D. Grupe. GRB 111222A: Swift/UVOT observations. *GRB Coordinates Network*, 12717:1, 2011.

M. F. Skrutskie et al. The Two Micron All Sky Survey (2MASS). *AJ*, 131:1163–1183, February 2006. doi: 10.1086/498708.

A. M. Soderberg et al. The Afterglow, Energetics, and Host Galaxy of the Short-Hard Gamma-Ray Burst 051221a. *ApJ*, 650:261–271, October 2006a. doi: 10.1086/506429.

A. M. Soderberg et al. Relativistic ejecta from X-ray flash XRF 060218 and the rate of cosmic explosions. *Nature*, 442:1014–1017, August 2006b. doi: 10.1038/nature05087.

M. Stamatikos et al. GRB 110112A: Swift detection of a possible short burst. *GRB Coordinates Network*, 11553:1, 2011.

K. Z. Stanek et al. Spectroscopic Discovery of the Supernova 2003dh Associated with GRB 030329. *ApJL*, 591:L17–L20, July 2003. doi: 10.1086/376976.

R. L. C. Starling et al. Discovery of the nearby long, soft GRB 100316D with an associated supernova. *MNRAS*, 411:2792–2803, March 2011. doi: 10.1111/j.1365-2966.2010.17879.x.

G. Stratta et al. A study of the prompt and afterglow emission of the short GRB 061201. *AAP*, 474:827–835, November 2007. doi: 10.1051/0004-6361:20078006.

D. Suzuki et al. GRB100625A : MOA optical upper limit. *GRB Coordinates Network*, 10885:1, 2010.

K. M. Svensson et al. The host galaxies of core-collapse supernovae and gamma-ray bursts. *MNRAS*, 405:57–76, June 2010. doi: 10.1111/j.1365-2966.2010.16442.x.

N. R. Tanvir and A. J. Levan. GRB 100625A gemini-north 2nd epoch imaging. *GRB Coordinates Network*, 10905:1, 2010.

N. R. Tanvir, R. Chapman, A. J. Levan, and R. S. Priddey. An origin in the local Universe for some short γ-ray bursts. *Nature*, 438:991–993, December 2005. doi: 10.1038/nature04310.

N. R. Tanvir et al. A γ-ray burst at a redshift of z˜8.2. *Nature*, 461:1254–1257, October 2009. doi: 10.1038/nature08459.

N. R. Tanvir et al. Late-time Observations of GRB 080319B: Jet Break, Host Galaxy, and Accompanying Supernova. *ApJ*, 725:625–632, December 2010a. doi: 10.1088/0004-637X/725/1/625.

N. R. Tanvir et al. GRB 100816A: VLT and Gemini-N revised redshift. *GRB Coordinates Network*, 11123:1, 2010b.

N. R. Tanvir et al. A 'kilonova' associated with the short-duration γ-ray burst GRB130603B. *Nature*, 500:547–549, August 2013. doi: 10.1038/nature12505.

C. Thompson and R. C. Duncan. Neutron star dynamos and the origins of pulsar magnetism. *ApJ*, 408:194–217, May 1993. doi: 10.1086/172580.

T. A. Thompson, M. D. Kistler, and K. Z. Stanek. A High Rate of White Dwarf-Neutron Star Mergers and Their Transients. *ArXiv e-prints*, December 2009.

C. Thöne et al. GRB060313: optical observations of the afterglow candidate. *GRB Coordinates Network*, 4874:1, 2006.

C. C. Thöne et al. Variable Lyα sheds light on the environment surrounding GRB 090426. *MNRAS*, page 433, March 2011. doi: 10.1111/j.1365-2966.2011.18408.x.

K. Tibbets-Harlow et al. in prep.

N. Tominaga et al. The Connection between Gamma-Ray Bursts and Extremely Metal-poor Stars: Black Hole-forming Supernovae with Relativistic Jets. *ApJL*, 657:L77–L80, March 2007. doi: 10.1086/513193.

E. Troja et al. Different progenitors of short hard gamma-ray bursts. *MNRAS*, 385: L10–L14, March 2008. doi: 10.1111/j.1745-3933.2007.00421.x.

R. L. Tunnicliffe et al. On the nature of the 'hostless' short GRBs. *MNRAS*, 437: 1495–1510, January 2014. doi: 10.1093/mnras/stt1975.

V. V. Usov. Millisecond pulsars with extremely strong magnetic fields as a cosmological source of gamma-ray bursts. *Nature*, 357:472–474, June 1992. doi: 10.1038/357472a0.

J. Řípa et al. Search for gamma-ray burst classes with the RHESSI satellite. *AAP*, 498:399–406, May 2009. doi: 10.1051/0004-6361/200810913.

A. J. van der Horst et al. Optical Classification of Gamma-Ray Bursts in the Swift Era. *ApJ*, 699:1087–1091, July 2009. doi: 10.1088/0004-637X/699/2/1087.

J. van Paradijs et al. Transient optical emission from the error box of the γ-ray burst of 28 February 1997. *Nature*, 386:686–689, April 1997. doi: 10.1038/386686a0.

Gilbert Vedrenne and Jean-Luc Atteia. *Gamma-Ray Bursts. The brightest explosions in the Universe*. Praxis Publishing Ltd., Chichester, UK, 2009.

J. S. Villasenor et al. Discovery of the short γ-ray burst GRB 050709. *Nature*, 437: 855–858, October 2005. doi: 10.1038/nature04213.

J. C. Wheeler, I. Yi, P. Höflich, and L. Wang. Asymmetric Supernovae, Pulsars, Magnetars, and Gamma-Ray Bursts. *ApJ*, 537:810–823, July 2000. doi: 10.1086/309055.

R. S. White. Some requirements of a colliding comet source of gamma ray bursts. *Astrophysics and Space Science*, 208:301–311, October 1993. doi: 10.1007/BF00657945.

K. Wiersema et al. GRB 050724: WHT optical observations. *GRB Coordinates Network*, 3699:1, 2005.

T.-W. Wong, B. Willems, and V. Kalogera. Constraints on Natal Kicks in Galactic Double Neutron Star Systems. *ApJ*, 721:1689–1701, October 2010. doi: 10.1088/0004-637X/721/2/1689.

S. E. Woosley. Gamma-ray bursts from stellar mass accretion disks around black holes. *ApJ*, 405:273–277, March 1993. doi: 10.1086/172359.

S. E. Woosley and J. S. Bloom. The Supernova Gamma-Ray Burst Connection. *ARAA*, 44:507–556, September 2006. doi: 10.1146/annurev.astro.43.072103.150558.

S. E. Woosley and T. A. Weaver. The Evolution and Explosion of Massive Stars. II. Explosive Hydrodynamics and Nucleosynthesis. *ApJS*, 101:181, November 1995. doi: 10.1086/192237.

S. E. Woosley, R. G. Eastman, and B. P. Schmidt. Gamma-Ray Bursts and Type IC Supernova SN 1998BW. *ApJ*, 516:788–796, May 1999. doi: 10.1086/307131.

J. Wren et al. GRB 051221A: RAPTOR fading counterpart constraint. *GRB Coordinates Network*, 4380:1, 2005.

L.-P. Xin et al. Probing the nature of high-z short GRB 090426 with its early optical and X-ray afterglows. *MNRAS*, page 1404, September 2010. doi: 10.1111/j.1365-2966.2010.17419.x.

L. P. Xin et al. GRB110112A: TNT optical afterglow candidate. *GRB Coordinates Network*, 11554:1, 2011.

D. Xu, I. Ilyin, and J. P. U. Fynbo. GRB 101224A: NOT optical observation. *GRB Coordinates Network*, 11492:1, 2010.

D. Xu et al. In Search of Progenitors for Supernovaless Gamma-Ray Bursts 060505 and 060614: Re-examination of Their Afterglows. *ApJ*, 696:971–979, May 2009. doi: 10.1088/0004-637X/696/1/971.

T. Yi et al. On the spectral lags of the short gamma-ray bursts. *MNRAS*, 367: 1751–1756, April 2006. doi: 10.1111/j.1365-2966.2006.10083.x.

M. Yoshida et al. GRB 090426: Okayama Mitsume optical observation. *GRB Coordinates Network*, 9266:1, 2009.

M. Zemp, E. Ramirez-Ruiz, and J. Diemand. Halo Retention and Evolution of Coalescing Compact Binaries in Cosmological Simulations of Structure Formation: Implications for Short Gamma-ray Bursts. *ApJL*, 705:L186–L190, November 2009. doi: 10.1088/0004-637X/705/2/L186.

B. Zhang et al. Discerning the Physical Origins of Cosmological Gamma-ray Bursts Based on Multiple Observational Criteria: The Cases of z = 6.7 GRB 080913, z = 8.2 GRB 090423, and Some Short/Hard GRBs. *ApJ*, 703:1696–1724, October 2009. doi: 10.1088/0004-637X/703/2/1696.

H. Ziaeepour et al. Swift report on GRB 061217. *GCN Report*, 21.2, 2007a.

H. Ziaeepour et al. Swift report on GRB 070724A. *GCN Report*, 74.2, 2007b.